ERDC/EL TR-00-10

Environmental Laboratory

US Army Corps
of Engineers®
Engineer Research and
Development Center

Water Quality Model of Florida Bay

Carl F. Cerco, Barry W. Bunch, Allen M. Teeter, and
Mark S. Dortch

September 2000

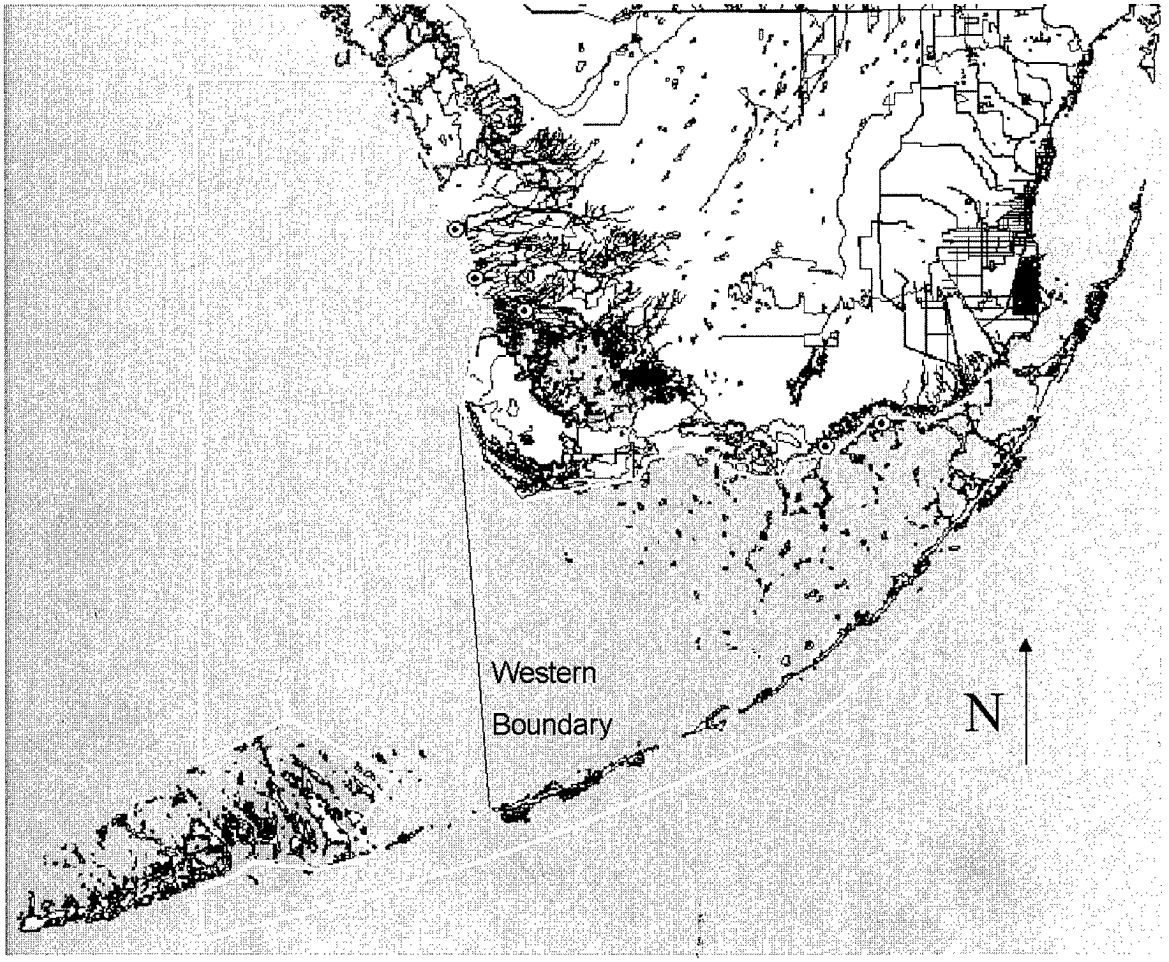

The contents of this report are not to be used for advertising, publication, or promotional purposes. Citation of trade names does not constitute an official endorsement or approval of the use of such commercial products.

The findings of this report are not to be construed as an official Department of the Army position, unless so designated by other authorized documents.

PRINTED ON RECYCLED PAPER

ERDC/EL TR-00-10
September 2000

Water Quality Model of Florida Bay

by Carl F. Cerco, Barry W. Bunch, Allen M. Teeter, Mark S. Dortch

Environmental Laboratory
U.S. Army Engineer Research and Development Center
3909 Halls Ferry Road
Vicksburg, MS 39180-6199

Final report

Prepared for U.S. Army Engineer District, Jacksonville
Jacksonville, FL

Engineer Research and Development Center Cataloging-in-Publication Data

Water quality model of Florida Bay / by Carl F. Cerco ; prepared for U.S. Army Engineer District, Jacksonville.
275 p. : ill. ; 28 cm. – (ERDC/EL ; TR-00-10)
Includes bibliographic references.
1. Water quality – Florida – Florida Bay – Mathematical models. 2. Florida Bay – Mathematical models. 3. Marine plants – Florida – Florida Bay – Mathematical models. 4. Sediments (Geology) – Florida – Florida Bay – Mathematical models. 5. Florida Bay (Fla.) I. Cerco, Carl F. II. United States. Army. Corps of Engineers. Jacksonville District. III. Engineer Research and Development Center (U.S.) IV. Environmental Laboratory (U.S.) V. Series: ERDC/EL TR ; 00-10.
TA7 E8 no.ERDC/EL TR-00-10

Contents

List of Figures

Preface

A water quality model of Florida Bay was developed and applied during the period January 1998 and February 2000. This study was requested, funded, and managed by the U.S. Army Engineer District, Jacksonville (CESAJ). Mr. Michael L. Choate served as the CESAJ technical point of contact (POC).

Dr. Mark S. Dortch, Chief, Water Quality and Contaminant Modeling Branch (WQCMB), Environmental Processes and Effects Division (EPED), Environmental Laboratory (EL), U.S. Army Engineer Research and Development Center (ERDC), Waterways Experiment Station (WES), was the overall ERDC study manager and POC. The water quality model development and application was conducted by Dr. Carl F. Cerco, with assistance by Dr. Barry W. Bunch, both of the WQCMB, EL, under the direct supervision of Dr. Dortch and the general supervision of Dr. Richard E. Price, Chief, EPED. Mr. Allen M. Teeter of ERDC's Coastal and Hydraulics Laboratory (CHL) developed and verified the sediment resuspension model. Mr. Teeter works under the general supervision of Dr. Rob McAdory, Chief, Tidal Hydraulics Branch, CHL. This report was prepared primarily by Dr. Cerco, with Dr. Bunch and Mr. Teeter contributing Chapters 4 and 5, respectively. Dr. Dortch provided technical editorial comments and revisions.

The assistance provided by numerous scientists that have studied Florida Bay is gratefully acknowledged. Without their assistance and suggestions and the data they provided, this study would not have been possible.

At the time of publication of this report, Acting Director of CHL was Mr. Thomas W. Richardson, Acting Director of EL was Dr. John W. Keeley, and Director of ERDC was Dr. James R. Houston. Commander of ERDC was COL James S. Weller, EN.

This report should be cited as follows:

> Cerco, C. F., Bunch, B. W., Teeter, A. M., and Dortch, M. S. (2000). "Water Quality Model of Florida Bay," ERDC/EL TR-00-10, U.S. Army Engineer Research and Development Center, Vicksburg, MS.

1 Introduction

Florida Bay

Florida Bay is a shallow, triangular water body bordered on the north by the Florida mainland and on the southeast by the Florida Keys (Figure 1). At the northeast apex, Cross Key separates the bay from adjacent Barnes Sound. The western boundary of the bay is not well-defined but can be represented by a north-south line drawn from Cape Sable, on the mainland, to Marathon, in the Keys. The physical, geological, hydrographic, and ecological characteristics of the bay have been described by Fourqurean (1992) and Fourqurean and Roblee (1999). Summary characteristics of the bay, presented below, are drawn from these sources and from data developed during this study.

As defined above, Florida Bay has a surface area of 2730 km^2. Distance from the western boundary to the northeast apex is roughly 83 km. Width, at the western boundary, is 60 km. Mean depth is 2 m. The bay is divided by mud banks into a series of semi-enclosed basins or lakes. Circulation between the lakes is restricted to channels that cut the banks. As a result of the shallow depth and restricted circulation, tides in the system are rapidly damped. Maximum tide range at the western boundary exceeds 1 m, while astronomical tides are practically nonexistent in the northeast portion of the bay. Wind effects, however, can significantly alter water level throughout the system.

The climate in Florida Bay is subtropical. Mean air temperature varies from 20 °C in January to 28 °C in August. The bay receives roughly 1 m of rainfall annually with the majority coming in a distinct wet season (April - November). Annual evaporation is the same order of magnitude as rainfall. Interannual and seasonal variability in rainfall and evaporation create periods in which net rainfall into the bay is positive (rainfall > evaporation) or negative (evaporation > rainfall). An excess of evaporation over rainfall, coupled with restricted circulation, leads to areas of hypersalinity with salinity exceeding 50 ppt in some basins.

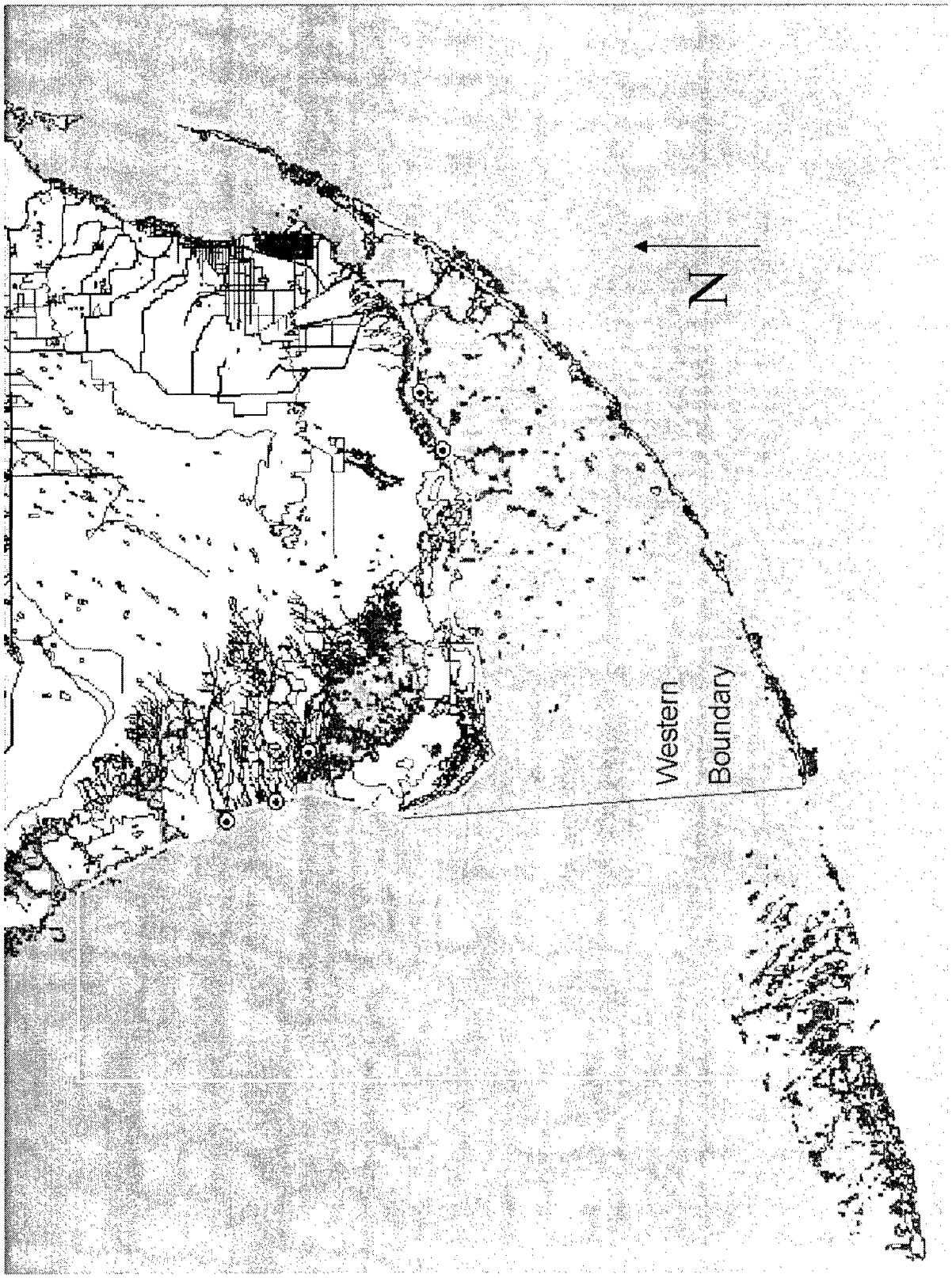

Figure 1. Florida Bay

The waters of Florida Bay are characterized by low nutrient and chlorophyll concentrations and high water clarity. The system is distinguished by a dense, highly developed seagrass community that covers 95% of the bottom. Recent occurrences of algal blooms, periods of elevated turbidity, and seagrass die-offs have led to enhanced concern for the viability of the bay.

Environmental Issues

Evidence of environmental deterioration in Florida Bay led to the formation of the Florida Bay Science Program. The goals of the Florida Bay Science Program are to understand the Florida Bay ecosystem and guide its restoration. The program is directed by a Program Management Committee composed of members from various state and federal water resource agencies.

In addition to seagrass die-off, one of the primary issues in Florida Bay is nutrient input, especially from freshwater sources. Nutrient-related questions posed by the Program Management Committee include:

- To what extent will increased freshwater flows into Florida Bay increase loadings of phosphorus and nitrogen?
- What are implications for nutrient inputs to Florida Bay of shifting some of the distribution of freshwater flows from Shark River Slough to Taylor Slough?
- What is the relationship of regional hydrologic restoration to the quality of water reaching Florida Bay?
- What is the relative importance of exogenous and endogenous nutrient sources in Florida Bay and how is this likely to change with restoration?
- To what extent are changes in nutrient loadings related to observed changes in seagrass and water column productivity?
- What is the spatial pattern in nutrient limitation across Florida Bay and the causes and consequences of the differences?
- What is the likelihood that increased freshwater flow into Florida Bay will adversely affect coral reefs?

A Florida Bay nutrient workshop was held in Key Largo, July 1-2, 1996, to exchange information and derive inferences about nutrient enrichment and how it might change as freshwater flows increase in association with hydrologic restoration of South Florida. A primary recommendation of the Science Oversight Panel convened for this workshop was that a numerical circulation/water quality model of Florida Bay should be developed to systematize data, pose hypotheses, and anticipate the effects of different water management scenarios. Specifically, the oversight panel recommended the model include:

- Coupled hydrodynamic-nutrient-phytoplankton-water quality variability;
- Suspended sediments and their influence on turbidity; and
- Seagrass populations and their influence on sediment resuspension, nutrient cycling, and geochemistry.

In response to the need for a Florida Bay water quality model, the U.S. Army Engineer District, Jacksonville, requested the U.S. Army Engineer Research and Development Center (ERDC) to assist with model planning. A workshop on design and specification for a Florida Bay water quality model was held in Key Largo, October 22-24, 1996, to facilitate the planning effort. A work plan (Dortch et al. 1997) was produced that addressed recommendations from the workshop and a Model Evaluation Group.

Objectives of the Present Study

The original work plan called for a four-year effort. Elements of the study included application of the Corps' CH3D-WES hydrodynamic model (Johnson et al. 1993) and the CE-QUAL-ICM water quality model (Cerco and Cole 1995) as well as development of new model components for the unique Florida Bay ecosystem. The need for rapid initial insights as well as resource constraints resulted in the present, two-year study. Major changes from the original work plan were employment of an existing hydrodynamic model, RMA-10, and limiting the development of new model components. The revised work plan included the following tasks:

1. **Data Acquisition.** Existing data will be acquired, reviewed, and built into model databases for both the hydrodynamic model (HM) and water quality model (WQM) applications.

2. **HM Application for WQM Calibration.** HM production runs will be made to develop circulation fields to drive the WQM application for 1996-1997. This task requires: development of input files; verification to the available salinity record for each production run; application of a recently developed projection procedure that forces local volume conservation; and assurance of compatibility of all HM results with the WQM. Results will be spatially integrated to provide flow fields consistent with the coarse-element WQM mesh.

3. **Linkage Setup and Testing.** Files must be developed that provide information to the WQM on the location of all computational cells with respect to each other and their geometric attributes, along with spatial correspondence to the HM mesh. Checks on volume and mass conservation will be conducted to ensure correct linkage. Additionally, salinity will be modeled during WQM application and compared with both the HM and observed salinity data to provide a final test of proper linkage.

4. **Resuspension Module Development.** Sediment resuspension will be added to the WQM. The resuspension formulation will be related to bottom shear stress caused by wave orbital velocity as estimated from wind speed and local depth.

5. **Physical Modifications.** The WQM will be modified to allow evaporation and rainfall and the associated change in computed concentrations.

6. **Seagrass Model Modifications.** The seagrass module in the WQM will be modified to represent the seagrasses of Florida Bay. Two species have been selected for simulation: *Thalassia testudinum* and *Halodule wrightii*. Presently, the model simulates a single dominant species in each model cell. Since *Thalassia* and *Halodule* can coincide or compete, modifications will be made to the model to allow competition.

7. **Loading and Boundary Concentration Estimates.** Mass loadings or boundary concentrations for nutrients and other WQM variables must be estimated for all possible entry points, including freshwater inflows, atmospheric loadings, septic tanks, stormwater runoff, groundwater, and the ocean boundaries.

8. **Initial WQM Application and Nutrient Budget Analysis.** The WQM will be calibrated for the period 1996-1997. Following calibration, nutrient budget and other analyses will be conducted to gain a better understanding of the relative importance of external nutrient loadings and internal nutrient cycling.

9. **HM Application for WQM Confirmation.** The HM will be used to develop circulation fields to drive a ten-year WQM confirmation. This will be accomplished by running conditions for each of three different years representing wet, dry, and average hydrology. The results of these runs will be spatially integrated and processed for the WQM mesh. Hydrodynamics from these years will be repeated and ordered to resemble the actual hydrology for the period 1988-1997.

10. **WQM Confirmation/Evaluation.** A long-term WQM confirmation will be performed for the period 1988-1997. The confirmation will evaluate the ability of the model to capture changes in seagrass coverage as well as long-term water quality conditions.

11. **Documentation Report.** The results of the two-year effort will be documented in a technical report. The report will include input data, description of the model, results of model calibration, nutrient budget analyses, model confirmation, and sensitivity analyses.

The present report comprises the documentation called for in item 11 above.

2 The Databases

The FIU Database

The primary database for calibration of the water quality model was provided in April 1998 by Dr. Joseph Boyer of Florida International University (FIU), Miami, Florida. The database provided extensive coverage including portions of the Keys, the western shelf, Biscayne Bay, and Whitewater Bay. The complete data set was pared down to 124 stations within the model domain (Figure 2). The database contained an extensive list of

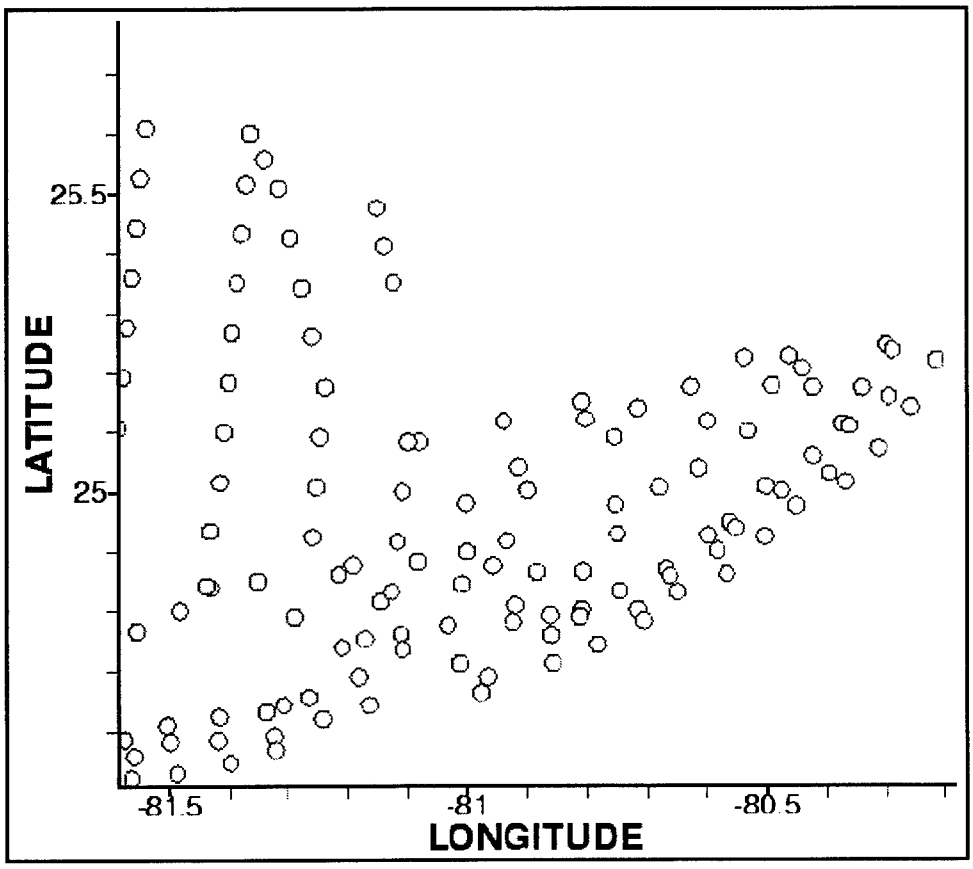

Figure 2. FIU sample stations within the model domain

parameters that was reduced to a set comparable with the model state variables (Table 1).

Table 1
Modeled Substances in FIU Database

Salinity	Temperature	Chlorophyll 'a'
Ammonium	Nitrate+nitrite	Organic nitrogen
Total nitrogen	Soluble reactive phosphorus	Total phosphorus
Total organic carbon	Dissolved oxygen	

Observations in Florida Bay were collected monthly from 1991 to 1997. Observations in the vicinity of the Keys and on the southwest shelf commenced in mid-1995 and were collected monthly thereafter. In the vicinity of the Keys, all observations were collected at surface, middepth, and bottom of the water column. Elsewhere, only salinity, temperature, and dissolved oxygen were observed at surface, middepth, and bottom. One sample at each station characterized the remaining substances.

Supplementary Observations

Additional observations in the water column were provided in October 1999 by Dr. James Fourqurean of FIU. Observations were collected at roughly monthly intervals at 16 stations (Figure 3) from June 1989 through March 1991. Substances sampled were the same as those listed in Table 1.

Light attenuation observations were provided for 23 stations (Figure 4) in the model domain by Dr. Boyer. Observations were collected on ten occasions from November 1994 to December 1995.

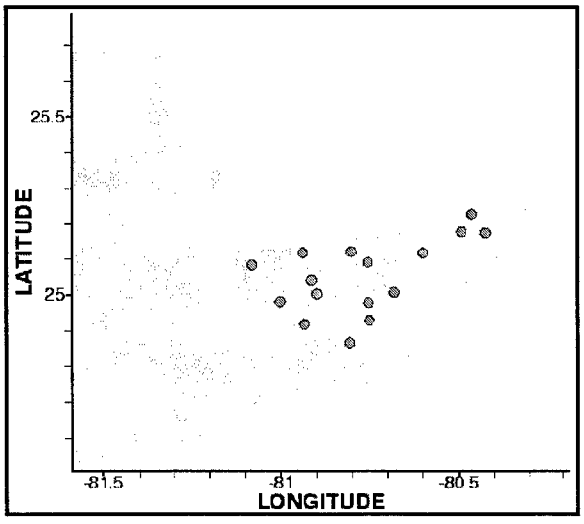

Figure 3. Water column observations 1989-1991

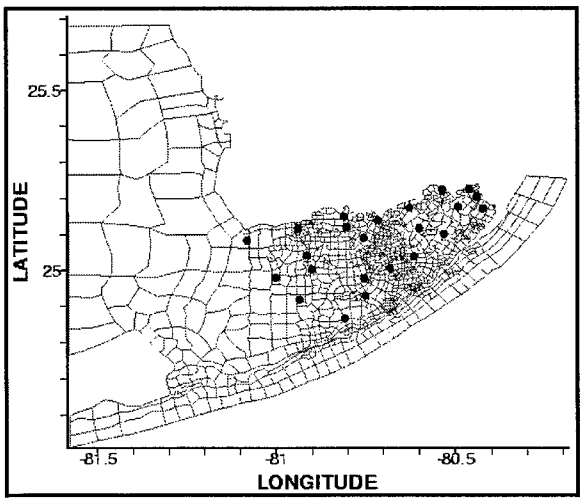

Figure 4. Light attenuation observations 1994-1995

Seagrass Observations

Seagrass observations were provided in July 1999 by Drs. Fourqurean, Michael Durako of University of North Carolina, Wilmington, and Lee Hefty, Miami-Dade Department of Environmental Resources Management (DERM), Miami, Florida. The database consisted of extensive observations collected at locations in Florida Bay (Figure 5), around the Keys, and on the western shelf (Figure 6). The primary observations employed in the model were SAV abundance, quantified as Braun-Blanquet score, collected from 1996 through 1998.

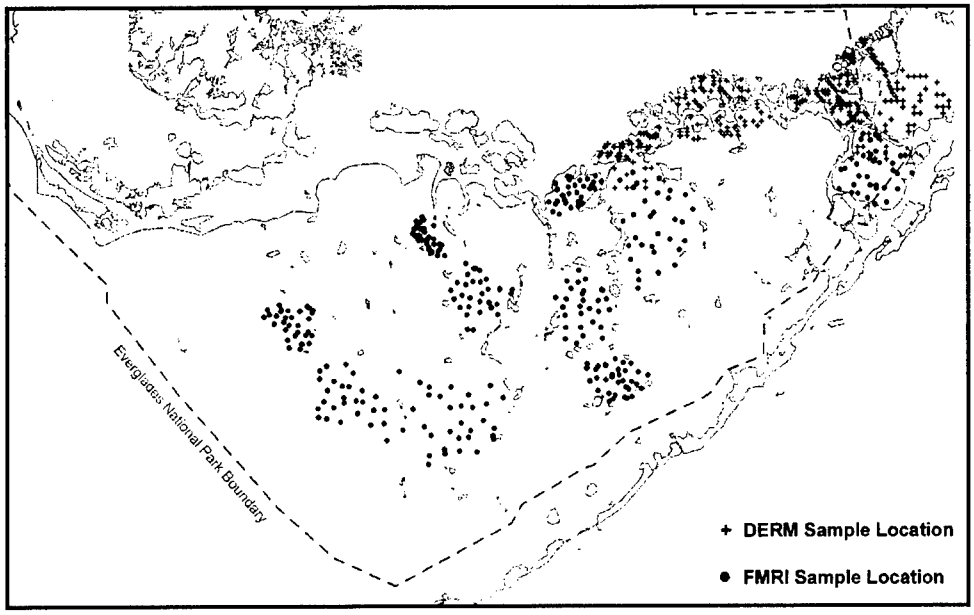

Figure 5. SAV observations in Florida Bay, after Fourqurean et al. (in press)

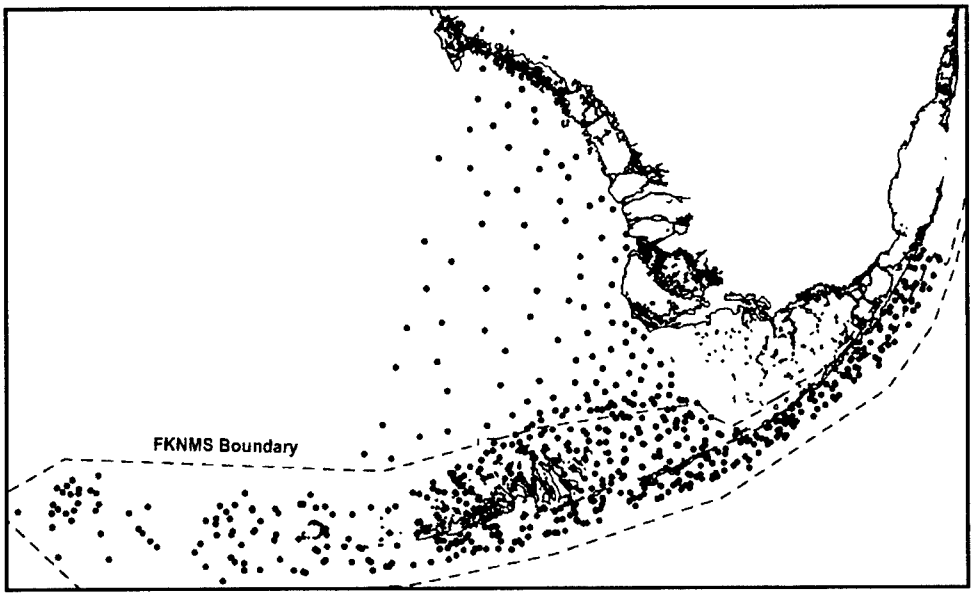

Figure 6. SAV observations in the Keys and Western Shelf, after Fourqurean et al. (in press)

Sediment-Water Exchange Measurements

Sediment-water oxygen and nutrient exchange measures were provided in July 1999 by Dr. Paul Carlson, Florida Marine Research Institute (FMRI), St. Petersburg, Florida, and in September 1999 by Dr. David Rudnick, South Florida Water Management District, West Palm Beach. Exchange was measured in chambers which enclosed water, SAV, benthos, and the sediment-water interface. Exchanges were corrected for activity in the water column before they were provided for this study. The Carlson database consisted of exchanges measured in the dark at six locations (Figure 7) on five occasions between 1997 and 1999. Observations were provided for ammonium, dissolved organic nitrogen, total nitrogen, soluble reactive phosphorus, dissolved organic phosphorus, and total phosphorus. The Rudnick database consisted of exchanges measured in the light and dark at four locations (Figure 7) on nine occasions between 1996 and 1998. Observations included the substances measured by Carlson as well as nitrate, dissolved organic carbon, and dissolved oxygen.

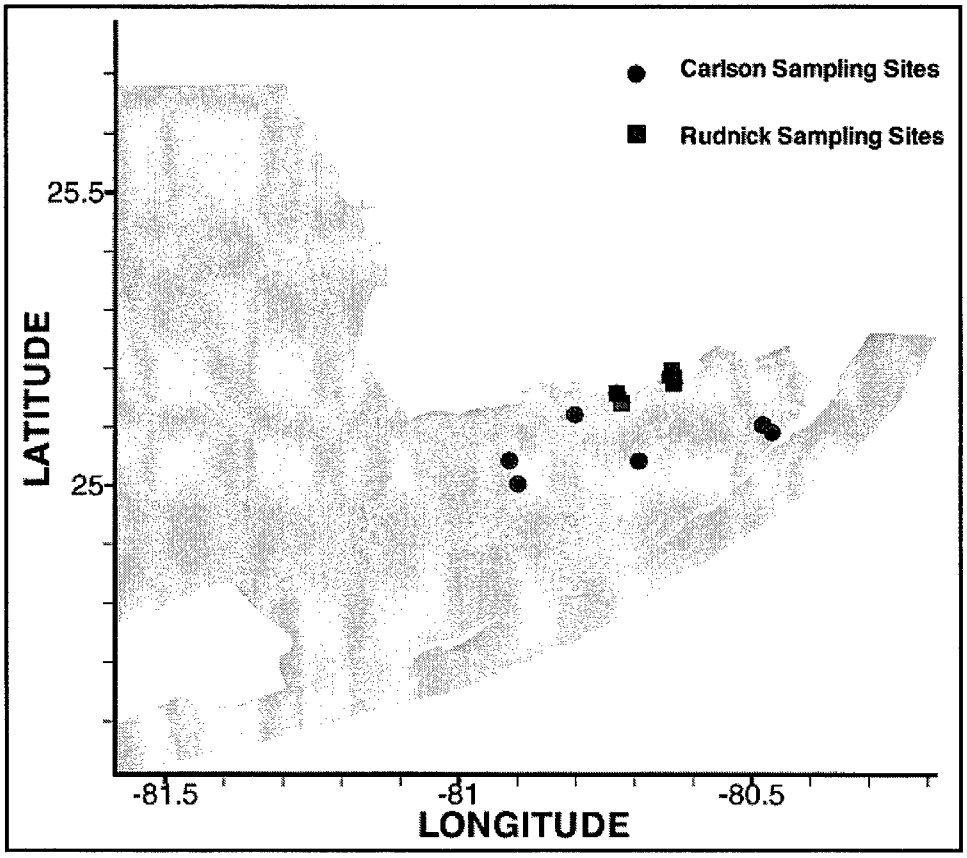

Figure 7. Location of sediment-water exchange measurements

Sediment Properties

Observations of sediment properties were downloaded from the Atlantic Oceanographic and Meteorological Laboratory web site (http://www.aoml.noaa.gov/ocd/sferpm) in July 1999. Observations included sediment total phosphorus, bulk nitrogen, bulk phosphorus, available phosphate (dissolved + sorbed), and chlorophyll. Observations were obtained as color maps and were digitized to the level of accuracy allowed by the spatial resolution and color interval.

In Situ Suspended Solids

Suspended solids observations, collected in situ, were provided in September 1999, by Dr. E. J. Phlips of the University of Florida, Gainesville. Observations were collected at 17 stations (Figure 8) at intervals of one to two months between January 1994 and July 1996. These observations were supplemented with summary information, including light attenuation and its relation to solids, presented by Phlips, Lynch, and Badylak (1995).

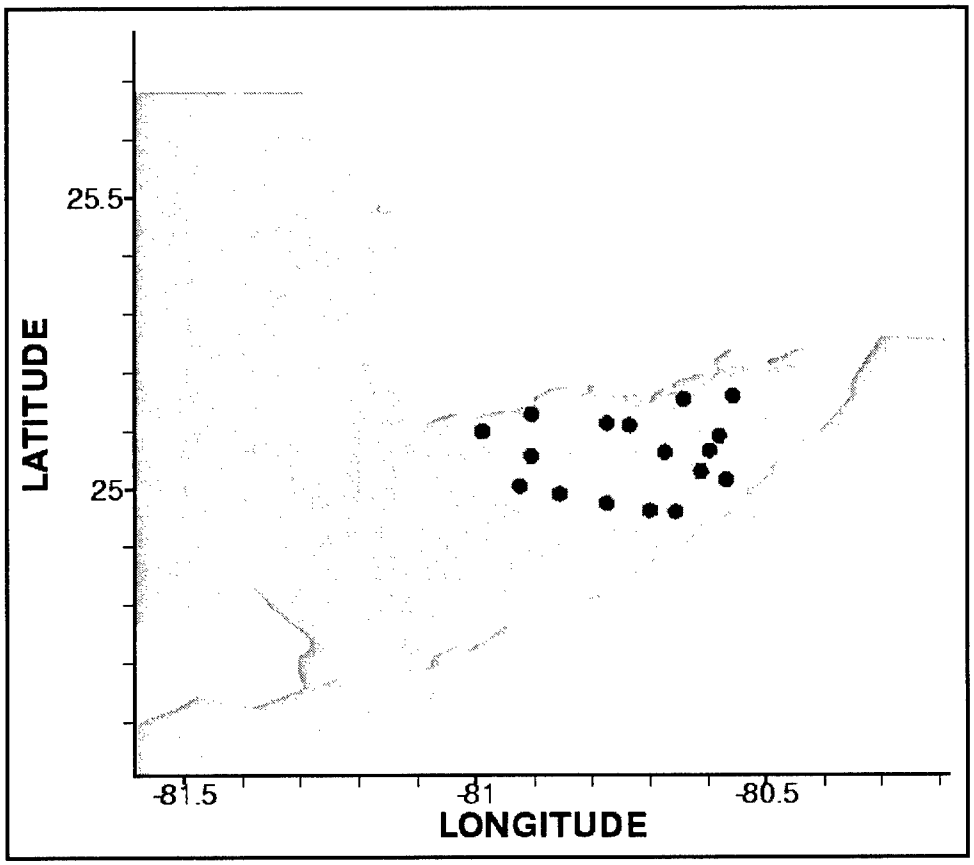

Figure 8. Location of in situ suspended solids observations

Remotely Sensed Suspended Solids

Sea-surface reflectance was obtained from a CD-ROM entitled "Florida Bay Imagery and Information" dated September 1998 and distributed by NOAA Coastal Services Center. Reflectance, determined by Advanced Very High Resolution Radiometer, was available on a 1-km grid on a monthly basis from 1985 through 1998. Data for each month represented the mean of all overflights during that month. Reflectance on the 1-km grid was spatially averaged into values at the center of each cell on the model grid. Reflectance was converted to suspended solids concentration using a formula provided by Richard Stumpf of the NOAA National Ocean Service, Silver Spring Maryland, in January 1999.

$$TSS = 4 \cdot (R - 1) \tag{1}$$

in which

TSS = total suspended solids (gm m^{-3})

R = reflectance (%)

Meteorological Data

Meteorological observations including temperature, relative humidity, cloud cover, and wind speed were obtained for Key West, Florida. These were employed in computations of solar radiation and water-atmosphere heat and gas exchange. A second, alternate representation of the wind field was employed for sediment resuspension computations. Winds for these computations were extracted from the global data set produced by the NCEP/NCAR Reanalysis Project (www.scd.ucar.edu/dss/pub/reanalysis). A grid transformation was employed to interpolate winds in the database (2-degree grid) down to 0.2-degree resolution for Florida Bay.

3 Runoff, Loading, and Boundary Conditions

Introduction

Runoff from the mainland and Keys and loads from the mainland, Keys, and atmosphere were computed by William W. Walker of Walker Enterprises, Concord, MA. Details and complete results of the computations may be obtained at http://www2.shore.net/~wwwalker/flabay/index.htm. A duplicate copy of the web page has been archived at the U.S. Army Engineer Research and Development Center. A summary of methods and results is presented below.

Runoff from the Mainland

Monthly runoff for the period 1987-1997 was computed for eight South Florida drainage basins (Figure 9). Of these, six discharge into the model domain: West, Broad, Shark Slough, Cape Sable, Taylor Slough, and Coastal. Runoff for each basin was computed by a water balance based on gaged inflow, evaporation and rainfall, and change in elevation within the basins.

Seasonal runoff

For use in the model, monthly runoff was averaged into runoff for the wet season and dry season of each year. Wet season and dry season were determined by examination of a ten-year rainfall record, 1951-1960, at Key West (Zieman 1982). The record indicated a distinct pattern in rainfall; the dry months (December-April) averaged 43 mm/month while the wet months (May-November) averaged 108 mm/month (Table 2). Examination of total rainfall from a contemporary record also clearly shows the dichotomy in seasons (Figure 10). Total rainfall during the dry season averages 25 cm compared to 82 cm in the wet season.

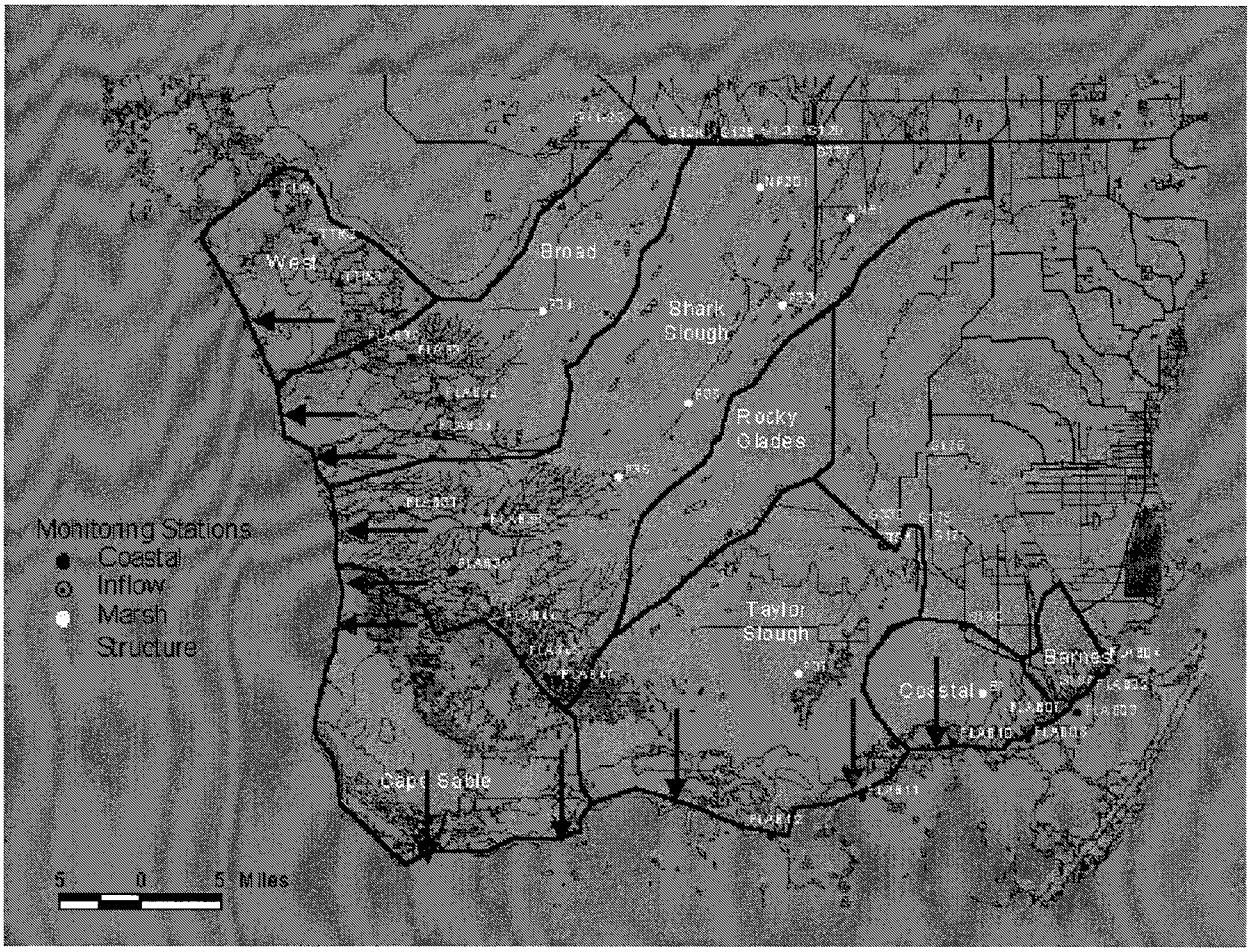

Figure 9. South Florida Drainage Basins. Arrows show locations where runoff was input to the model

Table 2
Monthly Rainfall at Key West (after Zieman 1982)

Month	Rainfall (mm)
January	44.0
February	54.8
March	36.9
April	40.7
May	85.6
June	93.5
July	91.8
August	101.0
September	165.8
October	115.9
November	99.8
December	40.6

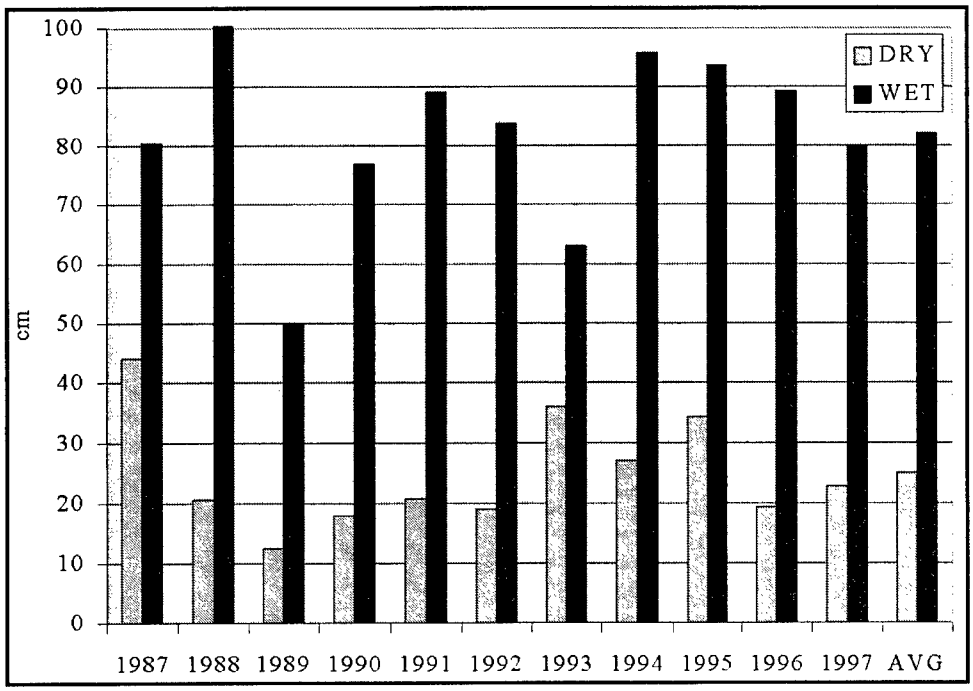

Figure 10. Wet and dry season rainfall at Key West, 1987-1997

For the period of record (1987-1997), Shark Slough was by far the largest contributor of runoff to the model domain while the Taylor Slough basin was the largest source to Florida Bay (Table 3, Figure 11). Basins along the western coast contributed the majority of runoff to the system: 84% in the dry season and 69% in the wet season.

Table 3
Mean Flows 1987-1997

Basin	Season	Flow, $m^3 s^{-1}$	Summary	Flow, $m^3 s^{-1}$
West	dry	0.92		
	wet	2.34		
Broad	dry	8.93		
	wet	11.83		
Shark Slough	dry	29.41	West Coast	39.26
	wet	37.37		51.54
Cape Sable	dry	1.55		
	wet	3.66		
Taylor Slough	dry	3.2		
	wet	11.93		
Coastal	dry	2.7		
	wet	7.5		
Keys (bay side)	dry	0.38	Florida Bay	7.83
	wet	0.68		23.77

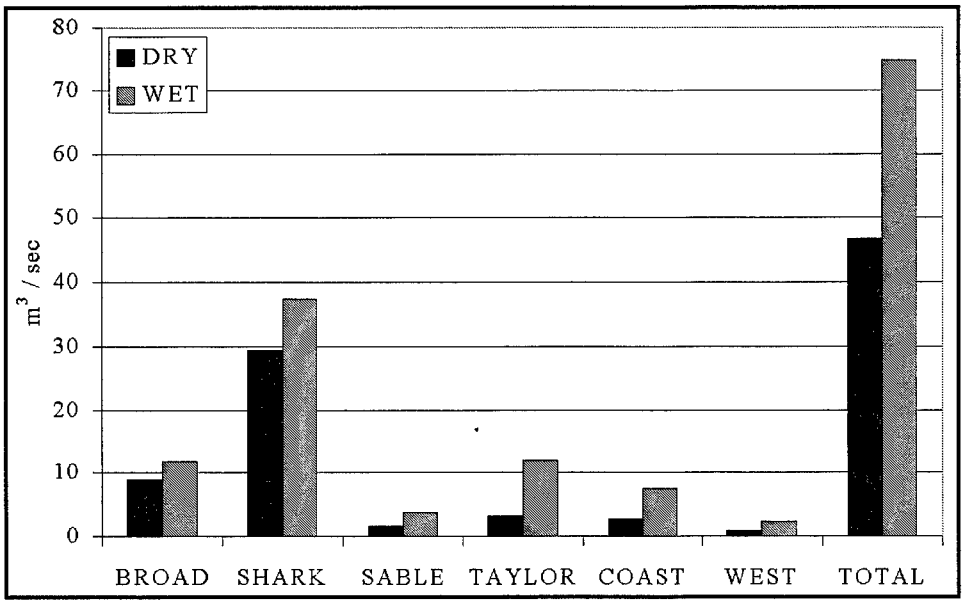

Figure 11. Mean runoff from the mainland, 1987-1997

A ten-year period, 1988-1997, was selected for model application. The period encompassed a wide range of runoff conditions (Table 4, Figure 12). The year 1995 had the highest runoff in the period of record. The years 1989 and 1990 exhibited far less than average runoff. Inspection of the record indicates that recurrent "wet" and "dry" seasons exist only on a long-term average basis. In individual years, runoff in the nominal dry season may exceed runoff in the wet season. Also, dry season runoff in wet years may exceed wet-season runoff in dry years.

Table 4
Total Runoff 1988-1997

Year	Dry, $m^3 s^{-1}$	Wet, $m^3 s^{-1}$
1988	27.8	88.9
1989	13.6	12.2
1990	2.2	28.5
1991	11.5	98.1
1992	39.3	83.4
1993	67.4	51.1
1994	26.3	67.1
1995	185	189.3
1996	91.1	77
1997	31.1	103

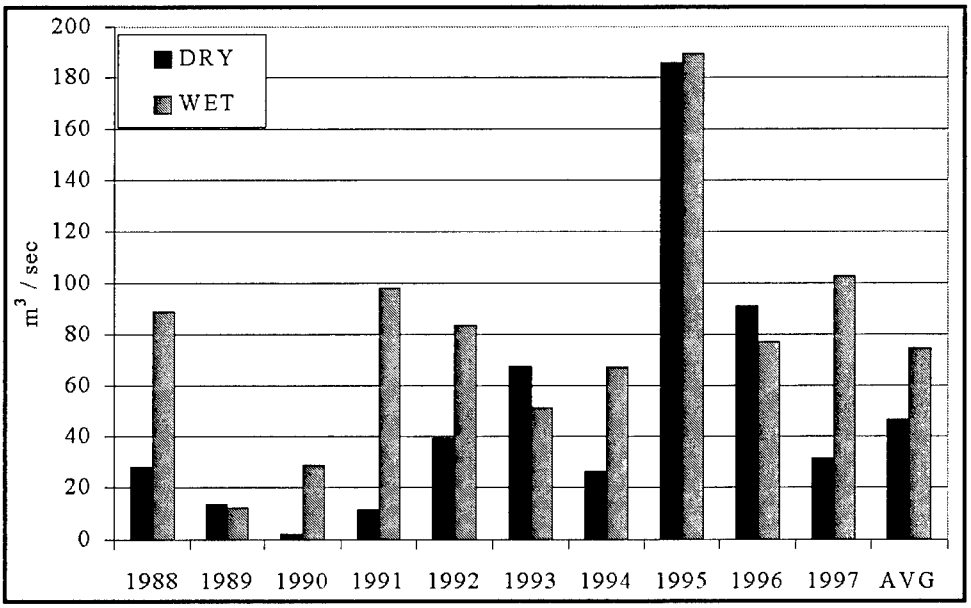

Figure 12. Seasonal runoff, 1988-1997

Location of Inflows

Locations of inflows from the mainland were not provided by the water-balance method. Runoff from the mainland may be diffuse or may follow defined channels depending on local topography and runoff volume. Topographic maps and personal experience provided guidance in locating eleven discrete locations for loading runoff into the model (Figure 9). For some basins, runoff was split between several defined channels (Table 5).

Table 5
Routing Basins to Inflow Locations

Location	Basins
Trout Creek	All of Coastal basin
Taylor River	75% of Taylor Slough basin
Alligator Creek	25% of Taylor Slough basin
Buttonwood Canal	33% of Cape Sable basin
East Cape Canal	33% of Cape Sable basin
Little Shark River	33% of Cape Sable basin + 25% of Shark Slough basin
Shark River	50% of Shark Slough basin
Harney River	25% of Shark Slough basin
Broad River	50% of Broad basin
Rogers River	50% of Broad basin
Lostmans River	All of West basin

Flow from the Florida Keys

Flow from the Florida Keys was considered from two sources: runoff and wastewater. Flow was computed for three divisions: upper, middle, and lower Keys. The lower Keys are outside the model domain and are not considered here.

Runoff was determined based on rainfall records and runoff coefficients. Runoff was arbitrarily split "fifty-fifty" with half going into Florida Bay and half into the waters on the other side of the Keys.

Flow from wastewater was computed based on reports from treatment plants and estimated numbers of septic tanks, cesspits, and live-aboard boats. All flows from treatment plants, 20% of flows from boats, and 50% of remaining flows were routed to the waters outside the Keys. The alternate fractions of the flows were routed to the bay side of the Keys.

Flows from the Keys were trivial compared to other flows in the system (Table 3) and were omitted from the model.

Nutrient Loads from the Mainland

Loads associated with runoff from the mainland were computed for numerous substances (Table 6). Of these, routine observations were available for calcium, salinity, and the nitrogen and phosphorus components. Concentrations were adapted or assumed for the other substances. Not all of the loads were used in the model. Calcium, silica, and alkalinity were not considered in this phase of the study. Specification of concentration boundary conditions rather than loading was utilized for organic carbon, salinity, total suspended solids, and chlorophyll. Substances input as loads were total nitrogen and total phosphorus, divided into fractions corresponding to model state variables.

Table 6
Loads Computed for These Substances

Total Phosphorus	Ortho Phosphorus
Total Nitrogen	Ammonium
Nitrate + Nitrite	Total Organic Nitrogen
Total Organic Carbon	Salinity
Total Suspended Solids	Dissolved Calcium
Dissolved Silica	Alkalinity
Chlorophyll 'a'	

Loads were computed for three locations in each basin: at the structural inflows, at the most downstream marsh station, and at the coastal outflow. From these, loads at the most downstream marsh station were selected as most relevant for model usage. Loads at the inflows were obviously inappropriate since they did not account for transformations in the marsh. Computation of loads at the coastal outflows was confounded by oscillating currents and mixing with bay water. Consequently, loads at the downstream marsh stations were used. Usage of these loads, however, does not account for transformations in the mangrove area that divides the mainland from the bay.

Loads were computed on a monthly basis as the product of flow and concentration. Observed concentrations were employed when available. Gaps in the record were filled by interpolation or substitution of appropriate values. Observed phosphorus and nitrogen fractions did not exactly correspond to model state variables. Model variables were derived from observations as follows.

Total phosphate

$$Tot\ PO4 = Ortho\ P + 0.1 \cdot (Total\ P - Ortho\ P) \quad (2)$$

The factor 0.1 was recommended by Walker to derive dissolved inorganic phosphorus from ortho and total phosphorus.

Dissolved organic phosphorus

$$DOP = FDOP \cdot (Total\ P - Tot\ PO4) \quad (3)$$

FDOP was assigned the value 0.8 based on observations collected in the Taylor Slough basin (Sutula 1999).

Particulate organic phosphorus

$$POP = Total\ P - Tot\ PO4 - DOP \quad (4)$$

All particulate organic phosphorus was assumed to be refractory based on experience with other systems.

Organic nitrogen

Dissolved organic nitrogen was assigned 90% of the reported total organic nitrogen, based on observations by Sutula (1999). The remaining, particulate, fraction was assumed to be entirely refractory, based on experience with other systems.

Summary

Average concentrations of modeled nitrogen and phosphorus fractions are reported in Table 7. In terms of total phosphorus, Shark Slough stands out as having roughly double the concentration of the remaining basins. Shark Slough is also distinctive in that roughly half the phosphorus is in dissolved organic form. For the other basins, phosphate comprises the majority of the total.

Table 7
Mean Nutrient Concentrations (g m^{-3}) in Runoff

Basin	Total P	Total PO4	DOP	RPOP	Total N	NO3	NH4	DON	RPON
Broad	0.00599	0.00397	0.00161	0.00040	1.05	0.02	0.02	0.92	0.10
Shark	0.01319	0.00587	0.00585	0.00146	1.55	0.08	0.05	1.28	0.14
Sable	0.00477	0.00354	0.00098	0.00024	0.83	0.04	0.02	0.69	0.08
Taylor	0.00507	0.00373	0.00108	0.00027	0.89	0.05	0.06	0.70	0.08
Coast	0.00555	0.00382	0.00138	0.00034	1.26	0.06	0.03	1.05	0.12
West	0.00583	0.00384	0.00160	0.00040	0.99	0.01	0.02	0.86	0.10
Keys	0.20883	0.13901	0.05586	0.01396	0.80	0.51	0.03	0.24	0.03

Total nitrogen concentration varies by a factor of two among the basins. As with phosphorus, Shark Slough exhibits the highest concentration but the distinction between this and the other basins is not so clear. One trend that is clear across all basins is that dissolved organic nitrogen is the predominant fraction (over 80%) followed by particulate organic nitrogen (roughly 10 %). Inorganic forms comprise only a small fraction of the total.

Long-term mean loadings from individual basins (Figures 13, 14; Table 8) reflect long-term mean flows. Shark Slough has the greatest runoff volume and the largest phosphorus and nitrogen loads. Loadings are higher in the wet season with one exception; mean phosphorus load from Shark Slough in the dry season exceeds mean load in the wet season.

Table 8
Mean Loads (kg d^{-1}) by Basin

	Phosphorus		Nitrogen	
Basin	Dry	Wet	Dry	Wet
Broad	4.6	5.2	792.5	1066.5
Shark	30.5	27.1	4270.8	4315.7
Sable	0.6	1.3	115.9	256.9
Taylor	1.3	4.6	248.9	832.7
West	0.5	1.0	75.5	202.2
Coast	1.2	3.2	314.0	663.5
Keys (bay side)	54.9	60.5	237.7	258.1

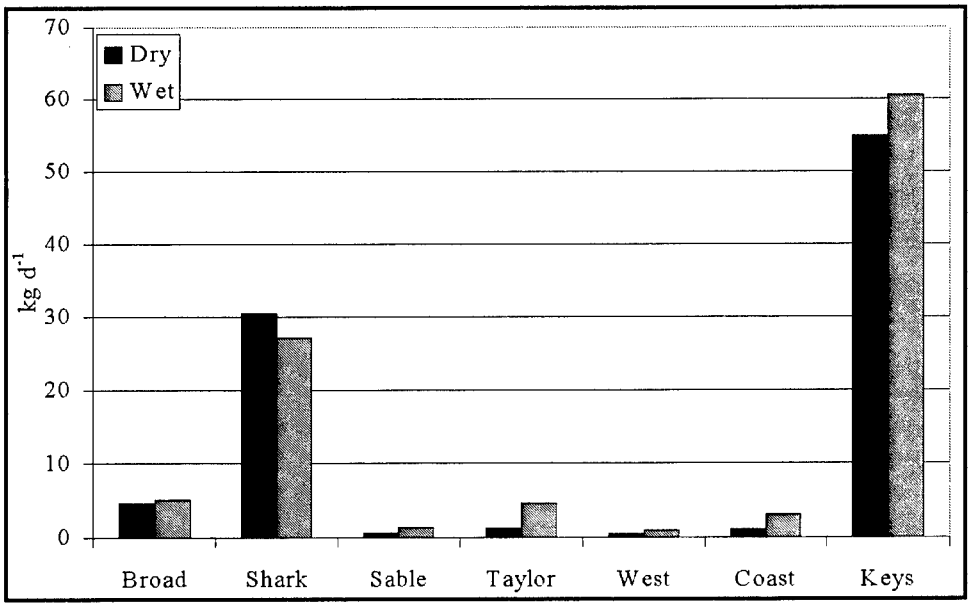

Figure 13. Mean phosphorus loading from mainland and Keys, 1988-1997

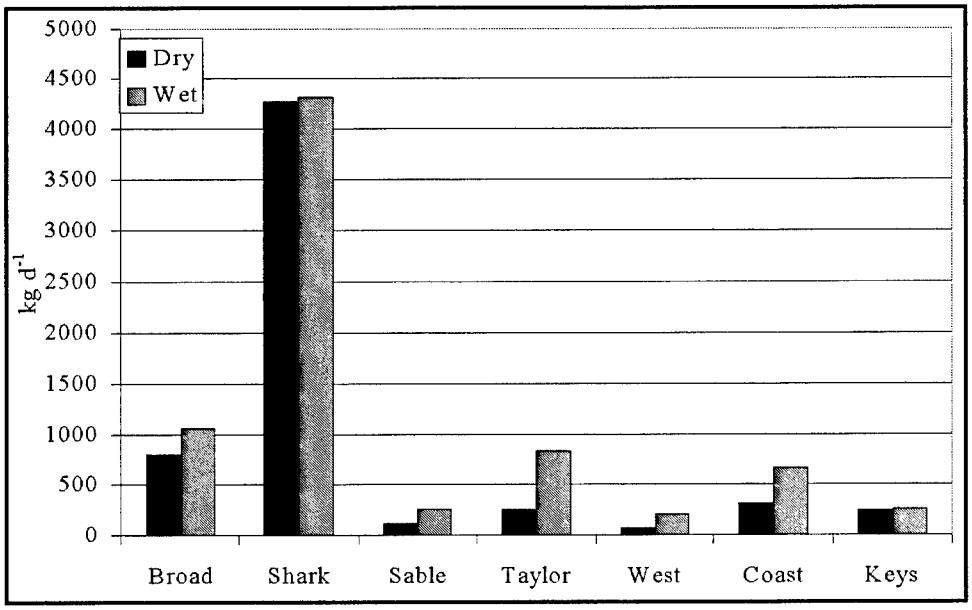

Figure 14. Mean nitrogen loading from mainland and Keys, 1988-1997

As with long-term mean loads, annual total loads (Figures 15, 16; Table 9) reflect total flows although one-to-one correspondence is absent. For example, 1991 was third in rank of wet-season flow but first in rank of wet-season phosphorus load. Although the wet season of 1995 exceeded the dry season in runoff volume, the dry season exceeded the wet season in nitrogen and phosphorus loading.

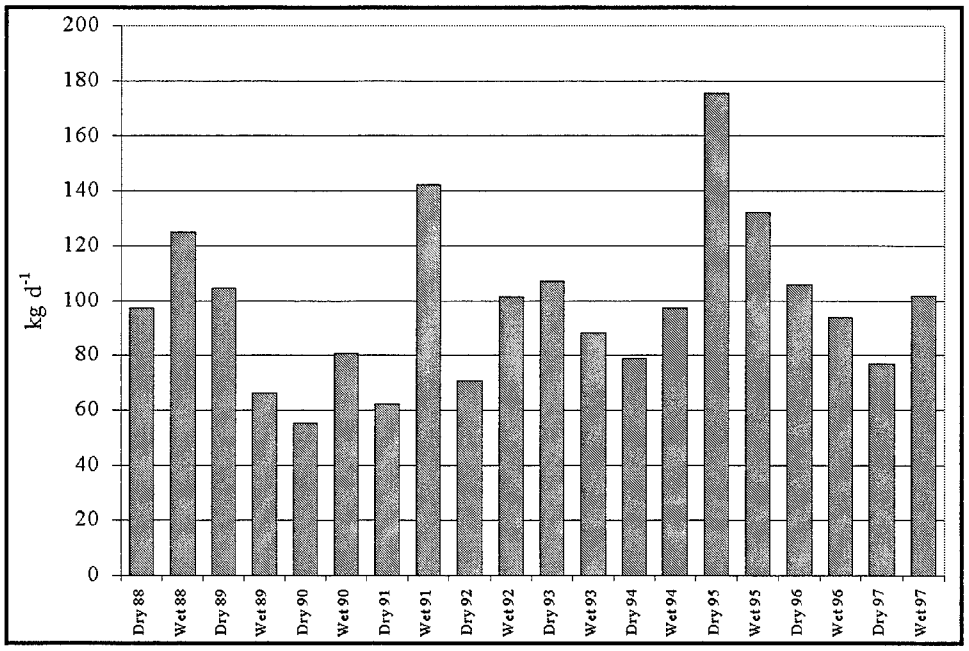

Figure 15. Seasonal phosphorus loads from mainland and Keys, 1988-1997

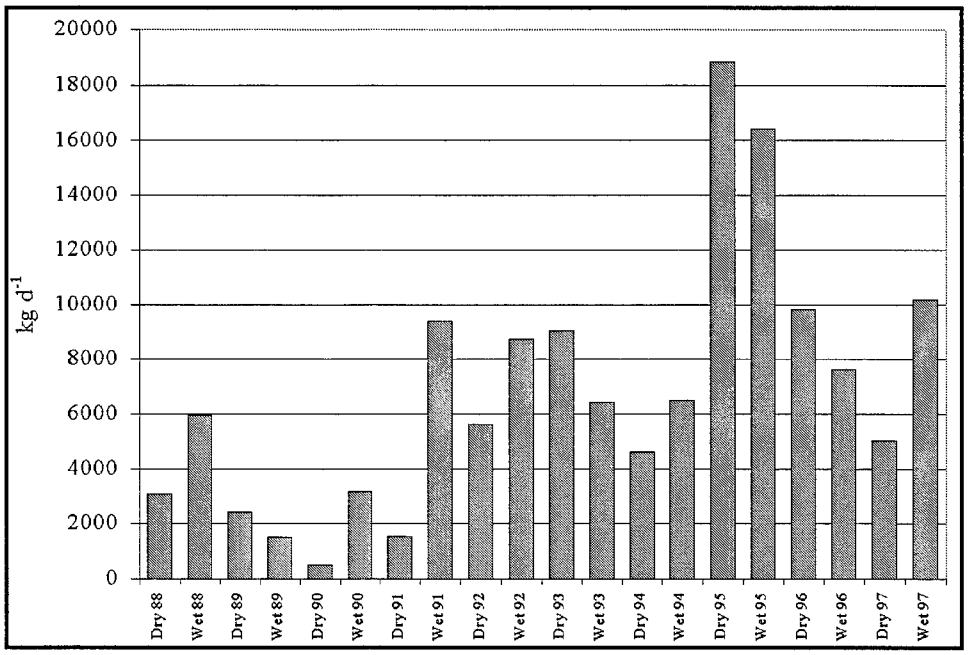

Figure 16. Seasonal nitrogen loads from mainland and Keys, 1988-1997

Table 9
Total Terrestrial Nutrient Loads (kg d^{-1}) 1988-1997

	Phosphorus	Nitrogen
Dry 88	97.2	3084.4
Wet 88	125.0	5973.2
Dry 89	104.5	2424.7
Wet 89	66.5	1501.4
Dry 90	55.3	498.1
Wet 90	80.7	3183.6
Dry 91	62.4	1545.6
Wet 91	142.2	9397.1
Dry 92	70.7	5619.0
Wet 92	101.3	8747.4
Dry 93	107.2	9051.0
Wet 93	88.2	6447.1
Dry 94	79.0	4617.6
Wet 94	97.2	6524.1
Dry 95	175.5	18833.8
Wet 95	132.0	16389.2
Dry 96	105.8	9830.1
Wet 96	94.0	7637.2
Dry 97	77.0	5047.8
Wet 97	101.9	10156.5

Location and frequency

Loads from runoff were input to the model at the same locations as corresponding flows (Figure 9). Although the summaries presented here are on a seasonal basis, loads were input to the model on a monthly schedule based on monthly runoff volume.

Loads from the Keys

Runoff-associated loads were generated as the product of runoff volume, an assumed runoff concentration, and an attenuation factor. The attenuation factor accounted for losses in transport between the load origin and the receiving water. As with volume, runoff-induced loads were calculated for three regions of the Keys and split "fifty-fifty" between Florida Bay and waters to the other side of the Keys. Loads to the lower Keys were outside the model domain and not considered.

Loads from wastewater were calculated based on flow volume and an assumed concentration. Loads discharged to groundwater were attenuated to account for losses in the aquifer. After the loads were initially estimated, phosphorus loads were revised downward to agree with previous estimates (Kruczynski 1998). Loads were routed to the bay and outside the Keys in accordance with the factors used to route flows.

Location

Loads from the Keys were distributed in eight locations on the bay side and eight locations on the outside of the Keys. Loads to the outside are included in the model but excluded from summaries of loads to Florida Bay.

Summary

Total phosphorus concentration in runoff from the Keys dwarfs total phosphorus in runoff from the mainland (Table 7). Presumably the excess is attributable to differences in land use and in attenuation between the Keys and the marsh basins. The volume of runoff is small, however (Table 3). The vast majority of phosphorus load (80 to 90%) from the Keys originates in wastewater. As a consequence of wastewater loads, phosphorus loads from the Keys to Florida Bay exceed all other terrestrial sources (Table 8).

Nitrogen concentration in runoff from the Keys is characteristic of concentrations in runoff from the mainland (Table 7). As with phosphorus, the majority of nitrogen load (80 to 90%) originates in wastewater, not runoff. Total nitrogen loading from the Keys to Florida Bay is comparable to several of the smaller mainland basins (Table 8).

Atmospheric Loads

Atmospheric loads were taken as annual mean values measured at Bahia Honda May 1978 - April 1979. These loads were 17 mg m^{-2} yr^{-1} total phosphorus and 320 mg m^{-2} yr^{-1} total nitrogen. For use in the model, atmospheric phosphorus loads were split evenly into dissolved inorganic and dissolved organic fractions. Atmospheric nitrogen loads were split 25% into ammonium, 50% into nitrate, and 25% into dissolved organic nitrogen. These splits were based on guidance from other systems.

Atmospheric loads, as kg d^{-1}, were obtained for each model cell as the product of areal load and cell surface area. Total loading to the model can be obtained from the total grid surface area, 8.04×10^9 m^2. Total atmospheric loads are 375 kg P d^{-1} and 7049 kg N d^{-1}.

Load Summary

A summary of long-term mean loads to the western shelf (model domain to the west of the Florida Bay boundary) and to Florida Bay indicates atmospheric loads are the dominant source (Table 10). Atmospheric loads comprise roughly 80% of the phosphorus loads to the western shelf and two-thirds the total loading to Florida Bay. Phosphorus loads from the Keys comprise most of the remaining load to Florida Bay. Phosphorus in runoff to Florida Bay is insignificant by comparison. Atmospheric nitrogen loads are more than a third of the total loading to the shelf and two-thirds of the loading to Florida Bay. The Keys are the least source of nitrogen directly to the bay.

Table 10
Load Summary

Source	Season	Phosphorus, kg d^{-1}	Nitrogen, kg d^{-1}
Runoff to western shelf	dry	35.6	5139
	wet	33.3	5584
Atmosphere to western shelf		177	3331
Runoff to Florida Bay	dry	3.0	679
	wet	9.1	1753
Keys to Florida Bay	dry	54.9	238
	wet	60.5	258
Atmosphere to Florida Bay		127	2393

Boundary Conditions

Concentration boundary conditions for all modeled substances were specified along the southern and western extent of the grid. Cells along these boundaries were divided into four regions: Upper Western Shelf, Lower Western Shelf, Upper Keys, and Lower Keys. Boundary conditions for each of these regions were derived on a quarterly basis from observations in the FIU database. These boundary conditions are summarized in Table 11.

Table 11
Open-Boundary Conditions

Substance	Western Boundary 1996	Southern Boundary 1996	Western Boundary 1997	Southern Boundary 1997
Salt (ppt)	34.1 - 36.6	35.3 - 36.1	34.0 - 36.0	35.9 - 36.6
Solids ($g\ m^{-3}$)	0.8 - 5.5	0.00 - 0.32	1.13 - 5.5	0.07 - 0.71
Chlorophyll ($mg\ m^{-3}$)	0.60 - 1.61	0.235 - 0.495	0.76 - 1.61	0.018 - 0.495
Total Organic Carbon ($g\ m^{-3}$)	1.83 - 4.13	1.56 - 2.27	2.46 - 4.16	1.85 - 3.03
Ammonium ($g\ m^{-3}$)	0.0039 - 0.0088	0.0031 - 0.0057	0.0031 - 0.014	0.0025 - 0.0048
Nitrate ($g\ m^{-3}$)	0.0004 - 0.0012	0.0018 - 0.0020	0.0004 - 0.0016	0.0012 - 0.0038
Organic Nitrogen ($g\ m^{-3}$)	0.201 - 0.305	0.112 - 0.142	0.185 - 0.332	0.103 - 0.136
Total Phosphate ($g\ m^{-3}$)	0.0006 - 0.0021	0.0002 - 0.001	0.0003 - 0.0029	0.0001 - 0.0007
Total Phosphorus ($g\ m^{-3}$)	0.009 - 0.014	0.0042 - 0.006	0.010 - 0.016	0.0048 - 0.0062
Dissolved Oxygen ($g\ m^{-3}$)	5.4 - 7.0	5.64 - 6.3	5.80 - 7.00	5.81 - 6.38

Observations did not correspond exactly to model variables. A partitioning process similar to that described for nutrient loads from the mainland was required. Dissolved organic fractions were assumed to comprise 90% of organic carbon, nitrogen, and phosphorus. The remaining organic matter was split fifty-fifty between labile and refractory particulate fractions.

Concentration boundary conditions were specified for salinity, organic carbon, suspended solids, chlorophyll, and dissolved oxygen in inflows from the mainland. These are summarized in Table 12. Dissolved organic carbon was assigned 90% of the total, based on observations from Sutula (1999). The remaining organic carbon was split fifty-fifty between labile and refractory particulate fractions.

Table 12
Runoff Boundary Concentrations

Year	Salt (ppt)	Solids ($g\ m^{-3}$)	Chlorophyll ($mg\ m^{-3}$)	Total Organic Carbon ($g\ m^{-3}$)	Dissolved Oxygen ($g\ m^{-3}$)
1996	0.0	2.0 - 65.9	0.66 - 6.84	4.17 - 15.7	4.52 - 8.45
1997	0.0	1.6 - 20.3	0.43 - 5.25	3.61 - 16.2	4.12 - 7.75

4 Linkage to Hydrodynamic Model

The RMA-10-WES Model and Grid

The two-dimensional version of RMA-10-WES, a finite element hydrodynamic model, was used to generate the flow field for the water quality model in Florida Bay. Typically, RMA-10-WES is used to compute water surface levels, tidal ranges, velocities, and flows. The RMA-10-WES grid for Florida Bay consists of 19253 triangular elements and 40609 nodes (Figure 17). The grid stretches from Barnes Sound in the east to the Gulf of Mexico north of Johnston Key in the west. The northern extent of the grid is the Gulf of Mexico and the Everglades, and the southern extent is the Florida Straits.

Several issues had to be addressed prior to using RMA-10-WES for water quality hydrodynamic generation. First, the mathematical formulation of RMA-10-WES conserves mass globally but not locally on an element control volume. Local mass conservation is a requirement for water quality modeling. Techniques had to be developed that would generate a locally mass conservative flow field. RMA-10-WES flow field information was output at hourly intervals. After the run was completed, the flow field was processed. An algorithm was used that redistributed the imbalance (or residual) among the nodes so that local flow conservation (and therefore mass conservation) was obtained. A second issue was that the resolution of the RMA-10-WES grid exceeded the practical resolution for water quality computations. It was not desirable to use a one-to-one overlay of the hydrodynamic grid as the fine resolution in many parts of the grid would cause unacceptably low timesteps and consequentially long runs. Using a coarser overlay allowed numerous small cells to be combined into one water quality cell so that reasonable timesteps were attainable. Furthermore, CE-QUAL-ICM did not have the capability to simulate wetting and drying of cells as RMA-10-WES did. Use of an overlay allowed RMA-10-WES cells to wet and dry without interfering with the water quality computations. Water quality cells were large enough that they would not be completely dry even though some of the RMA-10-WES cells comprising it became dry. The water quality overlay is shown in Figure 18. The water

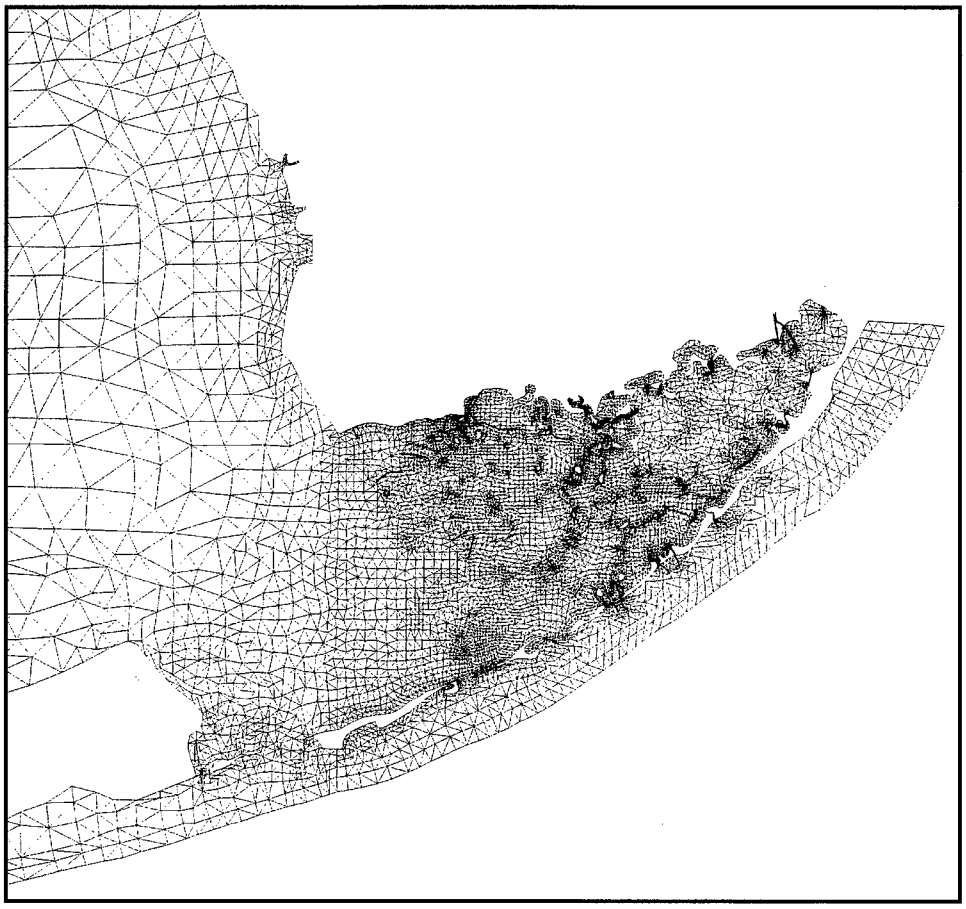

Figure 17. RMA-10-WES Hydrodynamic Model grid

quality model grid overlay had 1060 cells and 2268 flow faces. Water quality cells were irregular polygons with sides corresponding to the sides of RMA-10-WES elements. The two grids were congruent.

Wet Season/Dry Season Hydrodynamics

The computational requirements for RMA-10-WES precluded simulating a continuous two-year period for generation of a hydrodynamic data set for water quality computations. To mitigate these problems, seasonal hydrodynamic data sets were used for water quality computations. Seasonal hydrodynamic data sets were generated for the wet and dry seasons of 1996 and 1997 and the dry season of 1992. The dry season was defined as the period December 1 through April 30 and the wet period was May 1 through November 30. Each seasonal hydrodynamic data set varied hourly, but each was generated using seasonally averaged freshwater inflows and winds.

Figure 18. CE-QUAL-ICM Water Quality Model grid

Several different forms of input were required by RMA-10-WES. Constant river inflows for each season (Chapter 3) were applied at the tributaries (Table 13). The effects of rainfall and evaporation were included in the model as a net rainfall/evaporation rate (Table 14). Monthly rainfall data for Florida Bay, obtained as part of the effort to generate flows and loads (Chapter 3), was used to generate the seasonal rainfall rate. Long-term mean monthly evaporation rates, derived from the South Florida Water Management Model, were used to develop the seasonal evaporation rate. These were added to generate a single net rainfall/evaporation rate for the season. Positive net rainfall/evaporation rates indicate there was a net rainfall during that season while negative rates indicate a net evaporation. These rates were applied uniformly over the entire grid for the duration of the season. Seasonal average wind information, velocity and direction, obtained from the WES meteorological stations, was used to drive RMA-10-WES for the years 1996 and 1997. Wind information for 1992 was generated using the data from the National Center for Environmental Prediction (NCEP) Reanalyzed Winds data set. Water surface elevation boundary conditions for the RMA-10-WES hydrodynamic grid were developed using a regional vertically averaged numerical model, ADCIRC (Westerlink et al. 1992). Time varying water surface elevations were saved from the ADCIRC model at several locations along the Florida Bay grid

boundary. The water surface elevation boundary condition repeated every 28 days 23 hours.

Table 13
Uniform River Inflows (m^3/s)

Inflow	1996 Dry	1996 Wet	1997 Dry	1997 Wet	1992 Dry
Trout Creek	1.69	7.60	1.57	7.38	1.47
Taylor Slough	4.19	6.84	1.66	15.62	2.29
Alligator Creek	1.40	2.28	0.55	5.21	0.76
Buttonwood Canal	1.27	0.35	0.03	3.02	0.65
East Cape Canal	1.27	0.35	0.03	3.02	0.65
Little Shark River	15.74	11.46	5.37	15.03	7.15
Shark River	28.94	22.22	10.68	24.02	13
Harney Creek	14.47	11.11	5.34	12.01	6.5
Broad River	10.89	6.74	2.91	7.25	2.87
Rodgers River	10.89	6.74	2.91	7.25	2.87
Lostman's River	2.53	1.43	0.13	3.26	1.17

Table 14
Net Evaporation and Rainfall (cm/day)

	1996 Dry	1996 Wet	1997 Dry	1997 Wet	1992 Dry
Net Evaporation/ Rainfall	-0.17114	0.10650	-0.11828	0.10047	-0.16288

The total length of an RMA-10-WES seasonal hydrodynamic run was 57 days. The first 12 days of a run were discarded to remove initial conditions bias and compensate for model spin-up. The remaining 45 days of hydrodynamics were processed and projected to the water quality model grid to generate input for the water quality model. As these hydrodynamic data sets were less than the length of the season, they had to be repeated or "rewound" several times in order to simulate a season of six months. For the water quality model to perform correctly, the hydrodynamic conditions at the beginning and end of the hydrodynamic file should be similar to allow a smooth transition when the file is rewound.

The only time-varying forcing function in the hydrodynamic model was the tidal boundary condition. The tidal boundary condition record was 28 days 23 hours which necessitated that it be repeated to generate the seasonal hydrodynamic data set. As a result, conditions in the hydrodynamic model repeated on an approximately 29-day cycle in response to tidal activity. An example is shown for 1997 wet season in Figure 19. Use of a 29-day hydrodynamic record to drive the water quality model should allow smooth transitions when rewinding. A technique was developed for selecting this 29-day period from the 45-day hydrodynamic data set available.

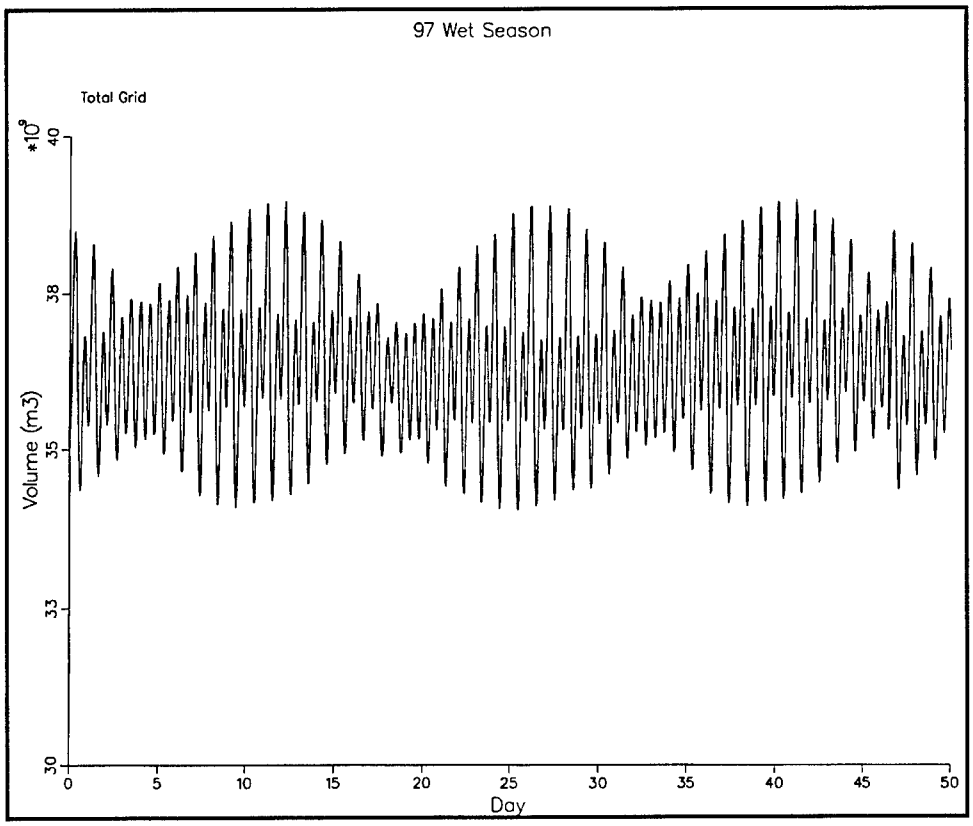

Figure 19. Total grid volume time series

The technique consisted of computing the total volumes within the entire grid and the total volume within Florida Bay for the duration of the hydrodynamic data set. Then, starting with the first iteration, the total volume and Florida Bay volume were compared to volumes in the future within a 4-hour window of the tidal cycle (28 days 21 hours to 29 days 1 hour). This was repeated until the end of the file was reached. The periods yielding the best agreement in terms of beginning and ending volumes were identified. A total of ten periods were identified for each hydrodynamic data set, five based on Florida Bay volumes, five based on total grid volume. From these ten, a final hydrodynamic period was selected and used to drive the water quality model. Criteria for selection included the relative magnitude of the imbalance in both the whole grid and Florida Bay. Final selections were made after visual inspection of time series plots. The 29-day hydrodynamic file for the 1997 wet season is shown in Figure 20.

There was a slight problem with using hydrodynamic data files of approximately 29 days length; it was impossible to combine the files in such a way as to get one year. Use of twelve seasonal hydrodynamic files would result in a simulation with a duration of approximately 348 days. This problem is not that significant for a one- to two-year water quality simulation as the inclusion of an additional 29-day hydro file would suffice. Ten-year simulations are another matter. If no corrections are made, the hydrodynamics would be 170 days, or approximately six months, out of phase by the end of the simulation. To counter this problem, three

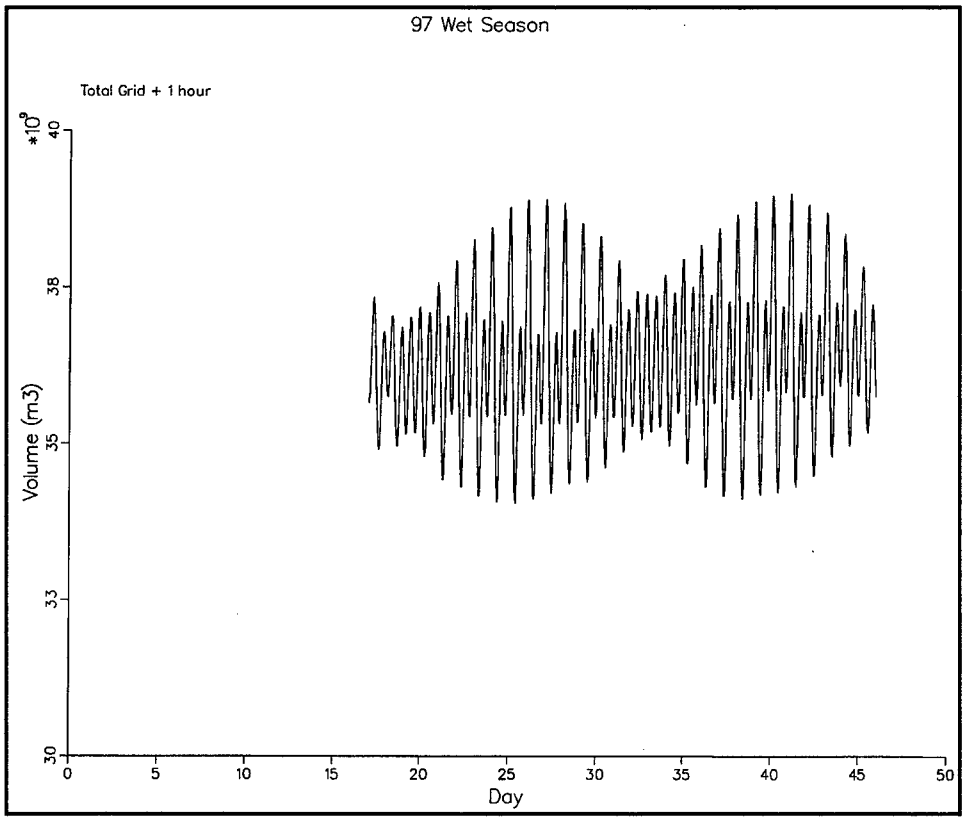

Figure 20. Total grid volume time series for water quality model seasonal hydrodynamic data set

additional hydrodynamic data files of approximately 17 days duration were generated. By including one of these files with twelve of the seasonal files, it was possible to simulate a complete year and maintain syncronicity between the hydrodynamics and other data. The 17-day file was extracted from the beginning of the original 29-day hydrodynamic record. The length of the file was adjusted slightly to provide a smother transition with the beginning of the next hydrodynamic file.

RMA-10-WES hydrodynamic time-varying data, flows, volumes, and surface areas, were output and stored in a file at 1-hour intervals. The information in this file was then projected to the water quality model grid and stored in a water quality model hydrodynamic file. This is the file from which the 29-day hydrodynamic records were extracted. The water quality model read the hydrodynamic file at 1-hour intervals during the simulation. Flows and surface areas were updated in the water quality model using new values obtained from the hydrodynamic file. Volumes obtained from the hydrodynamic file were compared against water quality model volumes. This check insures that the water quality model flow field is the same as that of RMA-10-WES. If there had been a problem with either the linkage of RMA-10-WES and the water quality model or in the projection algorithm, then the volumes of the two models would not match to an acceptable level. The volume balance check indicated that the water quality model was conserving volume.

Dye Studies

Continuous releases and instantaneous dumps of conservative tracers were used to compare transport in RMA-10-WES with that of the water quality model. These tests were performed to demonstrate that the transport properties of both models were similar. The locations of the continuous releases corresponded to the inflows of the Shark River and Trout Creek (Figure 21). A third location in western Florida Bay, water quality cell 373, was selected for an instantaneous tracer release (Figure 21). Boundary concentrations in the continuous releases were 100.0 mg/l while initial concentrations for the cells/elements receiving the instantaneous release were 1000.0 mg/l. Simulation duration was 45 days. Hydrodynamic data from the 1997 wet season were used for the dye studies.

Results for these tests were mixed. Generally, results for Florida Bay were good. Water quality model and RMA-10-WES results for simulation day 45 (Figures 22 and 23), for the continuous release at Trout Creek compare favorably as do instantaneous release results for ICM cell 373 (Figures 24 and 25). Although the water quality model used an overlay in these regions, the transport was not compromised in Florida Bay. However, water quality model concentrations resulting from the Shark River continuous tracer release were significantly lower than those generated by

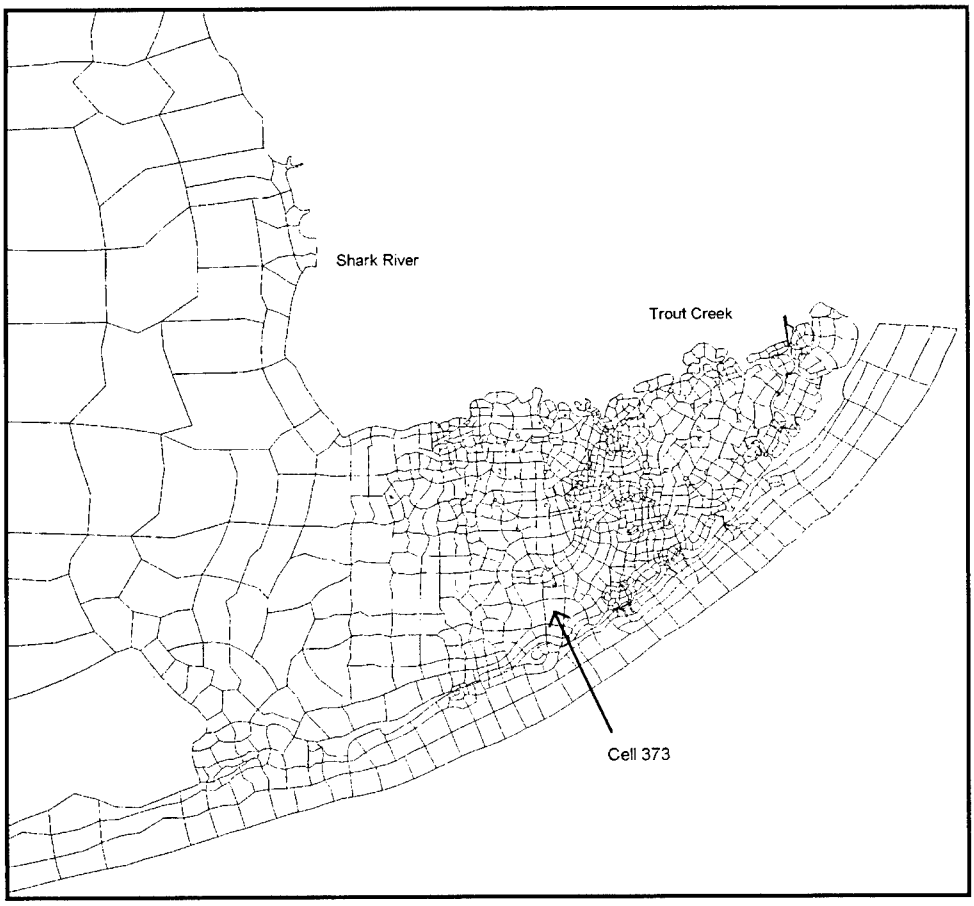

Figure 21. Transport comparison sites

Figure 22. Waver quality model tracer for Trout Creek

Figure 23. RMA-10-WES tracer for Trout Creek

Figure 24. Water quality model tracer, cell 373

Figure 25. RMA-10-WES tracer, cell 373

RMA-10-WES (Figures 26 and 27). These differences appear to result from increased numerical diffusion resulting from use of a coarse overlay over larger cells in the vicinity of the Shark River. The openness of this portion of the grid results in mass being moved quickly away from the loading site and dispersed throughout the system.

Summary

RMA-10-WES was used to generate a flow field that was projected onto a water quality model grid that was a coarse overlay of the RMA-10-WES grid. The projection algorithm used generated a locally and globally conservative flow field for the water quality model. Transport comparisons between RMA-10-WES and CE-QUAL-ICM using a conservative tracer indicated that the projection algorithm approach is working. Use of an overlay did not impact water quality results in the area of focus, Florida Bay. The use of a coarse overlay along the western boundary resulted in numerical diffusion which did not have an impact on the interior of Florida Bay. Overall, the results indicate that CE-QUAL-ICM and RMA-10-WES were linked together properly and that RMA-10-WES could be used to generate hydrodynamic flow fields for water quality modeling.

Figure 26. Water quality model tracer, Shark River continuous loading

Figure 27. RMA-10-WES tracer, Shark River continuous loading

5 Suspended Sediment Modeling

Introduction

A sediment resuspension model module was developed and implemented in the WQM for this study. Florida Bay water quality and submerged aquatic vegetation issues are related to water column turbidity and particulate resuspension. Water column suspended sediment concentrations modify the availability of photosynthetically active radiation to seagrasses and benthic algae. Conversely, seagrass and, to a lesser extent, benthic algae modify wave climates and sediment resuspension. To address water quality and seagrass issues, simulations of sediment resuspension are required to be coupled to the WQM. To perform this modeling, new capabilities were added to the WQM, and information on winds was assembled for model input. The sections to follow describe background information on resuspension, Florida Bay, the resuspension model module, development of wind climate, and resuspension module adjustment and verification.

Background

Coupling of sediment resuspension and seagrass

Resuspension is important to water quality in Florida Bay mainly as it impacts water clarity and light penetration to seagrasses. Seagrass greatly affects resuspension in Florida Bay. Areas bare of seagrass are prone to resuspension that can appreciably decrease water clarity and may prevent seagrass establishment or cause further seagrass decline. On the other hand, seagrass beds slow water movement, damp waves, and trap and hold sediments. Seagrass and macrophytes in general reduce wind-wave resuspension (Ward, Kemp, and Boynton 1984; James and Barko 1994; and Hamilton and Mitchell 1996). Seagrass reduces shear stress at the sediment bed below that which would occur on a bare bottom. At the same time,

seagrass greatly increases total resistance to flow and wave damping, absorbing shear stress, and sheltering the sediment in seagrass beds. Previous studies have documented the effects of submerged aquatic vegetation on total flow friction and on wind-wave damping (for example, see the bibliography of Dawson and Charlton 1988, and Fonseca and Cahalan 1992). Thus, there are feedbacks between the presence of seagrass, water clarity, and the establishment of new seagrass. These interactions are shown schematically in Figure 28.

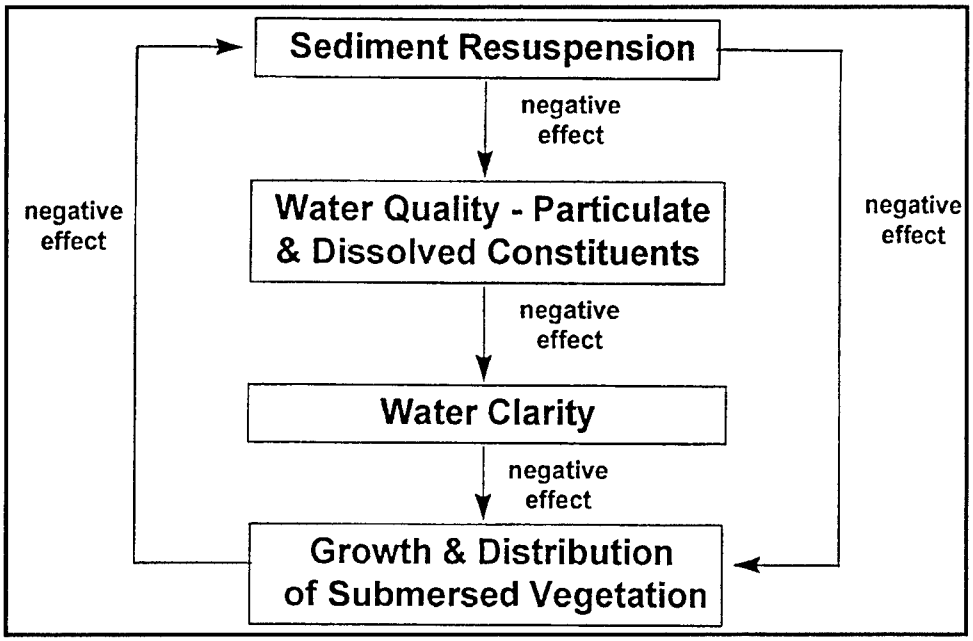

Figure 28. Sediment resuspension, water quality, and aquatic vegetation

Resuspension and flushing in Florida Bay

Resuspension is driven by bed shear stress generated by tidal and wind-driven mean currents and by wind waves. Tidal currents are generally weak except through bank cuts or passes. Wind-forced currents with subtidal periods are very important to circulation and flushing. Winds commonly move larger volumes of water than do tides in the interior of Florida Bay (Enos 1989), and 85 percent of alongshore velocity variance on nearby West Florida Shelf is in the subtidal frequency band (Mitchum and Sturges 1982).

Wind-generated currents and waves both create bed shear stresses that can resuspend bed material and mix it throughout the water column. Wind-generated currents transport salt, heat, and chemical constituents throughout the bay. Wind-wave resuspension is reported to be important to total suspended material (TSM) levels in the water column and therefore to turbidity. Phlips, Lynch, and Badylak (1995) made observations and sampled at 17 stations in Florida Bay monthly over a one-year period. Tripton (TSM minus algal biomass) levels ranged from 8 to 30 ppm, with higher values in the western bay. They reported that tripton was responsible for

54 to 92 percent of the water column light attenuation, with chlorophyll-containing particles the next most important contributor.

Physiography

Florida Bay is a 1,500-sq-km lagoon system consisting of largely interconnecting banks and associated islands semi-enclosing shallow 'lakes.' Banks are very shallow, restrict flows and flushing, and affect waves. The bay has 237 islands greater than 100 sq m which have a mean area of 0.11 sq km, median of 0.02 sq km, and maximum of 1.68 sq km (Enos 1989). Islands constitute 1.73 percent of the total bay area. The entire bay is underlain by pleistocene limestone at roughly 2- to 5-m depth deepening east to west. Windward (north and east) edges of islands and banks are mostly erosional and are composed primarily of sand- and gravel-sized material. Leeward (south and west) edges of banks are depositional and have finer sediment texture.

Bed sediments

Florida Bay sediments are predominantly biogenic carbonates which vary considerably in texture from place to place. Lake bottoms are primarily carbonate mud with sand- and gravel-sized components. Sediments migrate from lake bottoms, where most are produced, onto relatively stable banks, or out of the system (Bosence 1989). The northeastern or interior portion of the bay is sediment starved, with thin banks and some bare rock bottom (Bosence 1989). Thicker sediment beds occur in the central bay. The western portion of the bay contains a relatively deep (18 m) area called the 'sluiceway' which has a rock and shell bottom, and is reported to be frequently scoured (Schomer and Drew 1982).

Previous, rather sparse, sampling indicated that, overall, bay sediments are 52 percent finer than 62 μm and, on average, a bi-modal mix of sand, silt, and clay sized material. A recent study analyzed 600 samples from the bay and described sediment characteristics (Prager, Halley, and Hansen 1996).

Shallow water carbonate sediments are relatively rare, and few studies have reported on the erodibility of sediments such as those which occur in Florida Bay. Prager, Halley, and Hansen (1996) have undertaken an evaluation of bay sediment erodibility but this information is not yet available. Calcareous silt from the deep ocean, which might be similar to some fine sediments in the bay, has been previously found to be eroded by low near-bed current speeds (Southard, Young, and Hollister 1971). Erodibility of Florida Bay samples will depend on sediment characteristics as well as the nature and quantity of algae and other organic materials which generally reduce the erodibility of sediments.

Seagrass frictional effects

Data on the frictional characteristics of seagrasses are sparse. Fonseca and Cahalan (1992) performed laboratory wave-damping tests on several seagrass species from Laguna Madre, Texas. The percentage reduction in wave energy over a 1-m wave-flume test section was measured. Seagrass characteristics were:

Species	Leaf length, cm	Shoots per sq m
Halodule wrightii (H.w.)	17.2	1900-2870
Syringodium filiforme(S.f.)	41.4	230-1350
Thalassia testudinum (T.t.)	19.4	850-1500
Zostera marina (Z.m.)	23.4	750-1000

Two wave types were generated with wave periods of 0.7 sec and 0.4 sec and wave lengths of 0.68 m and 0.37 m, respectively. Two to four flow depths were used with each species to double the water-depth/leaf-length within each species. Waves were photographed entering and exiting the test section as the fifth generated waves passed. Percent wave energy reductions were about 40 percent for all species.

Species-averaged data from Fonseca and Cahalan (1992) were reanalyzed using energy considerations to obtain the following shear stress and friction factor estimates:

Species	h, cm	H_s, cm	τ_w, Pa	f_w
H.w.	9	2.1	0.24	0.082
S.f.	19	4.3	0.95	0.885
T.t.	11	3.1	0.52	0.143
Z.m.	16	3.4	0.48	0.304

where h is the flow depth, H_s is the significant wave height, τ_w is the total wave friction, and f_w is the wave friction factor,

$$\tau_w = \frac{1}{2}\rho f_w U_{wb}^2 \tag{5}$$

and ρ is water density, U_{wb} is the near-bottom velocity generated by waves. These f_w values are quite high compared to an expected turbulent f_w value of about 0.005 for the smooth, fine sand bed used in these experiments. However, the wave Reynolds numbers for these experiments were quite low (29-16), so that the bare-bed resistance is hard to estimate. Laminar-flow f_w's for these wave conditions range from 0.07 to 0.13. Fonseca and Cahalan (1992) state that no wave damping occurred when vegetation was not present in the flume.

In other flume experiments, Fonseca and Fisher (1986) measured the hydrodynamic characteristics of the same seagrass species for average current speeds U of about 20 cm/sec.

Species	h, cm	Y_k, cm	f
H.w.	23	6.5	0.37
S.f.	28	20.7	0.23
T.t.	23	13.9	1.26
Z.m.	21	8.0	0.76

where Y_k is the distance from the water surface to the top of the plant canopy, f is a Darcy friction factor defined as $U_* / U = (f / 8)^{0.5}$, and U_* is the friction velocity. It appears that, with respect to frictional characteristics, *T.* is most resistive, *H.* and *Z.* species are next, and *S.* is the least resistive seagrass species.

Fonseca and Fisher (1986) also measured a Shields' sediment entrainment function under seagrass canopies *(Fs')*. For the sediment particle size used in these experiments, a normal Shields entrainment function (for a bare bed) *Fs* of about 0.06 would be expected while Fonseca and Fisher (1986) found much higher values indicating that much of the total shear stress was not acting on the bed. The increased *Fs'* compared to *Fs* is interpreted as a decrease in the bed shear stress for the same total shear stress. Then the ratio *Fs / Fs'* expresses the fraction of the total shear stress reaching the bed. For the four seagrass species:

Species	*Fs / Fs'*
H.w.	0.21
S.f.	0.66
T.t.	0.12
Z.m.	0.21

The fraction of shear stress reaching the bed appears, in general, to be inversely related to the frictional effect expected from the seagrass species.

Modeling Wind-Wave Resuspension

Large, shallow water bodies such as lakes, estuaries, and lagoons are often subject to resuspension by wind-waves. Resuspension model studies of such systems have often used wave measurements or results from wave models to provide wave parameters for use in calculations of bottom shear stresses, and have been reasonably successful simulating TSM levels (Luettich, Harleman, and Somlyody 1990; Hawley and Lesht 1992; Sheng, Eliason, and Chen 1992; and others). In the case of Florida Bay water

quality modeling, simplifying assumptions such as a single grain class and independent erosion and deposition processes could be made (similar to the previous studies cited) to reduce resuspension model complexity and computational burden, as long as changes to sediments and depths are not varied for plan tests.

Previous studies stress the importance of winds and wind-waves to shallow water resuspension. Near-bed wave orbital velocity is a critical parameter for resuspension of bed sediments. Short-period oscillatory currents forced by wind-waves are more effective at developing bed shear stress than the same current magnitudes forced by tides due to boundary layer effects. Pejrup (1986) observed that, where wave heights and depths change appreciably, wind speed (being relatively constant over an area) may correlate better to TSM concentrations than wave height measured at a point. Analysis of time-series TSM from a micro-tidal estuary indicated that wind alone, regardless of direction, had the best correlation to TSM levels (Pejrup 1986). Arfi, Guiral, and Bouvyi (1993) tested an expression relating wind speed and water column buoyancy to calculate thresholds for resuspension and obtained results that were similar in magnitude to wave-based threshold estimators. Although wave characteristics are critical, wave shear stress and the overall balance of momentum input from the atmosphere are critical to resuspension in large shallow lagoons and estuaries. These shallow water bodies respond to winds at small spatial scales (for example, depth-limited wind-waves, Langmuir circulation cells, and buoyant eddy overturning).

Resuspension Model Description

Erosion and deposition

The depth-averaged conservation of sediment mass at a point, disregarding horizontal advection and diffusion, is

$$h\frac{dC}{dt} = E - W_s C \tag{6}$$

where C is depth- or cell-averaged suspended sediment concentration, h is the cell or water depth, t is time, E is the sediment bed erosion rate per unit area, and W_s is the sediment settling rate. The product of W_s and C is the depositional flux to the bed. As indicated by Equation 6, both erosion and deposition operate simultaneously and continuously in the resuspension model, as in the models of Leuttich, Harleman, and Somlyody (1990), Hawley and Lesht (1992), and Lick, Lick, and Ziegler (1994). Sanford and Halka (1993) found that single-grain class models that allow simultaneous erosion and deposition predicted resuspension concentrations more accurately than single-grain class models with mutually

exclusive erosion and deposition. However, a preponderance of laboratory data indicate that erosion and deposition are mutually exclusive processes (Teeter 2000). The formulation of the present model is intended to predict suspended sediment concentrations only and not bed elevation changes.

Erosion rate is computed in the model as

$$E = a_1 \tau_b^n \tag{7}$$

where a_1 and n are sediment-related parameters, and τ_b is the bed shear stress. The bed shear stress is related to the input of atmospheric momentum. For fully developed waves (constant wave spectra) over a bare bed, wave dissipation through bottom friction and whitecapping is equal to the atmospheric shear shress at the water surface. An infinite source of benthic sediment is assumed to be available for resuspension into the water column.

Atmospheric shear stress

Atmospheric shear stress τ_a is computed using a quadratic friction law as

$$\tau_a = \rho_a C_d U_a^2 \tag{8}$$

where ρ_a is the air density, C_d is a drag coefficient, and U_a is the wind speed at some height z. For neutral atmospheric stability and assumed logarithmic velocity profile

$$C_d = \frac{0.16}{(\ln z - \ln z_o)} \tag{9}$$

where z_o is the roughness height. The roughness height depends on wave characteristics, and Hsu (1974) found that

$$z_o = \frac{H_s U*_a^2}{g L_w} \tag{10}$$

where H_s is the significant wave height, $U*_a$ is the atmospheric shear velocity, and L_w is the wave length. Thus for a given U_a , τ_a is related to wave conditions' through the roughness height z_o. Using data from Laguna Madre, Texas, for h's of 1 to 2 m, an empirical equation for C_d was developed with the form

$$C_d = 0.0001 \times (6.49 + c_1 U_a) \tag{11}$$

where the parameter c_1 depends on the presence of seagrass, water depth, and fetch (wind direction) and, thus, varies spatially. Compared to deep coastal and oceanic areas, C_d's are lower in shallow lagoons and very much lower where seagrasses are present.

Water column partitioning of shear stress

The atmospheric shear stress is partitioned between that imparted to waves τ_w and to currents τ_o:

$$\tau_a = \tau_w + \tau_o \tag{12}$$

with 97 percent going to wave shear stress. At higher wind speeds, wave shear stress is partitioned between friction and dissipation by whitecapping using a simple power law developed from shallow-water data from Laguna Madre, Texas:

$$\tau_b = a_2 \tau_w, \quad U_a < 5 m/\sec \tag{13}$$

$$\tau_b = a_2 \tau_w / (U_a - 4)^{0.5}, \quad U_a > 5 m/\sec \tag{14}$$

where a_2 is a factor which ranges from 0.0 to 1.0 depending on seagrass conditions.

Model Validation

Wind data compilation

Two wind data sets were used. The verification period for the WQM was 1996-1997, and winds for this period were compiled from National Oceanic and Atmospheric Administration, National Center for Environmental Prediction (NCEP), Mid-Range Forecast (MRF) winds. MRF winds are produced on a 1° global grid. MRF winds were only available for 1994 through 1997. For the study prediction period of 1988 through 1997 NCEP's Reanalyzed Global (RG) winds were used. This data set covers 1976 through 1998 with a global grid of about 2°. There is tendency for the RG to be lower than the MRF winds.[1] A comparison of the MRF and RG winds is shown in Figure 29, and indicates that, indeed, the RG winds are lower for this period.

[1] Personal Communication, Rebbeca Brooks, November 12, 1999, CEERD Waterways Experiment Station, Vicksburg, MS.

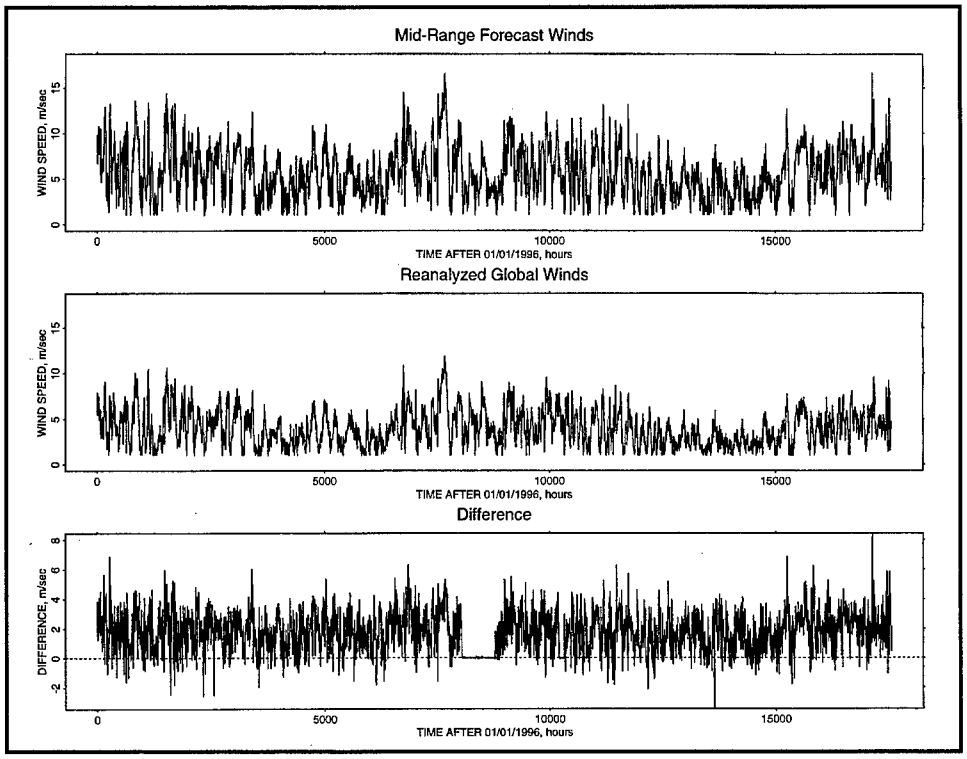

Figure 29. Comparison of MRF and RG winds for 1996 through 1997

Resuspension model verification

Initial simulations were performed for the 1996 through 1997 WQM verification using 13 months of data from Phlips, Lynch, and Badylak (1995) covering portions of 1993 and 1994. A rough verification was performed using means and standard deviations from 17 stations, and the MRF winds. Station locations are shown in Figure 30. The model was adjusted by regions or areas within which water column conditions were found to be similar, as previously suggested by Phlips, Lynch, and Badylak (1995). Areas are shown in Figure 31.

For the final model validation, a longer time-series data set was obtained for the same stations[1] which covered January 1994 through mid-1996 (937 days in all). Samples were collected about monthly. The winds for this period were extracted from the RG wind data set. The value for c_1 was set at 0.97 for all cells. Using aboveground biomass and patchiness to parameterize seagrass frictional effects, the model was adjusted such that an order of magnitude increase in this parameter decreased C_d by 20 percent and reduced the factor a_2 from 97 to 40 percent. A linear ramp was used between these end points. Model parameter n was set at 4.0 for all cells. The model parameter a_1 was adjusted spatially to improve the model

1 Personal Communication, Dr. E.J. Phlips, September 14, 1999, University of Florida, Gainesville, FL.

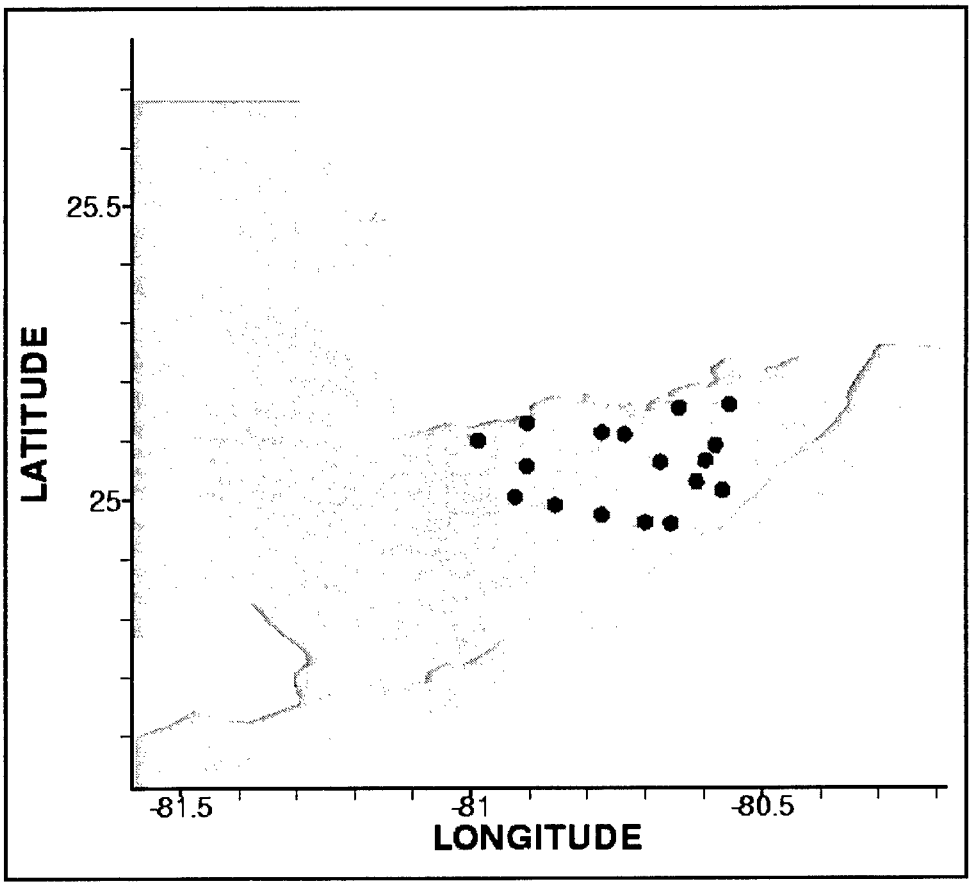

Figure 30. Phlips' station locations

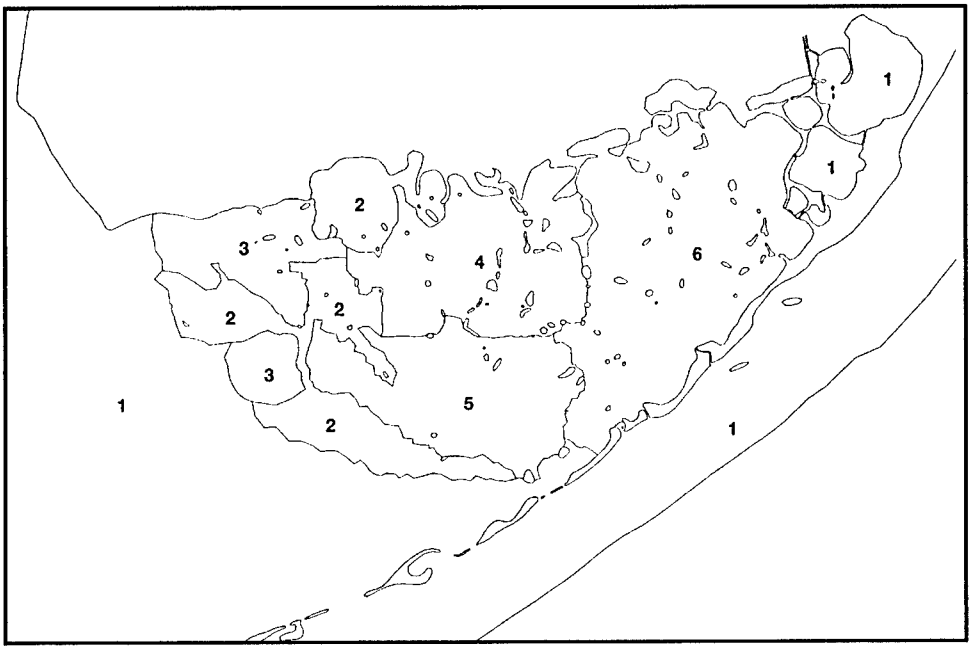

Figure 31. Areas used in rough verification

to field comparisons within the areas shown in Figure 31. The distributions of a_1 by area were as follows:

Area	Percentile		
	25	50	75
1	0.577	0.650	1.235
2	0.126	0.211	0.650
3	0.158	0.228	0.649
4	0.098	0.163	0.251
5	0.095	0.154	0.204
6	0.102	0.164	0.215
All	0.143	0.292	0.650

Final verification inorganic solids concentrations for the 17 stations are shown in Figure 32 for the period starting 1 January 1994. Means and standard deviations for model and field data are printed across the top of the plots shown in Figure 32. There were seven field data points not plotted in Figure 32. Station 4 had values of 166 and 235 g/m^3, and Stations 5, 6, 7, 11, and 17 had values of 218, 275, 317, 128, and 132 g/m^3, respectively. These extreme values affected mean and standard deviation values at these stations.

The timing of concentration peaks displayed in Figure 32 was not always predicted accurately by the model. The most important requirement of the model was to predict the central part of the frequency distributions critical to light availability and seagrass productivity. Statistical distributions for model and field data are shown in Figure 33 for the same stations. In Figure 33, inorganic solids are plotted on log scale against quantiles of the standard deviation about the median and straight lines indicate log-normal distributions.

Conclusions and Recommendations

The resuspension module successfully reproduced general characteristics of suspended sediment concentrations, at least in a statistical sense. The 25, 50, and 75 percentiles of the distributions are plotted in Figure 34. The algorithm does not add an appreciable numerical burden to the WQM. Further refinement of the algorithm is possible but would require additional synoptic information on wind, wave, and suspended sediment concentrations over bare and seagrass-covered bottoms. More field information is also needed on the short-term variability of suspended sediment fields and the effects of the seasonal occurrence of algal mats on resuspension.

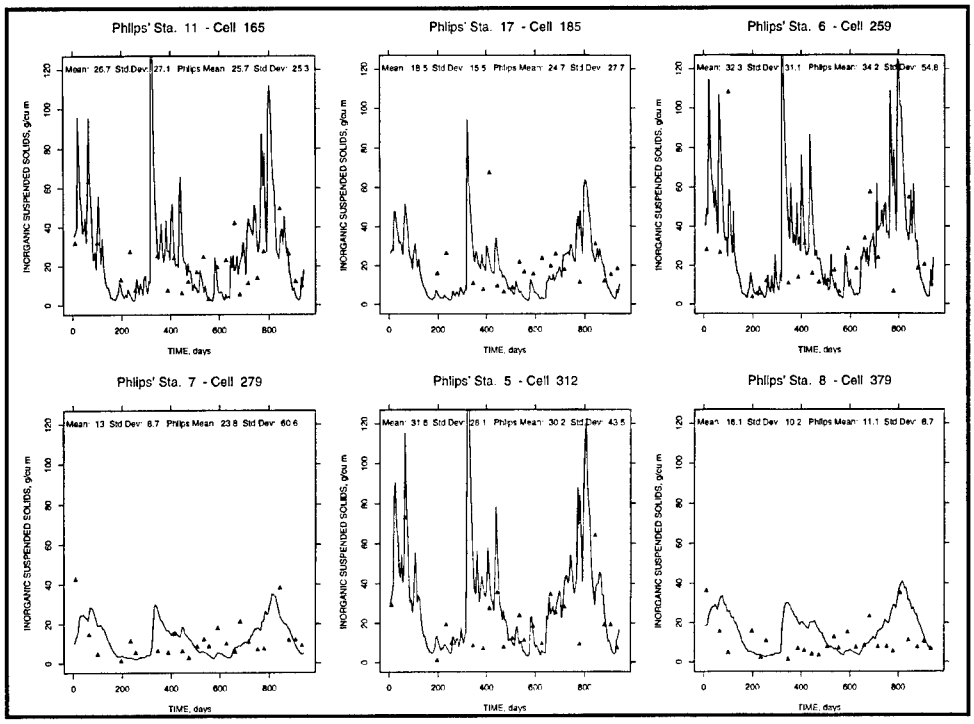

a. Phlips station locations, stations 11, 17, 6, 7, 5, and 8

Figure 32. Time-series comparison of model and field data starting 1 January 1994 (sheet 1 of 3)

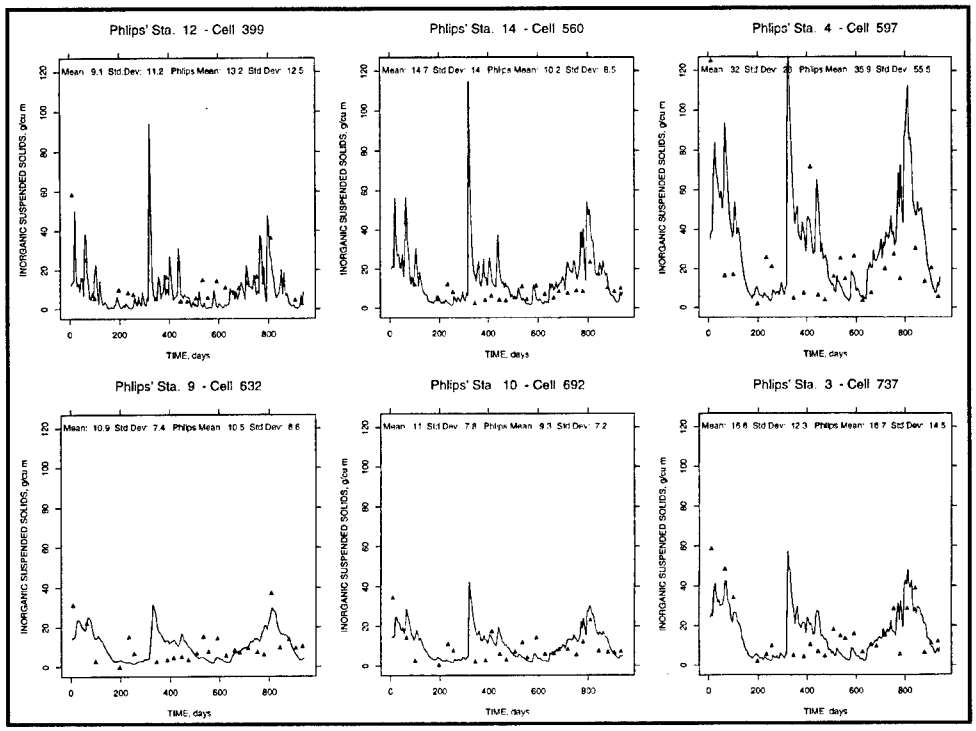

b. Phlips station locations, stations 12, 14, 4, 9, 10, and 3

Figure 32. (sheet 2 of 3)

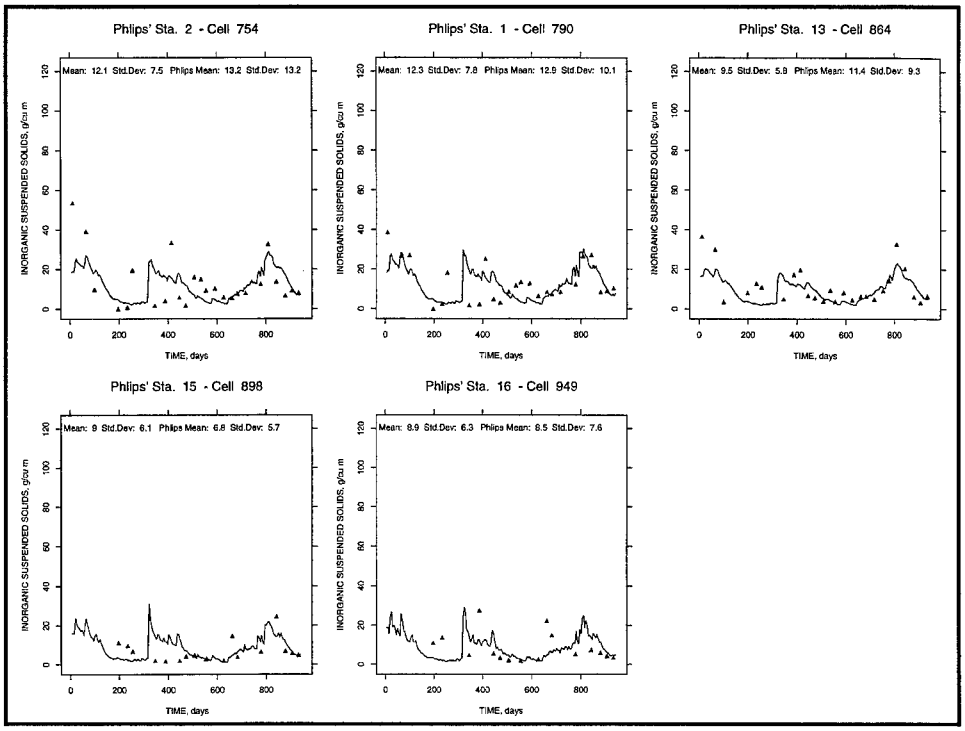

c. Phlips station locations, stations 2, 1, 13, 15, and 16

Figure 32. (sheet 3 of 3)

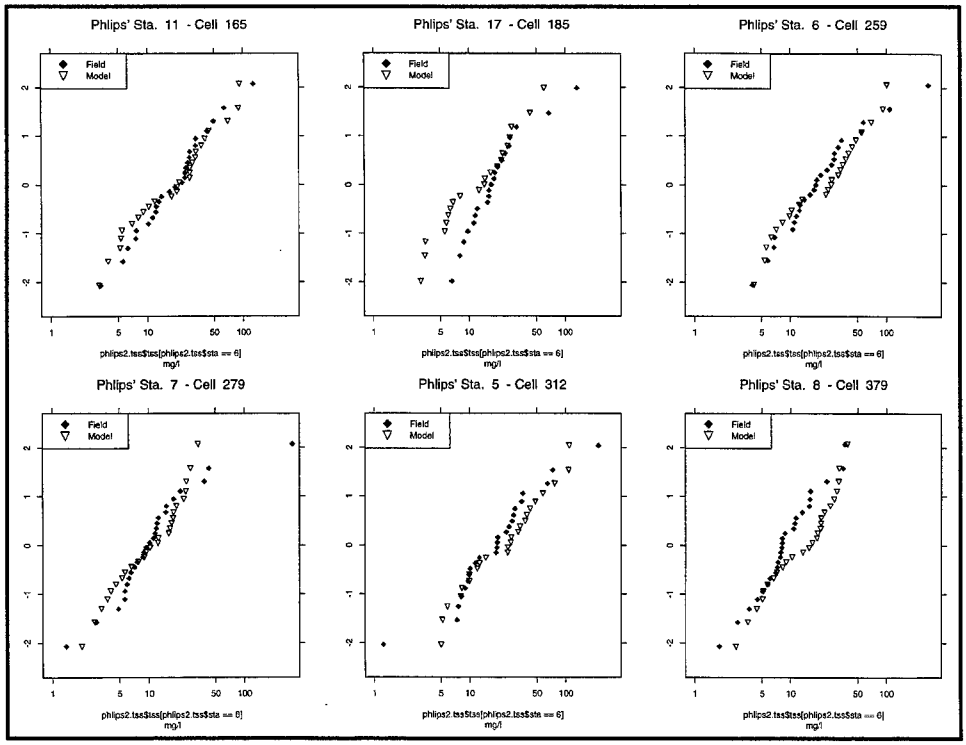

a. Phlips station locations, stations 11, 17, 6, 7, 5, and 8

Figure 33. Comparison of model and field distributions (sheet 1 of 3)

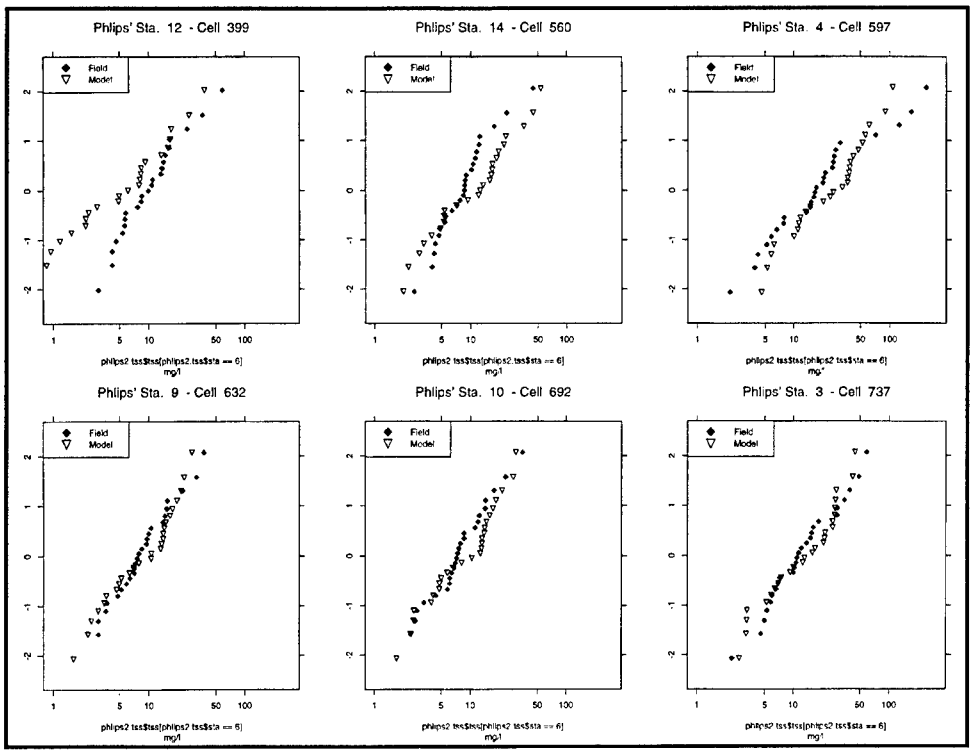

b. Phlips station locations, stations 12, 14, 4, 9, 10, and 3

Figure 33. (sheet 2 of 3)

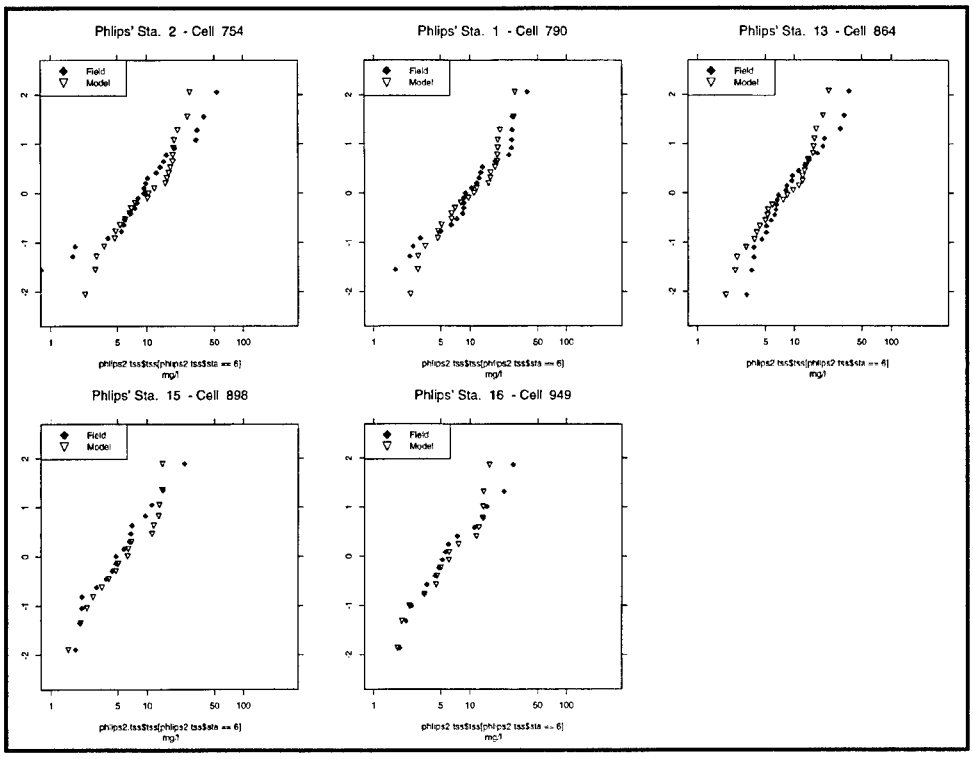

c. Phlips station locations, stations 2, 1, 13, 15, and 16

Figure 33. (sheet 3 of 3)

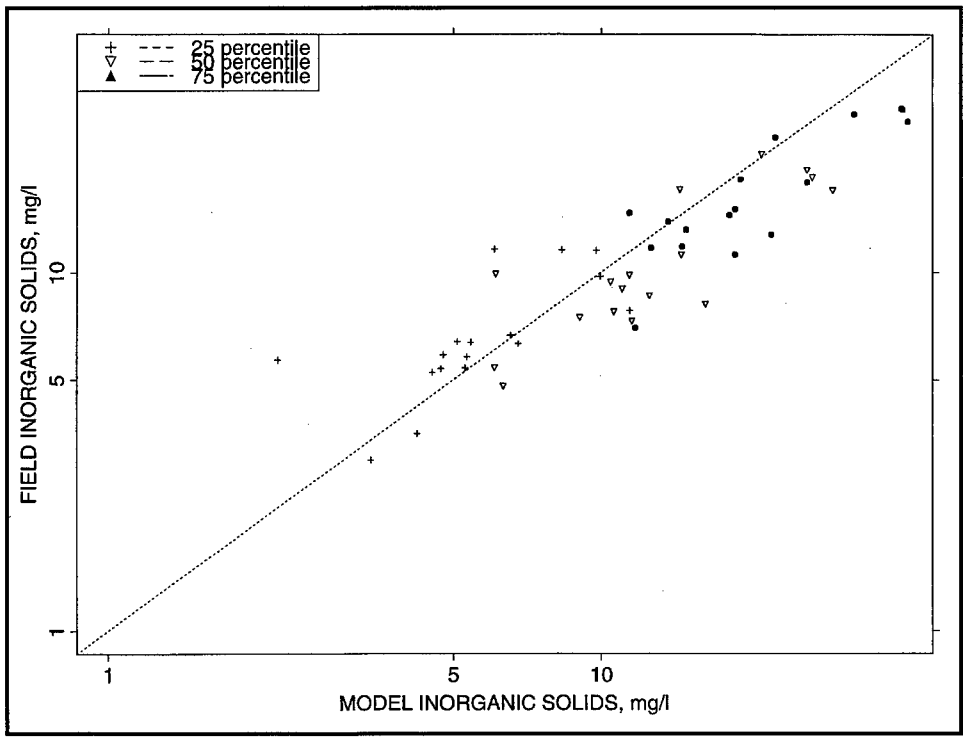

Figure 34. Overall model to field comparison for all stations

6 Water Quality Model Formulation

Introduction

CE-QUAL-ICM was designed to be a flexible, widely applicable eutrophication model. Initial application was to Chesapeake Bay (Cerco and Cole 1994). Subsequent additional applications included the Delaware Inland Bays (Cerco et al. 1994), Newark Bay (Cerco and Bunch 1997), and the San Juan Estuary (Bunch et al. 2000). Each model application employed a different combination of model features and required addition of system-specific capabilities. This chapter describes general features and site-specific developments of the model as applied to the water column of Florida Bay.

Conservation of Mass Equation

The foundation of CE-QUAL-ICM is the solution to the three-dimensional mass-conservation equation for a control volume. Control volumes correspond to cells on the model grid (Figure 18). CE-QUAL-ICM solves, for each volume and for each state variable, the equation

$$\frac{\delta V_j \cdot C_j}{\delta t} = \sum_{k=1}^{n} Q_k \cdot C_k + \sum_{k=1}^{n} A_k \cdot D_k \cdot \frac{\delta C}{\delta x_k} + \sum S_j \qquad (15)$$

in which

V_j = volume of j^{th} control volume (m^3)

C_j = concentration in j^{th} control volume (g m^{-3})

t, x = temporal and spatial coordinates

n = number of flow faces attached to j^{th} control volume

Q_k = volumetric flow across flow face k of j^{th} control volume ($m^3\ s^{-1}$)

C_k = concentration in flow across face k ($g\ m^{-3}$)

A_k = area of flow face k (m^2)

D_k = diffusion coefficient at flow face k ($m^2\ s^{-1}$)

S_j = external loads and kinetic sources and sinks in j^{th} control volume ($g\ s^{-1}$)

Solution of Equation 15 on a digital computer requires discretization of the continuous derivatives and specification of parameter values. The equation is solved explicitly using a time step of 14 minutes and upwind differencing to represent C_k. The remainder of this chapter is devoted to detailing the kinetics sources and sinks and to reporting parameter values. For notational simplicity, the transport terms are dropped in the reporting of kinetics formulations.

State Variables

At present, the CE-QUAL-ICM model incorporates 24 state variables in the water column including physical variables, multiple algal groups, two zooplankton groups, and multiple forms of carbon, nitrogen, phosphorus and silica. From these, a subset (Table 15) was selected for initial application to Florida Bay. Selection was influenced by the characteristics of the system, by the availability of data, and by the time available to complete the study.

Table 15
Water Quality Model State Variables

Temperature	Salinity
Fixed Solids	Algal Biomass
Dissolved Organic Carbon	Labile Particulate Organic Carbon
Refractory Particulate Organic Carbon	Ammonium
Nitrate	Dissolved Organic Nitrogen
Labile Particulate Organic Nitrogen	Refractory Particulate Organic Nitrogen
Total Phosphate	Dissolved Organic Phosphorus
Labile Particulate Organic Phosphorus	Refractory Particulate Organic Phosphorus
Chemical Oxygen Demand	Dissolved Oxygen

Algae

A single algal group is computed as carbonaceous biomass. A specified carbon-to-chlorophyll ratio is employed to compare computed algal carbon to observed chlorophyll.

Organic carbon

Three organic carbon state variables are considered: dissolved, labile particulate, and refractory particulate. Labile and refractory distinctions are based upon the time scale of decomposition. Labile organic carbon decomposes on a time scale of days to weeks while refractory organic carbon requires more time. Labile organic carbon decomposes rapidly in the water column or the sediments. Refractory organic carbon decomposes slowly, primarily in the sediments, and may contribute to sediment oxygen demand years after deposition.

Phosphorus

As with carbon and nitrogen, organic phosphorus is considered in three states: dissolved, labile particulate, and refractory particulate. Only a single mineral form, total phosphate, is considered. Total phosphate exists as several states within the model ecosystem: dissolved phosphate, phosphate sorbed to inorganic solids, and phosphate incorporated in algal cells. Equilibrium partition coefficients are used to distribute the total among the three states.

Nitrogen

Nitrogen is first divided into organic and mineral fractions. Organic nitrogen state variables are: dissolved organic nitrogen, labile particulate organic nitrogen, and refractory particulate organic nitrogen. Two mineral nitrogen forms are considered: ammonium and nitrate. Both are utilized to fulfill algal nutrient requirements although ammonium is preferred from thermodynamic considerations. The primary reason for distinguishing the two is that ammonium is oxidized by nitrifying bacteria into nitrate. This oxidation can be a significant sink of oxygen in the water column and sediments. An intermediate in the complete oxidation of ammonium, nitrite, also exists. Nitrite concentrations are often much less than nitrate and for modeling purposes nitrite is combined with nitrate. Hence the nitrate state variable actually represents the sum of nitrate plus nitrite.

Chemical oxygen demand

Chemical oxygen demand is the concentration of reduced substances that are oxidizable by inorganic means. The primary component of chemical oxygen demand is sulfide released from sediments. Oxidation of sulfide to sulfate may remove substantial quantities of dissolved oxygen from the water column.

Dissolved oxygen

Dissolved oxygen is required for the existence of higher life forms. Oxygen availability determines the distribution of organisms and the flows of energy and nutrients in an ecosystem. Dissolved oxygen is a central component of the water-quality model.

Salinity

Salinity is a conservative tracer that provides verification of the transport component of the model and facilitates examination of conservation of mass. Salinity also influences the dissolved oxygen saturation concentration and may be used in the determination of kinetics constants that differ in saline and fresh water.

Temperature

Temperature is a primary determinant of the rate of biochemical reactions. Reaction rates increase as a function of temperature although extreme temperatures may result in the mortality of organisms and a decrease in kinetics rates.

Fixed solids

Fixed solids are the mineral fraction of total suspended solids. In Florida Bay, fixed solids originate primarily through sediment resuspension. The solids contribute to light attenuation and may play a role in sediment-water phosphorus transfer and in buffering water column phosphorus concentration.

Algae

Algae play a central role in the carbon and nutrient cycles that comprise the model ecosystem. Algal sources and sinks in the conservation equation include production, metabolism, predation, and settling. These are expressed as

$$\frac{\delta}{\delta t}B = \left(G - BM - \frac{Wa}{H}\right)B - PR \quad (16)$$

in which

B = algal biomass, expressed as carbon (g C m^{-3})

G = growth (d^{-1})

BM = basal metabolism (d^{-1})

Wa = algal settling velocity (m d^{-1})

H = cell depth (m)

PR = predation (g C m^{-3} d^{-1})

Production

Production by phytoplankton is determined by the intensity of light, by the availability of nutrients, and by the ambient temperature.

Light

The influence of light on phytoplankton production is represented by a chlorophyll-specific production equation (Jassby and Platt 1976):

$$P = P\max\frac{1}{\sqrt{I^2 + Ik^2}} \quad (17)$$

in which

P = production (g C g^{-1} Chl d^{-1})

Pmax = production rate under optimal conditions (g C g^{-1} Chl d^{-1})

I = irradiance (E m^{-2} d^{-1})

Parameter Ik is defined as the irradiance at which the initial slope of the production vs. irradiance relationship (Figure 35) intersects the value of Pmax:

$$Ik = \frac{P}{\alpha} \quad (18)$$

in which

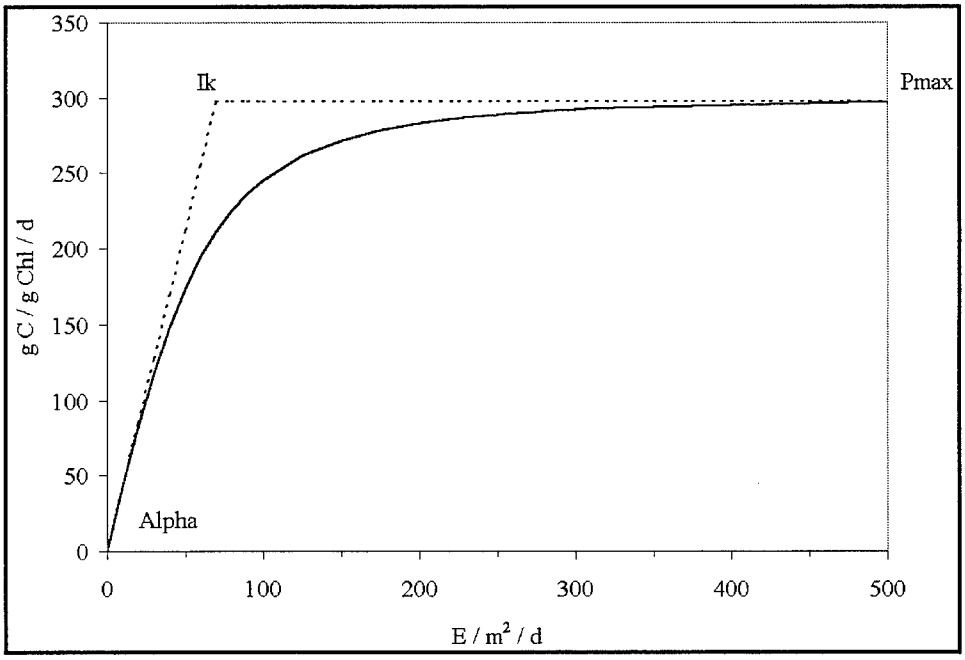

Figure 35. Production versus irradiance curve

α = initial slope of production vs. irradiance relationship (g C g^{-1} Chl $(E\ m^{-2})^{-1}$)

Chlorophyll-specific production rate is readily converted to carbon specific growth rate, for use in Equation 16, through division by the carbon-to-chlorophyll ratio:

$$G = \frac{P\max}{CChl} \tag{19}$$

in which

CChl = carbon-to-chlorophyll ratio (g C g^{-1} chlorophyll a)

Nutrients

Carbon, nitrogen, and phosphorus are the primary nutrients required for algal growth. Inorganic carbon is usually available in excess and is not considered in the model. The effects of the remaining nutrients on growth are described by the formulation commonly referred to as "Monod kinetics" (Figure 36; Monod 1949):

$$f(N) = \frac{D}{KHd + D} \tag{20}$$

in which

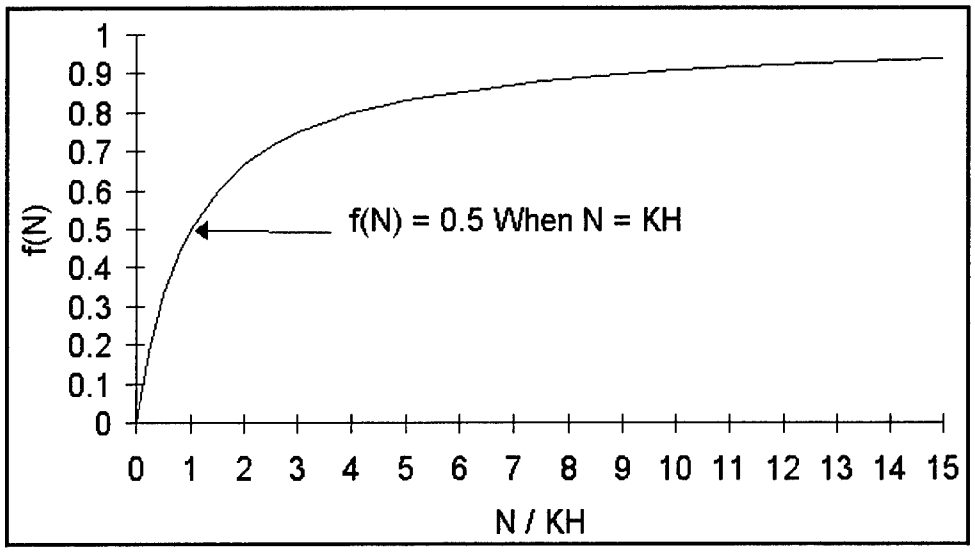

Figure 36. Monod formulation for nutrient-limited growth

f(N) = nutrient limitation on algal production ($0 \leq f(N) \leq 1$)

D = concentration of dissolved inorganic nutrient (g m^{-3})

KHd = half-saturation constant for nutrient uptake (g m^{-3})

Temperature

Algal production increases as a function of temperature until an optimum temperature or temperature range is reached. Above the optimum, production declines until a temperature lethal to the organisms is attained. Numerous functional representations of temperature effects are available. Inspection of growth versus temperature curves indicates a function similar to a Gaussian probability curve (Figure 37) provides a good fit to observations:

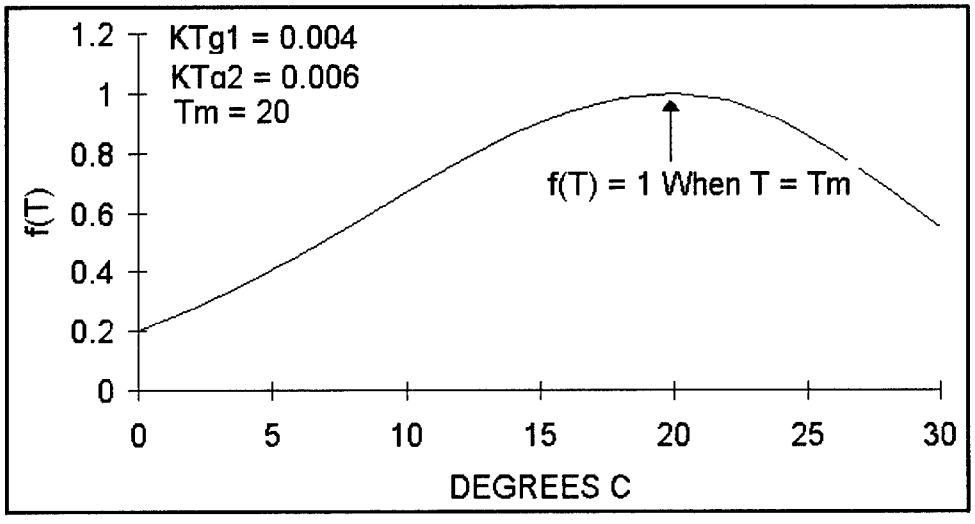

Figure 37. Relation of algal production to temperature

$$f(T) = e^{-KTg1\cdot(T-Topt)^2} \quad when \ T \le Topt$$
$$= e^{-KTg2\cdot(Topt-T)^2} \quad when \ T > Topt \tag{21}$$

in which

T = temperature (°C)

Topt = optimal temperature for algal growth (°C)

KTg1 = effect of temperature below Topt on growth ($°C^{-2}$)

KTg2 = effect of temperature above Topt on growth ($°C^{-2}$)

Combining effects of light, nutrients, and temperature

Phytoplankton models which consider multiple nutrients commonly invoke Leibig's "law of the minimum" (Odum 1971) so that the nutrient limitation on growth is determined by the single most limiting nutrient (Ambrose et al. 1991, Cerco and Cole 1994, Cole and Buchak 1995). This logic is not always extended to incorporate the light limitation, however. Often, the nutrient limitation is multiplied by the light limit (Di Toro et al. 1971, Ambrose et al. 1991). As an alternative, Leibig's law can be extended to include light so that growth limitation is determined by the minimum of light or one of two nutrients. At present, models that functionally combine the effects of light and a single nutrient have been presented (Laws and Chalup 1990; Cloern et al. 1995) but no unifying theory for the effects of light and multiple nutrients exists. In the absence of this theory, extension of Leibig's law to include light seems most rational. That is, it takes a fixed ratio of nutrients and photons to produce a unit of carbon. Production will be limited by whichever one of these is most limiting. Thus, algal production is modeled:

$$P = P\max \cdot f(T)$$
$$\cdot minimum\left(\frac{NH_4 + NO_3}{KHn + NH_4 + NO_3}, \frac{PO_4d}{KHp + PO_4d}, \frac{1}{\sqrt{I^2 + Ik^2}}\right) \tag{22}$$

in which

NH_4 = ammonium concentration (g N m^{-3})

NO_3 = nitrate concentration (g N m^{-3})

KHn = half-saturation concentration for nitrogen uptake (g N m^{-3})

PO_4d = dissolved phosphate concentration (g P m^{-3})

KHp = half-saturation concentration for phosphorus uptake (g P m^{-3})

Basal metabolism

Basal metabolism is considered to be an exponentially increasing function (Figure 38) of temperature:

$$BM = BMr \cdot e^{KTb \cdot (T-Tr)} \tag{23}$$

in which

BMr = metabolic rate at Tr (d^{-1})

KTb = effect of temperature on metabolism ($°C^{-1}$)

Tr = reference temperature for metabolism (°C)

Predation

Predation is modeled by assuming zooplankton and other predators clear a specific volume of water per unit biomass:

$$PR = F \cdot B \cdot Z \tag{24}$$

in which

F = filtration rate (m^3 g^{-1} zooplankton C day^{-1})

Z = zooplankton biomass (g C m^{-3})

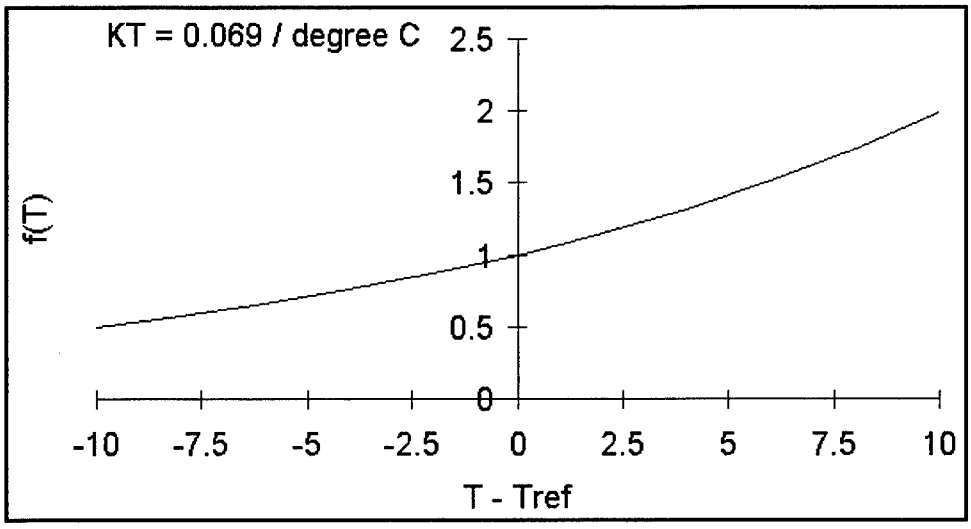

Figure 38. Relation of algal metabolism to temperature

Absent an explicit zooplankton model, specification of the spatial and temporal distribution of the predator population is impossible. One approach is to assume zooplankton biomass is proportional to algal biomass, $Z = \gamma B$, in which case Equation 24 can be rewritten:

$$PR = \gamma \cdot F \cdot B^2 \tag{25}$$

Since neither γ nor F are known precisely, the logical approach is to combine their product into a single unknown, Phtl, determined during the model calibration procedure. Effect of temperature on predation is represented with the same formulation as the effect of temperature on respiration.

Effect of algae on phosphorus

Model phosphorus state variables include total phosphate (dissolved, sorbed, and algal), dissolved organic phosphorus, labile particulate organic phosphorus, and refractory particulate organic phosphorus. The amount of phosphorus incorporated in algal biomass is quantified through a stoichiometric ratio. Thus, total phosphorus in the model is expressed

$$TotP = PO_4d + PO_4p + Apc \cdot B + DOP + LPOP + RPOP \tag{26}$$

in which

TotP = total phosphorus (g P m^{-3})

PO_4d = dissolved phosphate (g P m^{-3})

Apc = algal phosphorus-to-carbon ratio (g P g^{-1} C)

PO_4p = particulate inorganic phosphate (g P m^{-3})

DOP = dissolved organic phosphorus (g P m^{-3})

LPOP = labile particulate organic phosphorus (g P m^{-3})

RPOP = refractory particulate organic phosphorus (g P m^{-3})

Algae take up dissolved phosphate during production and release dissolved phosphate and organic phosphorus through respiration. The division of respired phosphorus into mineral and organic fractions is determined by empirical distribution coefficients. A second set of distribution coefficients determines the fate of algal phosphorus lost through predation.

Effect of algae on nitrogen

Model nitrogen state variables include ammonium, nitrate, dissolved organic nitrogen, labile particulate organic nitrogen, and refractory particulate organic nitrogen. The amount of nitrogen incorporated in algal biomass is quantified through a stoichiometric ratio. Thus, total nitrogen in the model is expressed as

$$TotN = NH_4 + NO_3 + Anc \cdot B + DON + LPON + RPON \quad (27)$$

where

TotN = total nitrogen (g N m^{-3})

NH_4 = ammonium (g N m^{-3})

NO_3 = nitrate (g N m^{-3})

Anc = algal nitrogen-to-carbon ratio (g N g^{-1} C)

DON = dissolved organic nitrogen (g N m^{-3})

LPON = labile particulate organic nitrogen (g N m^{-3})

RPON = refractory particulate organic nitrogen (g N m^{-3})

Algae take up ammonium and nitrate during production and release ammonium and organic nitrogen through respiration. Nitrate is internally reduced to ammonium before synthesis into biomass occurs (Parsons et al. 1984). Trace concentrations of ammonium inhibit nitrate reduction so that, in the presence of ammonium and nitrate, ammonium is utilized first. The "preference" of algae for ammonium is expressed by an empirical function (Thomann and Fitzpatrick 1982) with two limiting values (Figure 39). When nitrate is absent, the preference for ammonium is unity. When ammonium is absent, the preference is zero. In the presence of ammonium and nitrate, the preference depends on the abundance of both forms relative to the half-saturation constant for nitrogen uptake. When both ammonium and nitrate are abundant, the preference for ammonium approaches unity. When ammonium is scarce but nitrate is abundant, the preference decreases in magnitude and a significant fraction of algal nitrogen requirement comes from nitrate.

As with phosphorus, the fate of algal nitrogen released by metabolism and predation is represented by distribution coefficients.

Organic Carbon

Organic carbon undergoes innumerable transformations in the water column. The model carbon cycle (Figure 40) consists of the following elements:

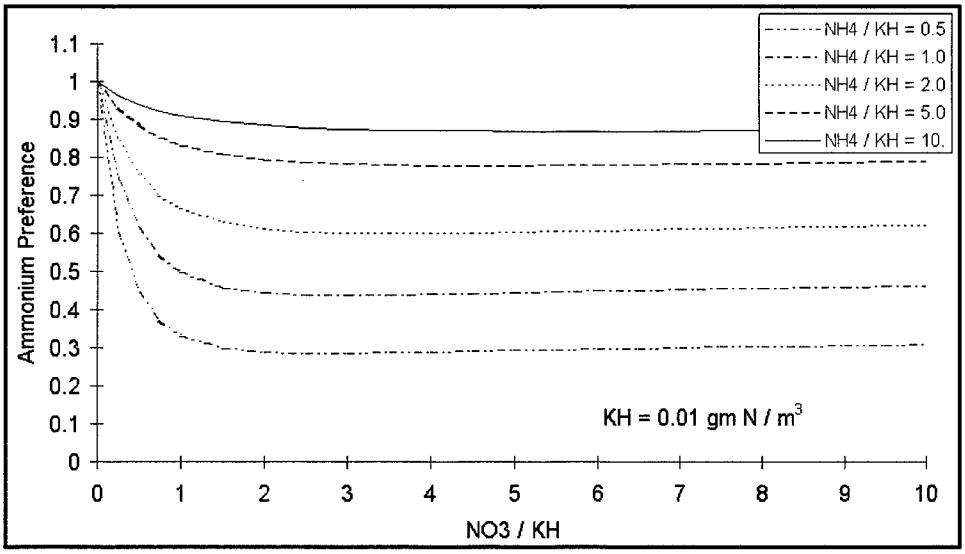

Figure 39. Algal ammonium preference

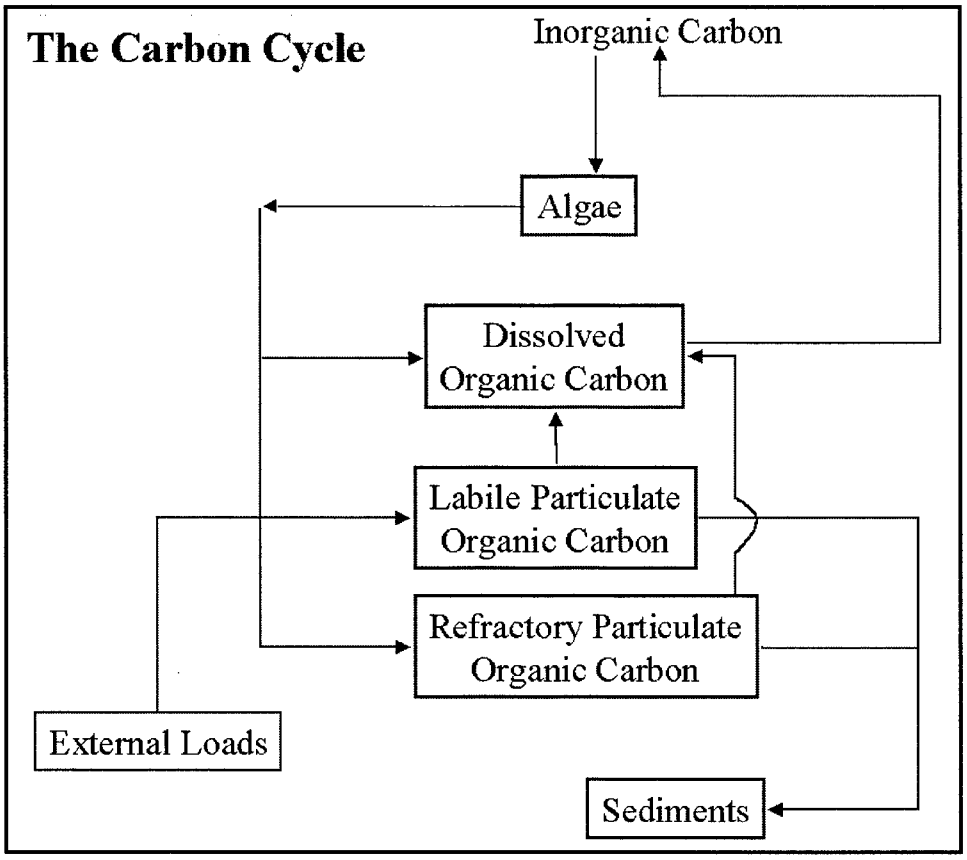

Figure 40. Model carbon cycle

Phytoplankton production
Phytoplankton exudation
Predation on phytoplankton
Dissolution of particulate carbon
Heterotrophic respiration
Settling and resuspension

Algal production is the primary carbon source although carbon also enters the system through external loading. Predation on algae releases particulate and dissolved organic carbon to the water column. A fraction of the particulate organic carbon undergoes first-order dissolution to dissolved organic carbon. Dissolved organic carbon produced by phytoplankton exudation, by predation, and by dissolution is respired at a first-order rate to inorganic carbon. Particulate organic carbon which does not undergo dissolution settles to the bottom sediments. A portion of this material may be later resuspended by wind action.

Dissolved organic carbon

The complete representation of dissolved organic carbon sources and sinks in the model ecosystem is

$$\frac{\delta}{\delta t} DOC = FCDP \cdot PR + Klpoc \cdot LPOC + Krpoc \cdot RPOC - Kdoc \cdot DOC + \frac{BENDOC}{H} + \frac{SAVDOC}{H} \quad (28)$$

in which

DOC = dissolved organic carbon (g m^{-3})
LPOC = labile particulate organic carbon (g m^{-3})
RPOC = refractory particulate organic carbon (g m^{-3})
FCDP = fraction of predation on algae released as DOC ($0 < FCDP < 1$)
Klpoc = dissolution rate of LPOC (d^{-1})
Krpoc = dissolution rate of RPOC (d^{-1})
Kdoc = respiration rate of DOC (d^{-1})
BENDOC = release of DOC from sediments and benthic algae (g C m^{-2} d^{-1})
SAVDOC = release of DOC from seagrass (g C m^{-2} d^{-1})

Labile particulate organic carbon

The complete representation of labile particulate organic carbon sources and sinks in the model ecosystem is

$$\frac{\delta}{\delta t} LPOC = FCLP \cdot PR - Klpoc \cdot LPOC - \frac{Wl}{H} \cdot LPOC + \frac{BENLPOC}{H} + \frac{SAVLPOC}{H} \quad (29)$$

in which

FCLP = fraction of predation on algae released as LPOC (0 < FCLP < 1)

Wl = settling velocity of labile particles (m d^{-1})

BENLPOC = resuspension of LPOC from sediments (g C m^{-2} d^{-1})

SAVLPOC = release of LPOC from seagrass (g C m^{-2} d^{-1})

Refractory particulate organic carbon

The complete representation of refractory particulate organic carbon sources and sinks in the model ecosystem is

$$\frac{\delta}{\delta t} RPOC = FCRP \cdot PR - Krpoc \cdot RPOC - \frac{Wr}{H} \cdot RPOC + \frac{BENRPOC}{H} + \frac{SAVRPOC}{H} \quad (30)$$

in which

FCRP = fraction of predation on algae released as RPOC (0 < FCRP < 1)

Wr = settling velocity of refractory particles (m d^{-1})

BENRPOC = resuspension of RPOC from sediments (g C m^{-2} d^{-1})

SAVRPOC = release of RPOC from seagrass (g C m^{-2} d^{-1})

Phosphorus

The model phosphorus cycle (Figure 41) includes the following processes:

Algal production and metabolism
Predation
Hydrolysis of particulate organic phosphorus
Mineralization of dissolved organic phosphorus
Settling and resuspension
Exchange with inorganic solids

External loads provide the ultimate source of phosphorus to the system. Dissolved phosphate is incorporated by algae during growth and released as phosphate and organic phosphorus through respiration and predation. A portion of the particulate organic phosphorus hydrolyzes to dissolved organic phosphorus. The balance settles to the sediments. Dissolved organic phosphorus is mineralized to phosphate. A portion of the phosphate sorbs to inorganic solids and settles to the sediments. Within the sediments, particulate phosphorus is mineralized and recycled to the water column as dissolved phosphate.

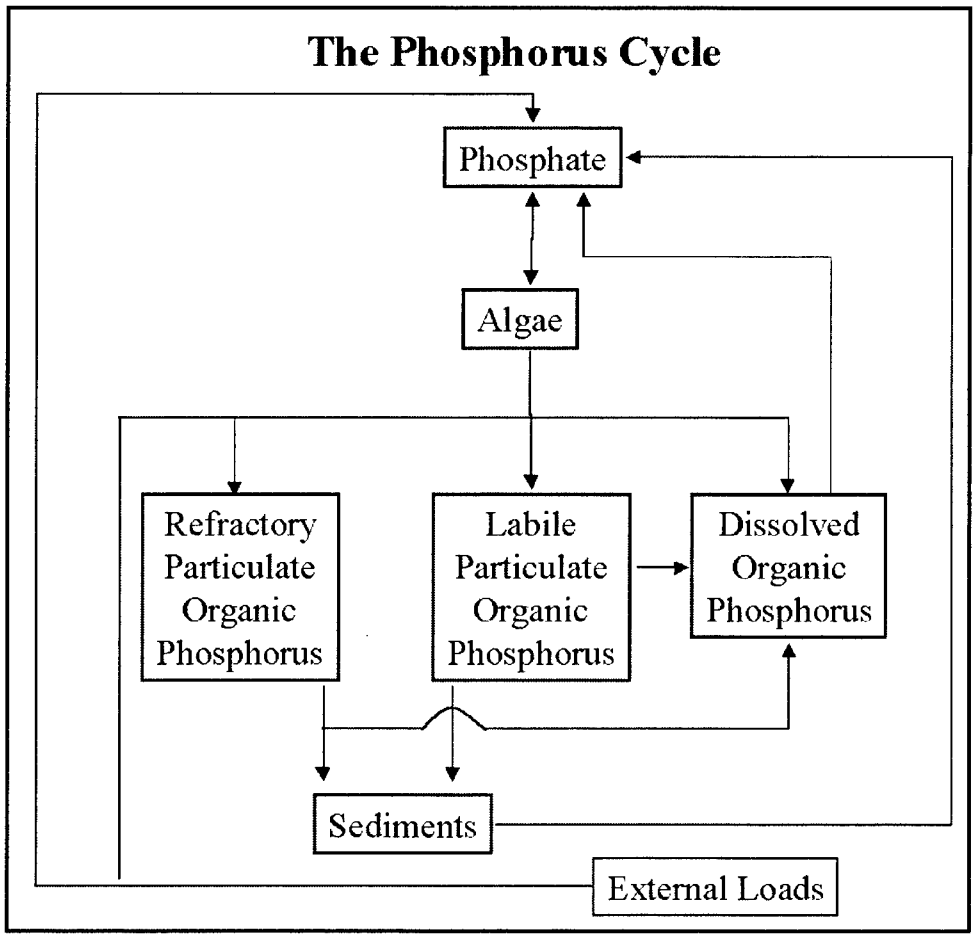

Figure 41. Model phosphorus cycle

Hydrolysis and mineralization

Within the model, hydrolysis is defined as the process by which particulate organic substances are converted to dissolved organic form. Mineralization is defined as the process by which dissolved organic substances are converted to dissolved inorganic form. Conversion of particulate organic phosphorus to phosphate proceeds through the sequence of hydrolysis and mineralization. Direct mineralization of particulate organic phosphorus does not occur.

Mineralization of organic phosphorus is mediated by the release of nucleotidase and phosphatase enzymes by bacteria (Ammerman and Azam 1985; Chrost and Overbeck 1987) and algae (Matavulj and Flint 1987; Chrost and Overbeck 1987; Boni et al. 1989). Since the algae themselves release the enzyme and since bacterial abundance is related to algal biomass, the rate of organic phosphorus mineralization is related, in the model, to algal biomass. A most remarkable property of the enzyme process is that alkaline phosphatase activity is inversely proportional to ambient phosphate concentration (Chrost and Overbeck 1987; Boni et al. 1989). Put in different terms, when phosphate is scarce, algae stimulate production of an enzyme that mineralizes organic phosphorus to phosphate. This phenomenon is simulated by relating mineralization to the algal phosphorus nutrient limitation. Mineralization is highest when algae are strongly phosphorus limited and is least when no limitation occurs.

The expression for mineralization rate is

$$Kdop = Kdp + \frac{KHp}{KHp + PO_4d} \cdot Kdpalg \cdot B \tag{31}$$

in which

Kdop = mineralization rate of dissolved organic phosphorus (d^{-1})

Kdp = minimum mineralization rate (d^{-1})

KHp = half-saturation concentration for algal phosphorus uptake ($g\ P\ m^{-3}$)

PO_4d = dissolved phosphate ($g\ P\ m^{-3}$)

Kdpalg = constant that relates mineralization to algal biomass ($m^3\ g^{-1}\ C\ d^{-1}$)

Potential effects of algal biomass and nutrient limitation on the mineralization rate are shown in Figure 42. When nutrient concentration greatly exceeds the half-saturation concentration for algal uptake, the rate roughly equals the minimum. Algal biomass has little influence. As nutrient becomes scarce relative to the half-saturation concentration, the rate increases. The magnitude of increase depends on algal biomass. Factor of two to three increases are feasible.

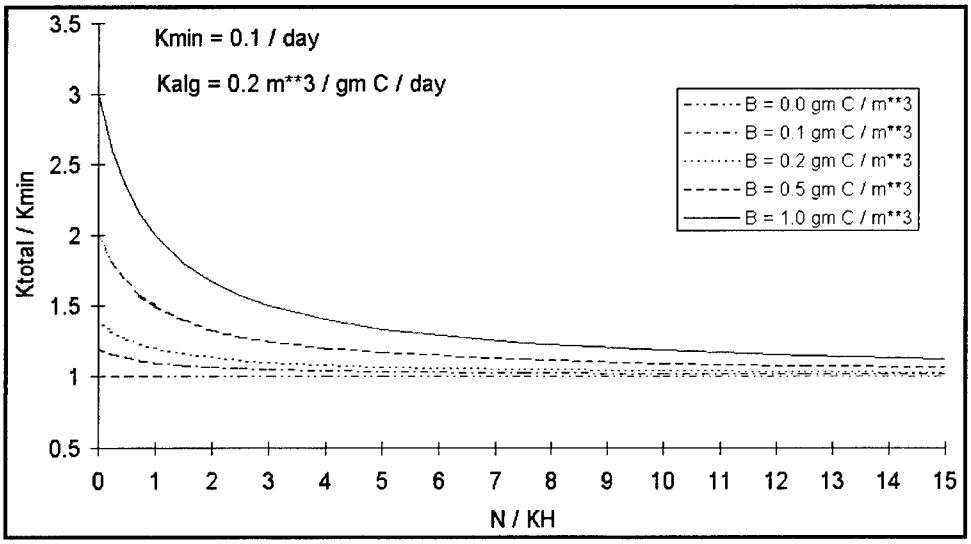

Figure 42. Effect of algal biomass and nutrient concentration on phosphorus mineralization

An exponential function (Figure 37) relates mineralization and hydrolysis rates to temperature.

The total phosphate system

The model phosphate state variable is defined as the sum of dissolved phosphate, sorbed phosphate, and algal phosphorus content:

$$PO_4t = PO_4d + PO_4p + PO_4a \tag{32}$$

in which

PO_4t = total phosphate (g P m^{-3})

PO_4d = dissolved phosphate (g P m^{-3})

PO_4p = particulate (sorbed) phosphate (g P m^{-3})

PO_4a = algal phosphorus (g P m^{-3})

Algal phosphorus is computed in the model as the product of algal biomass and APC, the algal phosphorus-to-carbon ratio. Particulate and dissolved fractions of total phosphate are determined by equilibrium partitioning of the non-algal fraction:

$$PO_4d = \frac{1}{1 + Kadpo4 \cdot ISS} \cdot (PO_4t - PO_4a) \tag{33}$$

and

$$PO_4p = \frac{Kadpo4 \cdot ISS}{1 + Kadpo4 \cdot ISS} \cdot (PO_4t - PO_4a) \quad (34)$$

in which

Kadpo4 = partition coefficient ($m^3\ g^{-1}$)

ISS = inorganic (fixed) solids concentration ($g\ m^{-3}$)

Mass-balance equations

Once the interactions of dissolved, particulate, and algal phosphate are made explicit, the mass balance equations for the phosphorus state variables are straightforward summations of previously described sources and sinks.

Total phosphate

$$\frac{\delta}{\delta t} PO_4t = Kdop \cdot DOP - APC \cdot \left[(1 - FPI) \cdot BM \cdot B + (1 - FPIP) \cdot PR\right] - \frac{Wa}{H} \cdot PO_4a - \frac{Wss}{H} \cdot PO_4p + \frac{BENPO4}{H} + \frac{SAVPO4}{H} \quad (35)$$

in which:

FPI = fraction of algal metabolism released as total phosphate ($0 \le FPI \le 1$)

FPIP = fraction of predation released as total phosphate ($0 \le FPIP \le 1$)

Wa = algal settling rate ($m\ d^{-1}$)

Wss = solids settling rate ($m\ d^{-1}$)

BENPO4 = sum (diagenesis + benthic algae + resuspension) of sediment water phosphorus transfer ($g\ P\ m^{-2}\ d^{-1}$)

SAVPO4 = phosphate release from seagrass ($g\ P\ m^{-2}\ d^{-1}$)

Algal uptake and release of phosphate represents an exchange of phosphate fractions rather than a phosphate source or sink. Consequently, no algal source or sink terms are included in the phosphate mass-conservation equation. The settling terms are required to represent the settling of particulate phosphate incorporated in algal biomass or sorbed to particles.

Dissolved organic phosphorus

$$\frac{\delta}{\delta t}DOP = APC \cdot (BM \cdot B \cdot FPD + PR \cdot FPDP) + Klpop \cdot LPOP + Krpop \cdot RPOP - Kdop \cdot DOP + \frac{BENDOP}{H} + \frac{SAVDOP}{H} \quad (36)$$

in which

DOP = dissolved organic phosphorus (g P m^{-3})

LPOP = labile particulate organic phosphorus (g P m^{-3})

RPOP = refractory particulate organic phosphorus (g P m^{-3})

FPD = fraction of algal metabolism released as DOP ($0 < FPD < 1$)

FPDP = fraction of predation on algae released as DOP ($0 < FPDP < 1$)

Klpop = hydrolysis rate of LPOP (d^{-1})

Krpop = hydrolysis rate of RPOP (d^{-1})

Kdop = mineralization rate of DOP (d^{-1})

BENDOP = release of DOP from sediments and benthic algae (g P m^{-2} d^{-1})

SAVDOP = release of DOP from seagrass (g P m^{-2} d^{-1})

Labile particulate organic phosphorus

$$\frac{\delta}{\delta t}LPOP = APC \cdot (BM \cdot B \cdot FPL + PR \cdot FPLP) - Klpop \cdot LPOP - \frac{Wl}{H} \cdot LPOP + \frac{BENLPOP}{H} + \frac{SAVLPOP}{H} \quad (37)$$

in which

FPL = fraction of algal metabolism released as LPOP ($0 < FPL < 1$)

FPLP = fraction of predation on algae released as LPOP ($0 < FPLP < 1$)

BENLPOP = resuspension of LPOP from sediments (g P m^{-2} d^{-1})

SAVLPOP = release of LPOP from seagrass (g P m^{-2} d^{-1})

Refractory particulate organic phosphorus

$$\frac{\delta}{\delta t} RPOP = APC \cdot (BM \cdot B \cdot FPR + PR \cdot FPRP) - Krpop \cdot RPOP - \frac{Wr}{H} \cdot RPOP + \frac{BENRPOP}{H} + \frac{SAVRPOP}{H} \quad (38)$$

in which

FPR = fraction of algal metabolism released as RPOP (0 < FPR < 1)

FPRP = fraction of predation on algae released as RPOP (0 < FPRP < 1)

BENRPOP = resuspension of RPOP from sediments (g P m^{-2} d^{-1})

SAVRPOP = release of RPOP from seagrass (g P m^{-2} d^{-1})

Nitrogen

The model nitrogen cycle (Figure 43) includes the following processes:

Algal production and metabolism
Predation
Hydrolysis of particulate organic nitrogen
Mineralization of dissolved organic nitrogen
Settling
Nitrification

External loads provide the ultimate source of nitrogen to the system. Inorganic nitrogen is incorporated by algae during growth and released as ammonium and organic nitrogen through respiration and predation. A portion of the particulate organic nitrogen hydrolyzes to dissolved organic nitrogen. The balance settles to the sediments. Dissolved organic nitrogen is mineralized to ammonium. In an oxygenated water column, a fraction of the ammonium is subsequently oxidized to nitrate through the nitrification process. Particulate nitrogen that settles to the sediments is mineralized and recycled to the water column, primarily as ammonium. Nitrate moves in both directions across the sediment-water interface, depending on relative concentrations in the water column and sediment interstices.

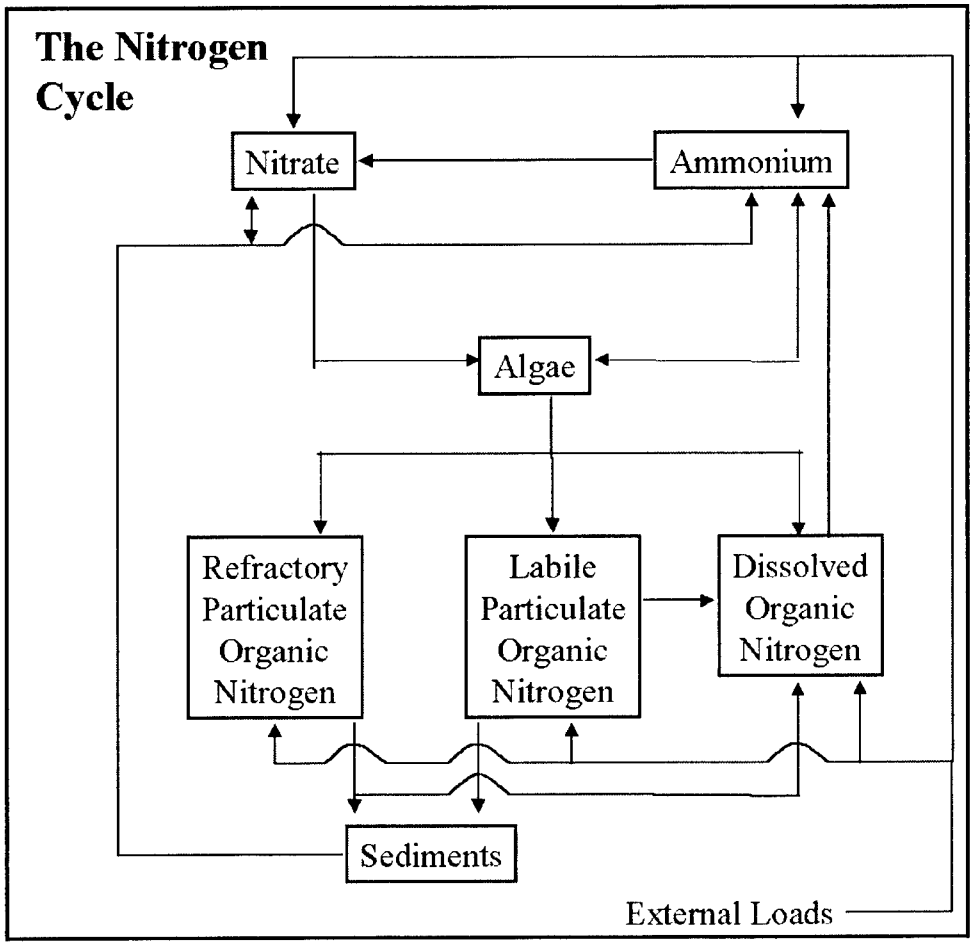

Figure 43. Model nitrogen cycle

Nitrification

Nitrification is a process mediated by specialized groups of autotrophic bacteria that obtain energy through the oxidation of ammonium to nitrite and oxidation of nitrite to nitrate. A simplified expression for complete nitrification (Tchobanoglous and Schroeder 1987) is

$$NH_4^+ + 2O_2 \rightarrow NO_3^- + H_2O + 2H^+ \quad (39)$$

The simplified stoichiometry indicates that two moles of oxygen are required to nitrify one mole of ammonium into nitrate. The simplified equation is not strictly true, however. Cell synthesis by nitrifying bacteria is accomplished by the fixation of carbon dioxide so that less than two moles of oxygen are consumed per mole of ammonium utilized (Wezernak and Gannon 1968).

The kinetics of complete nitrification are modeled as a function of available ammonium, dissolved oxygen, and temperature:

$$NT = \frac{DO}{KHont + DO} \cdot \frac{NH_4}{KHnnt + NH_4} \cdot f(T) \cdot NTm \qquad (40)$$

in which

NT = nitrification rate (g N m^{-3} d^{-1})

KHont = half-saturation constant of dissolved oxygen required for nitrification (g O_2 m^{-3})

KHnnt = half-saturation constant of NH_4 required for nitrification (g N m^{-3})

NTm = maximum nitrification rate at optimal temperature (g N m^{-3} day^{-1})

The kinetics formulation (Figure 44) incorporates the products of two "Monod" functions. The first function diminishes nitrification at low dissolved oxygen concentration. The second function expresses the influence of ammonium concentration on nitrification. When ammonium concentration is low, relative to KHnnt, nitrification is proportional to ammonium concentration. For NH4 << KHnnt, the reaction is approximately first-order. (The first-order decay constant = NTm/KHnnt.) When ammonium concentration is large, relative to KHnnt, nitrification approaches a maximum rate. This formulation is based on a concept proposed by Tuffey et al. (1974). Nitrifying bacteria adhere to benthic or suspended sediments. When ammonium is scarce, vacant surfaces suitable for nitrifying bacteria exist. As ammonium concentration increases, bacterial biomass increases, vacant surfaces are occupied, and the rate of nitrification increases. The bacterial population attains maximum density when all surfaces suitable for bacteria are occupied. At this point, nitrification proceeds at a maximum rate independent of additional increase in ammonium concentration.

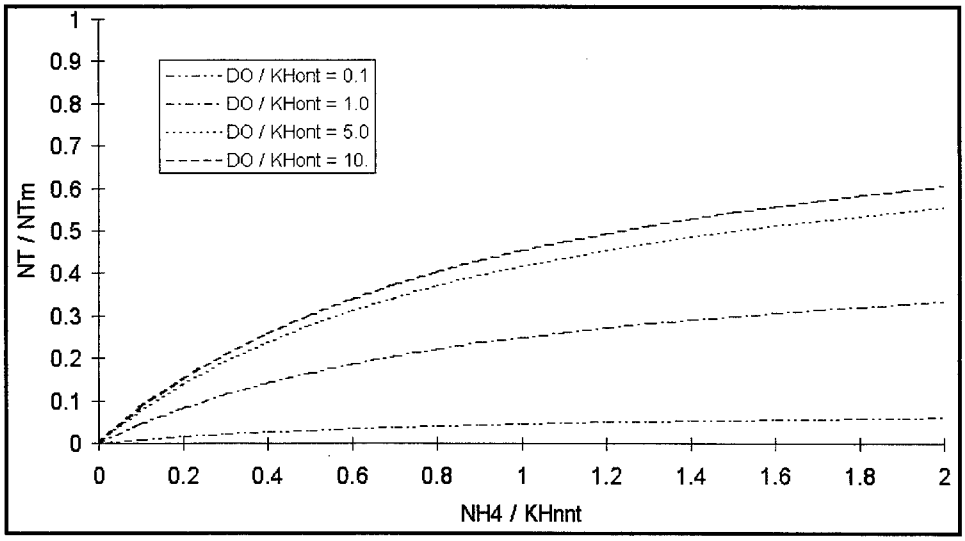

Figure 44. Effect of dissolved oxygen and ammonium concentration on nitrification rate

The optimal temperature for nitrification may be less than peak temperatures that occur in coastal waters. To allow for a decrease in nitrification at superoptimal temperature, the effect of temperature on nitrification is modeled in the Gaussian form of Equation 21.

Nitrogen mass balance equations

The mass-balance equations for nitrogen state variables are written by summing all previously-described sources and sinks:

Ammonium

$$\frac{\delta}{\delta t} NH_4 = ANC \cdot \left[(BM \cdot FNI - PN \cdot P) \cdot B + PR \cdot FNIP \right] + Kdon \cdot DON - NT + \frac{BENNH4}{H} + \frac{SAVNH4}{H} \quad (41)$$

in which

FNI = fraction of algal metabolism released as NH4 ($0 \leq FNI \leq 1$)

PN = algal ammonium preference ($0 \leq PN \leq 1$)

FNIP = fraction of predation released as NH4 ($0 \leq FNIP \leq 1$)

BENNH4 = release of ammonium from sediments and benthic algae (g N m^{-2} d^{-1})

SAVNH4 = release of ammonium from seagrass (g N m^{-2} d^{-1})

Nitrate

$$\frac{\delta}{\delta t} NO_3 = -ANC \cdot (1 - PN) \cdot P \cdot B + NT + \frac{BENNO3}{H} - \frac{SAVNH4}{H} \quad (42)$$

in which

BENNO3 = release of nitrate from sediments and benthic algae (g N m^{-2} d^{-1})

SAVNH4 = nitrate uptake by seagrass (g N m^{-2} d^{-1})

Dissolved organic nitrogen

$$\frac{\delta}{\delta t} DON = ANC \cdot \left(BM \cdot B \cdot FND + PR \cdot FNDP\right) + Klpon \cdot LPON + Krpon \cdot RPON - Kdon \cdot DON + \frac{BENDON}{H} + \frac{SAVDON}{H} \quad (43)$$

in which

DON = dissolved organic nitrogen (g P m^{-3})

LPON = labile particulate organic nitrogen (g P m^{-3})

RPON = refractory particulate organic nitrogen (g P m^{-3})

FND = fraction of algal metabolism released as DON (0 < FND < 1)

FNDP = fraction of predation on algae released as DON (0 < FNDP < 1)

Klpon = hydrolysis rate of LPON (d^{-1})

Krpon = hydrolysis rate of RPON (d^{-1})

Kdon = mineralization rate of DON (d^{-1})

BENDON = release of DON from sediments and benthic algae (g P m^{-2} d^{-1})

SAVDON = release of DON from seagrass (g P m^{-2} d^{-1})

Labile particulate organic nitrogen

$$\frac{\delta}{\delta t} LPON = ANC \cdot \left(BM \cdot B \cdot FNL + PR \cdot FNLP\right) - Klpon \cdot LPON - \frac{Wl}{H} \cdot LPON + \frac{BENLPON}{H} + \frac{SAVLPON}{H} \quad (44)$$

in which

FNL = fraction of algal metabolism released as LPON (0 < FNL < 1)

FNLP = fraction of predation on algae released as LPON (0 < FNLP < 1)

BENLPON = resuspension of LPON from sediments (g N m^{-2} d^{-1})

SAVLPON = release of LPON from seagrass (g N m^{-2} d^{-1})

Refractory particulate organic nitrogen

$$\frac{\delta}{\delta t} RPON = ANC \cdot (BM \cdot B \cdot FNR + PR \cdot FNRP) - Krpon \cdot RPON - \frac{Wr}{H} \cdot RPON + \frac{BENRPON}{H} + \frac{SAVRPON}{H} \quad (45)$$

in which

FNR = fraction of algal metabolism released as RPON (0 < FNR < 1)

FNRP = fraction of predation on algae released as RPON (0 < FNRP < 1)

BENRPON = resuspension of RPON from sediments (g N m^{-2} d^{-1})

SAVRPON = release of RPON from seagrass (g N m^{-2} d^{-1})

Chemical Oxygen Demand

Chemical oxygen demand is the concentration of reduced substances that are oxidizable through inorganic means. The source of chemical oxygen demand in saline water is sulfide released from sediments. A cycle occurs in which sulfate is reduced to sulfide in the sediments and reoxidized to sulfate in the water column. In freshwater, methane is released to the water column by the sediment model. Both sulfide and methane are quantified in units of oxygen demand and are treated with the same kinetics formulation:

$$\frac{\delta}{\delta t} COD = -\frac{DO}{KHocod + DO} \cdot Kcod \cdot COD \quad (46)$$

in which

COD = chemical oxygen demand concentration (g oxygen-equivalents m^{-3})

KHocod = half-saturation concentration of dissolved oxygen required for exertion of chemical oxygen demand (g O_2 m^{-3})

Kcod = oxidation rate of chemical oxygen demand (d^{-1})

An exponential function (Figure 37) describes the effect of temperature on exertion of chemical oxygen demand.

Dissolved Oxygen

Sources and sinks of dissolved oxygen in the water column (Figure 45) include:

Algal photosynthesis
Atmospheric reaeration
Algal respiration
Heterotrophic respiration
Nitrification
Chemical oxygen demand

Reaeration

The rate of reaeration is proportional to the dissolved oxygen deficit in model segments that form the air-water interface:

$$\frac{\delta}{\delta t} DO = \frac{Kr}{H} \cdot (DOs - DO) \tag{47}$$

in which

DO = dissolved oxygen concentration (g O^2 m^{-3})

Kr = reaeration coefficient (m d^{-1})

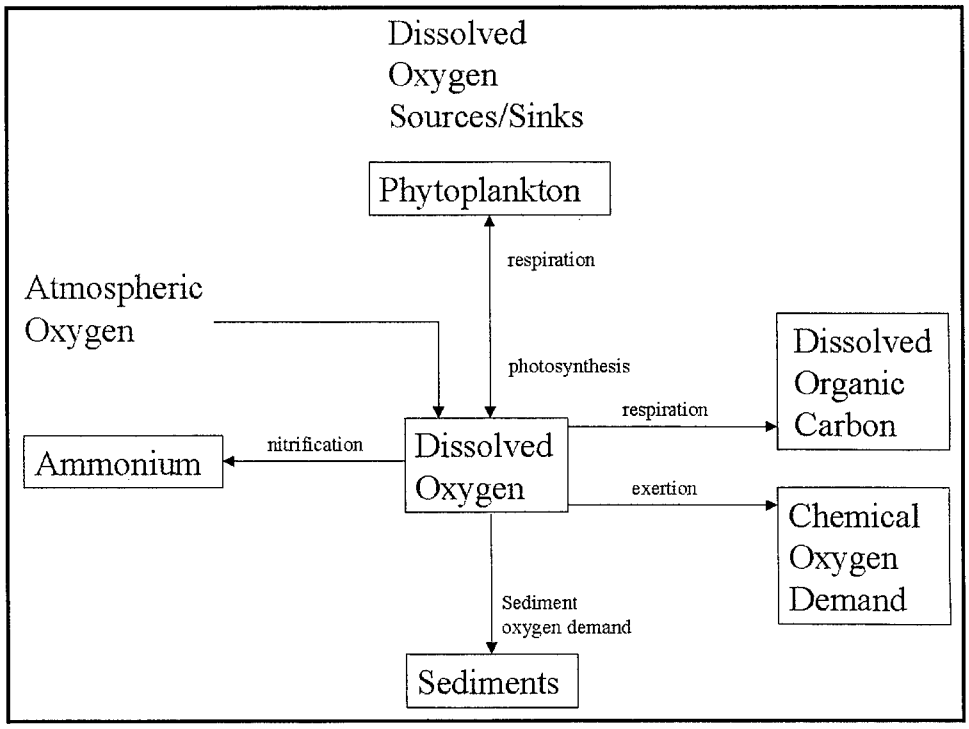

Figure 45. Dissolved oxygen sources and sinks

DOs = dissolved oxygen saturation concentration (g O_2 m^{-3})

In free-flowing streams, the reaeration coefficient depends largely on turbulence generated by bottom shear stress (O'Connor and Dobbins 1958). In lakes and coastal waters, however, wind effects may dominate the reaeration process (O'Connor 1983). For Florida Bay, a relationship for wind-driven gas exchange (Hartman and Hammond 1985) was employed:

$$Kr = 0.157 \cdot Rv \cdot Wms^{1.5} \tag{48}$$

in which

Rv = ratio of kinematic viscosity of pure water at 20 °C to kinematic viscosity of water at specified temperature and salinity

Wms = wind speed measured at 10 m above water surface (m s^{-1})

An empirical function that fits (Figure 46) tabulated values of Rv is

$$Rv = 0.54 + 0.0233 \cdot T - 0.0020 \cdot S \tag{49}$$

in which

S = salinity (ppt)

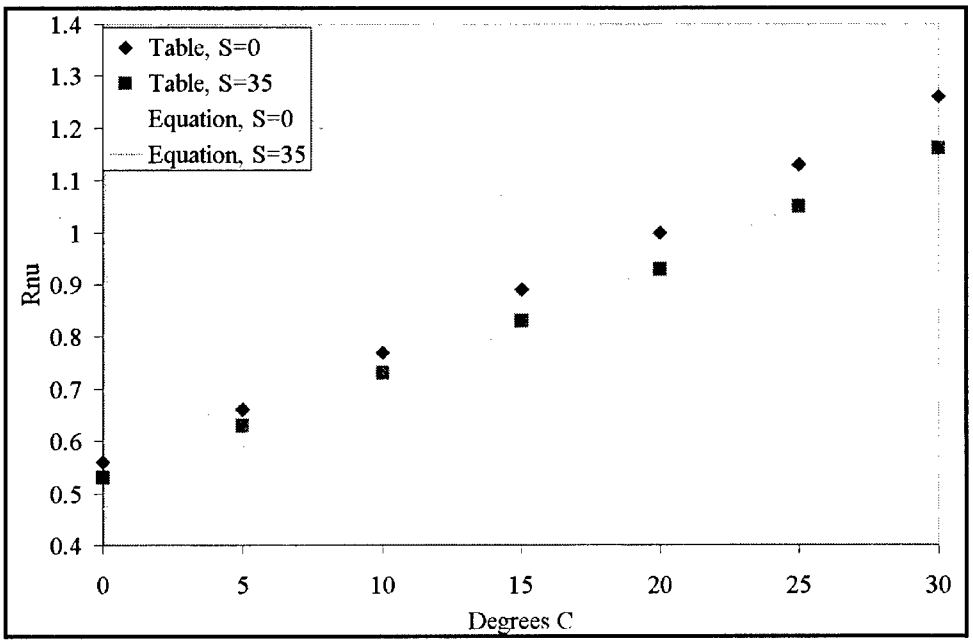

Figure 46. Computed and tabulated values of Rv

Saturation dissolved oxygen concentration diminishes as temperature and salinity increase. An empirical formula that describes these effects (Genet et al. 1974) is

$$DOs = 14.5532 - 0.38217 \cdot T + 0.0054258 \cdot T^2 - CL \cdot \left(1.665 \times 10^{-4} - 5.866 \times 10^{-6} \cdot T + 9.796 \times 10^{-8} \cdot T^2\right) \quad (50)$$

in which

CL = chloride concentration (= salinity/1.80655)

T = temperature (°C)

Mass balance equation for dissolved oxygen

$$\frac{\delta}{\delta t} DO = AOCR \cdot (P - BM) \cdot B - AONT \cdot NT - AOCR \cdot Kdoc \cdot DOC - Kcod \cdot COD + \frac{Kr}{H} \cdot (DOs - DO) + \frac{BENDO}{H} + \frac{SAVDO}{H} \quad (51)$$

in which

AOCR = oxygen-to-carbon mass ratio in production and respiration (= 2.67 g O_2 g^{-1} C)

AONT = oxygen consumed per mass ammonium nitrified (= 4.33 g O_2 g^{-1} N)

BENDO = sediment oxygen flux (g DO m^{-2} d^{-1})

SAVDO = seagrass dissolved oxygen production (g DO m^{-2} d^{-1})

Temperature

Computation of temperature employs a conservation of internal energy equation that is analogous to the conservation of mass equation. For practical purposes, the internal energy equation can be written as a conservation of temperature equation. The only source or sink of temperature considered is exchange with the atmosphere. Atmospheric exchange is considered proportional to the temperature difference between the water surface and a theoretical equilibrium temperature (Edinger et al. 1974):

$$\frac{\delta}{\delta t}T = \frac{KT}{\rho \cdot Cp \cdot H} \cdot (Te - T) \tag{52}$$

in which

T = water temperature (°C)

Te = equilibrium temperature (°C)

KT = heat exchange coefficient (watt m^{-2} $°C^{-1}$)

Cp = specific heat of water (4200 watt s kg^{-1} $°C^{-1}$)

ρ = density of water (1000 kg m^{-3})

Inorganic (Fixed) Solids

Resuspension and settling

The only internal sources and sinks of fixed solids are resuspension and settling:

$$\frac{\delta}{\delta t}ISS = -\frac{Wiss}{H} \cdot ISS + \frac{BENISS}{H} \tag{53}$$

in which

ISS = fixed solids concentration (g m^{-3})

Wiss = solids settling velocity (m d^{-1})

BENISS = resuspension rate (g m^{-2} d^{-1})

Computation of resuspension was presented in Chapter 5.

Light attenuation

Fixed solids are one component of light attenuation which is computed:

$$Kess = Keb + Kevss \cdot VSS + Keiss \cdot ISS \tag{54}$$

in which

Kess = diffuse light attenuation (m^{-1})

Keb = background light attenuation (m^{-1})

Kevss = attenuation coefficient for volatile solids ($m^2\ g^{-1}$)

VSS = volatile solids concentration ($g\ m^{-3}$)

Keiss = attenuation coefficient for fixed solids ($m^2\ g^{-1}$)

ISS = fixed solids concentration ($g\ m^{-3}$)

Volatile solids are computed from the sum of algal biomass and particulate organic carbon. These state variables, as carbon, are converted to solids using a ratio 2.5 g solids g^{-1} C (assuming organic matter is composed of carbon, hydrogen, and oxygen in the atomic ratio 1:2:1). Attenuation by phytoplankton chlorophyll is taken into account in the parameter that relates attenuation to volatile solids.

Salinity

Salinity is modeled by the conservation of mass equation with no internal sources or sinks.

Parameter Values

Model parameter evaluation is a recursive process. Parameters are selected from a range of feasible values, tested in the model, and adjusted until satisfactory agreement between predicted and observed variables is obtained. Ideally, the range of feasible values is determined by observation or experiment. For some parameters, however, no observations are available. Then, the feasible range is determined by parameter values employed in similar models or by the judgment of the modeler. For Florida Bay, an initial parameter set was adapted from the Chesapeake Bay study (Cerco and Cole 1994), the most extensive model application to date. Parameter values were adjusted, where appropriate, for the subtropical environment. Subsequent adjustment was performed to improve agreement between model and observations. A complete set of parameter values is provided in Table 16.

Table 16
Parameters In Kinetics Equations

Symbol	Definition	Value	Units
ANC	nitrogen-to-carbon ratio of algae	0.175	g N g^{-1} C
AOCR	dissolved oxygen-to-carbon ratio in respiration	2.67	g O_2 g^{-1} C
AONT	mass dissolved oxygen consumed per mass ammonium nitrified	4.33	g O_2 g^{-1} N
APC	algal phosphorus-to-carbon ratio	0.0167	g P g^{-1} C
BMr	basal metabolic rate of algae at reference temperature Tr	0.1	d^{-1}
CChl	carbon-to-chlorophyll ratio of algae	75	g C mg^{-1} chl
FCDP	fraction of dissolved organic carbon produced by predation	0.25	$0 \leq FCDP \leq 1$
FCLP	fraction of labile particulate carbon produced by predation	0.5	$0 \leq FCLP \leq 1$
FCRP	fraction of refractory particulate carbon produced by predation	0.25	$0 \leq FCRP \leq 1$
FNI	fraction of inorganic nitrogen produced by metabolism of algae	0.1	$0 \leq FNI \leq 1$
FNIP	fraction of inorganic nitrogen produced by predation	0.1	$0 \leq FNIP \leq 1$
FND	fraction of dissolved organic nitrogen produced by metabolism of algae	0.5	$0 \leq FND \leq 1$
FNDP	fraction of dissolved organic nitrogen produced by predation	0.5	$0 \leq FNDP \leq 1$
FNL	fraction of labile particulate nitrogen produced by metabolism of algae	0.25	$0 \leq FNL \leq 1$
FNLP	fraction of labile particulate nitrogen produced by predation	0.25	$0 \leq FNLP \leq 1$
FNR	fraction of refractory particulate nitrogen produced by metabolism of algae	0.15	$0 \leq FNR \leq 1$
FNRP	fraction of refractory particulate nitrogen produced by predation	0.15	$0 \leq FNRP \leq 1$
FPD	fraction of dissolved organic phosphorus produced by metabolism by algae	0.5	$0 \leq FPD \leq 1$
FPDP	fraction of dissolved organic phosphorus produced by predation	0.4	$0 \leq FPDP \leq 1$
FPL	fraction of labile particulate phosphorus produced by metabolism of algae	0.0	$0 \leq FPL \leq 1$
FPLP	fraction of labile particulate phosphorus produced by predation	0.07	$0 \leq FPLP \leq 1$
FPR	fraction of refractory particulate phosphorus produced by metabolism of algae	0.0	$0 \leq FPR \leq 1$
FPRP	fraction of refractory particulate phosphorus produced by predation	0.03	$0 \leq FPRP \leq 1$
Kadpo4	partition coefficient of sorbed vs. dissolved phosphate	0.2	m^3 g^{-1}
Kcod	oxidation rate of chemical oxygen demand	20	d^{-1}

(Sheet 1 of 3)

Table 16 (Continued)

Symbol	Definition	Value	Units
Kdoc	dissolved organic carbon respiration rate	0.01	d^{-1}
Kdon	dissolved organic nitrogen mineralization rate	0.01	d^{-1}
Kdp	minimum mineralization rate of dissolved organic phosphorus	0.2	d^{-1}
Kdpalg	constant that relates mineralization rate to algal biomass	0.2	$m^3 g^{-1} C d^{-1}$
Keb	background light attenuation	0.13	m^{-1}
Keiss	light attenuation coefficient for fixed solids	0.085	$m^2 g^{-1}$
Kevss	light attenuation coefficient for volatile solids	0.085	$m^2 g^{-1}$
KHn	half-saturation concentration for nitrogen uptake by algae	0.03	$g N m^{-3}$
KHnnt	half-saturation concentration of NH_4 required for nitrification	1.0	$g N m^{-3}$
KHocod	half-saturation concentration of dissolved oxygen required for exertion of COD	0.5	$g O_2 m^{-3}$
KHodoc	half-saturation concentration of dissolved oxygen required for oxic respiration	0.5	$g O_2 m^{-3}$
KHont	half-saturation concentration of dissolved oxygen required for nitrification	3.0	$g O_2 m^{-3}$
KHp	half-saturation concentration for phosphorus uptake by algae	0.005	$g P m^{-3}$
Klpoc	labile particulate organic carbon dissolution rate	0.02	d^{-1}
Klpon	labile particulate organic nitrogen hydrolysis rate	0.03	d^{-1}
Klpop	labile particulate organic phosphorus hydrolysis rate	0.12	d^{-1}
Krpoc	refractory particulate organic carbon dissolution rate	0.005	d^{-1}
Krpon	refractory particulate organic nitrogen hydrolysis rate	0.005	d^{-1}
Krpop	refractory particulate organic phosphorus hydrolysis rate	0.005	d^{-1}
KTb	effect of temperature on basal metabolism of algae	0.0322	$°C^{-1}$
KTg1	effect of temperature below Tm on growth of algae	0.004	$°C^{-2}$
KTg2	effect of temperature above Tm on growth of algae	0.012	$°C^{-2}$
KThdr	constant that relates hydrolysis rates to temperature	0.069	$°C^{-1}$
KTmnl	constant that relates mineralization rates to temperature	0.069	$°C^{-1}$
KTnt1	effect of temperature below Tmnt on nitrification	0.003	$°C^{-2}$
KTnt2	effect of temperature above Tmnt on nitrification	0.003	$°C^{-2}$
NTm	maximum nitrification rate at optimal temperature	0.01	$g N m^{-3} d^{-1}$
Phtl	predation rate on algae	0.02	$m^3 g^{-1} C d^{-1}$

(Sheet 2 of 3)

Table 16 (Concluded)

Symbol	Definition	Value	Units
Pmax	production rate of algae under optimal conditions	300	g C g^{-1} Chl d^{-1}
Topt	optimal temperature for growth of algae	25	°C
Tmnt	optimal temperature for nitrification	30	°C
Tr	reference temperature for metabolism	20	°C
Trhdr	reference temperature for hydrolysis	20	°C3
Trmnl	reference temperature for mineralization	20	°C
Wa	algal settling rate	0.01	m d^{-1}
Wl	settling velocity of labile particles	0.03	m d^{-1}
Wr	settling velocity of refractory particles	0.03	m d^{-1}
Wss	settling velocity of fixed solids	0.03	m d^{-1}
α	initial slope of production vs. irradiance relationship	5.0	g C g^{-1} Chl (E m^{-2})$^{-1}$

(Sheet 3 of 3)

7 The Seagrass Model

Introduction

Three components are required to make up a system-wide seagrass model. The first is a unit-level model of a plant. The second is an environmental model that provides light, temperature, nutrient concentrations, and other forcing functions to the plant component. The third is a coupling algorithm that links the system-wide environmental model to the local-scale plant model. The environmental model was described in Chapter 6. In this chapter, the unit model, the coupling between the unit model and the environmental model, and parameters employed in the unit model are described.

The Seagrass Unit Model

The seagrass unit model (Figure 47) incorporates two state variables: shoots (above-ground biomass) and roots (below-ground biomass). Shoots exchange nutrients with the water-column component of the eutrophication model while roots exchange nutrients with the diagenetic sediment component (Chapter 8). Light available to the shoots is computed via a series of sequential attenuations by color, fixed and organic solids in the water column, epiphytes, and self-shading. The selection of state variables and the basic principles of the model are based on principles established by Wetzel and Neckles (1986) and Madden and Kemp (1996).

Shoots

The governing equation for shoots establishes a balance between sources and sinks of above-ground biomass:

$$\frac{dSH}{dt} = \left(Fleaf \cdot P - Rsh\right) \cdot SH + Trrs \qquad (55)$$

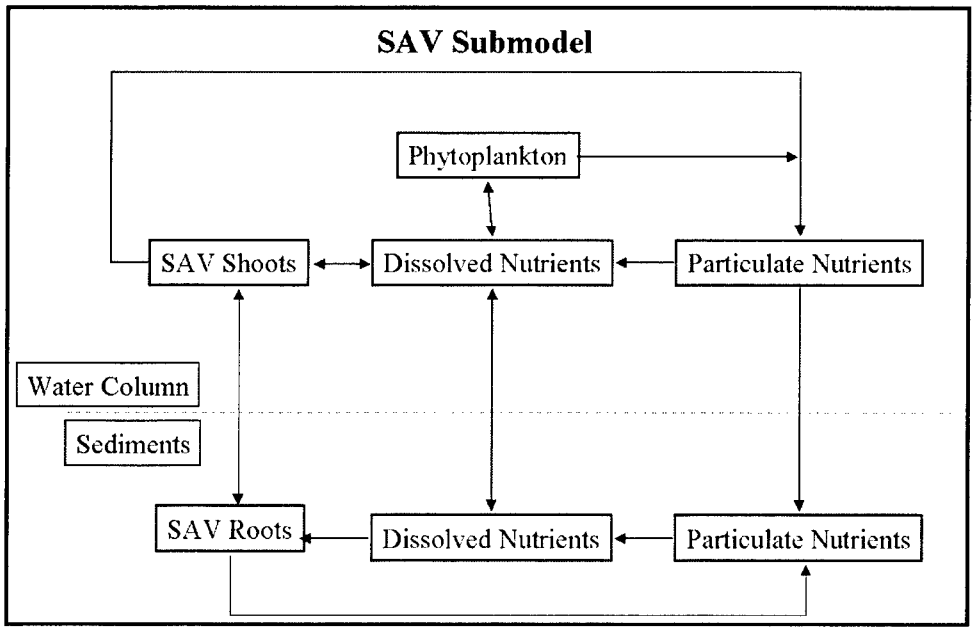

Figure 47. Seagrass model state variables (boxes) and mass flows (arrows)

in which

SH = shoot biomass (g C m^{-2})

Fleaf = photosynthetic fraction of above-ground biomass ($0 \leq Fleaf \leq 1$)

P = specific production (d^{-1})

Rsh = shoot respiration (d^{-1})

Trrs = carbon transport from root to shoot (g C m^{-2} d^{-1})

Production is computed as the product of a specified maximum rate (a function of temperature) and a limiting factor. The limiting factor is the minimum of independently evaluated light, nitrogen, and phosphorus limitations. Light limitation is represented as a rectangular hyperbola.

$$f(I) = \frac{Ish}{Ish + Ik} \tag{56}$$

in which

f(I) = light limitation

Ish = irradiance at leaf surface (E m^{-2} day^{-1})

Parameter Ik is derived from two specified parameters.

$$Ik = \frac{P\max(T)}{\alpha} \tag{57}$$

in which

Pmax = maximum production as a function of temperature ($g\ C\ g^{-1}\ DW\ d^{-1}$)

α = initial slope of production versus irradiance curve ($g\ C\ g^{-1}\ DW\ (E\ m^{-2})^{-1}$)

Nutrient limitations for nitrogen and phosphorus are evaluated using a formula (Madden and Kemp 1996) that combines individual Monod-like functions for the roots and shoots.

$$f(N) = \frac{Nw + K^* \cdot Ns}{Khw + Nw + K^* \cdot Ns} \tag{58}$$

in which

f(N) = nutrient limitation

Nw = nutrient concentration ($g\ m^{-3}$) in water column

Ns = nutrient concentration ($g\ m^{-3}$) in sediment pore water

Khw = half-saturation concentration for nutrient uptake by shoots ($g\ m^{-3}$)

Khs = half-saturation concentration for nutrient uptake by roots ($g\ m^{-3}$)

K^* = Khw / Khs

Specific production, P, is obtained from maximum production, Pmax, through division by parameter Acdw, the plant carbon-to-dry weight ratio.

The dependence of production on temperature is a Gaussian curve that identifies a temperature of maximum production and declines at higher and lower temperatures (Equation 21; Figure 37). An exponential function (Equation 23; Figure 38) describes the dependence of respiration on temperature.

Roots

The governing equation for roots establishes a balance between sources and sinks of below-ground biomass

$$\frac{d\,RT}{dt} = -Rrt \cdot RT - Trrs \tag{59}$$

in which

Rrt = root respiration (d^{-1})

Root - shoot material exchange

Carbon is produced by photosynthesis in seagrass leaves. A portion of this carbon is transferred to the below-ground roots and rhizomes. During growth spurts or periods of environmental stress, biomass from below ground can be transferred back to the leaves and shoots. Mechanistic computation of these transfers requires detailed modeling of plant physiology and the response of plants to the environment. A simpler approach is adopted here. The proportion of plant biomass in shoots and roots is specified, on a time-varying basis, based on observations. Material exchanges between above- and below-ground biomass are computed to maintain the specified distribution.

$$\begin{aligned} &If \frac{SH}{RT} > SRobs \quad then \quad Trrs = -Ktrrs \cdot SH \\ &\qquad\qquad\qquad\quad else \quad Trrs = Ktrrs \cdot RT \end{aligned} \tag{60}$$

in which

SRobs = observed ratio of above- to below-ground biomass

Ktrrs = transfer rate between above- and below-ground biomass (d^{-1})

Seagrass composition and nutrient cycling

A fundamental assumption of the model is that plants have uniform, constant composition. Nitrogen and phosphorus in plant biomass are quantified as fractions of the carbonaceous biomass. Nutrients are taken up in stoichiometric relation to net production. Proportions removed from the water column and sediments are determined by the relative nutrient limits in each pool. Respiration returns appropriate quantities of nutrients to the sediments and water column.

The Light Field

A conceptual model has been long-established in which light reaching seagrass shoots is first attenuated by dissolved and particulate matter in the water column and next by epiphytic material (e.g. Kemp et al. 1983). No consensus exists for the representation of self-shading by shoots. One approach is to incorporate density-limiting functions into the model that simulate both self-shading and space limitations (Wetzel and Neckles 1986; Madden and Kemp 1996). A second approach, adopted here, explicitly considers self-shading.

Light available to seagrass shoots is computed through a series of sequential attenuations. First, light at the top of the canopy is computed

$$Ic = Io \cdot e^{-(Kw+Ki \cdot ISS+Kv \cdot Vss)Ztc} \tag{61}$$

in which

Ic = light at the canopy top (E m^{-2} day^{-1})

Io = light at water surface (E m^{-2} day^{-1})

Kw = attenuation due to color (m^{-1})

Ki = attenuation coefficient for fixed solids (m^2 g^{-1})

ISS = fixed solids concentration (g m^{-3})

Kv = attenuation coefficient for volatile solids (m^2 g^{-1})

VSS = volatile solids concentration (g m^{-3})

Ztc = depth to canopy (m)

Next, mean light within the canopy is evaluated. Assuming that attenuation by shoots follows an exponential relationship analogous to Equation 61 (Titus and Adams 1979), the mean light field within the canopy is

$$Iwc = \frac{Ic}{Ksh \cdot SH} \cdot \left(1 - e^{-Ksh \cdot SH}\right) \tag{62}$$

in which

Iwc = mean light within the canopy (E m^{-2} day^{-1})

Ksh = attenuation by seagrass shoots (m^2 g^{-1} C)

Although epiphyte accumulation in several systems has been related to nutrient concentration (Twilley et al. 1985; Borum 1985), only a weak relationship has been observed in Florida Bay (Frankovich and Fourqurean 1997). Furthermore, only a small fraction of the epiphytic material on Florida Bay seagrass is viable algae (Frankovich and Fourqurean 1997).

Consequently, a fully predictive model of autotrophic epiphytes is not required for Florida Bay. Instead, a constant epiphyte biomass is specified based on observations. Light reaching the shoots through the epiphyte layer is computed

$$Ish = Iwc \cdot e^{-Kep \cdot Acla \cdot EP} \tag{63}$$

in which

Ish = light available to shoots (E m^{-2} day^{-1})

Kep = attenuation by epiphytes (m^2 leaf surface g^{-1} DW)

Acla = shoot biomass-to-surface-area ratio (g shoot C m^{-2} shoot surface)

EP = epiphyte density (g DW g^{-1} shoot C)

From the Unit to the System

The Florida Bay model operates by dividing the continuum of the bay into a grid of discrete cells. In the present grid, the surface plane of the bay and adjacent waters is sectioned into 1060 cells with a length scale of 2 to 3 km. The major problem in coupling the system-wide model with the unit model is the difference in scales represented by the two models. The minimum scale represented by the bay model is on the order of kilometers while the scale on which seagrass is distributed is orders of magnitude smaller. A scaling factor, patchiness, is employed to relate biomass on the unit level to abundance on the grid scale. Abundance within each cell is then

$$M = SH \cdot A \cdot P \tag{64}$$

in which

M = above-ground abundance (g C)

A = cell surface area (m^2)

P = patchiness ($0 \leq P \leq 1$)

An identical relationship defines below-ground abundance.

The relationship of shoot (and root) biomass to abundance allowed uptake and release of materials by plants on a unit area basis to be converted to a mass basis for employment in the mass-balance equation applied to each cell (Chapter 6).

Selection of Species

Six seagrass species are commonly found in south Florida (Fourqurean et al. in press). From these, three dominant species were selected for the model: *Thalassia testudinum*, *Syringodium filiforme*, and *Halodule wrightii*. Although these species coexist, each has properties which yield a competitive advantage in specific environments (Fourqurean 1992). *Halodule* has a high growth rate which yields an advantage in colonizing unvegetated areas. Its high requirement for phosphorus, however, limits its distribution to regions and periods when phosphorus is readily available. *Thalassia* requires more light but less phosphorus than *Halodule*. In shallow environments, *Thalassia* will succeed *Halodule* as available sediment phosphorus becomes sequestered in plant material. *Syringodium* has a higher ratio of photosynthetic material to plant biomass than *Thalassia*. Consequently, *Syringodium* requires less light than *Thalassia* and the median depth at which *Syringodium* occurs is greater than *Thalassia*.

Model Parameters

Parameters for photosynthesis, respiration, biomass distribution, and composition (Table 17) were obtained from Fourqurean (1992). For some parameters, small adjustments were made to improve model fit or to adjust reported parameters to model reference temperatures. Fourqurean divided plants into four fractions: leaf, short shoot, rhizome, and root. The model considers only two fractions: shoots and roots. In determining parameters, biomass-weighted values for leaf and short shoot were employed for model shoots. Biomass-weighted values for rhizome and root were employed for model roots.

Table 17
Seagrass Production, Respiration, Biomass, and Composition

Parameter	Definition	Thalassia	Syringodium	Halodule	Units
Pmax	maximum production at optimum temperature	0.115	0.088	0.212	g C g^{-1} DW d^{-1}
α	initial slope of Pvsl curve	0.0030	0.0040	0.0044	g C g^{-1} DW $(E\ m^{-2})^{-1}$
Fleaf	photosynthetic fraction of above-ground biomass	0.30	0.75	0.77	
Rsh	shoot respiration	0.0048	0.0100	0.025	d^{-1}
Rrt	root respiration	0.0027	0.0036	0.006	d^{-1}
SRobs	shoot-to-root biomass ratio	1.42	0.58	0.77	
Andw	nitrogen-to-dry-weight ratio	0.022	0.022	0.027	g N g^{-1} DW
Apdw	phosphorus-to-dry-weight ratio	0.0009	0.0009	0.002	g P g^{-1} DW

Canopy height was taken as the median of measures conducted in the Indian River lagoon.[1] Additional parameters (Table 18) were adapted from previous applications of the seagrass model (Cerco and Moore 2000) or determined during the model calibration process.

Table 18
Additional Parameters In Seagrass Model

Parameter	Definition	Thalassia	Syringodium	Halodule	Units
Hcan	canopy height	0.25	0.25	0.13	m
Acdw	carbon-to-dry-weight ratio	0.37	0.37	0.37	g C g^{-1} DW
Ktrrs	transfer rate between above- and below-ground biomass	0.05	0.05	0.05	d^{-1}
Ksh	attenuation by shoots	0.02	0.02	0.02	m^2 g^{-1} C
Kep	attenuation by epiphytes	0.1	0.1	0.1	m^2 leaf surface g^{-1} DW
EP	epiphyte density	0.4	0.4	0.4	g DW g^{-1} leaf C
Acla	shoot biomass-to-surface-area ratio	10	10	8	g shoot C m^{-2} leaf surface
Khnw	half-saturation concentration for nitrogen uptake by shoots	3.0	3.0	3.0	g N m^{-3}
Khns	half-saturation concentration for nitrogen uptake by roots	0.3	0.3	0.3	g N m^{-3}
Khpw	half-saturation concentration for phosphorus uptake by shoots	0.6	0.6	0.6	g P m^{-3}
Khps	half-saturation concentration for phosphorus uptake by roots	0.12	0.12	0.12	g P m^{-3}
Trpm	optimum temperature for production	30	30	30	°C
Trbm	reference temperature for respiration	27	27	27	°C
Ktps1	effect of suboptimal temperature on production	0.006	0.006	0.006	$°C^{-2}$
Ktps2	effect of superoptimal temperature on production	0.06	0.06	0.06	$°C^{-2}$
Ktbm	effect of temperature on respiration	0.12	0.12	0.12	$°C^{-1}$

[1] Personal communication, June 1999, Lori Morris, St. Johns River Water Management District, Palatka, FL.

Patchiness

The fraction of each model cell covered by seagrass was derived from the Braun-Blanquet abundance data (Chapter 2). The Braun-Blanquet scale consists of seven cover classes (Fourqurean et al. in press). Cover is defined as the fraction of the bottom obscured by seagrass when viewed by a diver from above.

The observed total Braun-Blanquet abundance was interpolated to provide cell-centered values for all model cells, including those in which no observations were available. Since the Braun-Blanquet scale is discrete, the interpolated values were rounded to the nearest integer, providing a cover class for each model cell. Since each cover class encompasses a range of coverage, each class was assigned a single coverage value (Table 19). Coverage for this class was equated to patchiness (Figure 48) in the cell.

Table 19
Braun-Blanquet Coverage and Patchiness

Cover Class	Description	Patchiness
0	Absent	0.0
0.1	Solitary individual ramet, less than 5% cover	0.0
0.5	Few individual ramets, less than 5% cover	0.0
1	Many individual ramets, less than 5% cover	0.025
2	5% to 25% cover	0.15
3	25% to 50% cover	0.375
4	50% to 75% cover	0.625
5	75% to 100% cover	0.875

Nitrogen fixation

The role of nitrogen fixation in the nitrogen budget of Florida Bay has not been established although nitrogen fixation by cyanobacteria has been observed (Phlips, Zeman, and Hansen 1989). Without knowledge of nitrogen fixation rates and the environmental factors that influence these rates, comprehensive representation of nitrogen fixation cannot be included in the model. Nevertheless, at least a first approximation can be included. Measurements have established that nitrogen fixation is associated with the root and shoot zones of *Thalassia* (Capone and Taylor 1980). Based on these measures, ammonium was introduced to the water column and sediments in proportion to seagrass coverage. The rates were 0.003 g N m^{-2} d^{-1} in the water and 0.011 g N m^{-2} d^{-1} in the sediments. The effective area was taken as the product of model cell surface area and seagrass patchiness. The total amounts introduced were 2300 kg N d^{-1} to the water column of Florida Bay and 8450 kg N d^{-1} to the sediments.

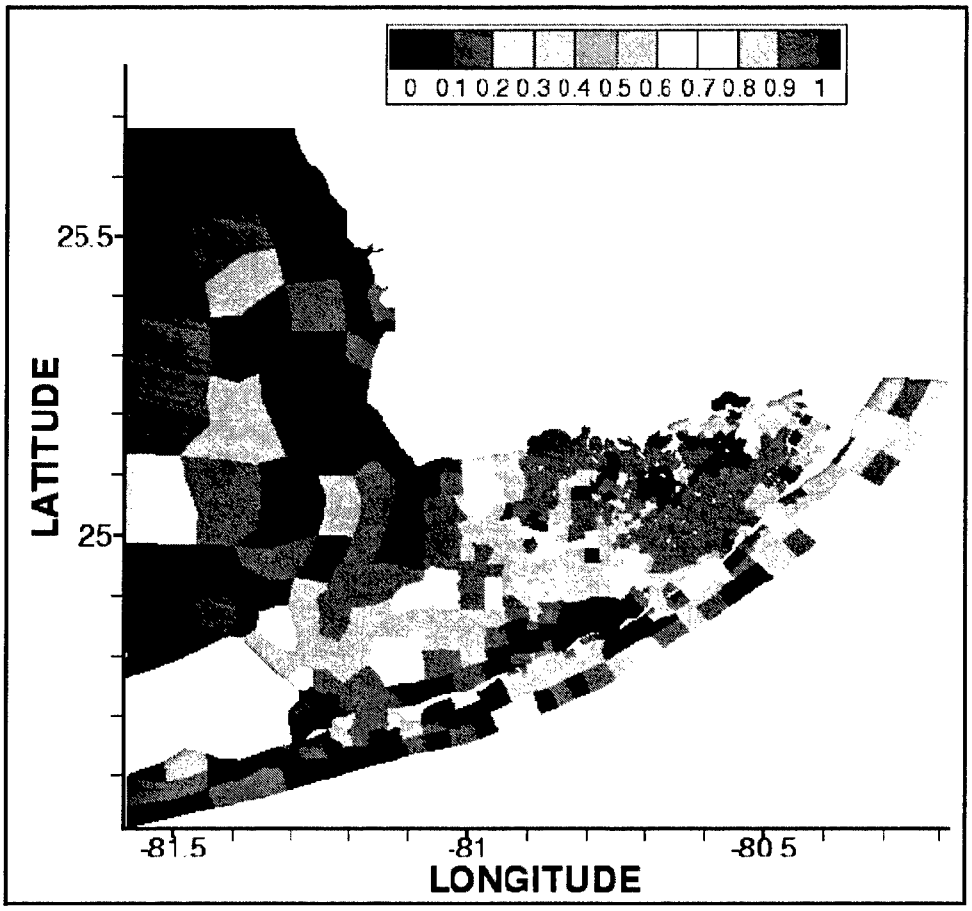

Figure 48. Seagrass coverage in model cells

8 Sediment-Water Interactions

Introduction

Representations of sediment-water interactions in Florida Bay employ three interactive submodels: a sediment diagenesis model, a benthic algae model, and a resuspension model. The diagenesis model computes the diagenesis (decay) of organic matter in the sediments, the resulting production of oxygen demand and nutrients, and the movement of diagenesis products between sediments and water column. Benthic algae occupy the sediment-water interface. They intercept nutrients released from sediments and may remove nutrients from the water column as well. The resuspension model transfers particulate carbon and nutrients from the sediments to the water column as a result of wind-driven wave action.

The Diagenesis Model

The predictive diagenetic submodel was developed as one component of the Chesapeake Bay eutrophication model study (Cerco and Cole 1994). The model (Figure 49) is driven by net settling of organic matter from the water column to the sediments. In the sediments, the model simulates the diagenesis (decay) of the organic matter. Diagenesis produces oxygen demand and inorganic nutrients. Oxygen demand, as sulfide (in saltwater) or methane (in freshwater), takes three paths out of the sediments: export to the water column as chemical oxygen demand, oxidation at the sediment-water interface as sediment oxygen demand, or burial to deep, inactive sediments. Inorganic nutrients produced by diagenesis take two paths out of the sediments: release to the water column, or burial to deep, inactive sediments.

Additional details of the model, required to understand the coupling of the sediment submodel to the model of the water column, are provided below. Complete model documentation is provided by DiToro and

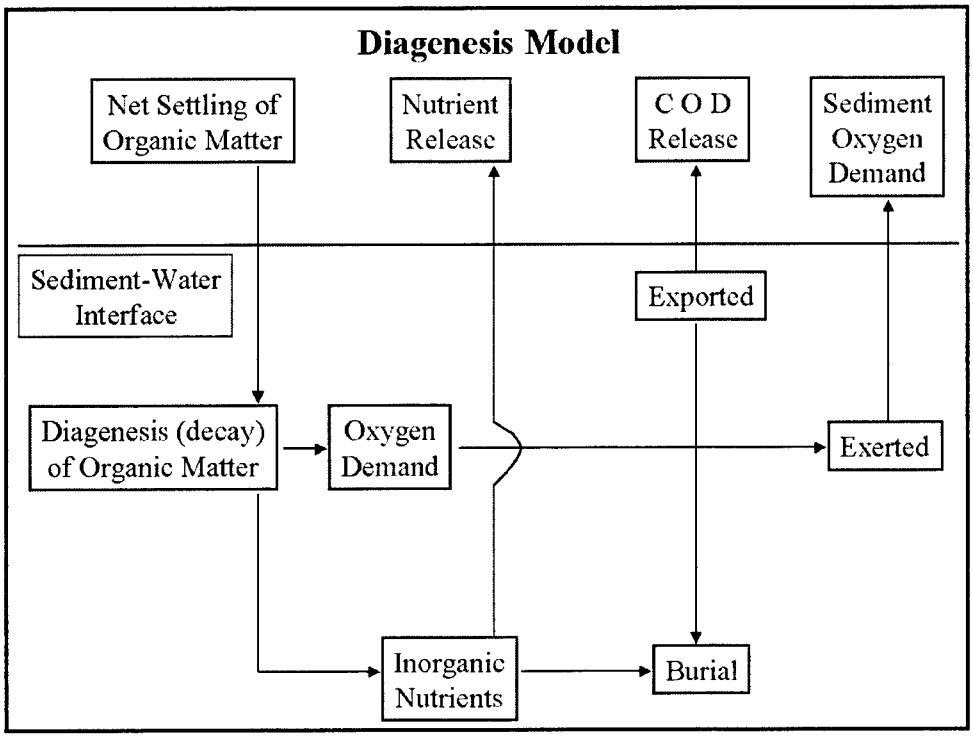

Figure 49. Diagenesis model schematic

Fitzpatrick (1993). A listing of sediment model state variables and predicted sediment-water fluxes is provided in Table 20.

Table 20
Diagenesis Model State Variables and Fluxes

State Variable	Sediment-Water Flux
Temperature	
Particulate Organic Carbon	Sediment Oxygen Demand
Sulfide/Methane	Release of Chemical Oxygen Demand
Particulate Organic Nitrogen	
Ammonium	Ammonium Flux
Nitrate	Nitrate Flux
Particulate Organic Phosphorus	
Phosphate	Phosphate Flux

Description

Benthic sediments are represented as two layers with a total depth of 10 cm (Figure 50). The 10-cm depth was specified as the approximate limit of the depth of bioturbation. The upper layer, in contact with the water column, may be oxic or anoxic depending on dissolved oxygen concentration in the water. The lower layer is permanently anoxic. The thickness of the

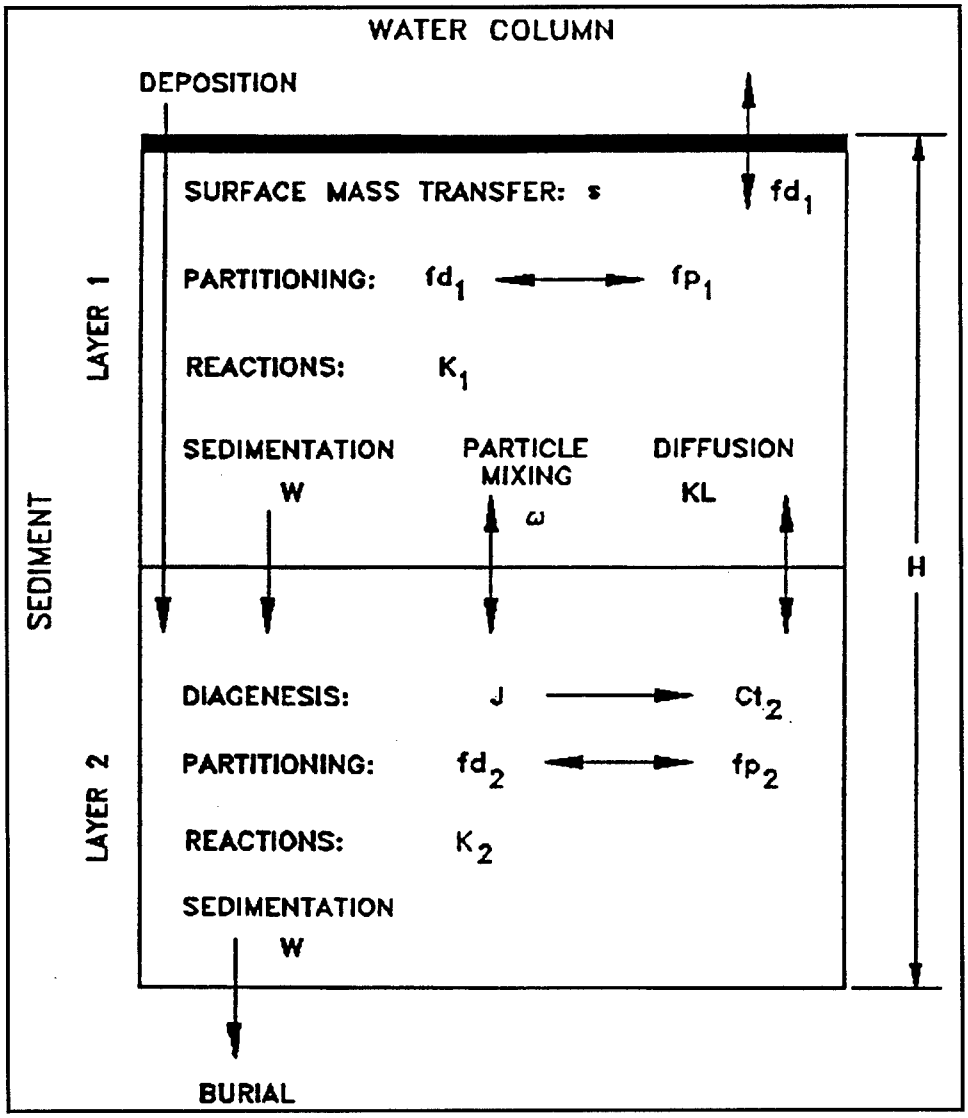

Figure 50. Diagenesis model layers and definitions

upper layer is determined by the penetration of oxygen into the sediments. At its maximum thickness, the oxic layer depth is only a small fraction of the total.

The diagenesis model consists of three basic processes. The first is deposition of particulate organic matter from the water column to the sediments. Due to the negligible thickness of the upper layer, deposition proceeds from the water column directly to the lower, anoxic layer. Within the lower layer, organic matter is subject to the second basic process, diagenesis (or decay). The third basic process is flux of substances produced by diagenesis to the upper sediment layer, to the water column, and to deep, inactive sediments. The flux portion of the model is the most complex. Computation of flux requires consideration of reactions in both sediment layers, of partitioning between particulate and dissolved fractions in both

layers, of sedimentation from the upper to lower layer and from the lower layer to deep inactive sediments, of particle mixing between layers, of diffusion between layers, and of mass transfer between the upper layer and the water column.

Deposition

Deposition is one process which couples the model of the water column with the model of the sediments. Consequently, deposition is represented in both the sediment and water-column models. In the water column, deposition is represented by the settling term in the mass balance equation for particulate carbon and nutrients

$$\frac{\delta C}{\delta t} = [transport] + [kinetics] - \frac{Ws}{H} \cdot C \tag{65}$$

in which

C = concentration of particulate constituent (g m^{-3})

Ws = settling velocity (m d^{-1})

H = depth (m)

Diagenesis

Organic matter in the sediments is divided into three fractions, or G classes, in accordance with principles established by Westrich and Berner (1984). Division into G classes accounts for differential decay rates of organic matter fractions. The G1, labile, fraction has a half life of 20 days. The G2, refractory, fraction has a half life of one year. The G3, inert, fraction undergoes no significant decay before burial into deep, inactive sediments. Each G class has its own mass-conservation equation.

$$Hsed \cdot \frac{\delta Gi}{\delta t} = Ws \cdot fi \cdot C - Wb \cdot Gi - Hsed \cdot Ki \cdot Gi \cdot \theta i^{(T-20)} \tag{66}$$

in which

Hsed = total thickness of sediment layer (m)

Gi = concentration organic matter in G class i (g m^{-3})

fi = fraction of deposited organic matter assigned to G class i

Wb = burial rate (m day^{-1})

Ki = decay rate of G class i (d^{-1})

θi = constant that expresses effect of temperature on decay of G class i

Since the G3 class is inert, $K_3 = 0$.

Total diagenesis is the rate at which oxygen demand and nutrients are produced by diagenesis of the G1 and G2 fractions:

$$J = Hsed \cdot \left[K1 \cdot G1 \cdot \theta 1^{(T-20)} + K2 \cdot G2 \cdot \theta 2^{(T-20)} \right] \tag{67}$$

in which

J = total diagenesis (g m^{-2} d^{-1})

Flux

Total diagenesis provides the driving force for the flux portion of the model. Computation of flux requires mass-balance equations for oxygen demand and nutrients in both sediment layers. The upper layer is thin such that a steady-state approximation is appropriate:

$$s \cdot fd1 \cdot Ct1 = \omega \cdot \left[fp2 \cdot Ct2 - fp1 \cdot Ct1 \right] + KL \cdot \left[fd2 \cdot Ct2 - fd1 \cdot Ct1 \right] - Wb \cdot Ct1 \pm \sum K_1 \tag{68}$$

in which

s = sediment-water mass-transfer coefficient (m d^{-1})

fd1 = dissolved fraction of total substance in upper layer ($0 \leq fd \leq 1$)

Ct1 = total concentration in upper layer (g m^{-3})

ω = particle mixing velocity (m day^{-1})

fp2 = particulate fraction of total substance in lower layer

Ct2 = total concentration in lower layer (gm m^{-3})

fd2 = dissolved fraction of total substance in lower layer

fp1 = particulate fraction of total substance in upper layer (= 1 - fd1)

KL = diffusion velocity for dissolved fraction (m d^{-1})

ΣK_1 = sum of all sources and sinks due to reactions in upper layer (g m^{-2} d^{-1})

The left side of Equation 68 represents flux to the water column under the assumption that dissolved concentration in the water column is negligibly small compared to the sediments. The assumption is made here for notational simplicity. Effects of concentration in the overlying water are computed in the diagenesis model code. The terms on the right side are mass transport due to particle mixing, diffusion of dissolved substance, deposition to the lower layer, and reactive sources and sinks. The reactions include, for example, the oxidation of sulfide that results in sediment oxygen demand. The equation states that flux to the water column, deposition to deeper sediments, and reactive sources and sinks are balanced by mixing and diffusion from deeper sediments.

The mass balance equation for the lower layer accounts for temporal concentration variations:

$$\frac{\delta Ct2}{\delta t} = \frac{J}{Hsed} - \frac{\omega}{Hsed} \cdot [fp2 \cdot Ct2 - fp1 \cdot Ct1] - \frac{KL}{Hsed} \cdot [fd2 \cdot Ct2 - fd1 \cdot Ct1] + \frac{Wb}{Hsed} \cdot [Ct1 - Ct2] \pm \sum K_2 \quad (69)$$

in which

ΣK_2 = sum of all sources and sinks due to reactions in lower layer ($g\ m^{-2}\ d^{-1}$)

The first term on the right of Equation 69 represents the diagenetic source of oxygen demand or nutrient. The second term represents exchange of the particulate fraction with the upper layer. The third term represents exchange of the dissolved fraction with the upper layer. The fourth term represents deposition of total substance from the upper layer to the lower layer and burial from the lower layer to deep, inactive sediments. The last term is the sum of all internal sources and sinks due to reactions.

The mass balance equations, with appropriate sources and sinks, are solved within the diagenesis model for sulfide, methane, ammonium, nitrate, and phosphate. Details of the reactions and solution scheme may be found in the model documentation (DiToro and Fitzpatrick 1993).

The water-quality and diagenesis models interact on a time scale equal to the integration time step of the water-quality model. After each integration, predicted particle deposition, temperature, nutrient and dissolved oxygen concentrations are passed from the water-quality model to the sediment model. The sediment model computes sediment-water fluxes of dissolved nutrients and oxygen based on predicted diagenesis and concentrations in the sediments and water. The computed sediment-water fluxes are incorporated by the water-quality model into appropriate mass balances and kinetic reactions.

The Benthic Algae Model

Benthic algae are considered to occupy a thin layer between the water column and benthic sediments (Figure 51). Biomass within the layer is determined by the balance of production, respiration, and losses to predation.

$$\frac{\delta B}{\delta t} = (G - BM) \cdot B - PR \qquad (70)$$

in which

B = algal biomass, as carbon (g C m^{-2})

G = growth (d^{-1})

BM = basal metabolism (d^{-1})

PR = predation (g C m^{-2} d^{-1})

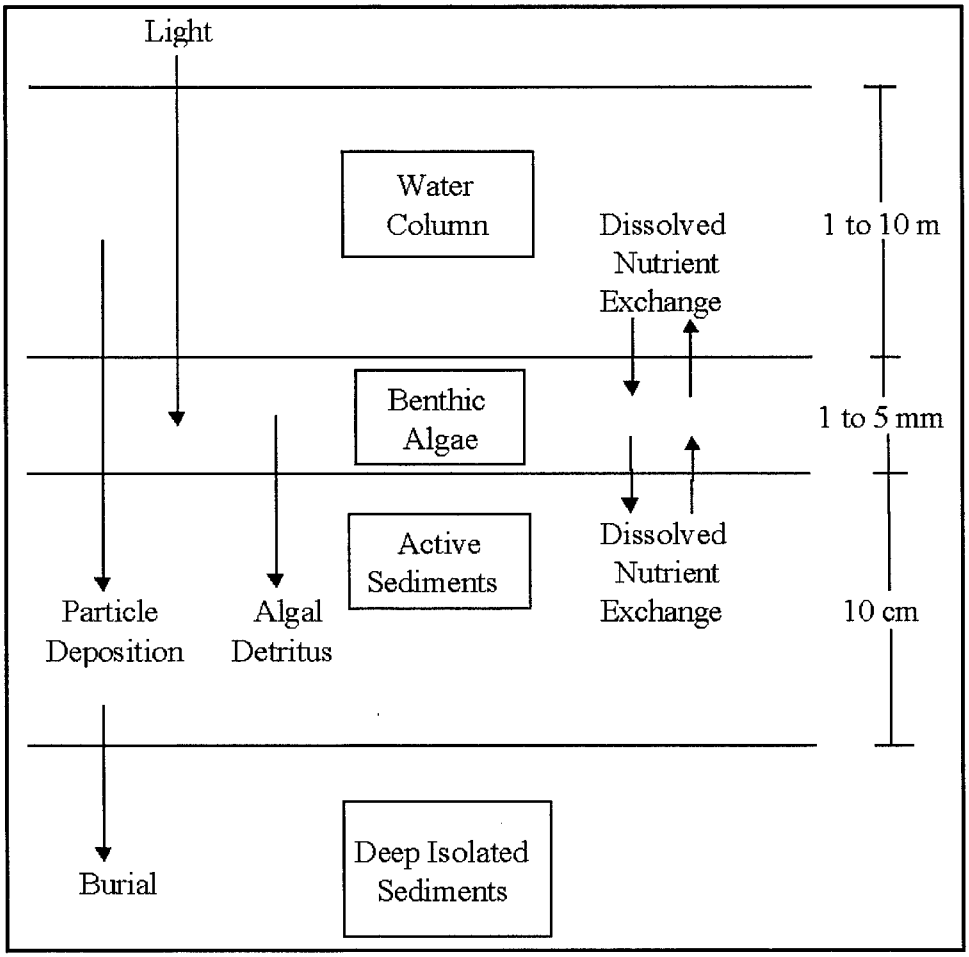

Figure 51. Benthic algae model schematic

Light and nutrient limits

Formulations for production, respiration, and predation largely follow the formulations for phytoplankton (Chapter 6). The formulation for available light accounts for self-shading within the algal mat. The mean irradiance within the mat is

$$Iavail = \frac{Iatbot}{B} \cdot \int_0^B e^{-Kba \cdot B} dB = \frac{Iatbot}{Kba \cdot B} \cdot \left[1 - e^{-Kba \cdot B}\right] \quad (71)$$

in which

Iavail = mean irradiance within algal mat (E m^{-2} d^{-1})

Iatbot = irradiance at bottom of water column (E m^{-2} d^{-1})

Kba = attenuation by benthic algae (m^2 g^{-1} C)

Due to their position at the sediment-water interface, benthic algae may utilize nutrients released from the sediments by diagenetic processes or they may remove nutrients from the water column. Since the thickness of the benthic algal layer is undefined, computation of nutrient concentration within the layer is impossible. Instead, an areal nutrient concentration that combines diagenetic nutrient flux with nutrients in the water column is computed.

$$N = Nflux \cdot \Delta t + Nwat \cdot H \quad (72)$$

in which

N = areal nutrient concentration (g m^{-2})

Nflux = sediment nutrient release (g m^{-2} d^{-1})

Δt = model time step (d)

Nwat = nutrient concentration in water column (g m^{-3})

H = depth of water column (m)

The areal nutrient concentration is employed in the Monod formulation (Equation 20) for nutrient limitation by nitrogen and phosphorus.

Influence of benthic algae on fluxes of dissolved substances

In the present model, sediment-water fluxes are quantified at the interface of the algal layer and the water column. Fluxes quantified at this interface are comparable to field measurements conducted in dome-like enclosures. The benthic algae modify fluxes that would otherwise occur between water and sediments. Benthic algae may enhance, diminish, or even reverse the direction of sediment-water nutrient fluxes by intercepting diagenetically produced nutrients, by scavenging nutrients from the overlying water, and by metabolic release of internal nutrient pools. Benthic algae may enhance, diminish, or reverse the direction of sediment-water oxygen flux through photosynthetic oxygen production and through respiration.

Ammonium flux

Diagenetic ammonium flux is enhanced by ammonium released through algal metabolism and predation on benthic algae. Diagenetic flux is diminished by uptake associated with algal production. These influences on sediment-water ammonium flux are represented

$$BENNH4 = DIANH4 + \left[\left(BM \cdot FNI - PN \cdot G\right) \cdot B + PR \cdot FNIP\right] \cdot ANC \cdot PATCHb \quad (73)$$

in which

BENNH4 = sediment-water ammonium flux (g N m^{-2} d^{-1})

DIANH4 = diagenetic ammonium flux (g N m^{-2} d^{-1})

BM = benthic algal metabolism (d^{-1})

FNI = fraction of metabolic products released as ammonium ($0 \le FNI \le 1$)

PN = nitrogen preference ($0 \le PN \le 1$)

PR = predation on benthic algae (g C m^{-2} d^{-1})

FNIP = fraction of predation products released as ammonium ($0 \le FNIP \le 1$)

ANC = nitrogen-to-carbon ratio of benthic algae (g N g^{-1} C)

PATCHb = fraction of bottom covered by algal mat ($0 \le PATCHb \le 1$)

In the absence of benthic algae, sediment-water ammonium flux is equivalent to diagenetic ammonium flux. Net algal production causes sediment-water ammonium flux to be less than flux of diagenetically-produced ammonium. In the presence of substantial algal production, demand may exceed availability of ammonium from sediments in which case

sediment-water flux is negative indicating removal of ammonium from the water column.

Nitrate flux

Benthic algal production enhances sediment nitrate uptake when ammonium is unavailable to satisfy algal requirements.

$$BENNO3 = DIANO3 - (1 - PN) \cdot P \cdot B \cdot ANC \cdot PATCHb \quad (74)$$

in which

BENNO3 = sediment-water nitrate flux (g N m^{-2} d^{-1})

DIANO3 = diagenetic nitrate flux (g N m^{-2} d^{-1})

Dissolved organic nitrogen flux

Fluxes of dissolved organic nitrogen are not considered by the diagenesis model. Sediment-water fluxes of dissolved organic nitrogen are produced through algal metabolism and predation on benthic algae. These processes are represented as

$$BENDON = (BM \cdot FND \cdot B + PR \cdot FNDP) \cdot ANC \cdot PATCHb \quad (75)$$

in which

BENDON = sediment-water dissolved organic nitrogen flux (g N m^{-2} d^{-1})

FND = fraction of metabolic products released as dissolved organic nitrogen ($0 \leq FNI \leq 1$)

FNDP = fraction of predation products released as dissolved organic nitrogen ($0 \leq FNDP \leq 1$)

Phosphorus fluxes

Sediment-water fluxes of dissolved phosphate and dissolved organic phosphorus are represented by relationships analogous to those for ammonium and dissolved organic nitrogen.

Dissolved oxygen and carbon

Oxygen demand generated by diagenetic processes is enhanced by algal metabolism and diminished by algal oxygen production. These influences on sediment oxygen demand are represented as

$$BENDO = DIADO - (BM \cdot FDO - P) \cdot AOCR \cdot B \cdot PATCHb \quad (76)$$

in which

BENDO = sediment oxygen demand (g O_2 m^{-2} d^{-1})

DIADO = diagenetic oxygen demand (g O_2 m^{-2} d^{-1})

FDO = fraction of metabolism represented by direct oxygen consumption ($0 \leq FDO \leq 1$)

AOCR = oxygen-to-carbon mass ratio in production and respiration (= 2.67 g O_2 g^{-1} C)

Since sediment oxygen demand is a flux into the sediments, it is a negative quantity in the model. Benthic algal production counters the influence of sediment oxygen demand. Substantial algal oxygen production can exceed the rate of oxygen consumption through sulfide oxidation and metabolism and produce oxygen release from the benthic algal layer to the water column.

Fluxes of dissolved organic carbon are not considered by the diagenesis model. Sediment-water fluxes of dissolved organic carbon are produced through algal metabolism and predation on benthic algae. These processes are represented as

$$BENDOC = (BM \cdot FCD \cdot B + PR \cdot FCDP) \cdot PATCHb \qquad (77)$$

in which

BENDOC = sediment-water dissolved organic carbon flux (g C m^{-2} d^{-1})

FCD = fraction of metabolic products released as dissolved organic carbon ($0 \leq FCD \leq 1$)

FCDP = fraction of predation products released as dissolved organic carbon ($0 \leq FCDP \leq 1$)

Effect of benthic algae on sediment organic matter

Algal detritus, produced in the model through metabolism and predation, contributes to the concentration of particulate organic matter in the sediments. The contribution of benthic algae to sediment particulate organic carbon is represented as

$$\frac{\delta POC}{\delta t} = \frac{1}{Hsed} \cdot \left[(FCL + FCR) \cdot BM \cdot B + (FCLP + FCRP) \cdot PR \right] \qquad (78)$$

in which

POC = sediment particulate organic carbon concentration (g m^{-3})

FCL = fraction of metabolic products released as labile particulate organic carbon ($0 \leq FCD \leq 1$)

FCR = fraction of metabolic products released as refractory particulate organic carbon ($0 \leq FCR \leq 1$)

FCLP = fraction of predation products released as labile particulate organic carbon ($0 \leq FCLP \leq 1$)

FCRP = fraction of predation products released as refractory particulate organic carbon ($0 \leq FCRP \leq 1$)

Labile particulate organic carbon produced by metabolism and predation is routed directly to the G1 carbon pool. Refractory particulate organic carbon produced by metabolism and predation is split between the G2 and G3 pools.

The contributions of benthic algae to sediment particulate organic nitrogen and phosphorus are described by relationships analogous to the relationship for carbon.

Parameters in benthic algae model

Parameters in the benthic algae model are summarized in Table 21.

Table 21
Parameters in Benthic Algae Model

Symbol	Definition	Value	Units
ANC	nitrogen-to-carbon ratio of algae	0.175	g N g^{-1} C
APC	phosphorus-to-carbon ratio of algae	0.0175	g P g^{-1} C
BMr	basal metabolic rate of algae at reference temperature Tr	0.05	d^{-1}
CChl	carbon-to-chlorophyll ratio of algae	75	g C mg^{-1} chl
FCDP	fraction of dissolved organic carbon produced by predation	0.25	$0 \leq FCDP \leq 1$
FCD	fraction of dissolved organic carbon produced by metabolism of algae	0.1	$0 \leq FCD \leq 1$
FCLP	fraction of labile particulate carbon produced by predation	0.5	$0 \leq FCLP \leq 1$
FCRP	fraction of refractory particulate carbon produced by predation	0.25	$0 \leq FCRP \leq 1$
FDO	fraction of metabolism represented by direct oxygen consumption	0.9	$0 \leq FDO \leq 1$
FNI	fraction of inorganic nitrogen produced by metabolism of algae	0.35	$0 \leq FNI \leq 1$
FNIP	fraction of inorganic nitrogen produced by predation	0.35	$0 \leq FNIP \leq 1$

(Continued)

Table 21 (Concluded)

Symbol	Definition	Value	Units
FND	fraction of dissolved organic nitrogen produced by metabolism of algae	0.15	$0 \le FND \le 1$
FNDP	fraction of dissolved organic nitrogen produced by predation	0.15	$0 \le FNDP \le 1$
FNL	fraction of labile particulate nitrogen produced by metabolism of algae	0.40	$0 \le FNL \le 1$
FNLP	fraction of labile particulate nitrogen produced by predation	0.40	$0 \le FNLP \le 1$
FNR	fraction of refractory particulate nitrogen produced by metabolism of algae	0.20	$0 \le FNR \le 1$
FNRP	fraction of refractory particulate nitrogen produced by predation	0.20	$0 \le FNRP \le 1$
FPI	fraction of dissolved inorganic phosphorus produced by metabolism of algae	0.5	$0 \le FPI \le 1$
FPIP	fraction of dissolved inorganic phosphorus produced by predation	0.5	$0 \le FPIP \le 1$
FPD	fraction of dissolved organic phosphorus produced by metabolism by algae	0.25	$0 \le FPD \le 1$
FPDP	fraction of dissolved organic phosphorus produced by predation	0.25	$0 \le FPDP \le 1$
FPL	fraction of labile particulate phosphorus produced by metabolism of algae	0.15	$0 \le FPL \le 1$
FPLP	fraction of labile particulate phosphorus produced by predation	0.15	$0 \le FPLP \le 1$
FPR	fraction of refractory particulate phosphorus produced by metabolism of algae	0.10	$0 \le FPR \le 1$
FPRP	fraction of refractory particulate phosphorus produced by predation	0.10	$0 \le FPRP \le 1$
Kba	light attenuation coefficient for benthic algae	0.25	$m^2\ g^{-1}\ C$
KHn	half-saturation concentration for nitrogen uptake by algae	0.025	$g\ N\ m^{-2}$
KHp	half-saturation concentration for phosphorus uptake by algae	0.005	$g\ Pm^{-2}$
KTb	effect of temperature on basal metabolism of algae	0.032	$°C^{-1}$
KTg1	effect of temperature below Tm on growth of algae	0.004	$°C^{-2}$
KTg2	effect of temperature above Tm on growth of algae	0.012	$°C^{-2}$
PATCHb	fraction of bottom covered by algal mats	0.25	$0 \le PATCHb \le 1$
Phtl	predation rate on algae	0.005	$m^2\ g^{-1}\ C\ d^{-1}$
Pmax	production rate of algae under optimal conditions	300	$g\ C\ g^{-1}\ Chl\ d^{-1}$
Topt	optimal temperature for growth of algae	25	°C
Tr	reference temperature for metabolism	20	°C
α	initial slope of production vs. irradiance relationship	5.0	$g\ C\ g^{-1}\ Chl\ (E\ m^{-2})^{-1}$

The Resuspension Model

Relationships developed to quantify wind-driven resuspension of solids from the bottom were described in Chapter 5. These solids are a mixture of mineral and organic particles. The resuspension of organic matter and particulate nutrients represents a potentially significant process in the recycling of material from benthic sediments to the water column.

Resuspension into the water column is considered by adding a term to the deposition relationship presented previously (Equation 65).

$$\frac{\delta C}{\delta t} = [transport] + [kinetics] - \frac{Ws}{H} \cdot C + \frac{ER}{H} \cdot \frac{Csed}{M} \tag{79}$$

in which

ER = erosion rate of total solids (g m^{-2} d^{-1})

Csed = bulk concentration of particulate constituent in sediment (g m^{-3})

M = bulk concentration of total solids in sediment (g m^{-3})

On the sediment side, resuspension is considered by adding a term to the conservation of mass relationship (Equation 66).

$$Hsed \cdot \frac{\delta Gi}{\delta t} = Ws \cdot fi \cdot C - Wb \cdot Gi - \frac{ER}{Hsed} \cdot \frac{Gi}{M} - Hsed \cdot Ki \cdot Gi \cdot \theta i^{(T-20)} \tag{80}$$

in which all terms have been previously described.

Resuspension is considered for particulate organic carbon, particulate organic nitrogen, particulate organic phosphorus, and particulate inorganic phosphorus. G1 fractions of the organic constituents in the sediment are routed to the labile particulate pool in the water column. The sum of the G2 and G3 fractions is routed to the refractory particulate pool in the water column. Sediment particulate inorganic phosphorus is routed to the total phosphate pool in the water column.

9 Water Column Calibration Results

The Calibration Period

Initial application of the model was to a two-year period, 1996–1997. More than fifty model runs were made in the effort to calibrate the model. In each run, model parameters or other factors were changed with the goal of optimizing agreement between observations and model results. The effort was halted when the judgment was reached that no substantial improvement in calibration status was likely. Run 48 was judged the best of all runs completed.

Hydrodynamics for the calibration were obtained by sequencing dry-season and wet-season hydrodynamic files of 29 days in length. The hydrodynamics were generated using seasonal-average flows and winds and an intertidal sequence of surface elevations at the open boundaries (Chapter 4).

Along the west coast, the 1996 dry-season flows were, in fact, the highest in the calibration period (Figure 52). Least flows occurred during the dry season of 1997. Wet-season flows in 1996 and 1997 were nearly equal and intermediate in magnitude. Flows to Florida Bay exhibited the expected sequence of dry- and wet-season flows (Figure 53). Highest seasonal flows occurred during the 1997 wet season while least seasonal flows occurred during the 1997 dry season.

Peak phosphorus loads from the west coast occurred in early 1996, a nominal dry season, and in late 1997, a nominal wet season (Figure 54). Surprisingly, the high runoff in September through November 1996 was not matched by concurrent loads. Nitrogen loads from the west coast followed the runoff record more closely. Peak loads occurred in early January 1996, November 1996, and July 1997.

Phosphorus loads to Florida Bay showed little correlation with runoff (Figure 55). Peak loads occurred in May 1996 and May 1997, two of the lowest flow months in the calibration period. These loads originated in the

estimated wastewater loads from the Keys. A lesser peak occurred in October 1996, concurrent with a runoff event. Nitrogen loads tracked runoff closely. Maximum loads occurred in January 1996, October 1996, and July 1996, and ranked in magnitude identically to flow events.

Wind magnitude during the calibration period exhibited a rough sinusoidal pattern with peak winds in the winter months and lower winds in the summer months (Figure 56). Deviations from this pattern were substantial, however. Periods of near calm occurred in the winter and occasional wind events occurred in summer. Peak wind took place in November 1996. A succession of wind events of only slightly lesser magnitude occurred in January and February of the same year. July and August of 1997 exhibited the lowest winds in the calibration interval.

Format

During the calibration process, comparisons between model and observations were conducted in a number of formats. These included spatial comparisons, time series comparisons, and scatterplots.

Spatial comparisons

Spatial comparisons (Figures 58-65 and 67-78) are plan-form views of the bay. Observations are represented as colored circles outlined in black. Unless otherwise noted, observations are arithmetic means of all samples collected during the 1997 dry and wet seasons. The observations are superimposed on a model grid. Cells are colored according to modeled concentrations. The modeled concentrations shown are arithmetic means of all values computed during the 1997 dry and wet seasons. Both observations and modeled concentrations are colored according to a scale at the top of each figure. When observations and model agree, within the scale interval, the circle and surrounding grid have the same color. Different colors in the circles and outside indicate discrepancies between observations and model.

Due to space considerations, only 1997 spatial plots are included. The characteristics of these plots are not substantially different from 1996. Electronic copies of the 1996 results are available upon request from the first author.

Time series

Time series plots (Figures 79-86) compare the temporal behavior of observations and model during the calibration period. Time series were constructed for six regions outlined by NOAA/AOML (Figure 57). In addition to the six regions, comparisons were also conducted for two regions in the model domain but outside Florida Bay: the Southwest Shelf Zone and

the Outer Keys Zone. The time series show monthly arithmetic mean and range of all observations collected within a region. The model mean, shown as a solid line, represents the arithmetic mean of all computed values within cells containing observations. Means were computed from model output at ten-day intervals. Computed range within these same cells is shown as a shaded background to the model mean. Days, shown on the horizontal axis, commence on January 1, 1996.

Scatterplots

Scatterplots (Figure 87) present a one-to-one comparison of computed and modeled values. Computed values are plotted on the horizontal axis and observations are plotted on the vertical axis. Perfect agreement between observed and computed values is indicated by the diagonal solid line. For the scatterplots, the observed and computed values are the seasonal means at individual stations from the dry and wet seasons of 1996 and 1997. Thus, the plots summarize the ability of the model to compute seasonal-average water quality throughout the model domain.

Statistics

Statistical summaries of the calibration are presented at the top of each scatterplot. The summaries are quantitative measures of the ability of the model to compute seasonal-average water quality throughout the model domain.

Mean error

The mean error is defined as

$$ME = \frac{\sum(O - P)}{n} \tag{81}$$

in which

ME = mean error

O = observation (seasonal average at a station)

P = model prediction (seasonal average at a station)

n = number of observations

A mean error of zero is ideal. Positive mean error indicates model predictions are less than observations, on average. A negative mean error indicates model predictions exceed observations, on average.

Absolute mean error

The absolute mean error is defined as

$$AME = \frac{\sum |O - P|}{n} \tag{82}$$

An absolute mean error of zero is ideal. The magnitude of the absolute mean error indicates the average deviation between predictions and observations.

Root-mean-square error

The-root-mean square error is defined as

$$RMS = \sqrt{\frac{\sum (O - P)^2}{n}} \tag{83}$$

A root-mean-square error of zero is ideal. The root-mean-square error is an indicator of the deviation between predictions and observations. The root-mean-square is an alternative to (and usually larger than) the absolute mean error.

Relative error

The relative error is defined

$$RE = \frac{\sum |O - P|}{\sum O} \cdot 100 \tag{84}$$

The relative error is the ratio of the absolute mean error to the mean of the observations and is expressed as a percent.

Temperature

The primary variability of temperature is temporal, not spatial. The time series analyses (Figures 79-86) indicate the model successfully reproduces the seasonal cycling of water temperature. Worth noting is that observed temperatures were lowest in early 1996 and trended upward, in winter and summer, thereafter. This trend was reproduced by the model. The scatter-plots (Figure 87) indicate a bi-modal temperature distribution in both the observations and model.

Salinity

Due to the seasonal, steady-state flows used in the model, the seasonal-average salinity distributions are the appropriate measures of model performance. The observed spatial salinity distribution is captured by the model (Figures 58, 59). Florida Bay water exhibits its lowest salinity at the northeast apex and grows saltier in a southwest direction. High-salinity water also prevails outside the barrier formed by the Keys. Overall, observed salinity in the system is ≈0.5 ppt higher than computed. In portions of the domain, notably adjacent to the mainland in Florida Bay, the discrepancy is larger, however. Several reasons can be advanced for this shortfall. One is that the mainland is modeled as an impermeable boundary. In reality, the transition from open water to land is not well-defined. During dry periods, water from the bay penetrates into the mangrove. The mangrove and area upland provide additional area for evapotranspiration and subsequent concentration of salt. The most complete remedy for this problem is to model the mangrove and marsh area as well as the bay. Less involved, more empirical remedies are also possible. For example, set salinity boundaries at the inflows to non-zero values or increase evaporation in the Northern Transition Zone.

Time-series plots in the Eastern and Central Zones (Figures 80, 81) indicate computed salinity never attains the observed peaks. Computations track the increasing salinity during the dry seasons but drop off too sharply during the switch to wet seasons. The immediate explanation is that the flows are seasonal averages, not instantaneous. Consequently, matching of computed salinity within each season cannot be expected. Certainly, inclusion of an exact runoff time series would improve computations but that explanation alone is too simple. It appears that the interior portion of the bay flushes too quickly. Material should remain longer and become more concentrated. The excess flushing may be a property of the hydrodynamic model or it may be an artifact of the overlay grid. We suspect cells in the overlay grid span mud banks and other features that restrict flow. Overlay of flow-restricting features creates artificial transport across these features and prevents concentration build-up. In addition, the larger overlay cells increase numerical diffusion which also diminishes concentration gradients.

Chlorophyll

Highest observed chlorophyll values tend to run in a band from the Central Zone in a southwest direction into the Gulf Transition Zone (Figures 60, 61). The mouth of the Shark River also exhibits consistently high chlorophyll concentrations. Lowest values occur in the northeast apex of the bay and outside the Keys. Distinct seasonality is not evident in the data but blooms are pronounced in some regions (e.g. Central Zone, Figure 81). The observed spatial pattern is reasonably reproduced in the model. The model also shows evidence of blooms. Modeled blooms are more

widespread than blooms in the bay and show little correlation with observed blooms. For example, the Central Zone exhibited blooms in November 1996 and September 1997 (Figure 81). Modeled blooms in the same zone occurred in April 1996 and February 1997. Random algal blooms are among the most difficult phenomena to model. Both increased understanding and more intense modeling effort are required to improve model capabilities in this area.

Ammonium

Observed ammonium concentrations exhibit a peak in the central portion of the bay and are uniformly low elsewhere (Figures 62, 63). The peak persists through both wet and dry seasons although the concentrations were higher in the dry season of 1997 than the wet season. The model does well in reproducing the observed spatial distribution although peak dry- season concentrations were underpredicted.

Nitrate+Nitrite

During the dry season of 1997, nitrate+nitrite was concentrated in the Central and Northern Transition Zones and at the mouth of the Shark River (Figure 64). During the wet season, the peak in the bay moved northeast toward the apex (Figure 65). Observed peaks in the apex and Shark River in the wet season are likely due to nitrate-enriched runoff. The dry-season concentration in the Central Zone was reproduced by the model although the wet-season apex peak was not well matched.

Total Nitrogen

The dominant property of observed total nitrogen is that the total greatly exceeds the sum of ammonium and nitrate+nitrite. Although the excess fraction is not clearly identified in the observations, stoichiometric conversion of the observed chlorophyll and analyses conducted at the mouths of several creeks (Sutula 1999) indicate the majority of the total nitrogen is in dissolved organic form. The dominance of organic nitrogen over mineral forms is well-represented in the model (Figure 66). Observed total nitrogen demonstrates a pronounced "hot spot" in the Central Zone that persists through wet and dry seasons. Highest concentrations occur in the Central, Eastern, and Northern Transition Zones. The model reproduces the spatial pattern (Figures 67, 68) but tends to underestimate total nitrogen over a broad portion of the bay (Figure 87). The origin of the deficit cannot be clearly identified from the calibration. Possible causes include

loading shortfalls and failure to isolate water in enclosed basins. These issues will be examined in subsequent sensitivity analyses.

Soluble Reactive Phosphorus

One fraction of the model total phosphate state variable is dissolved inorganic phosphate (Equation 33). Dissolved inorganic phosphate was equated with soluble reactive phosphorus analyzed in Florida Bay.

Observed soluble reactive phosphorus exhibits highest concentrations in the Western Shelf, the Gulf Transition Zone, and the mouth of the Shark River (Figures 69, 70). Least concentrations are in the apex of the bay, in the Central, Eastern, and Northern Transition Zones. The model reproduces the low concentrations well in the interior of the bay but tends to overestimate soluble reactive phosphorus elsewhere. The origin of the excess is not at all clear. Potential sources include the representation of phosphorus mineralization in the model, the employment of constant phytoplankton stoichiometry, interactions between dissolved and particulate phosphorus forms, and the use of seasonal average hydrodynamics. Several of these influences will be examined in subsequent sensitivity analyses.

Total Phosphorus

Observed total phosphorus exhibits highest concentrations in an arc that extends from the Western Shelf around Cape Sable into the Central Zone (Figures 71, 72). Interestingly, concentrations along the west coast are often higher than at the western boundary of the model domain, perhaps indicating a source in the Shark River or further up the coast. The model duplicates the broad pattern of higher concentrations to the west and lower concentrations in the interior of the bay. During the dry season of 1997, both observations and model exhibited a "hot spot" in the northern portion of the Central Zone.

The scatterplots (Figure 87) and summary statistics indicate a scattering of observations that exceed computations, but most prediction-observation pairs fall along the one-to-one line. As with nitrogen, the dissolved inorganic fraction is only a small portion of both the observed and computed total phosphorus (Figure 66). Also as with nitrogen, the calibration database does not allow the dominant phosphorus fraction to be identified. A summary of an independent data set (Fourqurean 1992) indicates 30% of total phosphorus is in particulate form and 65% is in dissolved organic form. In the model, these distributions are reversed. The largest phosphorus fraction is particulate and about half of that fraction is inorganic. The distribution of total phosphorus into fractions can be addressed through additional calibration of the model. Since the summary of observed

fractions was based on data collected outside the calibration period (1989–1990), however, the degree to which the modeled and observed fractions should agree is uncertain.

Total Organic Carbon

Observed total organic carbon declines from roughly 10 g m^{-3} in the interior of Florida Bay (Figures 79, 80) to 3 g m^{-3} at the open boundaries of the system. A large portion of the observed carbon near the mainland likely originates in the inflows. Observations at the mouths of several tidal creeks indicate concentrations of 10 to 20 g m^{-3} (Sutula 1999). Computed total organic carbon in the interior is uniformly less than observed. This property is consistent with other applications of CE-QUAL-ICM (e.g. Cerco and Cole 1994). The problem is that the model has only one class of dissolved organic carbon which decays at a constant rate. To match the observations, the model should include a large fraction of refractory dissolved organic carbon and a small fraction of labile dissolved organic carbon. This improvement can be readily installed in the model but is not of primary importance in Florida Bay.

Dissolved Oxygen

Both observed and computed dissolved oxygen (Figures 79-86) track the saturation concentration which is a function of salinity and temperature. Computed dissolved oxygen exceeds observed by an average of less than 0.1 gm m^{-3}. In turn, computed dissolved oxygen is roughly 0.1 gm m^{-3} less than saturation concentration. Although dissolved oxygen is not a critical parameter and computations are satisfactory, improved agreement may be possible by slight adjustment of the reaeration function (Equation 48).

Total Suspended Solids

Comparison of observed and computed total suspended solids for the calibration period is problematic. The solids resuspension algorithm was developed based on in situ solids observations collected in 1993–1994 (Phlips, Lynch, and Badylak 1995). For the calibration period, available solids data are from the AVHRR observations (see Chapter 2 and Stumpf et al. 1999). While the AVHRR observations were "ground truthed," direct correspondence between the two data sets has not been established.

The Phlips et al. data set indicates highest solids concentrations adjacent to the mainland in a patch extending from Cape Sable to Snake Bight (Figures 73, 74). Peak dry season concentrations are double peak wet

season concentrations, presumably because winter winds exceed summer winds. The model reasonably reproduces the observed spatial and temporal pattern. One key reason for the reproduction of the spatial pattern is that erosional properties of the model were specified to agree with the Phlips et al. data set.

On a spatial basis, the AVHRR observations indicate the highest solids concentrations in the eastern basin (Figures 75, 76). The factor-of-two ratio between dry and wet-season concentrations appears in this data set too. Modeled concentrations indicate two major resuspension events, in March and December 1996, that elevated sediment concentrations basin-wide (Figures 79-86). The AVHRR observations indicate these events too (e.g. Figure 80) but the magnitude is not as pronounced as in the model nor is the effect as widespread.

The resuspension algorithm reproduced the distribution of observed suspended solids (Chapter 4). Compared to the AVHRR observations, modeled solids are most often higher than observed (Figure 87). Improved agreement between the model and observations requires re-calibration of the resuspension algorithm to the AVHRR database.

Light Attenuation

Light attenuation was not universally monitored in the primary data set used to calibrate the model. A data set was assembled from various sources (Chapter 2) to provide an indication, at least, of the model's ability to compute light attenuation. The observations show a spatial trend in which attenuation is highest near the mainland ($> 2\ m^{-1}$), especially in the Central Zone, and declines with distance away from the mainland to reach minimum values outside the Keys ($< 0.25\ m^{-1}$). The model reproduces both the magnitude and the trend in the observations (Figures 77, 78) although it perhaps overestimates the attenuation during the dry season of 1997. Since few of the observations in the central bay were collected during the calibration interval, however, one-to-one correspondence between computations and observations cannot be expected.

Algal Growth-Limiting Factors

Several lines of evidence indicate algal abundance in Florida Bay is limited by phosphorus availability (Fourqurean, Jones, and Zieman 1993). These include: the occurrence of dissolved inorganic nitrogen and soluble reactive phosphorus in ratios greatly in excess of the Redfield ratio; the occurrence of total nitrogen and total phosphorus in ratios greatly in excess of the Redfield ratio; and a strong correlation between chlorophyll concentration and total phosphorus.

The model calculates strong phosphorus limitation on algal growth within the interior of the bay including the Northern Transition, Eastern, and Central Zones (Figure 88). The most limiting nutrient transitions from phosphorus to nitrogen in the southern and western extremes of the bay and becomes almost exclusively nitrogen in the Gulf Transition Zone and along the boundaries of the model domain. Occasionally, during resuspension events, light is computed to limit growth more than either nutrient but nutrient limitations generally prevail over light as limiting factors.

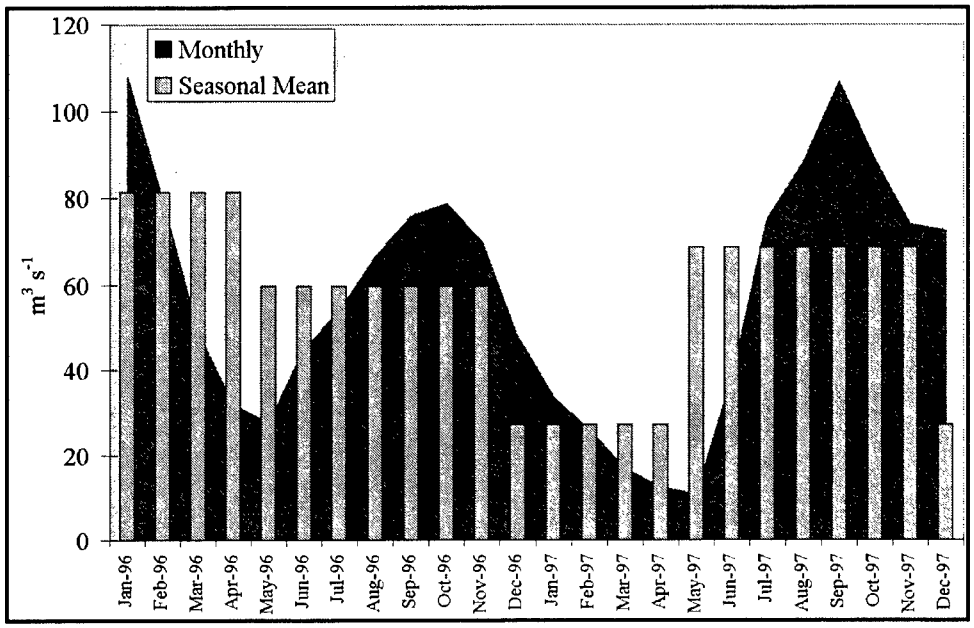

Figure 52. Runoff from the west coast

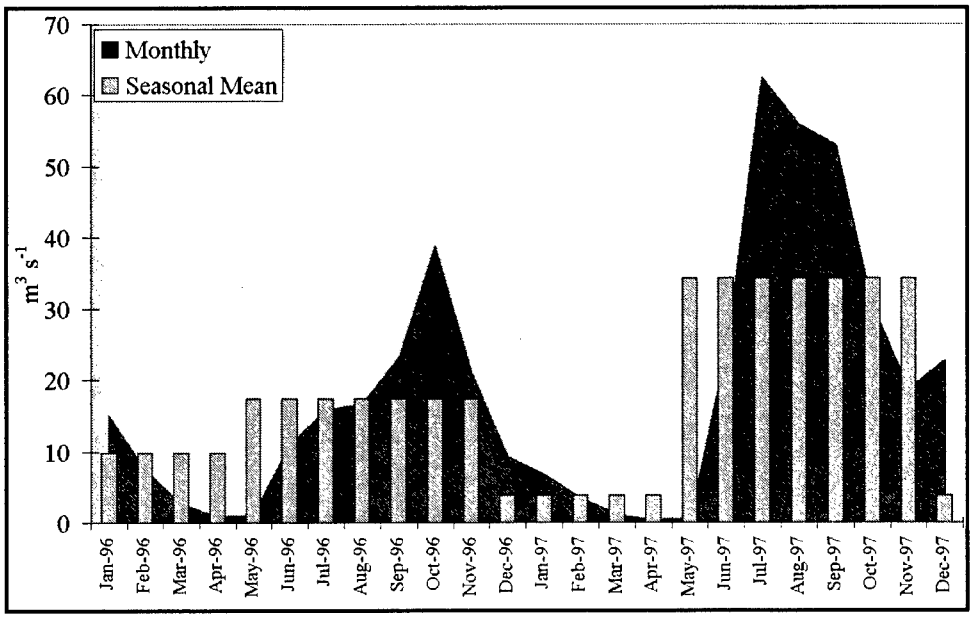

Figure 53. Runoff into Florida Bay

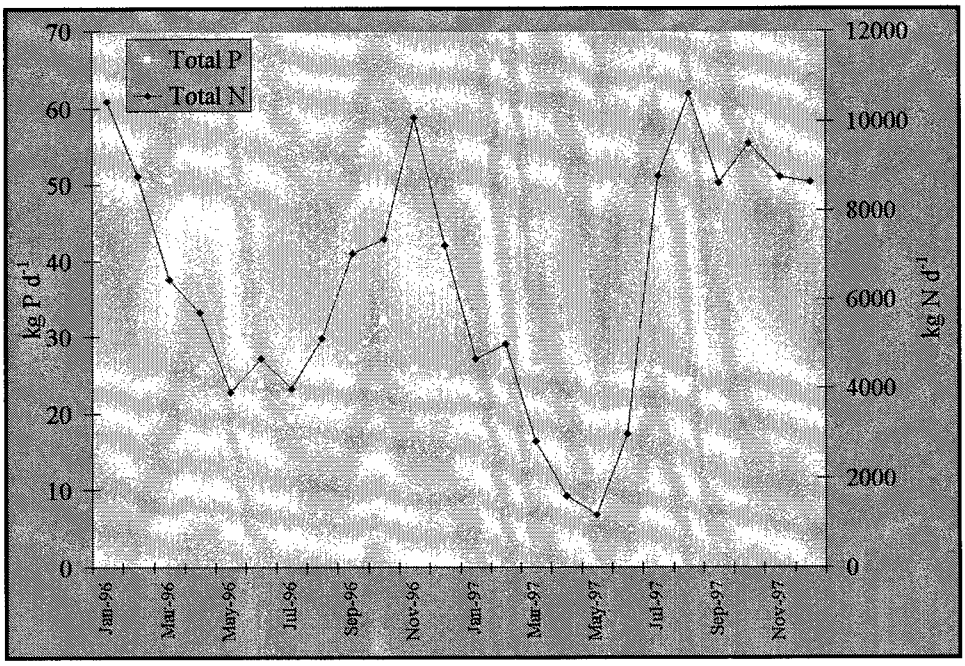

Figure 54. Phosphorus and nitrogen loads from the west coast

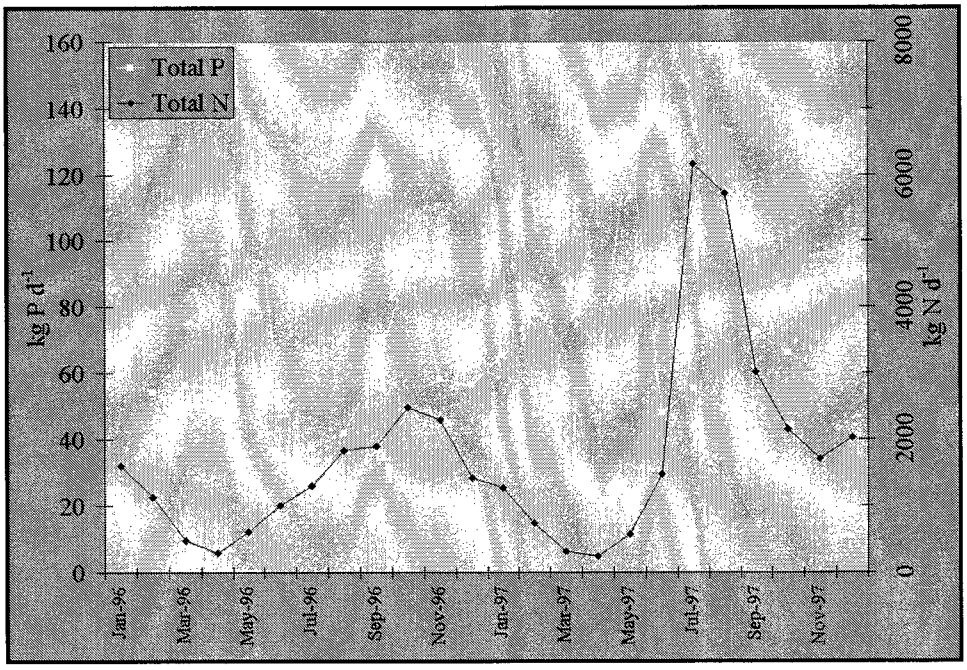

Figure 55. Phosphorus and nitrogen loads into Florida Bay

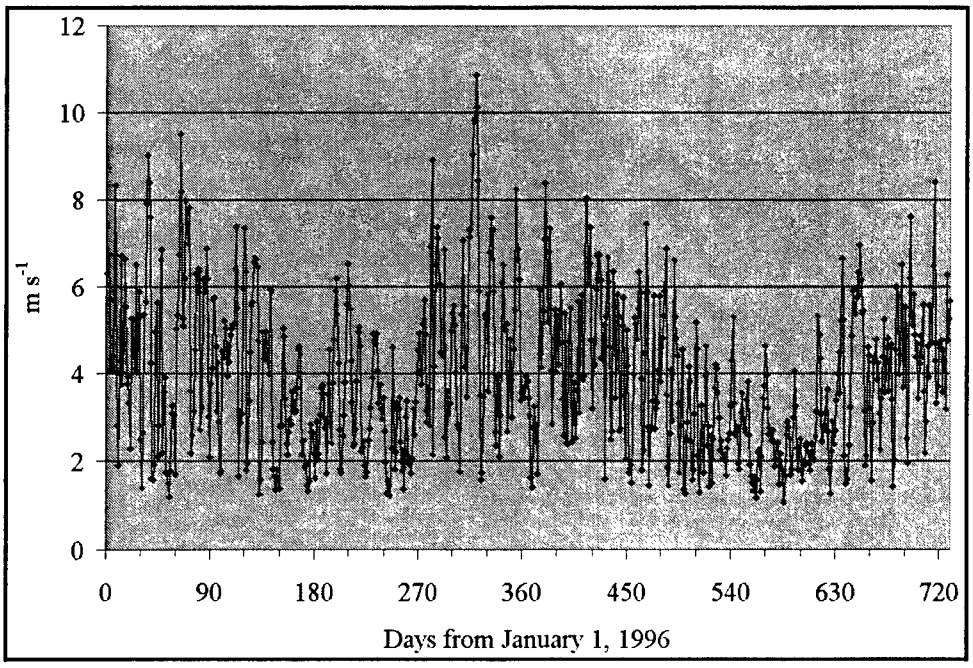

Figure 56. Daily-mean wind speed during the calibration period

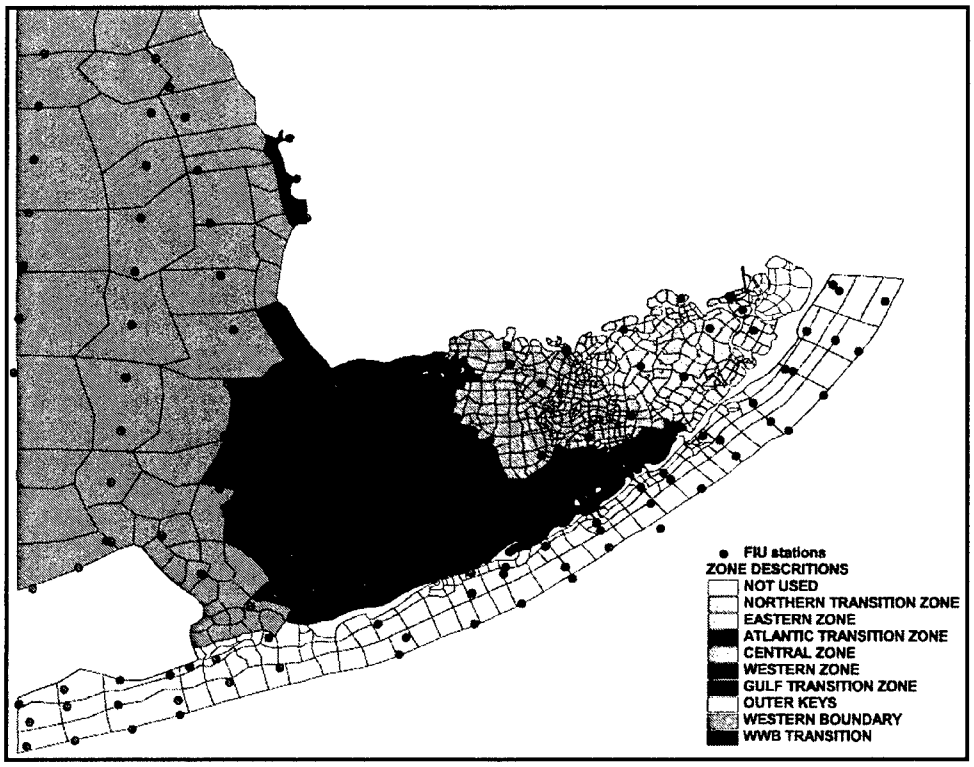

Figure 57. Regions for time-series comparisons

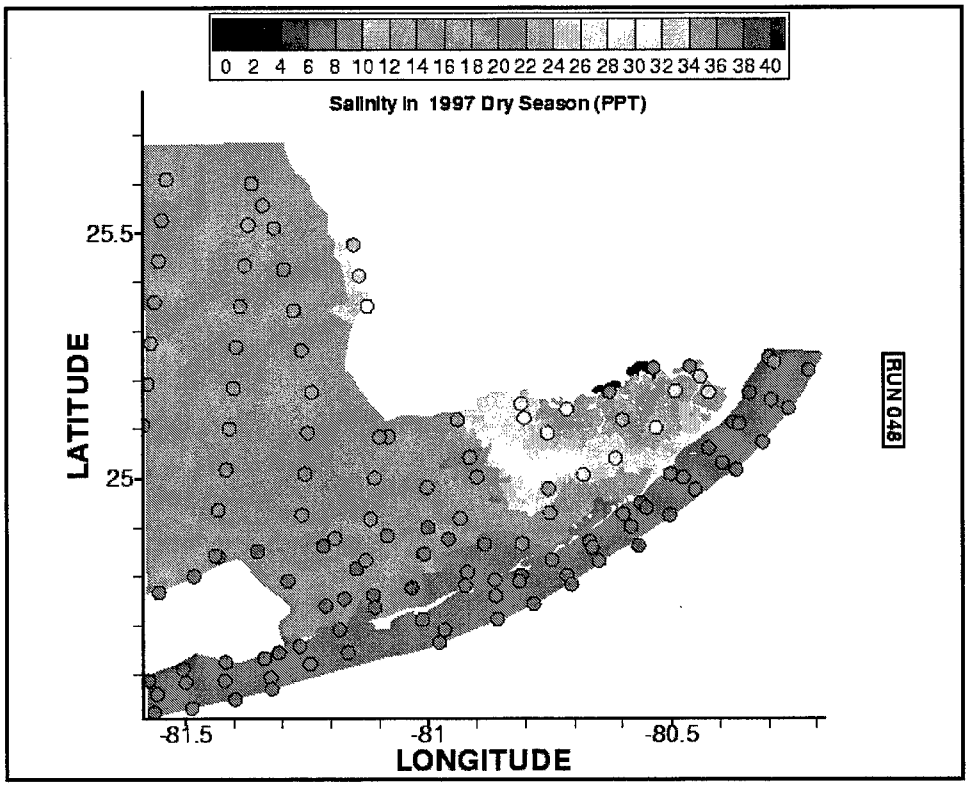

Figure 58. Salinity, dry season 1997

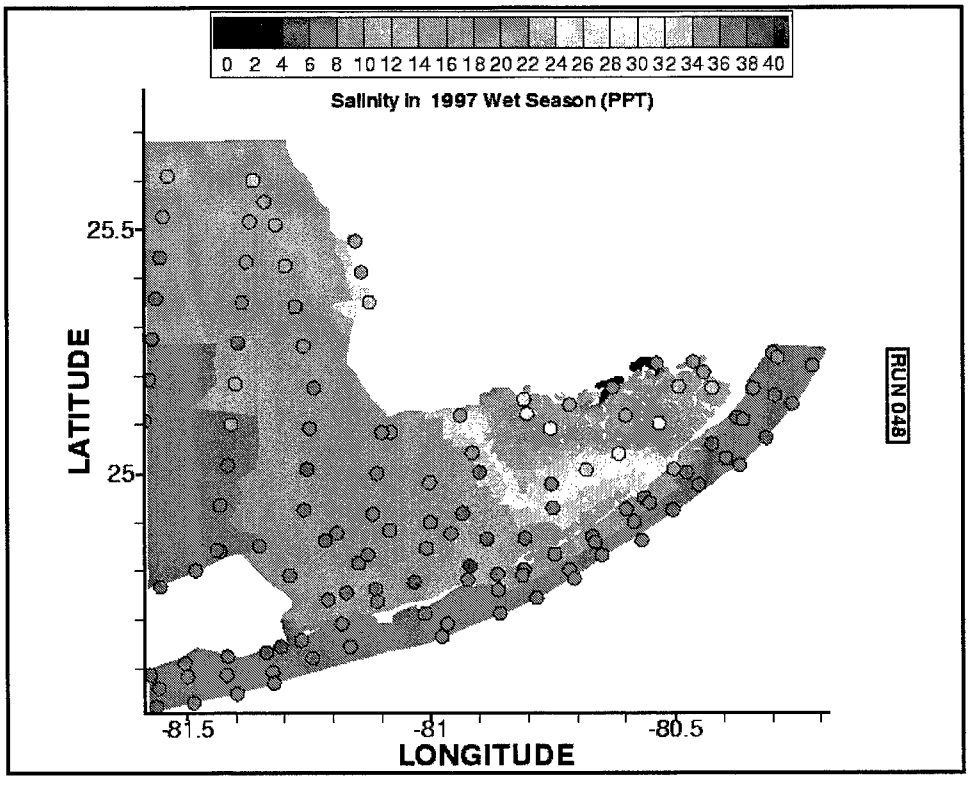

Figure 59. Salinity, wet season 1997

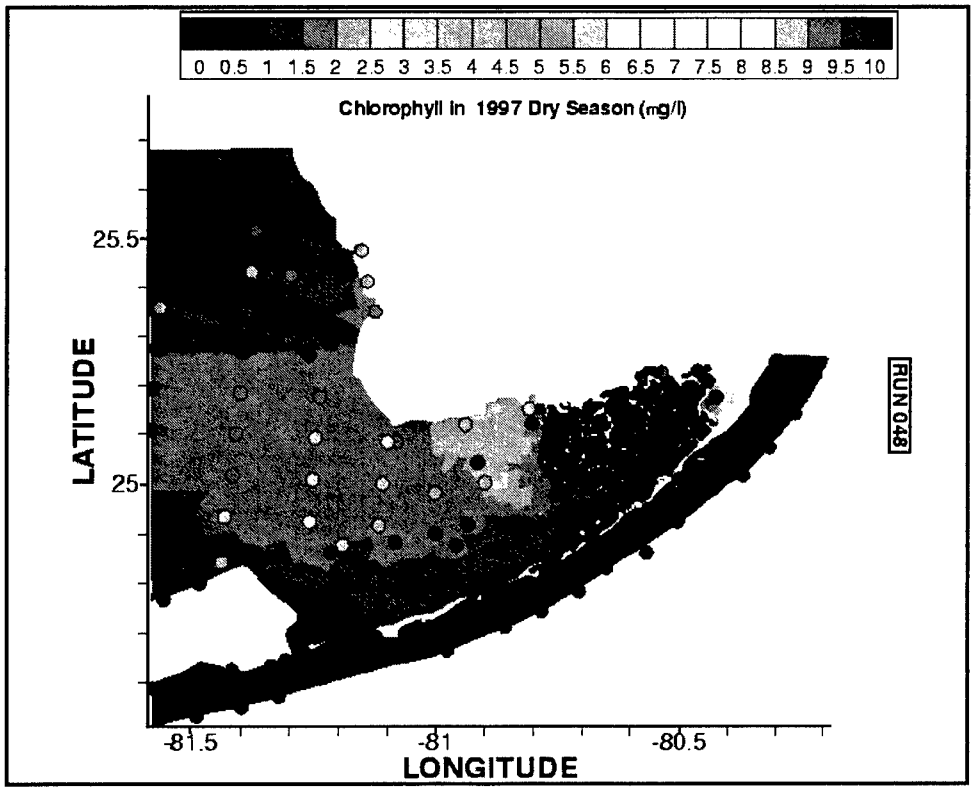

Figure 60. Chlorophyll, dry season 1997

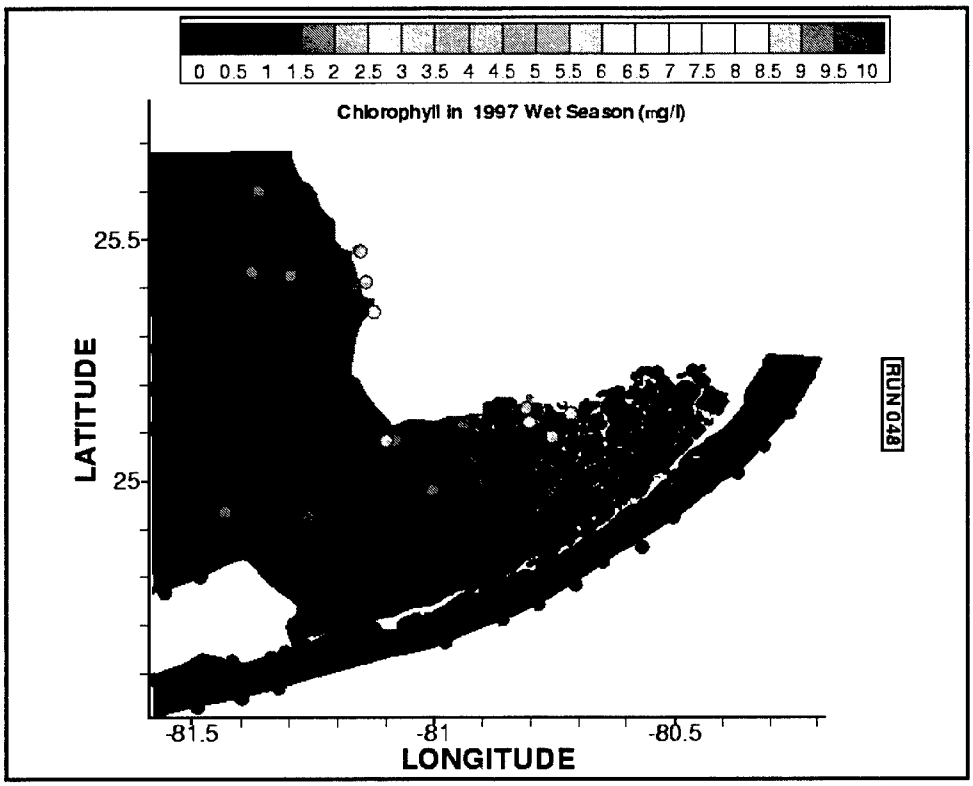

Figure 61. Chlorophyll, wet season 1997

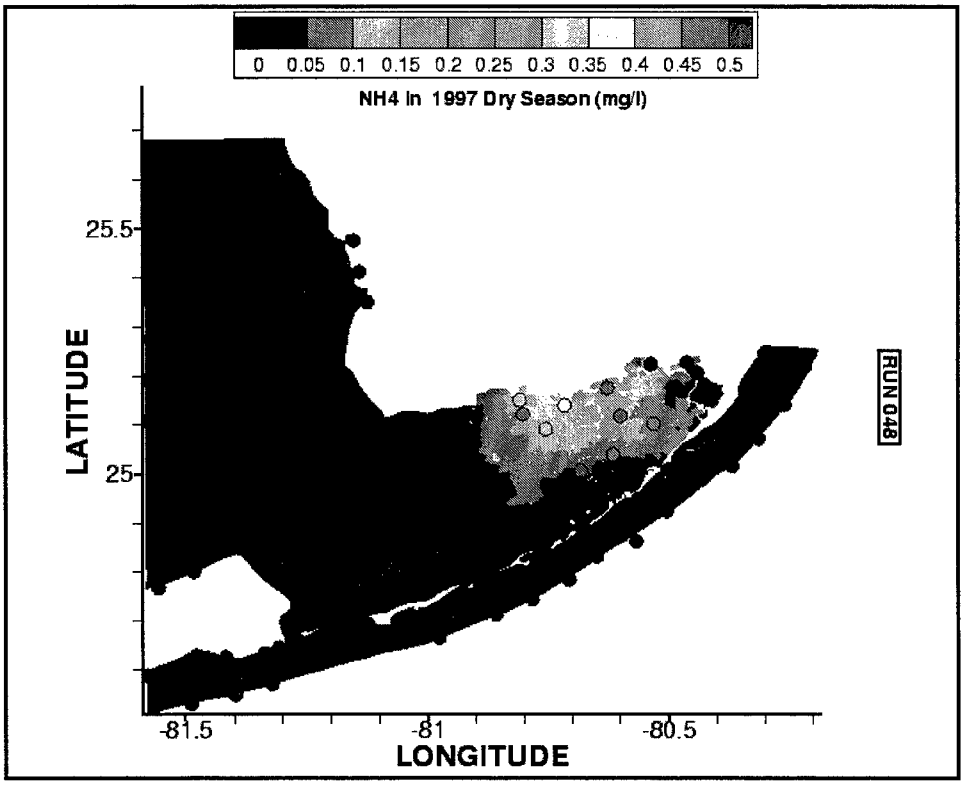

Figure 62. Ammonium, dry season 1997

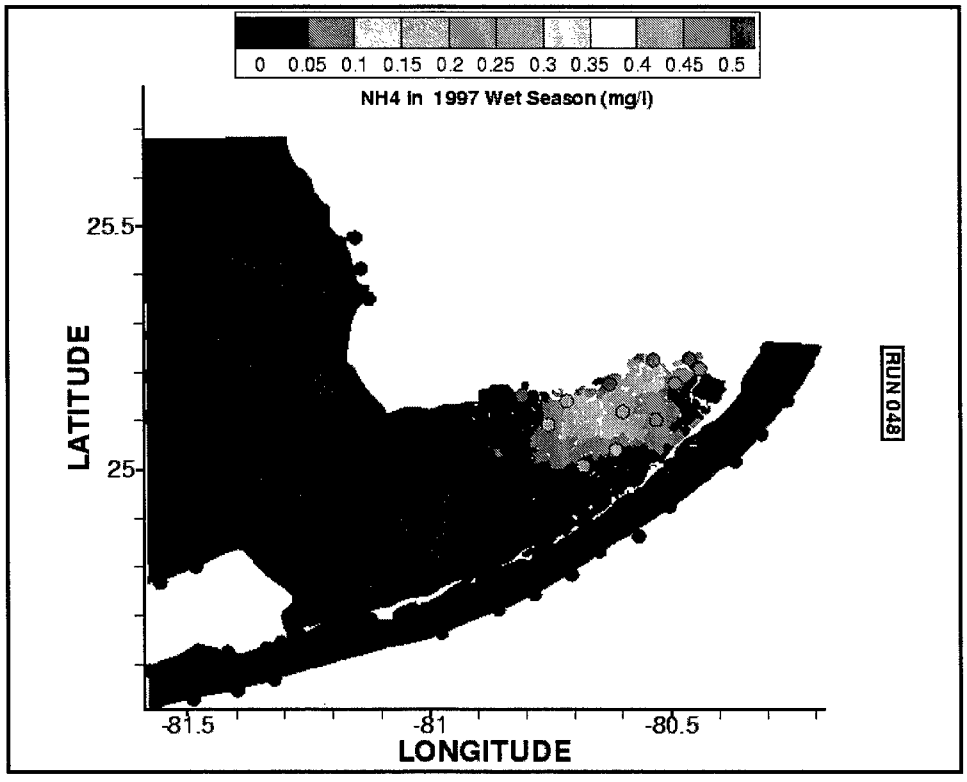

Figure 63. Ammonium, wet season 1997

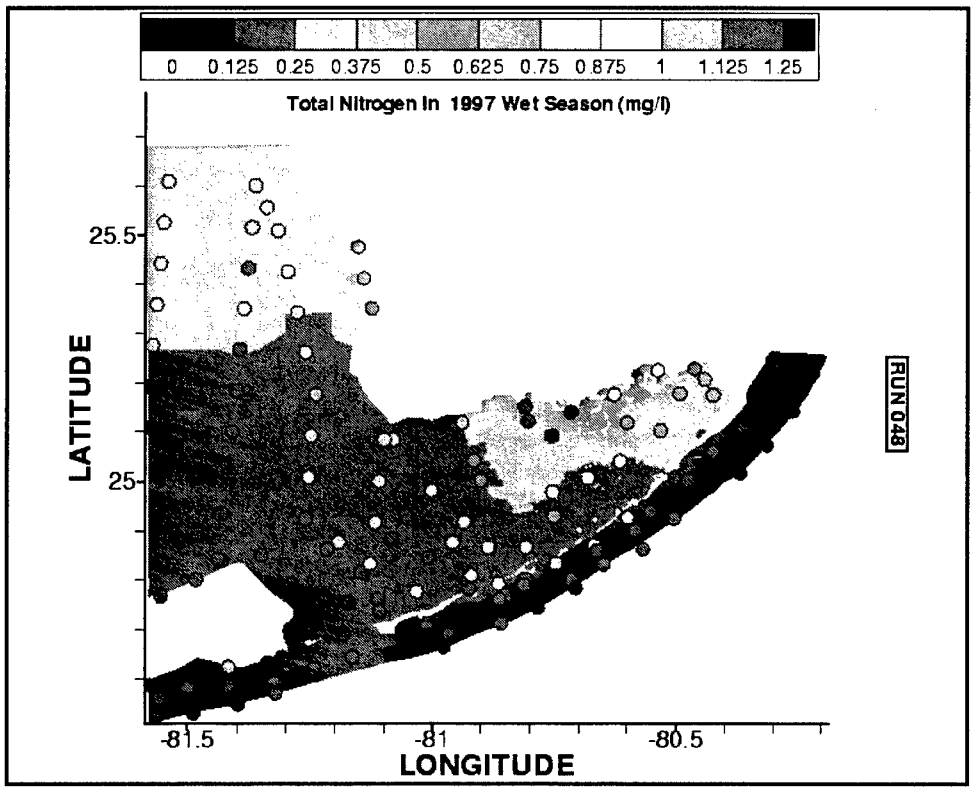

Figure 68. Total nitrogen, wet season 1997

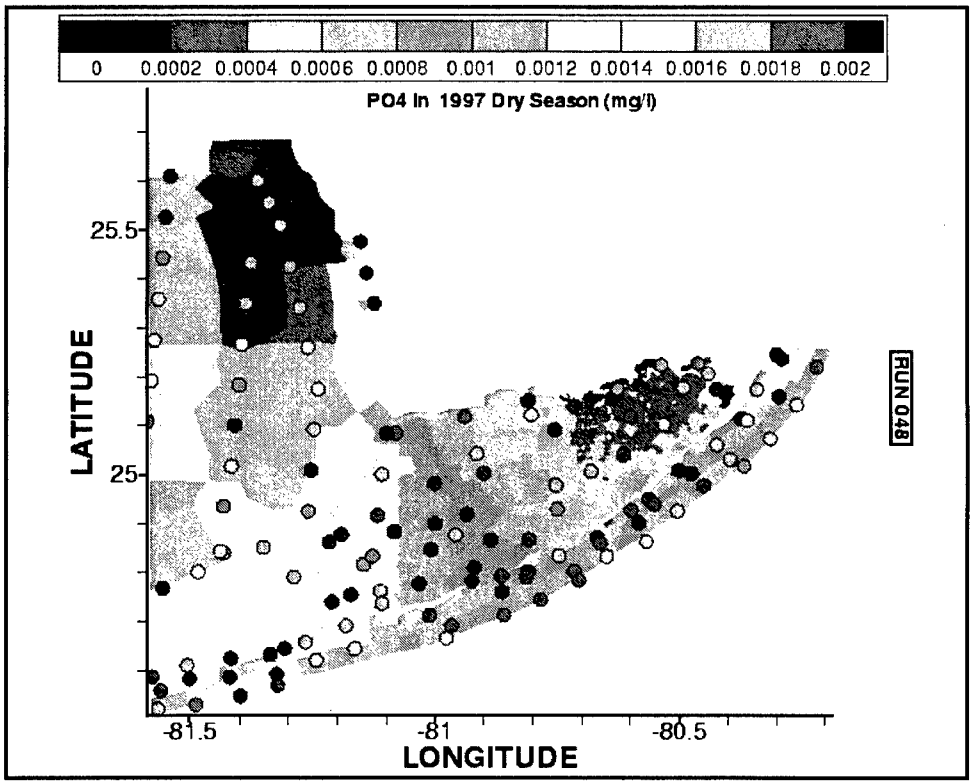

Figure 69. Soluble reactive phosphorus, dry season 1997

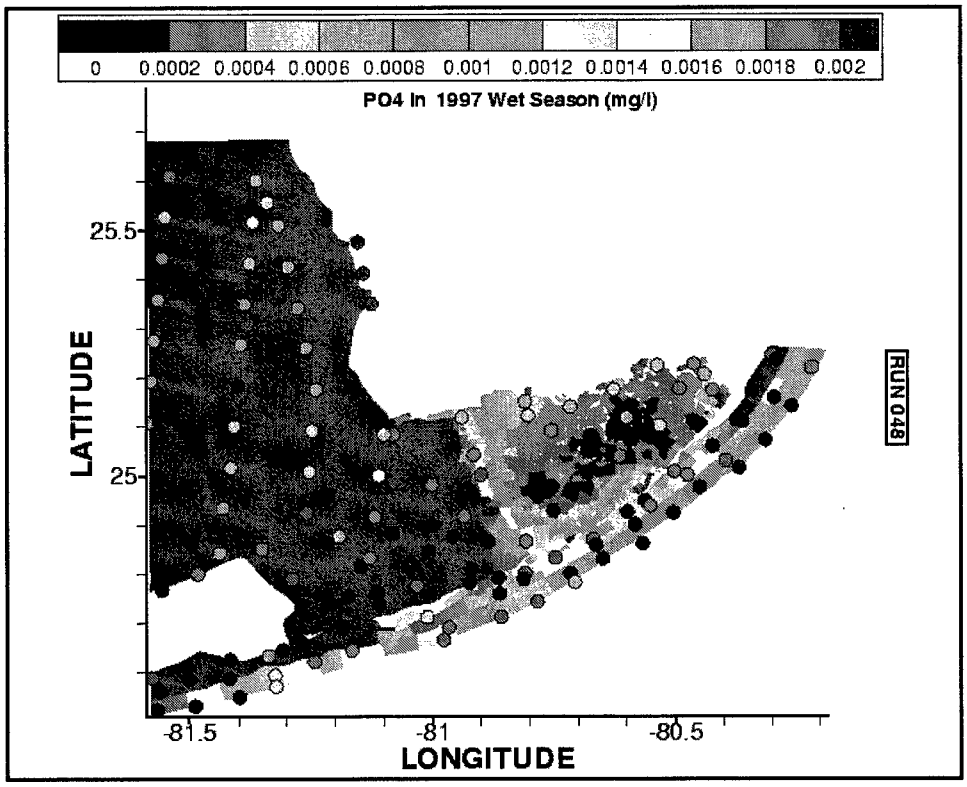

Figure 70. Soluble reactive phosphorus, wet season 1997

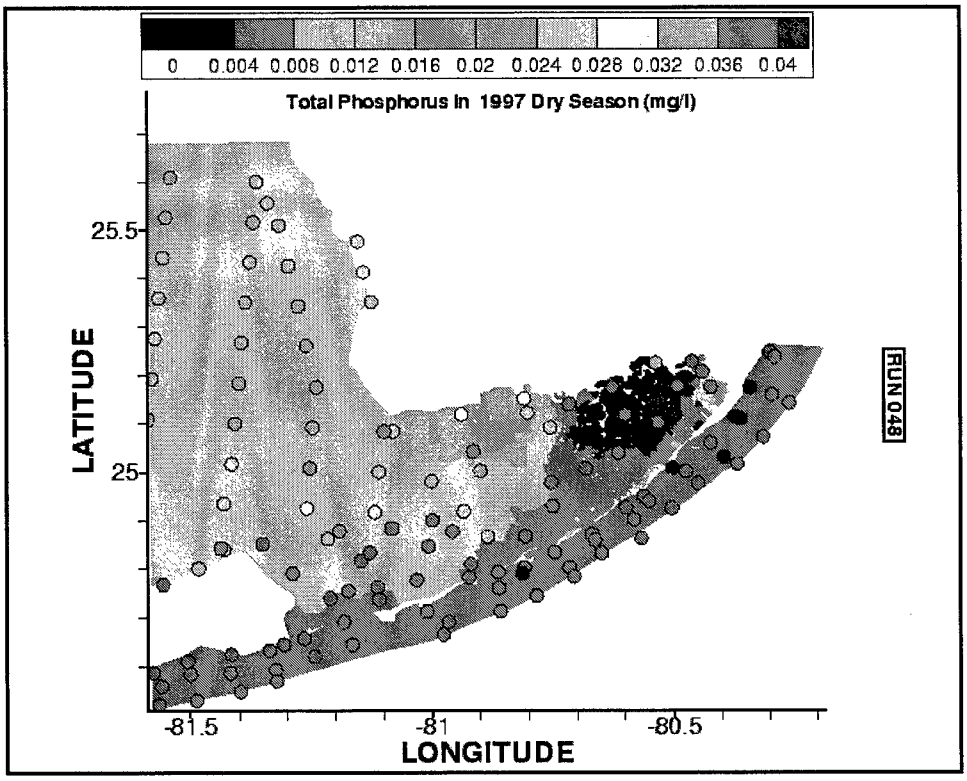

Figure 71. Total phosphorus, dry season 1997

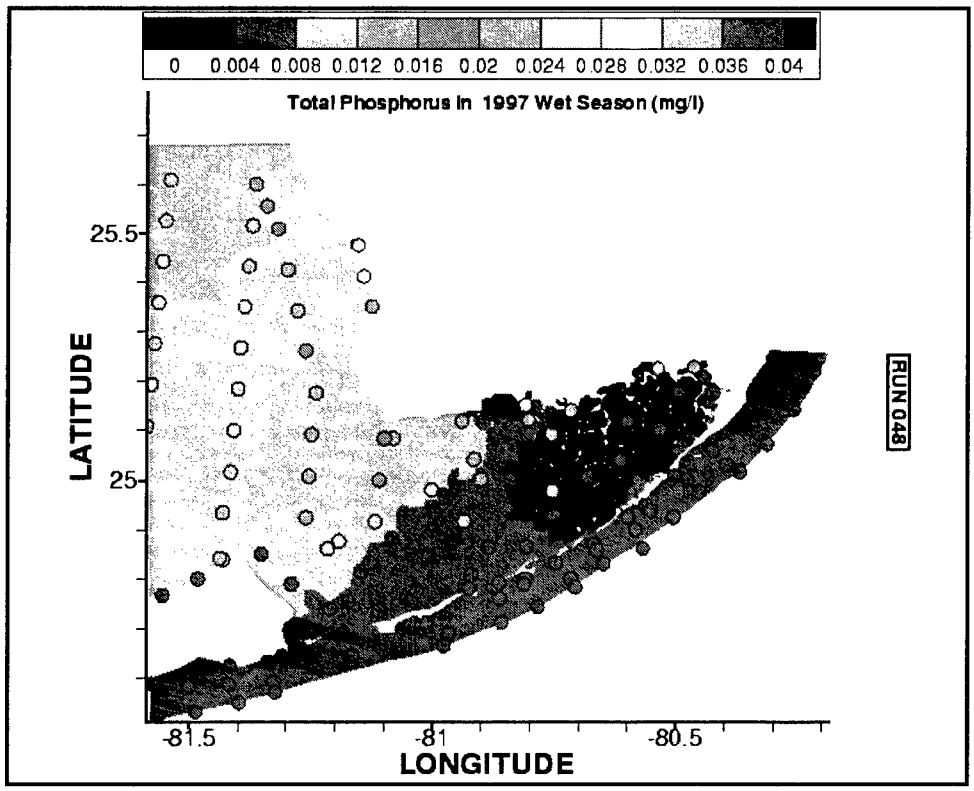

Figure 72. Total phosphorus, wet season 1997

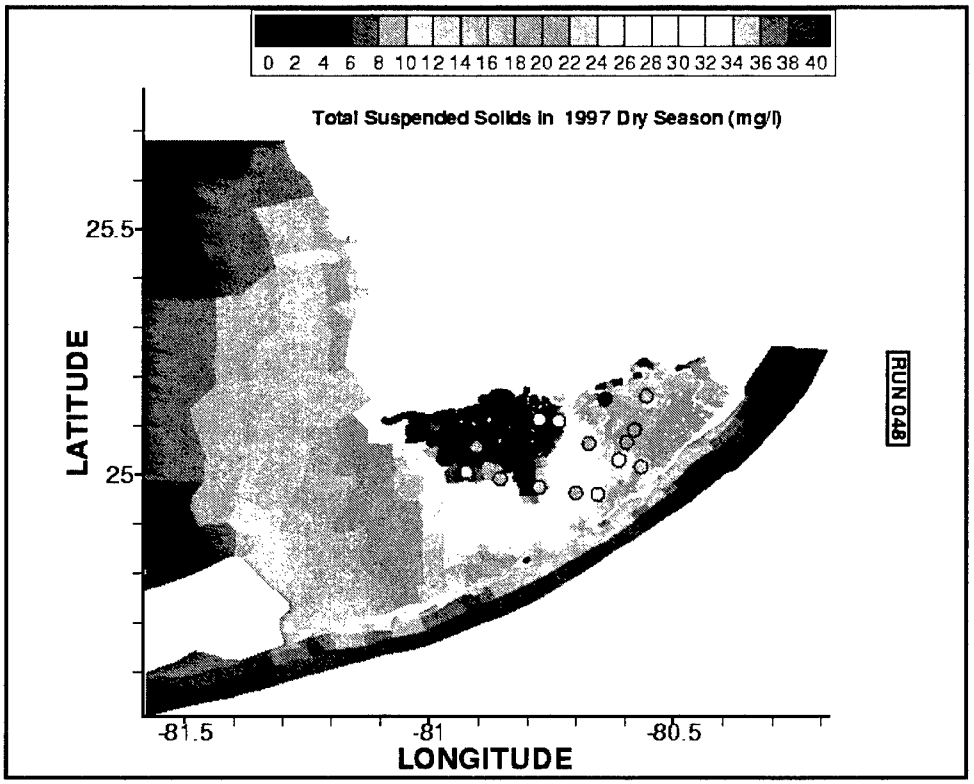

Figure 73. Total suspended solids, dry season 1997, compared to in situ observations from 1994-1996

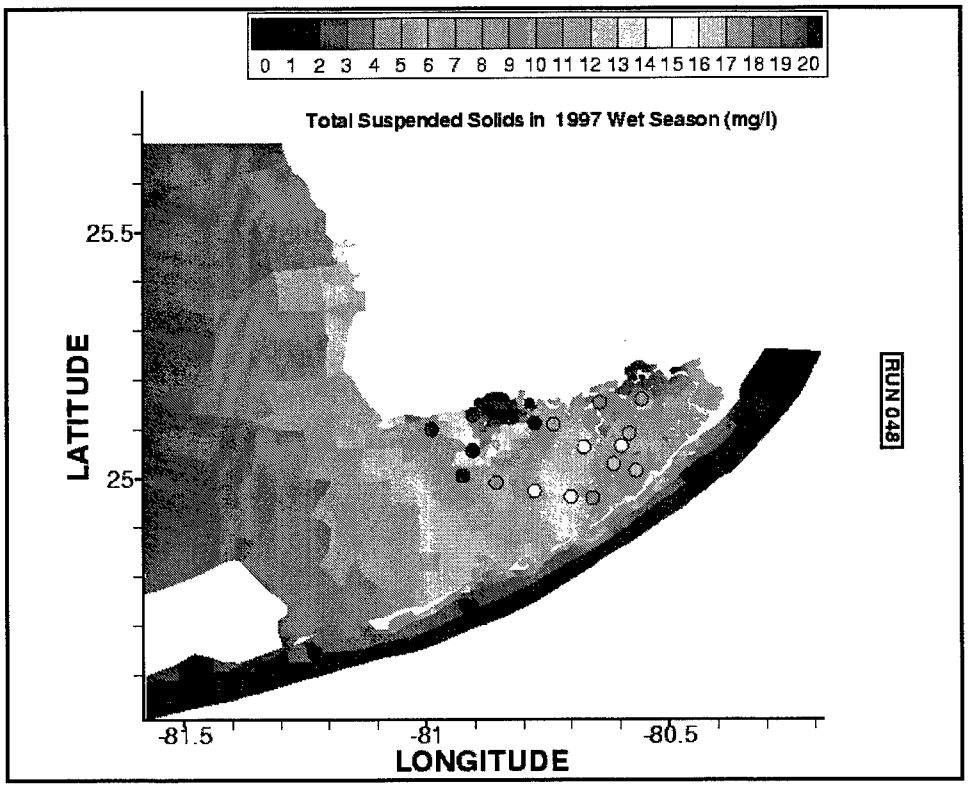

Figure 74. Total suspended solids, wet season 1997, compared to in situ observations from 1994-1996

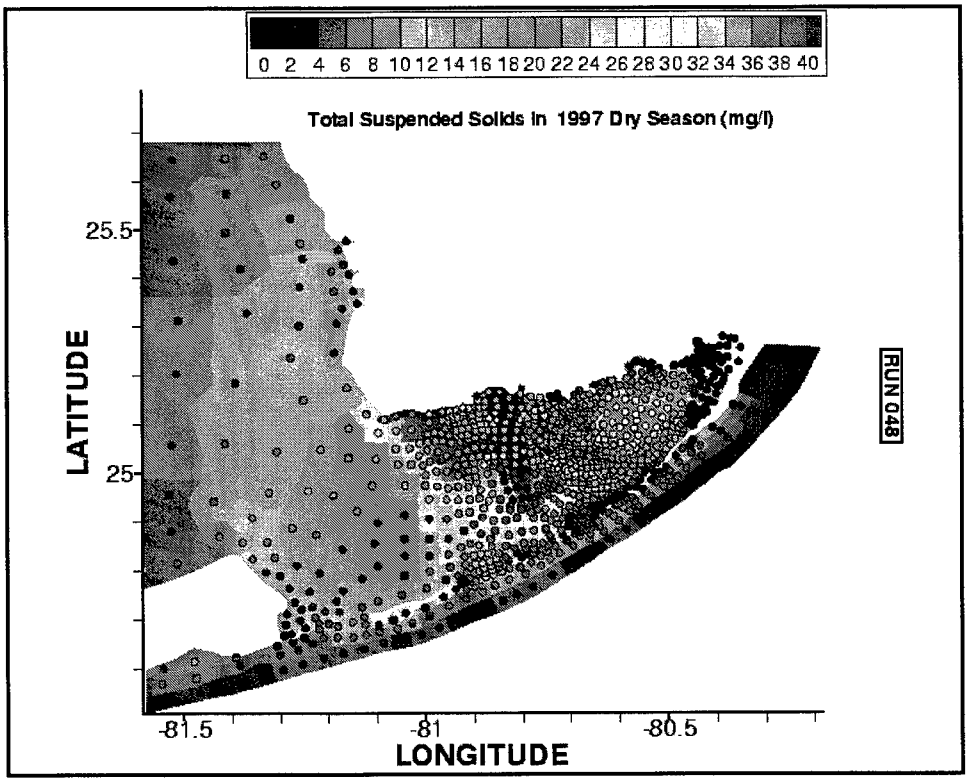

Figure 75. Total suspended solids, dry season 1997, compared to remotely sensed observations

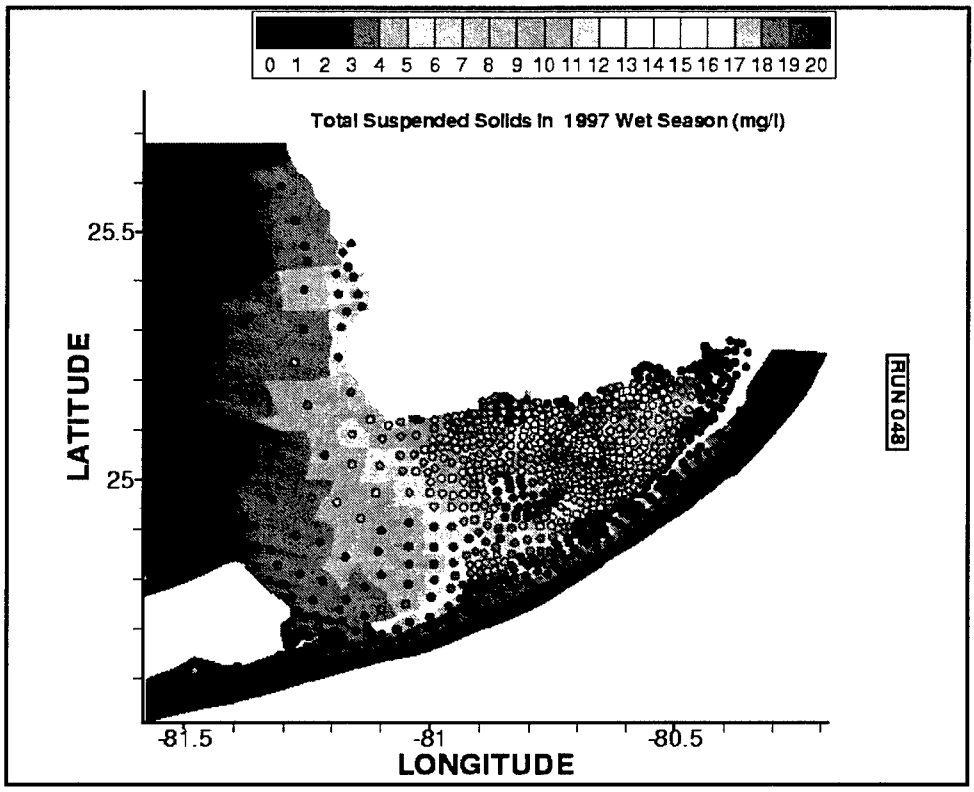

Figure 76. Total suspended solids, wet season 1997, compared to remotely sensed observations

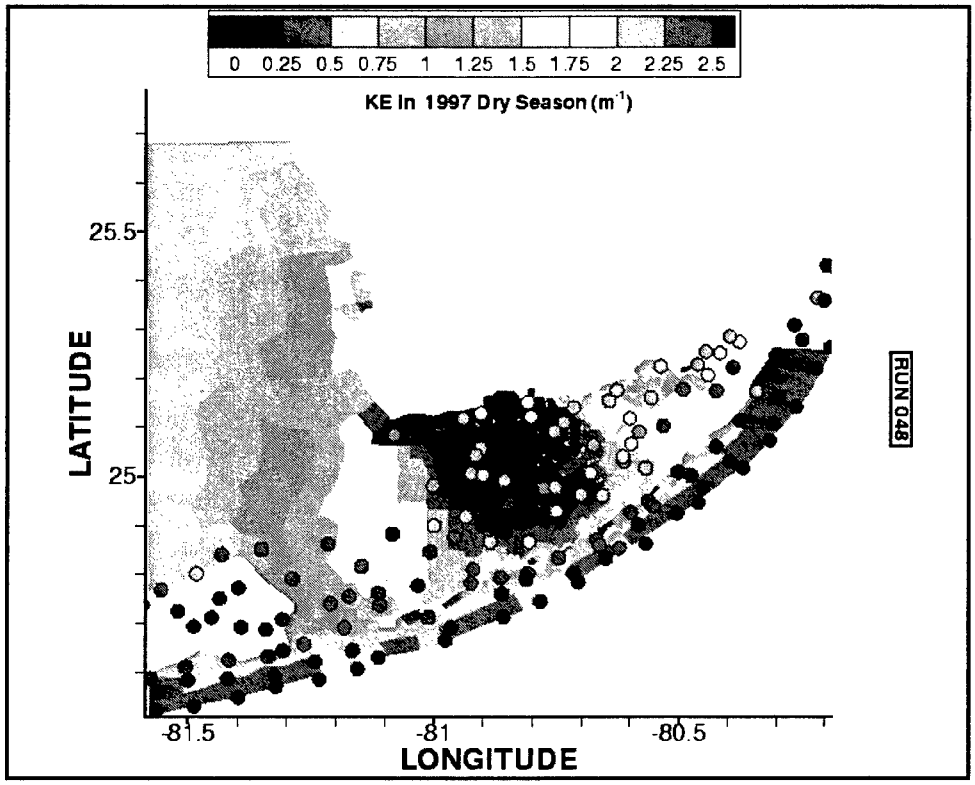

Figure 77. Light attenuation, dry season 1997, compared to observations from 1994-1995

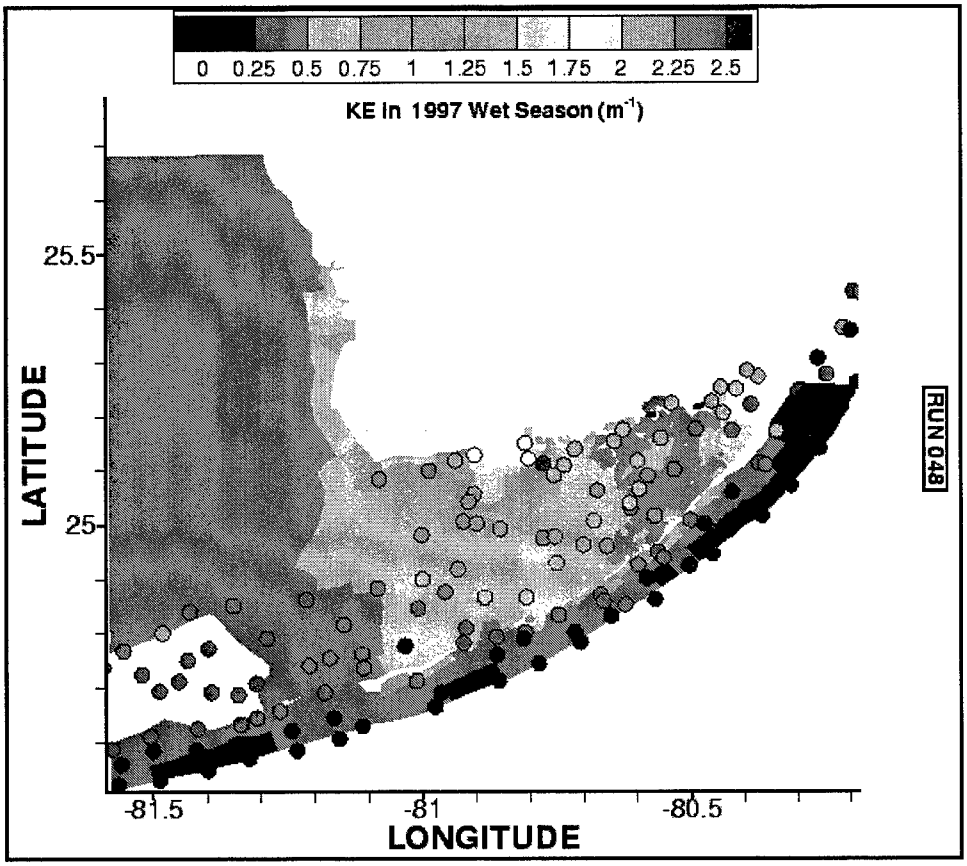

Figure 78. Light attenuation, wet season 1997, compared to observations from 1994-1995

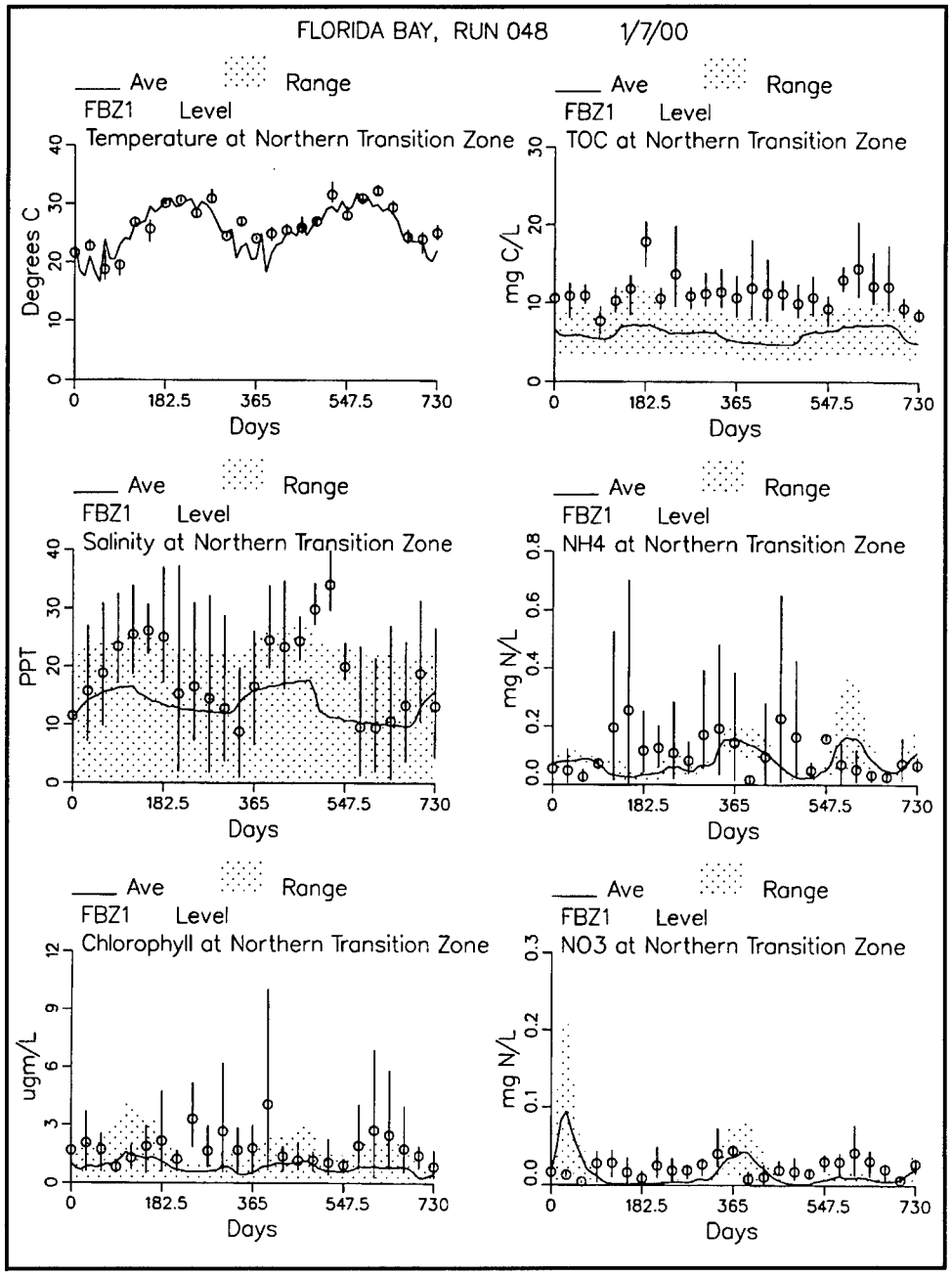

Figure 79. Time series in Northern Transition Zone (continued)

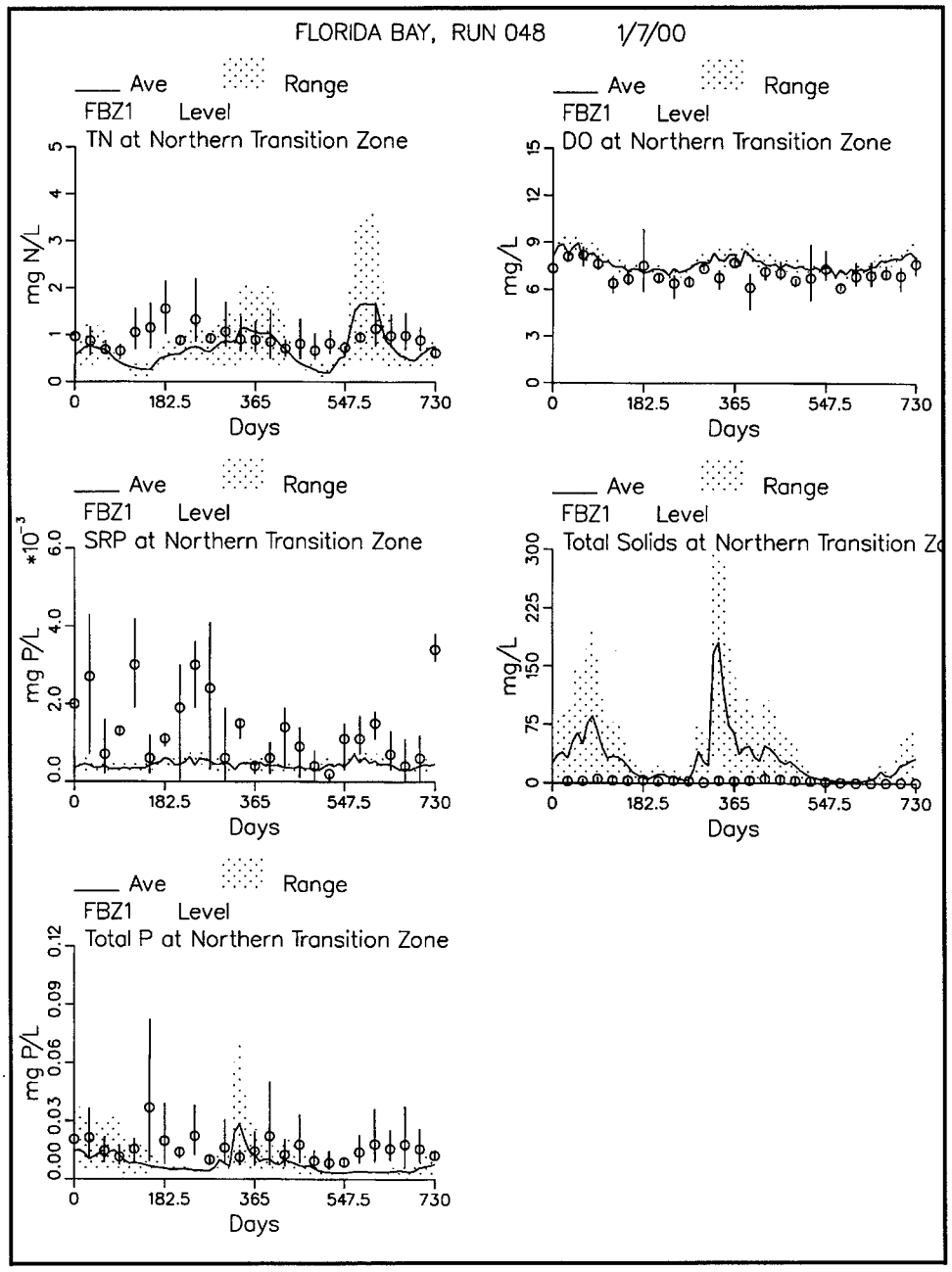

Figure 79. (concluded)

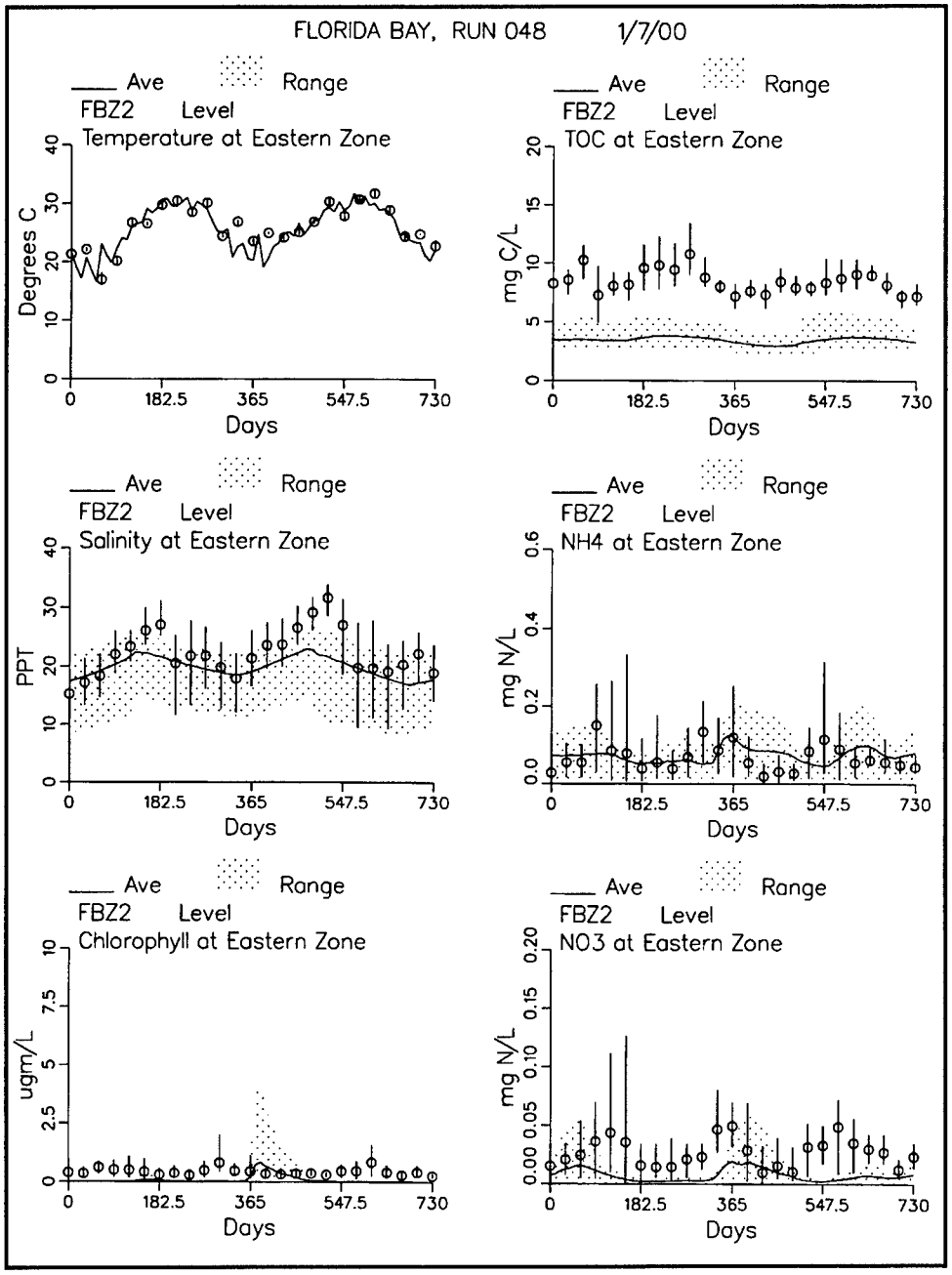

Figure 80. Time series in Eastern Zone (continued)

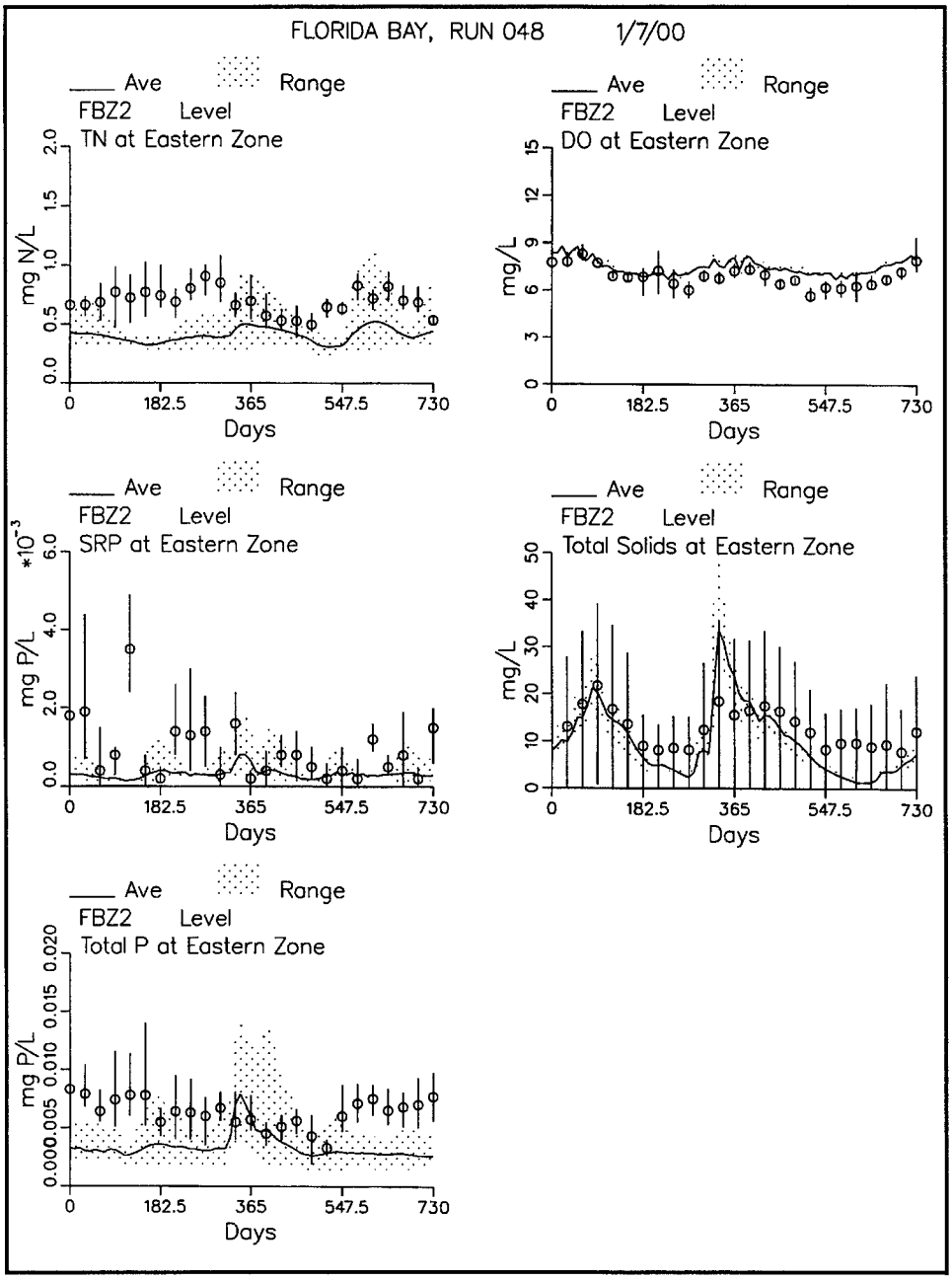

Figure 80. (concluded)

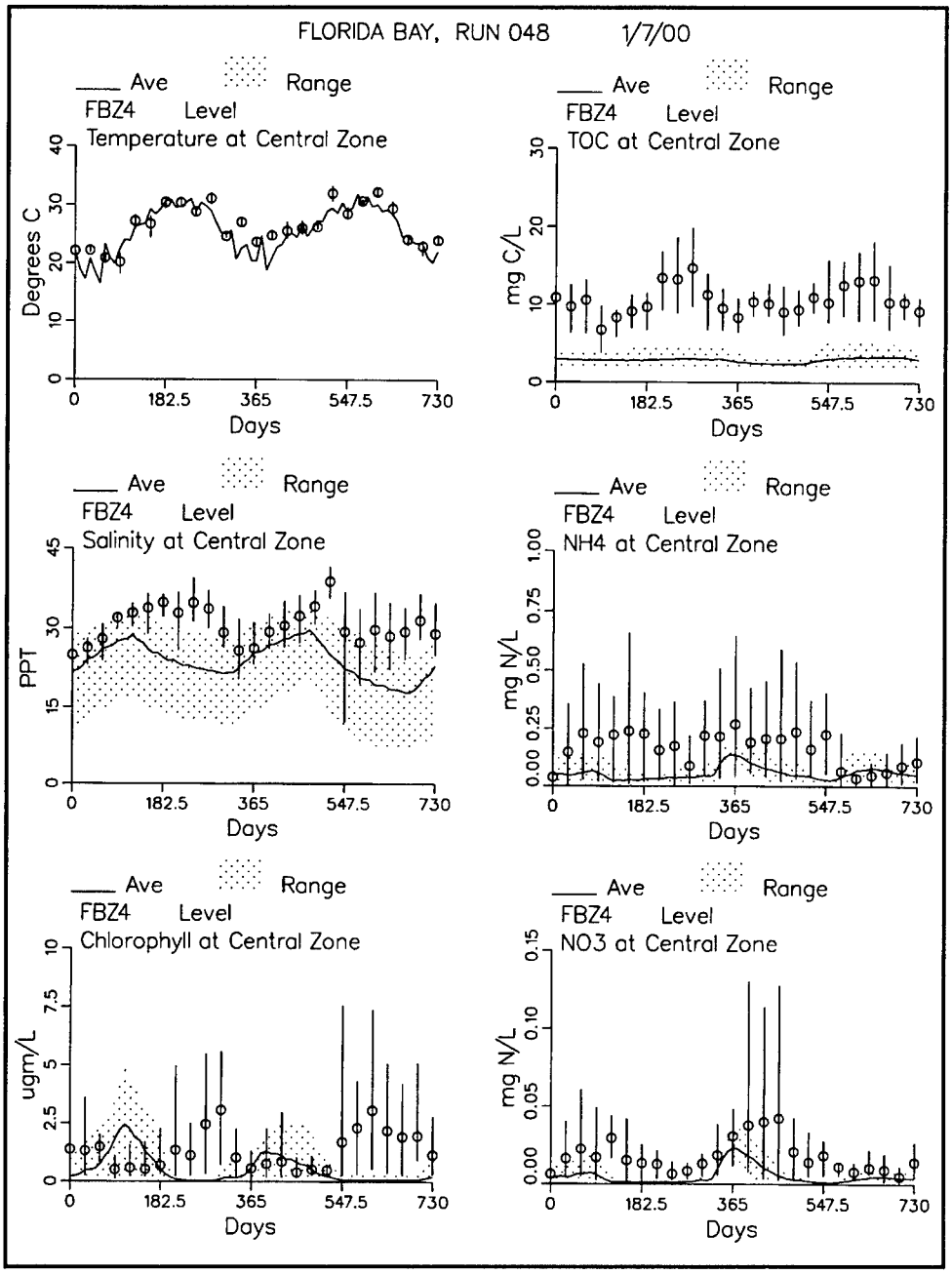

Figure 81. Time series in Central Zone (continued)

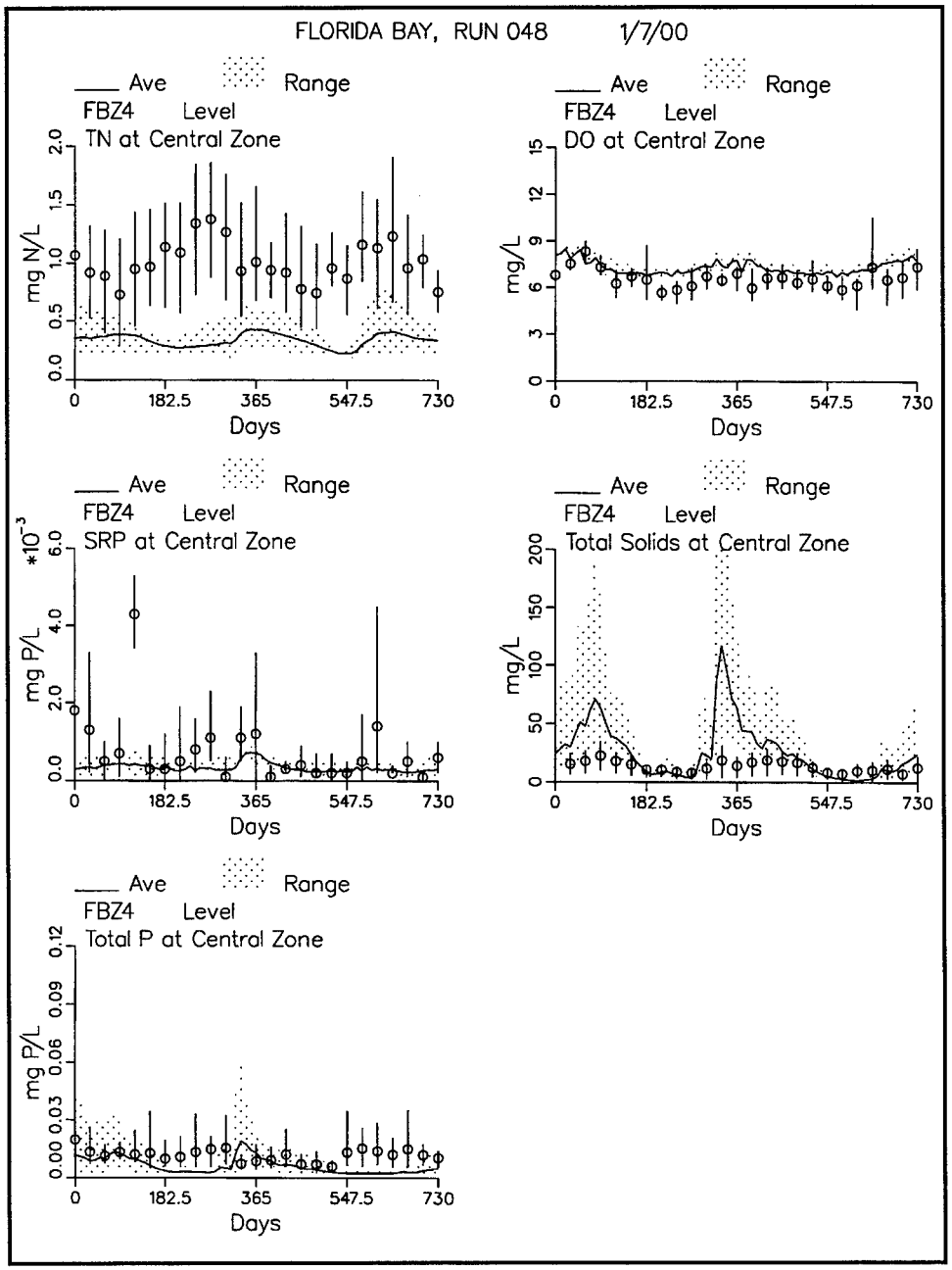

Figure 81. (concluded)

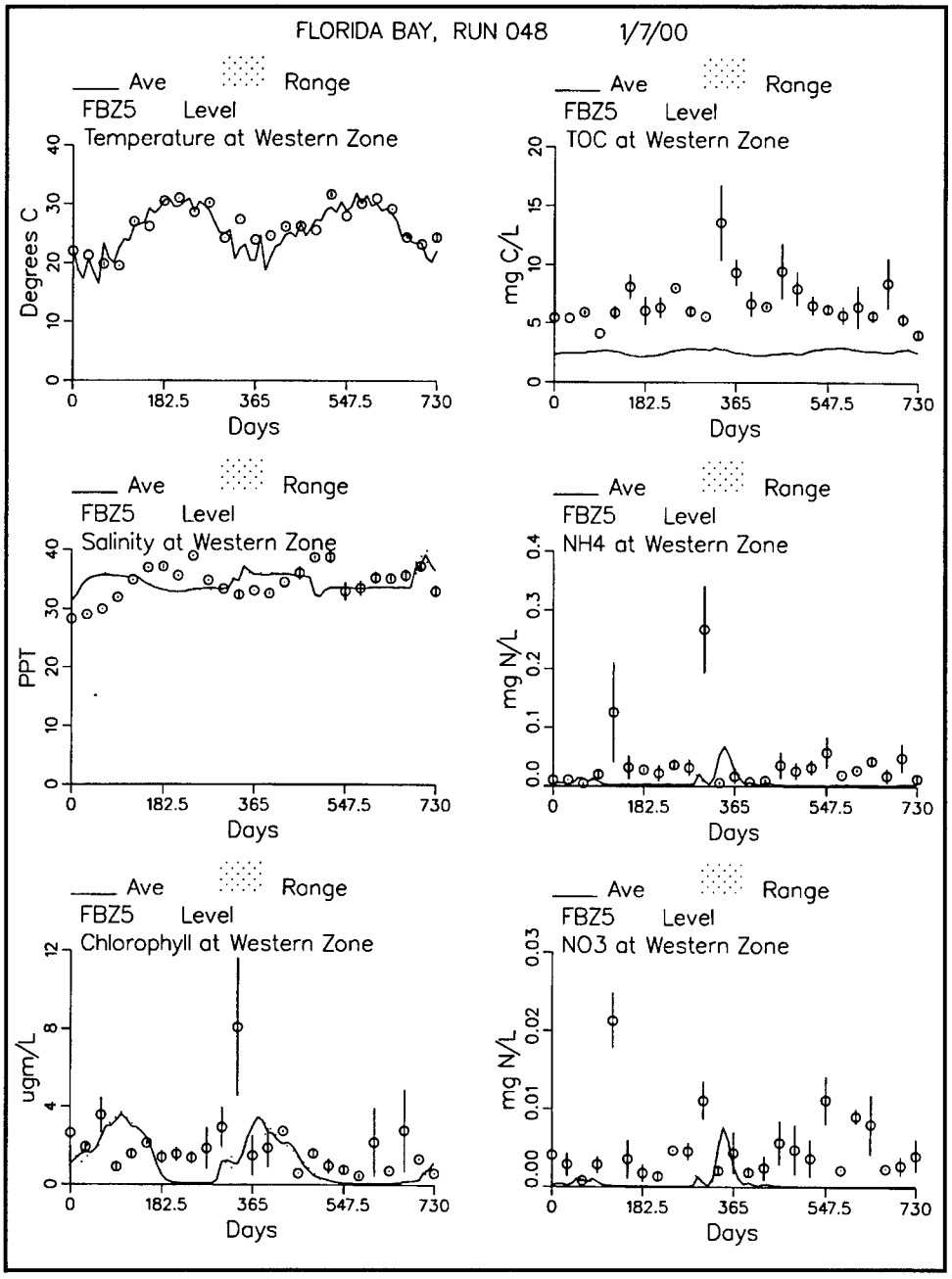

Figure 82. Time series in Western Zone (continued)

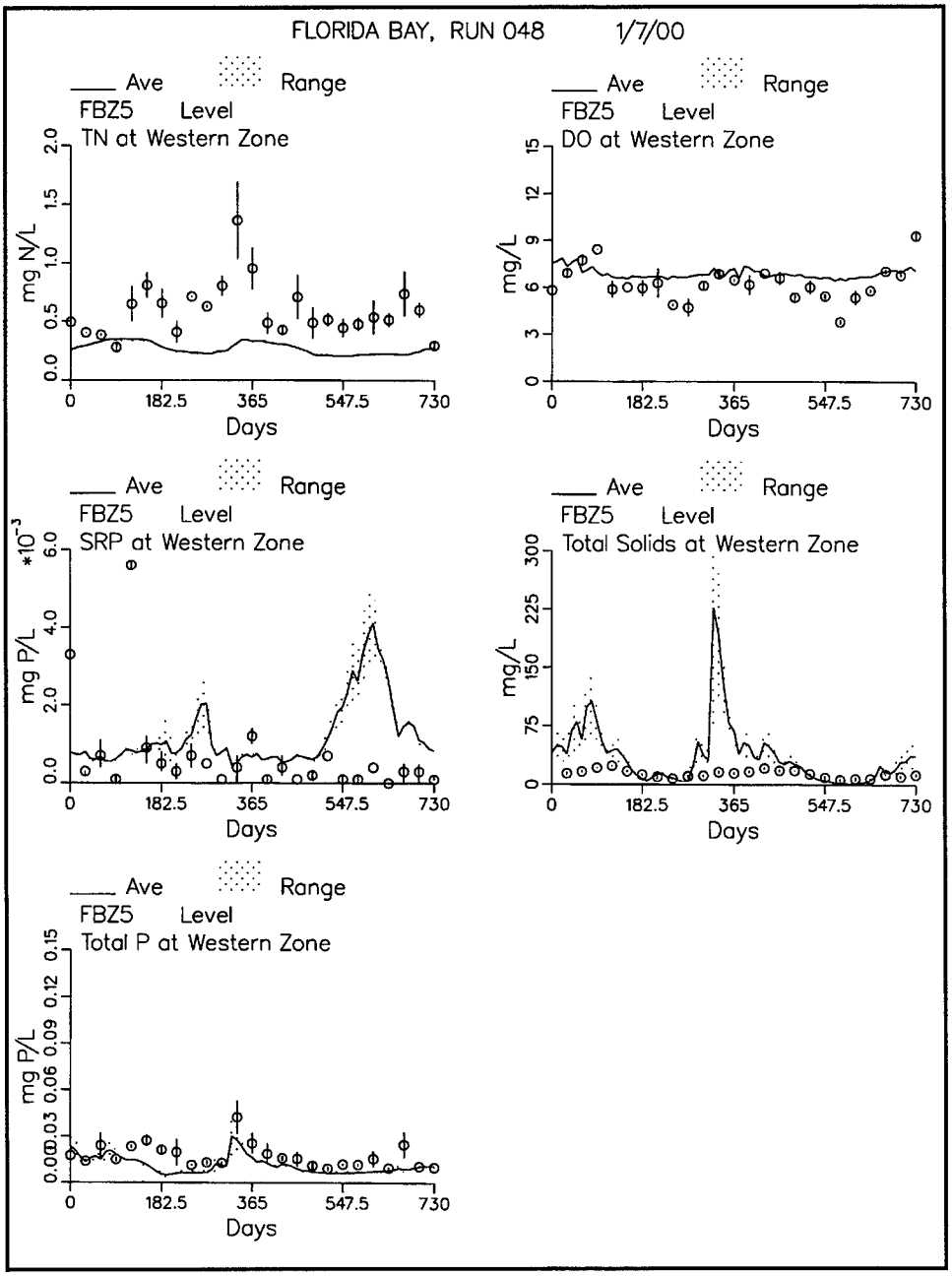

Figure 82. (concluded)

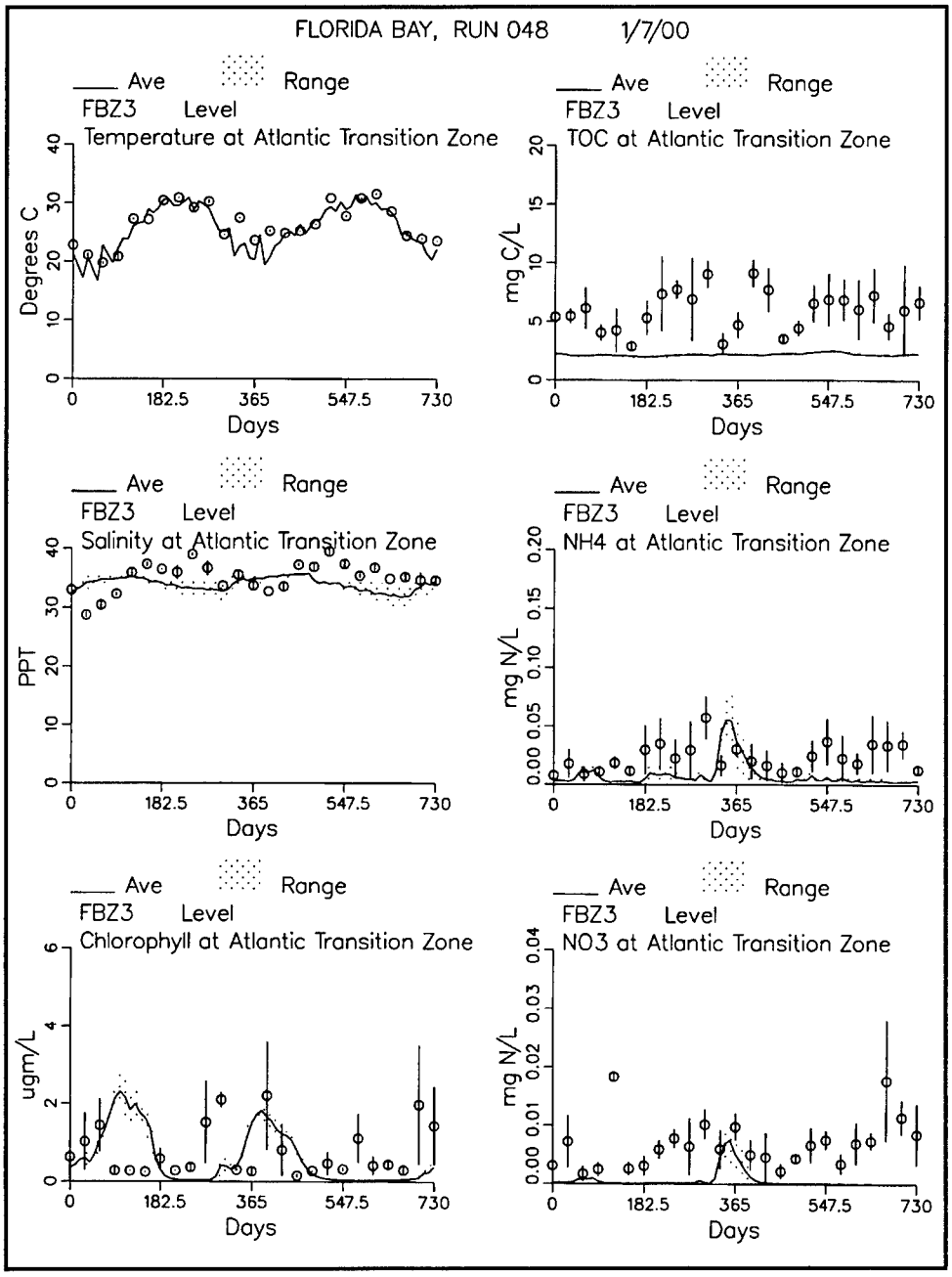

Figure 83. Time series in Atlantic Transition Zone (continued)

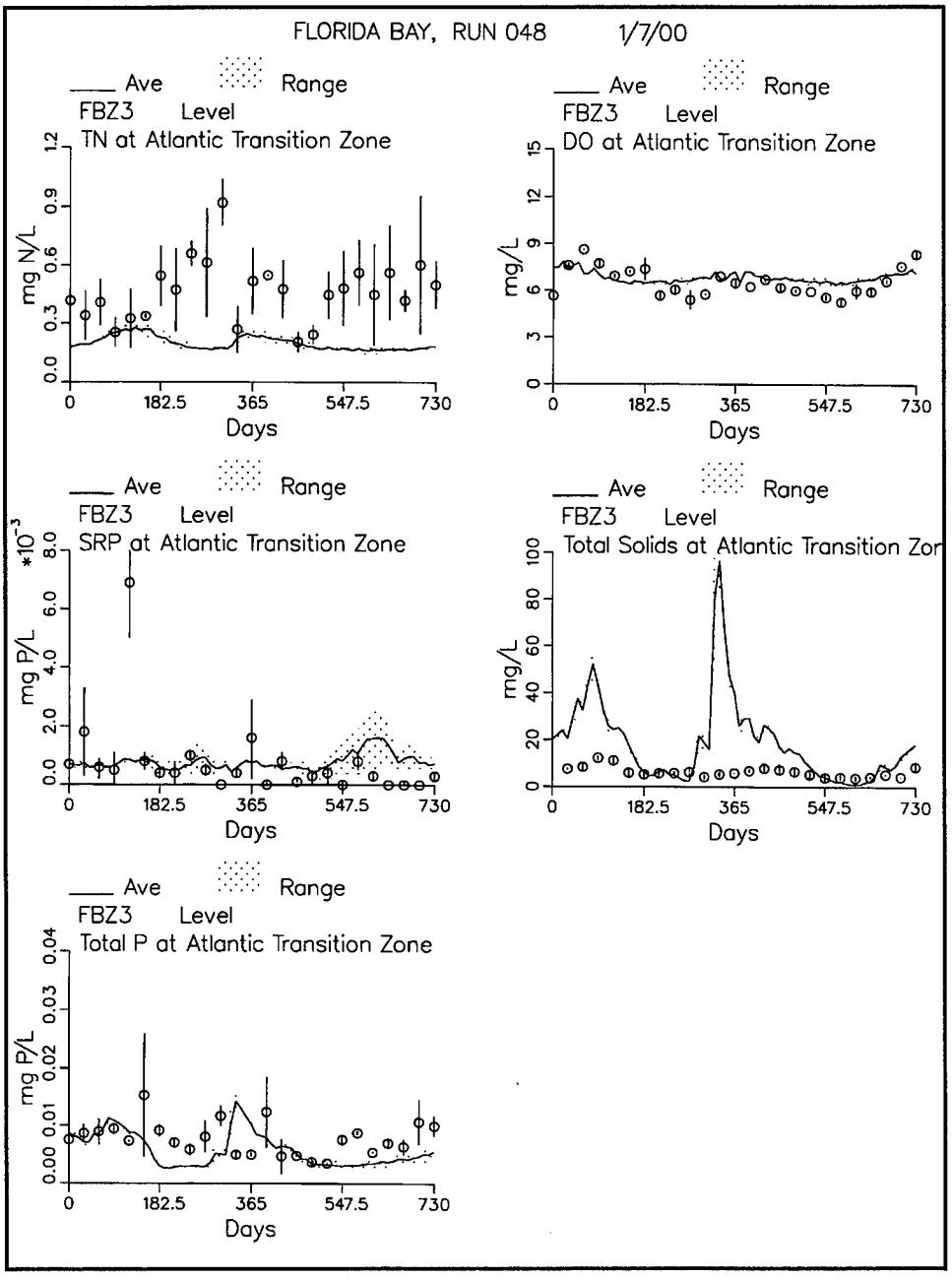

Figure 83. (concluded)

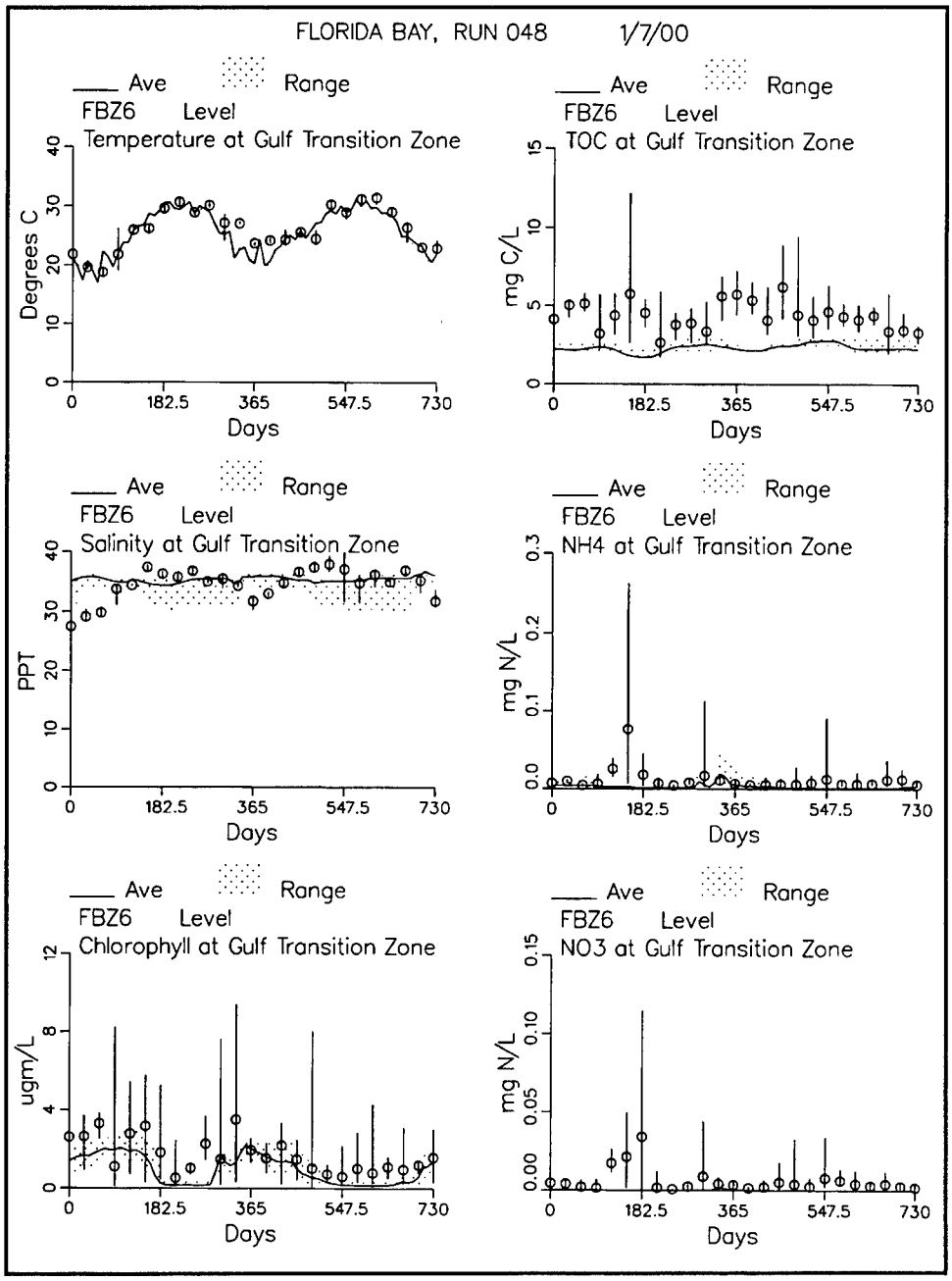

Figure 84. Time series in Gulf Transition Zone (continued)

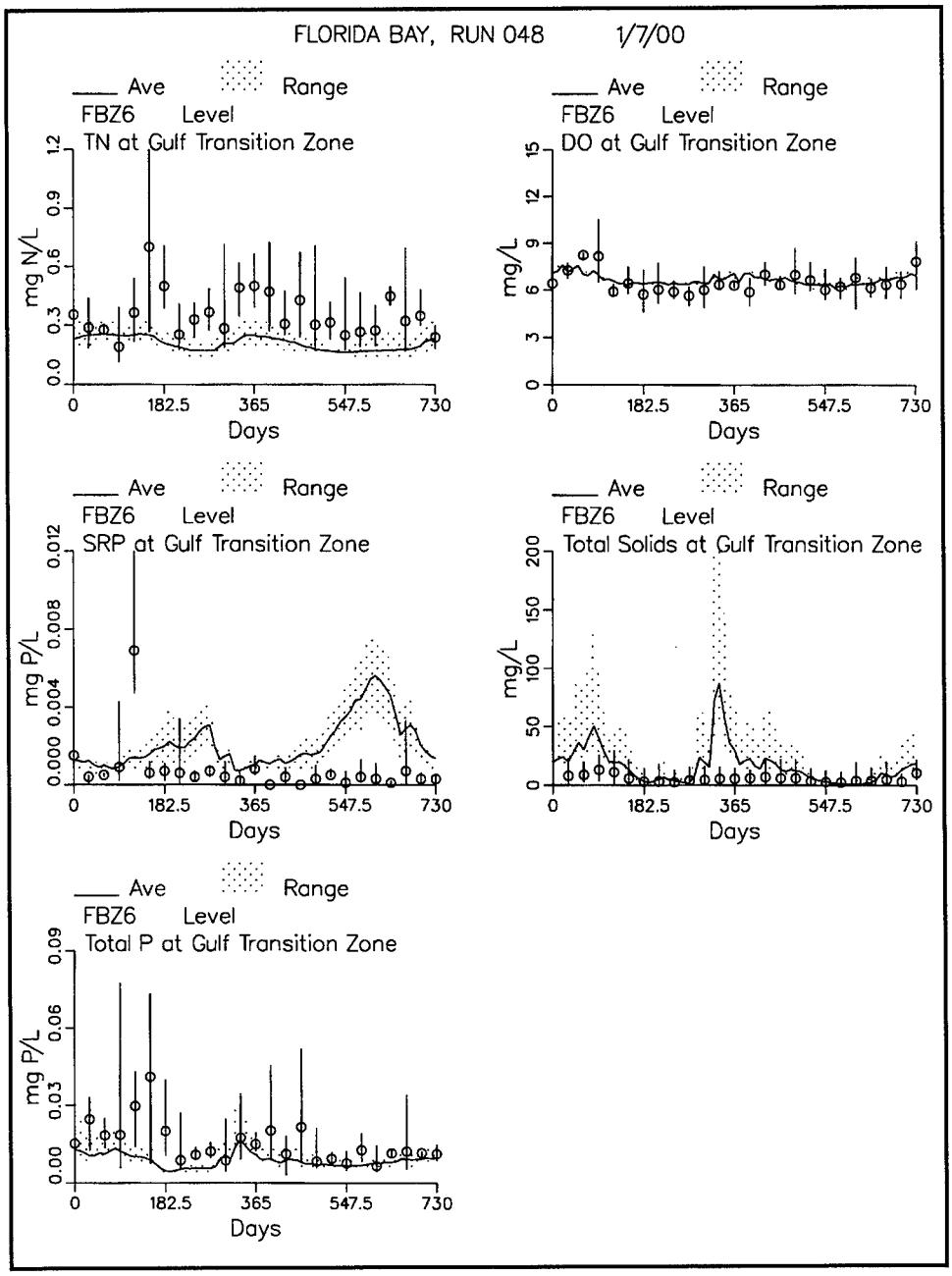

Figure 84. (concluded)

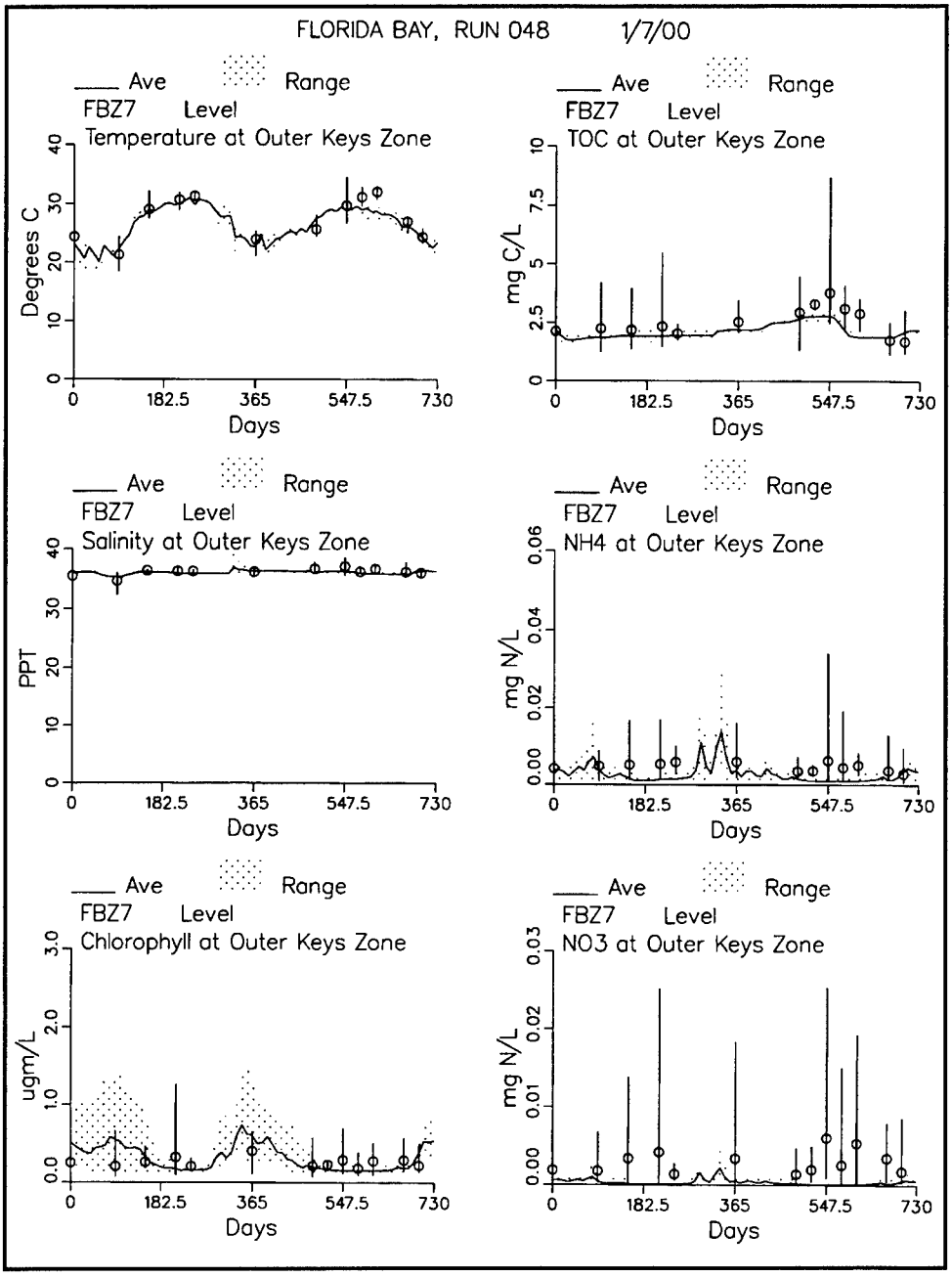

Figure 85. Time series in Outer Keys Zone (continued)

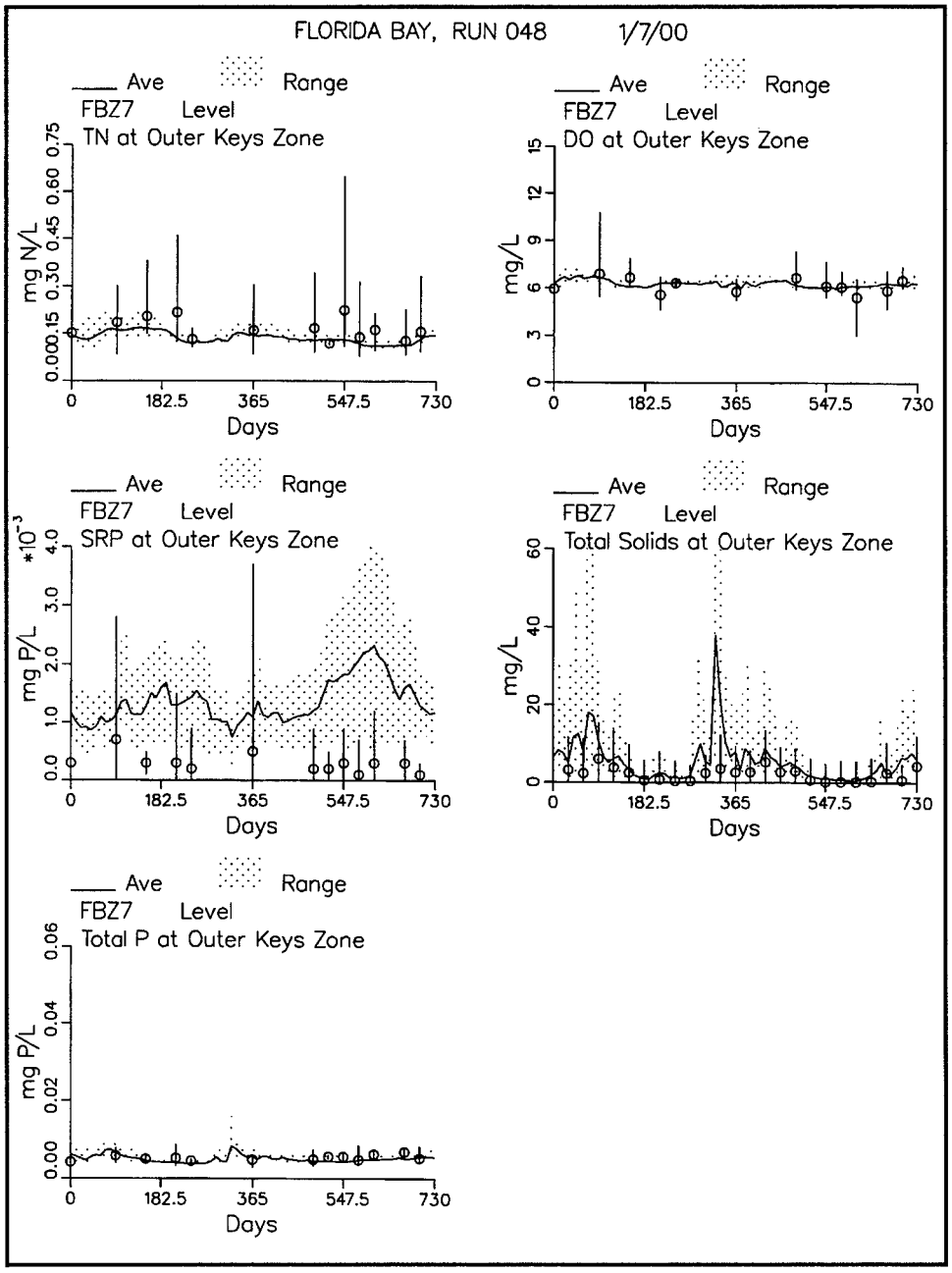

Figure 85. (concluded)

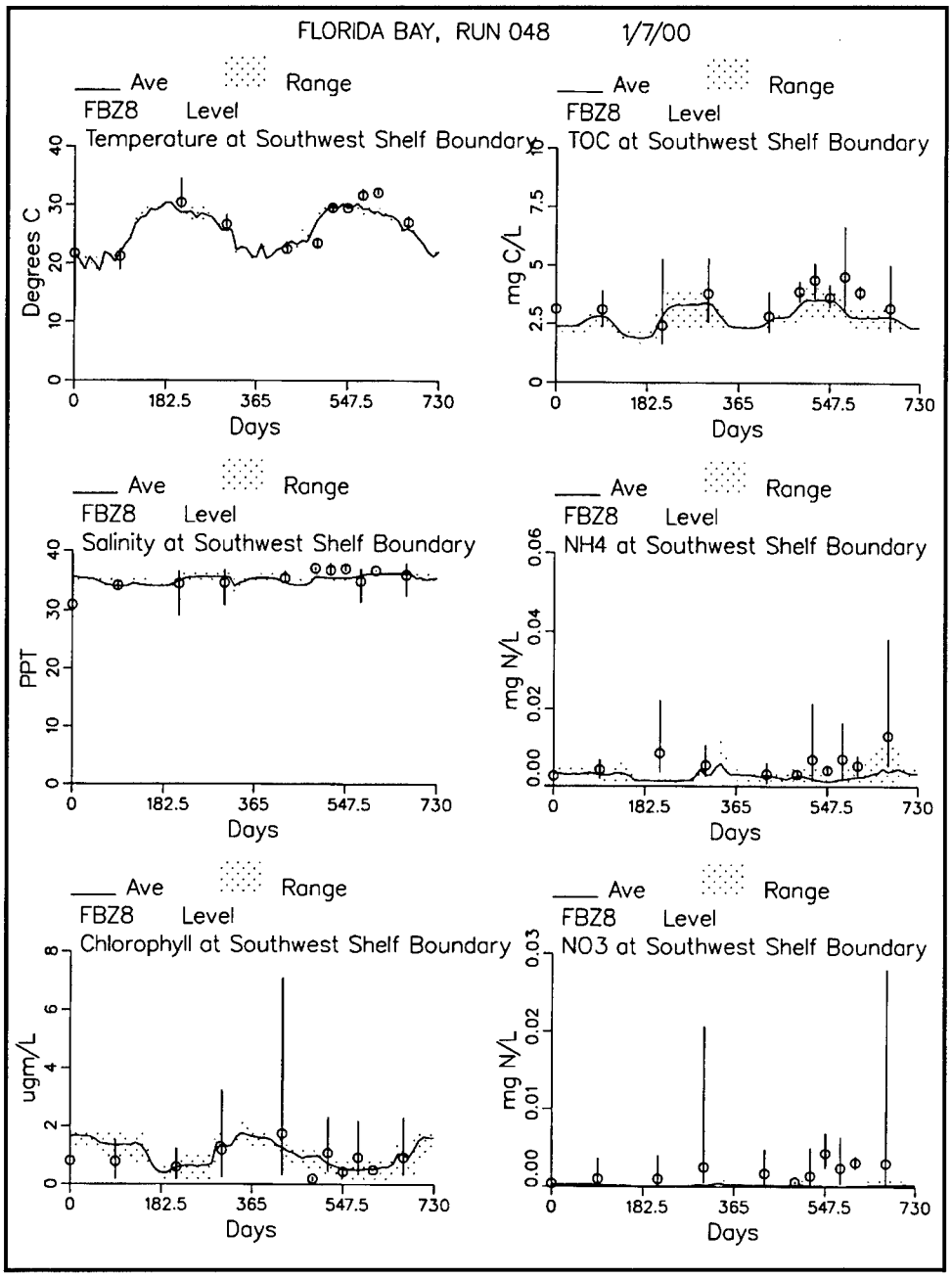

Figure 86. Time series in Southwest Shelf Zone (continued)

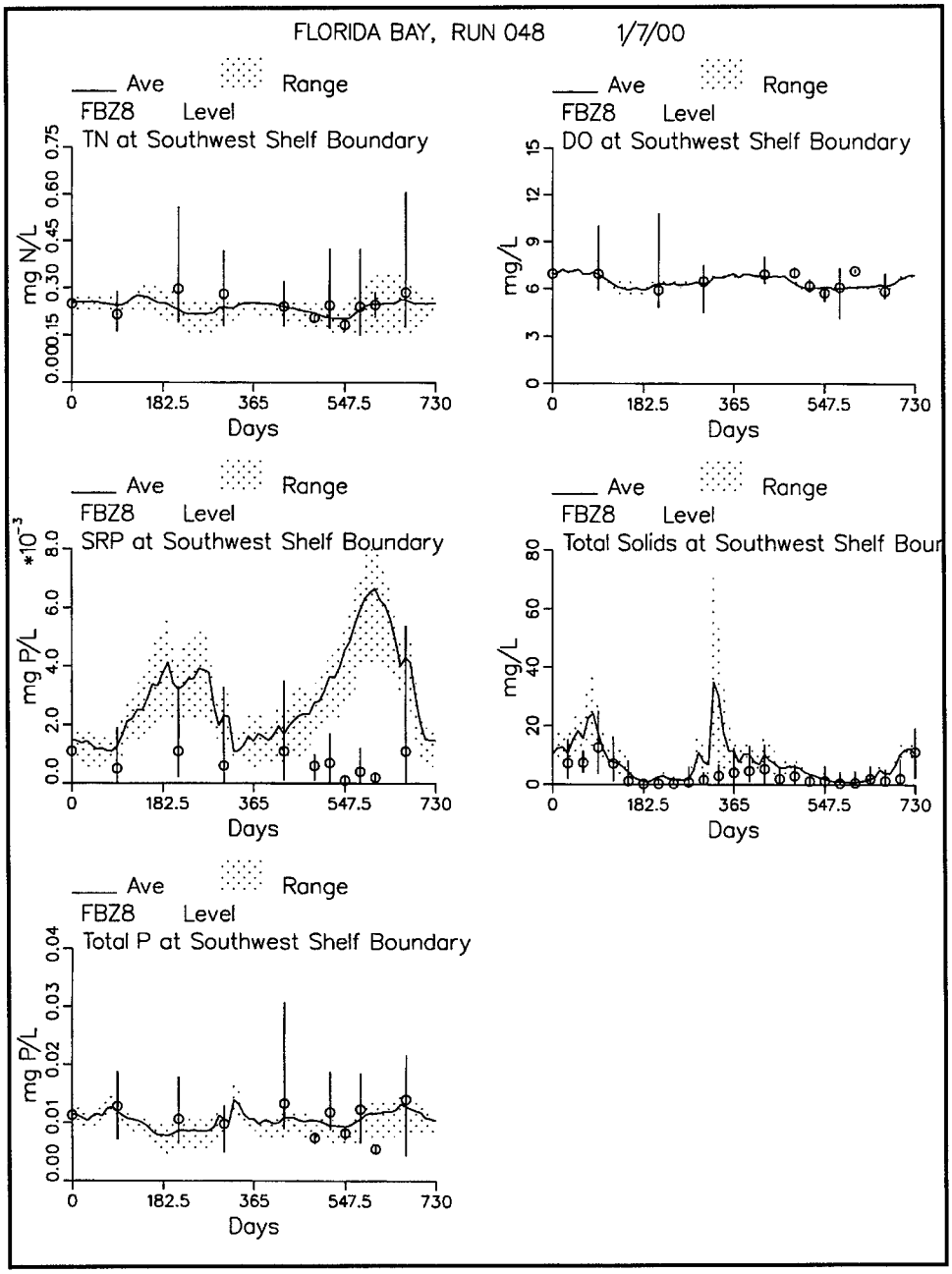

Figure 86. (concluded)

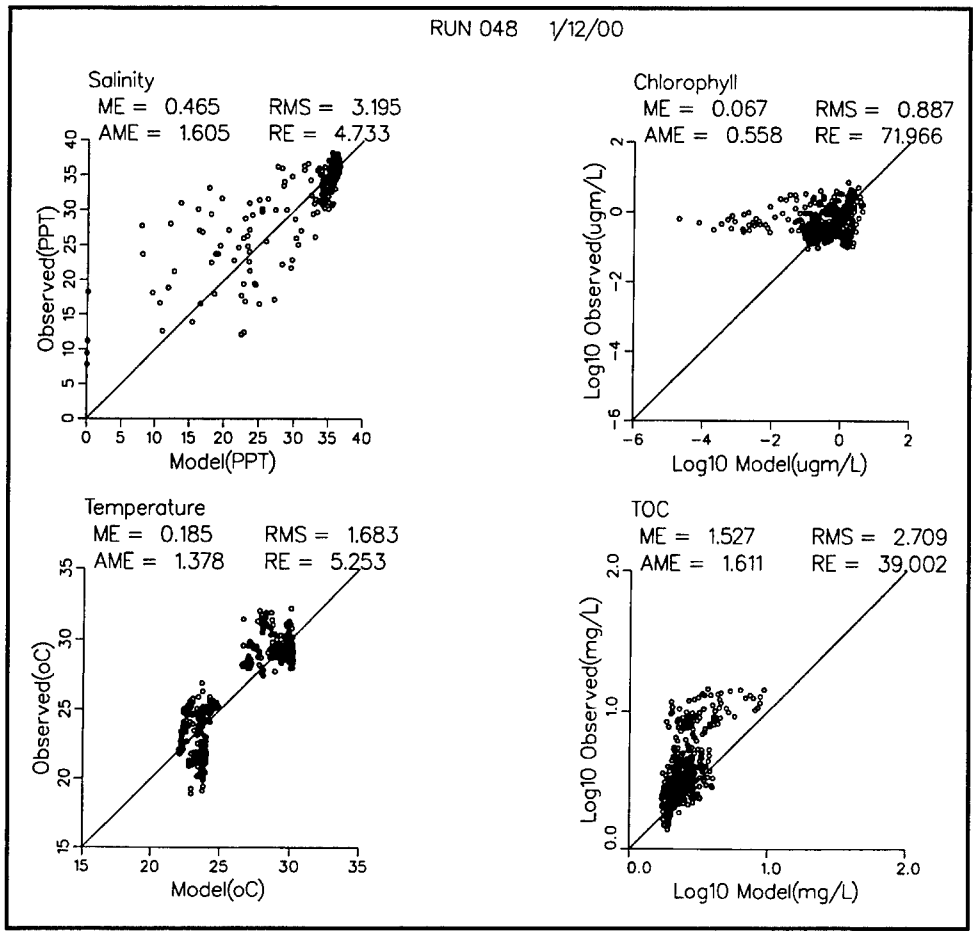

Figure 87. Scatterplots (sheet 1 of 3)

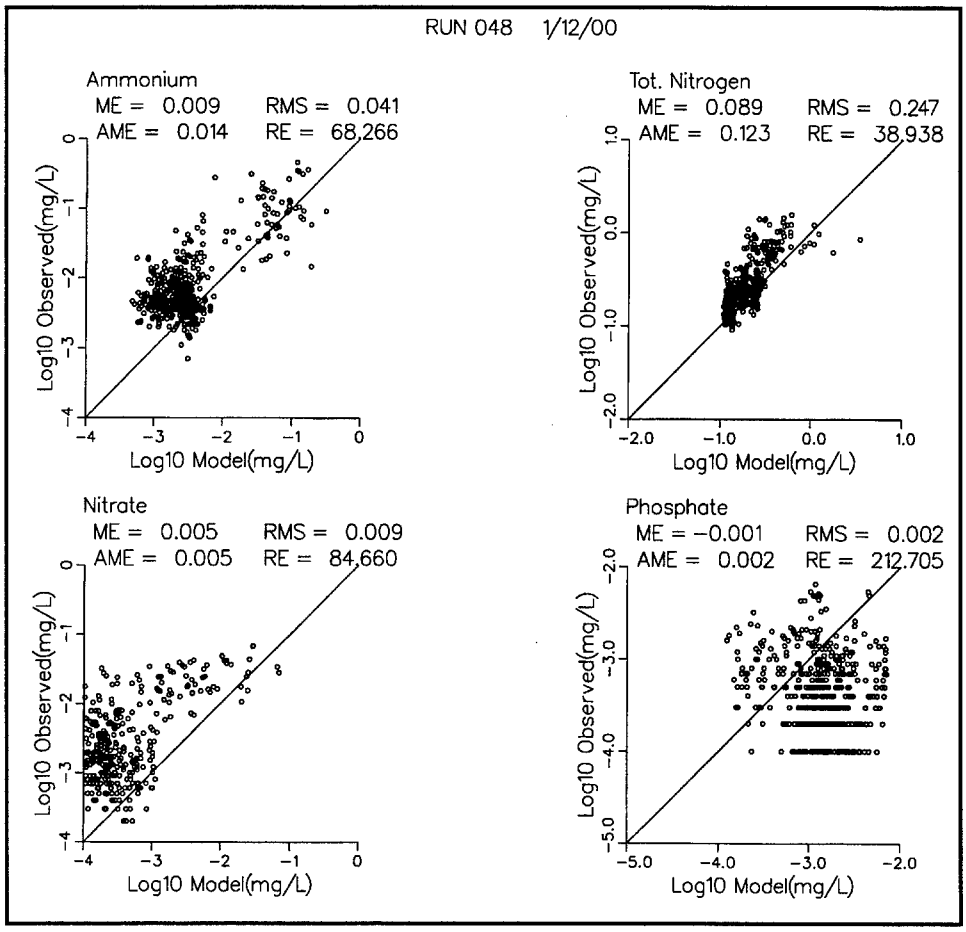

Figure 87. (sheet 2 of 3)

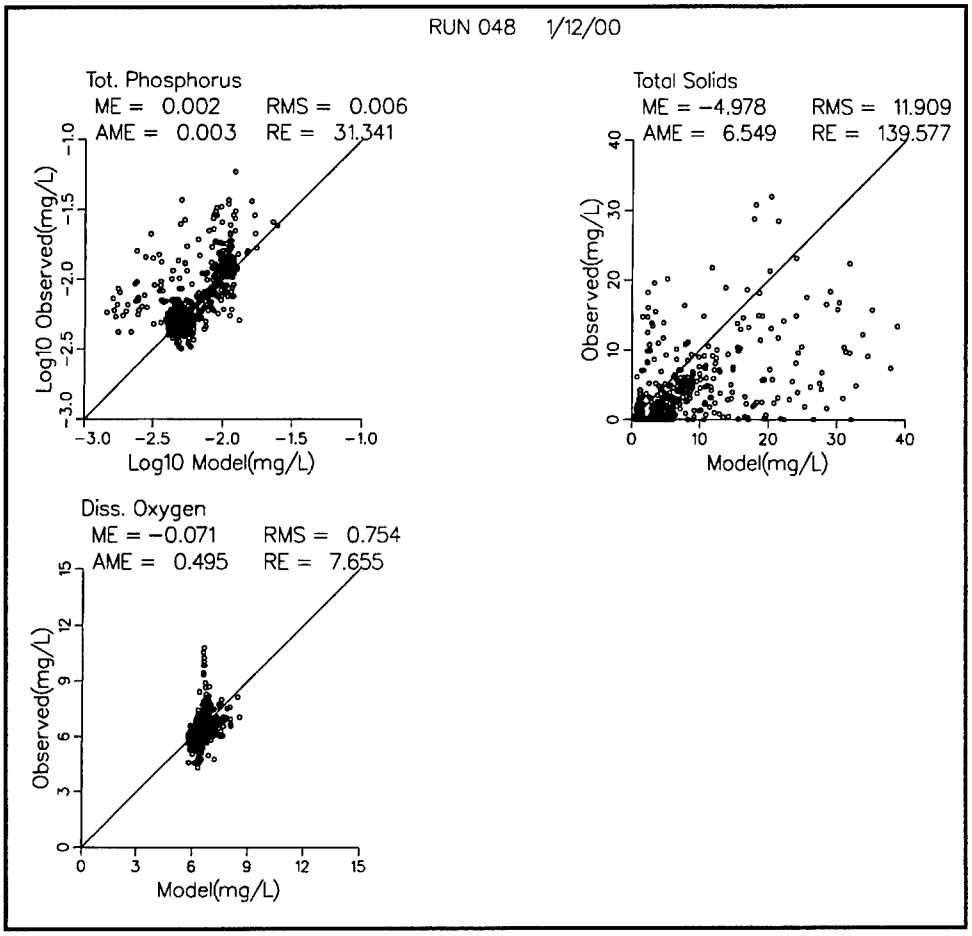

Figure 87. (sheet 3 of 3)

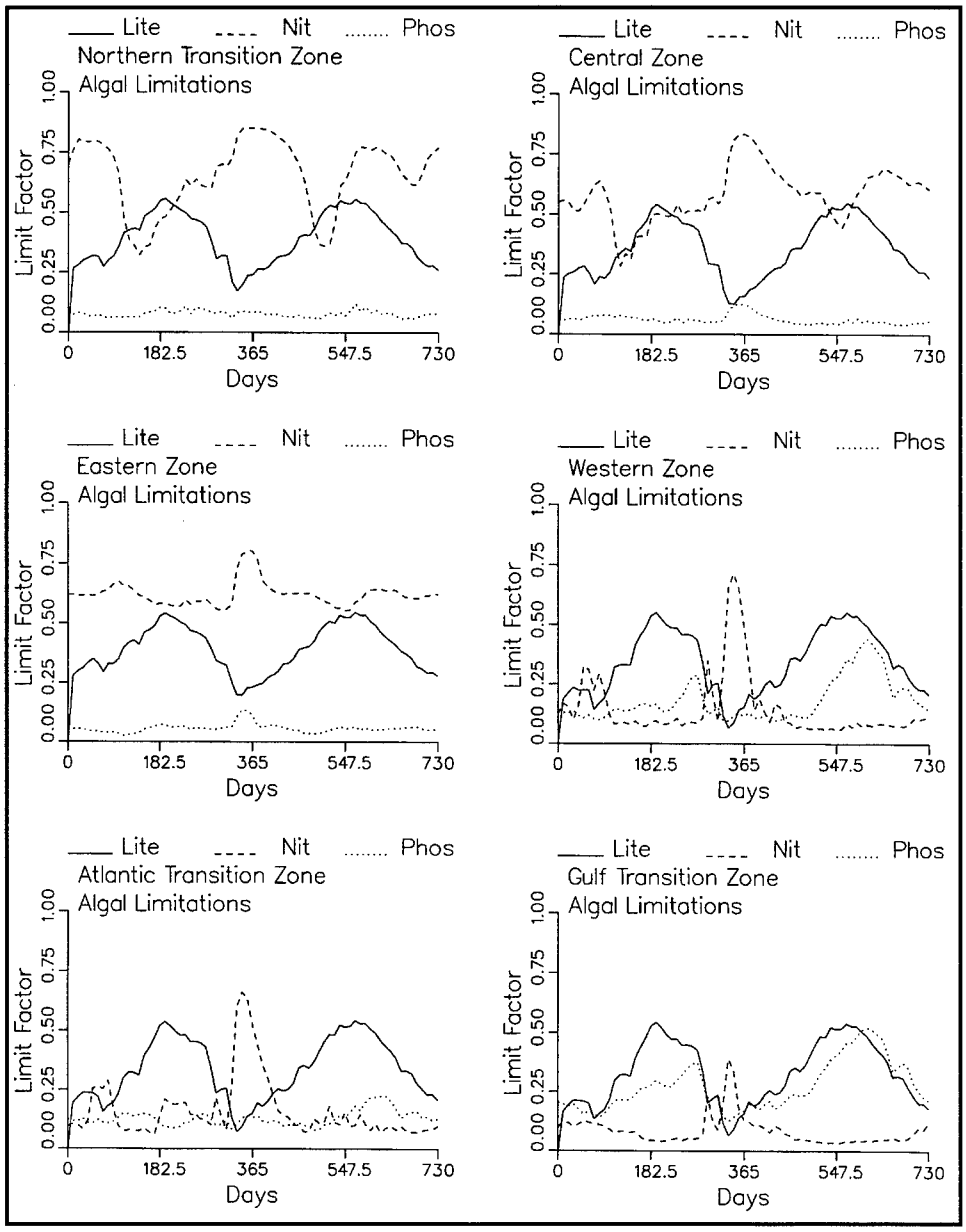

Figure 88. Algal growth-limiting factors. The lowest value of "Limit Factor" is most limiting (continued)

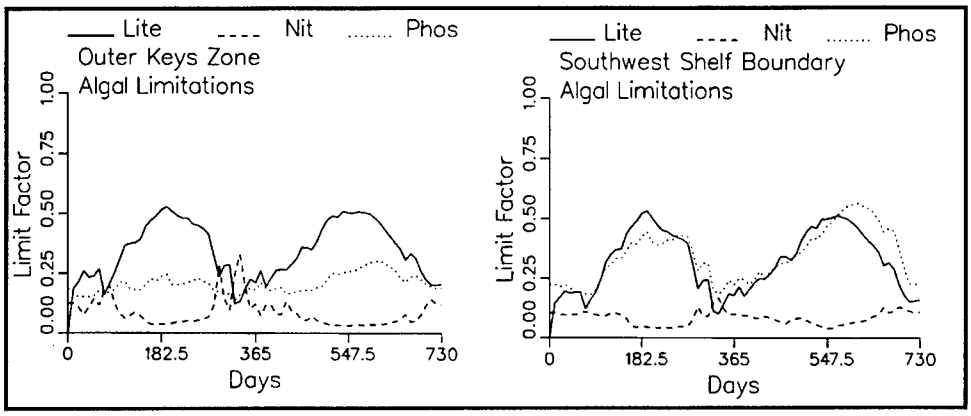

Figure 88. (concluded)

10 Seagrass Model Calibration Results

Introduction

The present chapter examines three computed properties of the seagrass model: spatial distribution of seagrass species, local density of seagrass species, and factors limiting seagrass production.

Spatial Distribution

The spatial distribution and relative abundance of seagrass species in Florida Bay and adjacent waters have been well-described (Fourqurean et al. in press). *Thalassia* is the most commonly encountered species and has the greatest areal extent. Within the model domain, density of *Thalassia* is greatest inside Florida Bay and in the area between the upper Keys and the reef tract (Figure 89). *Syringodium* is also commonly encountered although the distribution differs from *Thalassia*. *Syringodium* is more often found in deeper water and forms a dense bed north of the middle Keys, west of Florida Bay (Figure 90). *Halodule* is found sporadically throughout Florida Bay (Figure 91).

Initial conditions

The initial distribution of seagrass was specified based on observed Braun-Blanquet densities. Observed densities were converted to patchiness as described in Chapter 7. Patchiness is not a computed variable and remains at its specified value throughout a model run. One implication of this specification is the fraction of each cell covered with seagrass is fixed at the initial value throughout the simulation. A second implication is that modeled seagrass will not grow in cells in which seagrass does not presently exist (cover class 0.5 or less, patchiness = 0). Practically, this restriction is of little significance since cells without seagrass are mostly at the

western extreme of the grid and likely would not support seagrass if it were allowed to grow.

Initial density in each cell supporting seagrass was also based on reported Braun-Blanquet values. (In the model, shoot and roots are computed as mass per unit area and referred to as density. This same quantity is often referred to by community scientists as standing crop. Density in the model ***does not*** imply number of shoots per unit area.) The seagrass species having the highest reported Braun-Blanquet value was assigned initial density based on reported mean values (Fourqurean 1992). Remaining species were assigned small "seed" populations. We found this method yielded the greatest agreement with observed distributions. Otherwise, unrealistic distributions resulted. For example, when *Thalassia* and *Syringodium* were both initialized at mean values in the same cell, *Syringodium* out-competed *Thalassia*. When *Thalassia* was given an initial advantage, however, shading prevented *Syringodium* from catching up. This behavior has interesting ecological implications that are beyond the scope of the present effort. Some insight into species competition as modeled is presented in the ten-year simulation.

Following initialization, the model was run for eight years to allow computed seagrass to equilibrate with the model environment. The distribution and density that resulted from the ten-year equilibration were used as initial conditions in the two-year model calibration.

Results

The computed distribution of *Thalassia* (Figure 92) agrees well with the described distribution. *Thalassia* is computed almost exclusively in Florida Bay and in the shallow waters adjacent to the Keys. Computed *Syringodium* is nearly absent from Florida Bay and is concentrated instead on the Western Shelf and outside the Keys (Figure 93). While regions with observed *Syringodium* are represented in the model, the model computes extensive Syringodium along the west coast of Florida where none is found. These western regions do support *Halophila decipiens*, however (Figure 94). Since *Halophila* is not represented in the model, *Syringodium* is occupying regions that should be *Halophila* dominated. As with the observations, *Halodule* is sporadically distributed within Florida Bay (Figure 95). Both observations and model indicate greatest densities are southeast of Cape Sable and at the apex of Florida Bay.

Local Density and Limiting Factors

Density statistics for comparison with the model (Table 22) were obtained from Fourqurean (1992) who collected measures at a number of stations baywide. Reported values for leaf and short shoot were combined for comparison with the model shoot variable. Reported values for rhizome

and root were combined for comparison with the model root variable. Biomass as dry weight was converted to carbon using the ratio 0.37 g C g^{-1} DW.

Table 22
Seagrass Density (modified from Fourqurean 1992)

	Shoot (g C m^{-2})	Root (g C m^{-2})
Halodule		
Mean	9.7	12.6
SE	4	4.4
Minimum	3.5	0.9
Maximum	60.3	60.7
Syringodium		
Mean	40.6	70.6
SE	15.9	27.7
Minimum	2.7	3.3
Maximum	134.5	225
Thalassia		
Mean	194	136.9
SE	23.9	14.5
Minimum	38.4	33.6
Maximum	632.3	400

Within the Northern Transition Zone, mean *Thalassia* shoot density is roughly 50 g C m^{-2}, about one-quarter the reported mean (Figure 96). *Syringodium* is absent, and *Halodule* shoot density is 2 to 3 g C m^{-2}, also less than the reported mean. The computed most-limiting factor on growth is almost exclusively phosphorus.

Within the Eastern Zone, *Thalassia* shoot density is roughly 100 g C m^{-2} (Figure 97), less than reported mean values but well within the reported range. *Syringodium* is virtually absent and *Halodule* has mean shoot density roughly 1 g C m^{-2}, less than the reported minimum. The most limiting factor for *Thalassia* growth varies between light and nitrogen and the most limiting factor for *Halodule* growth varies between light and phosphorus.

The computed limit on *Thalassia* growth conflicts with common wisdom that availability of phosphorus is most limiting to growth (Fourqurean, Zieman, and Powell 1992a, 1992b). Two factors contribute to the difference. The first is that computed available phosphate in the sediment is often higher than reported values (Figure 108). The second is the method in which limiting factors are computed and reported. Self-shading is computed in the model and incorporated into the reported light limitation.

Self-shading is not commonly considered when field data are analyzed to obtain light limitation on seagrass.

The Atlantic Transition, Central, and Western Zones are all dominated by *Thalassia* which is most often light and nitrogen limited (Figures 98-100). Mean shoot densities are 25 to 75 g C m^{-2}, less than reported mean values. *Syringodium* is present at very low densities in all three zones. *Halodule* reaches its highest shoot density, 5 g C m^{-2}, in the Western Zone (Figure 100). There, the limiting factors are most often nitrogen and light. As previously noted, the computed limits are affected by a tendency to over-compute sediment available phosphorus. Sediment bulk nitrogen is often under-computed (Figure 106), perhaps leading to under-computing of available nitrogen. Also, the computed light limitation includes shading of *Halodule* by *Thalassia.*

In the Gulf Transition Zone (Figure 101), *Thalassia* is present at low shoot density (15 g C m^{-2}) while *Syringodium* achieves some of the highest computed values (shoots nearly 20 g C m^{-2}). *Syringodium* density is less than reported mean, however. *Halodule* is present at a very low density. Light is usually the most limiting growth factor on all species. Due to the greater depth of this region, computed light limitation here is more reasonable than in the shallow interior portions of the bay.

The Outer Keys Zone exhibits *Thalassia* shoot density greater than 75 g C m^{-2} and *Syringodium* of 10 to 15 g C m^{-2} (Figure 102). *Halodule* is absent. Light is most often the most limiting growth factor. As with the Gulf Transition Zone, greater depths outside the Keys make the computed light limitation more reasonable.

In the Southwest Shelf, *Thalassia* is present at low density, 5 g C m^{-2}, while *Syringodium* achieves shoot densities of nearly 30 g C m^{-2} (Figure 103). *Halodule* is present at very low density. Most limiting growth factor is most often light with occasional nitrogen limit. Due to the great depth of this region and the presence of phosphorus from the Gulf, the computed limitations are reasonable.

Overall, seagrass density is lower than reported mean values. More careful comparison of computed values at the exact locations of the samples may alter this conclusion. Also, inclusion of cells with zero density can artificially lower the computed density over a zone. A more appropriate measure may be mean density of only cells in which seagrass occurs.

Nitrogen limits computed seagrass growth to a greater extent than reported. Additional nitrogen loading to the system, routed to the sediments, may alleviate this limit and contribute to overall higher seagrass density.

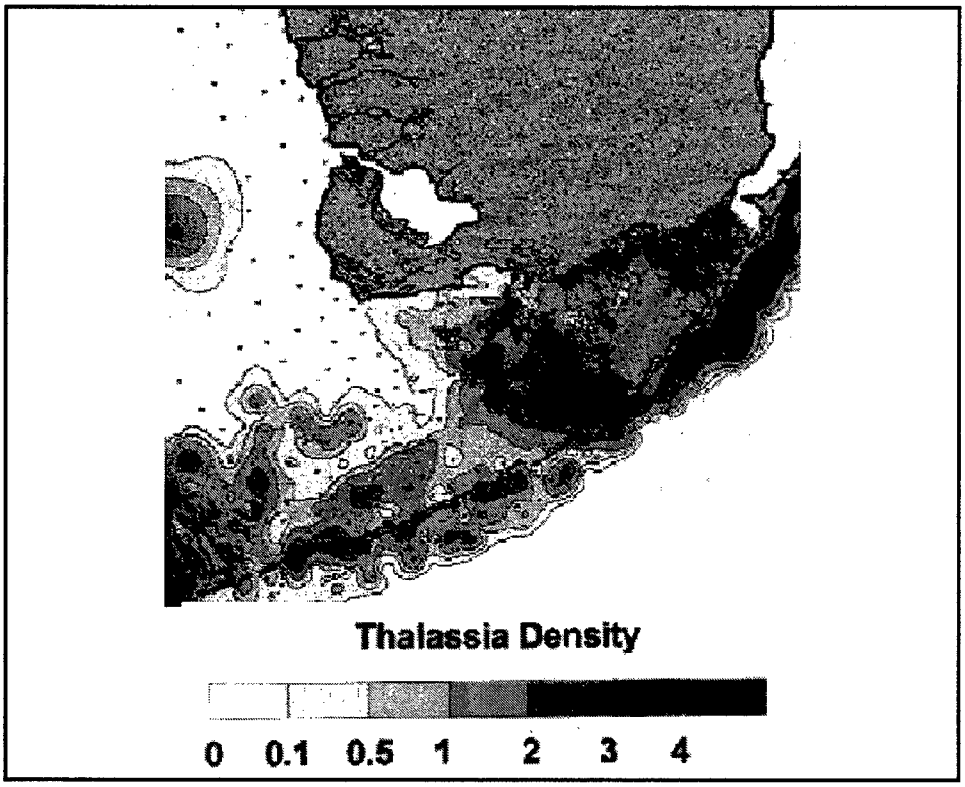

Figure 89. Observed *Thalassia* distribution, as Braun-Blanquet density (after Fourqurean et al. in press)

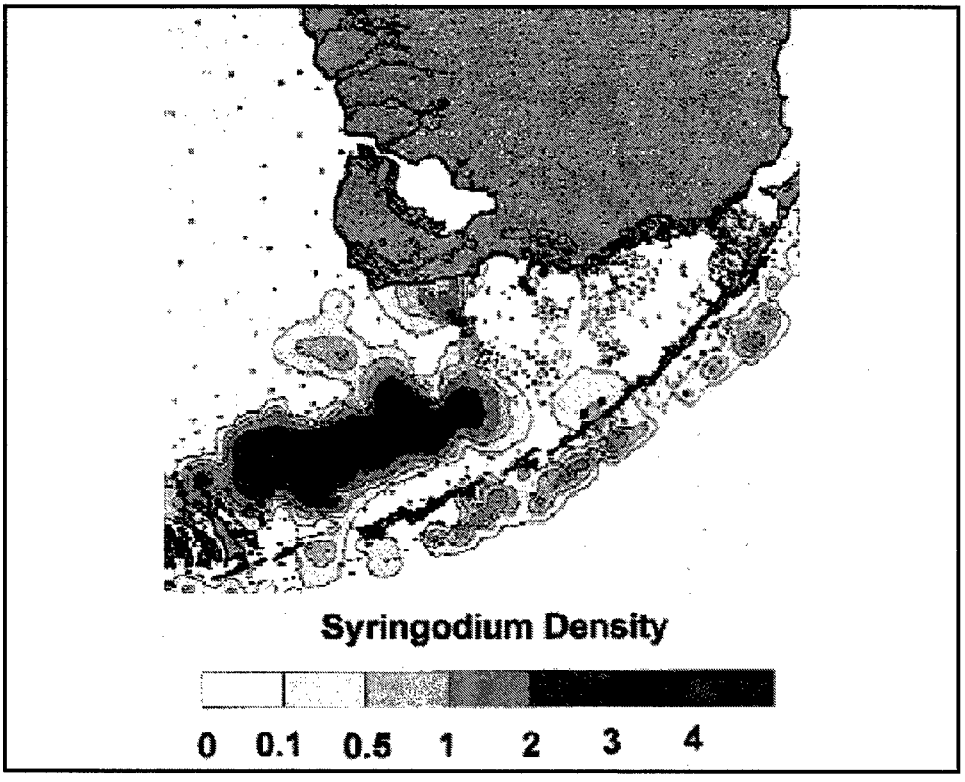

Figure 90. Observed *Syringodium* distribution, as Braun-Blanquet density (after Fourqurean et al. in press)

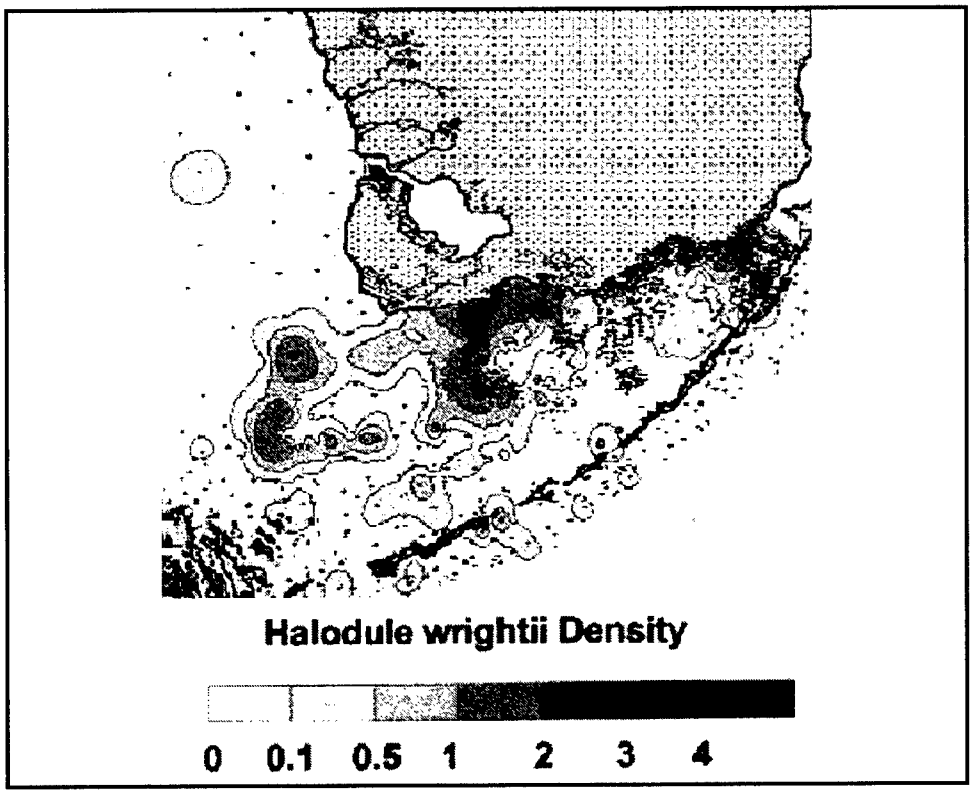

Figure 91. Observed *Halodule* distribution, as Braun-Blanquet density (after Fourqurean et al. in press)

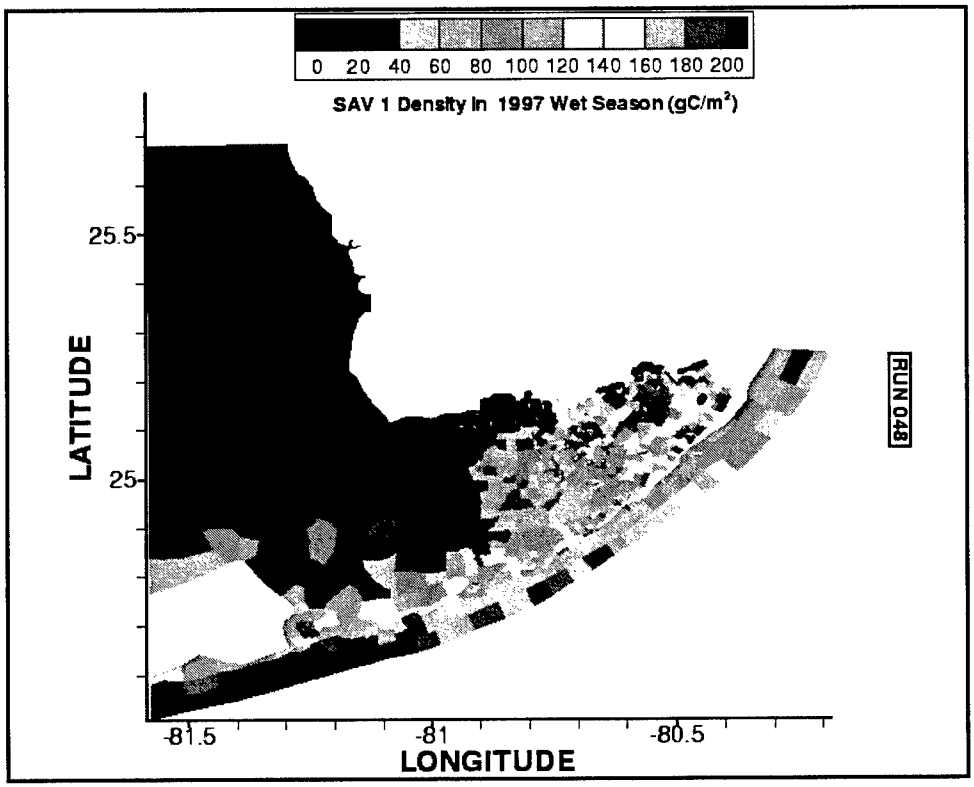

Figure 92. Computed *Thalassia* density, 1997 wet season

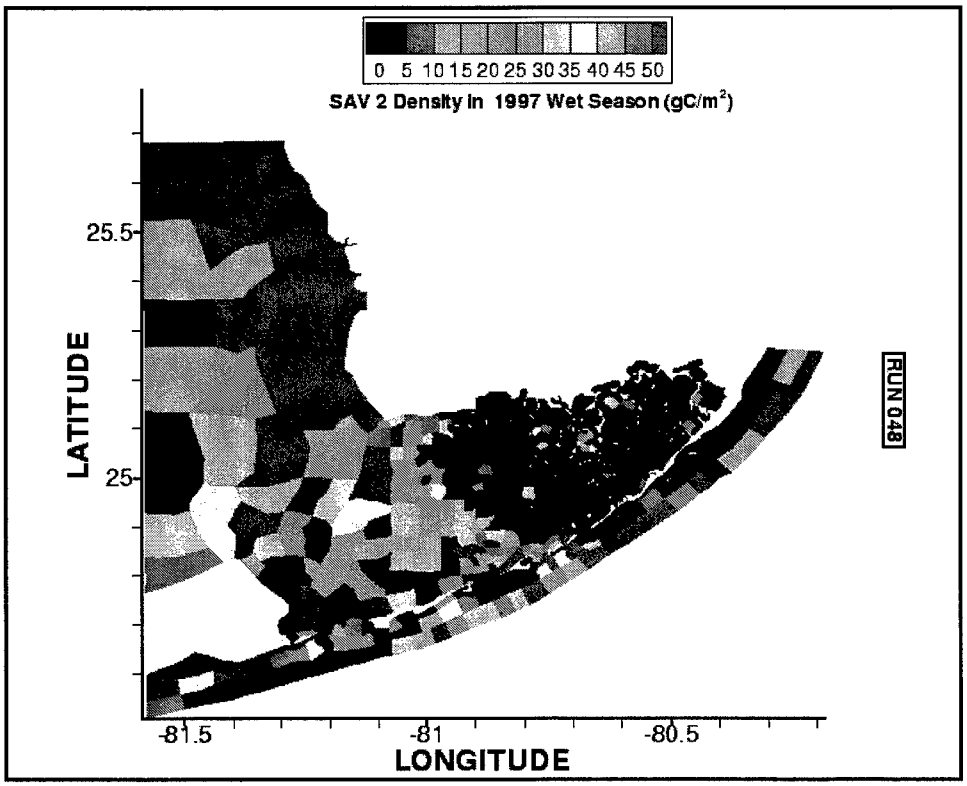

Figure 93. Computed *Syringodium* density, 1997 wet season

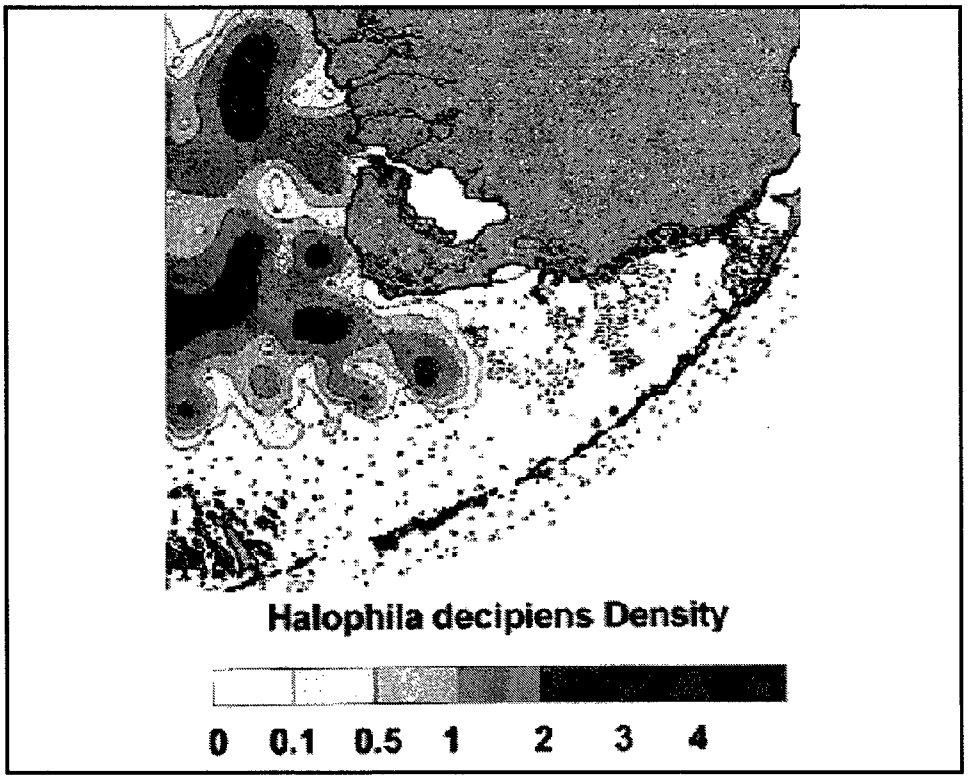

Figure 94. Observed *Halophila* distribution, as Braun-Blanquet density (after Fourqurean et al. in press)

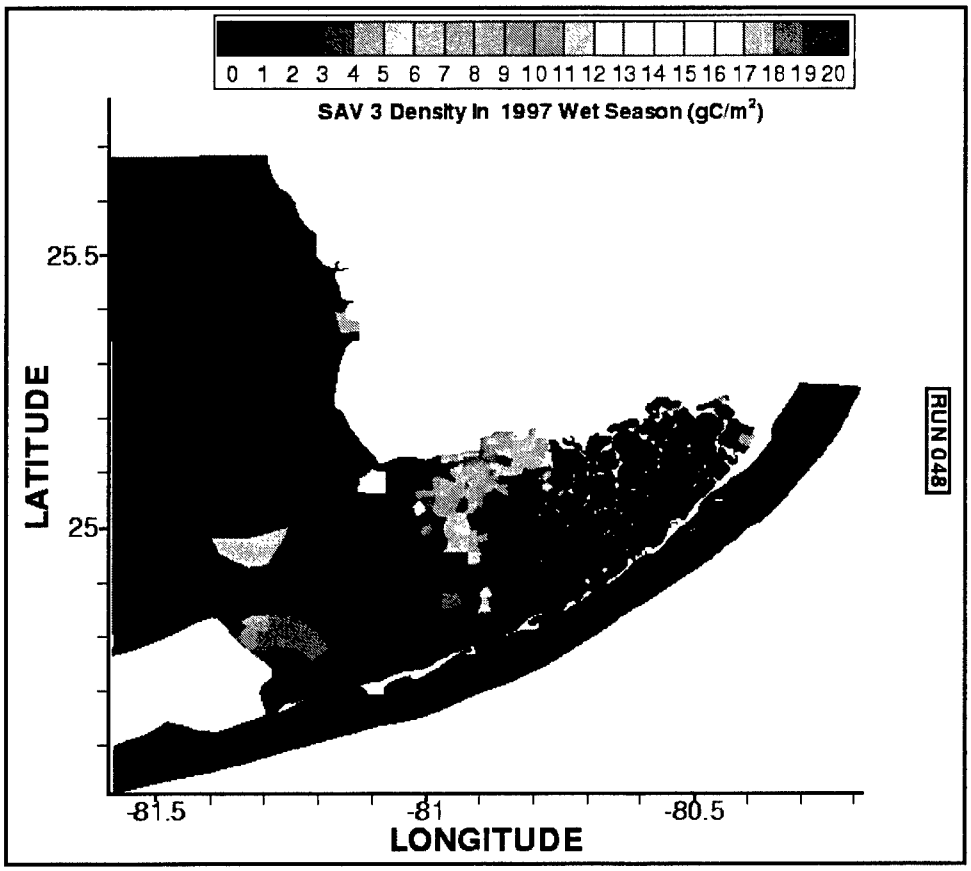

Figure 95. Computed *Halodule* density, 1997 wet season

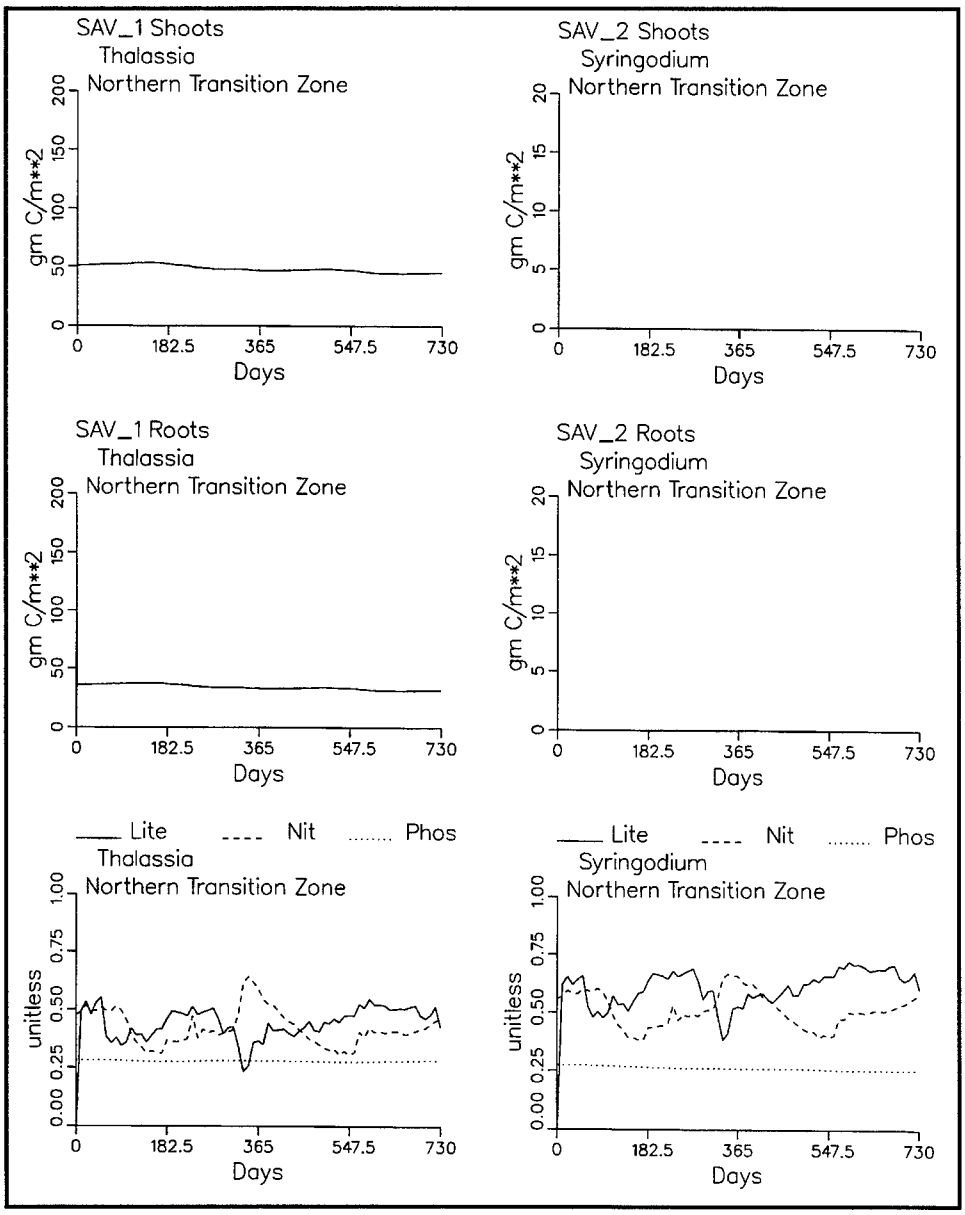

Figure 96. Computed densities and limiting factors, Northern Transition Zone (continued)

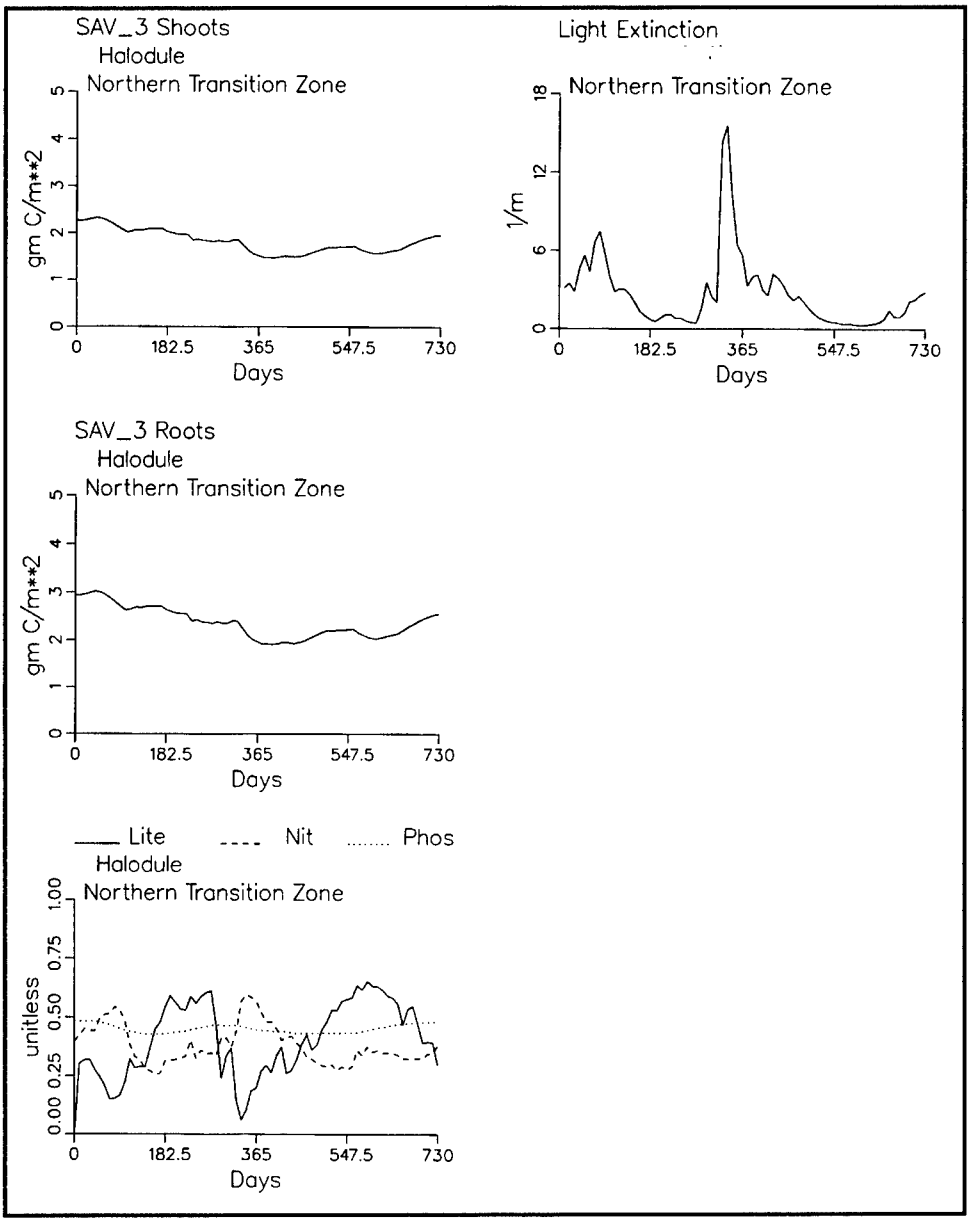

Figure 96. (concluded)

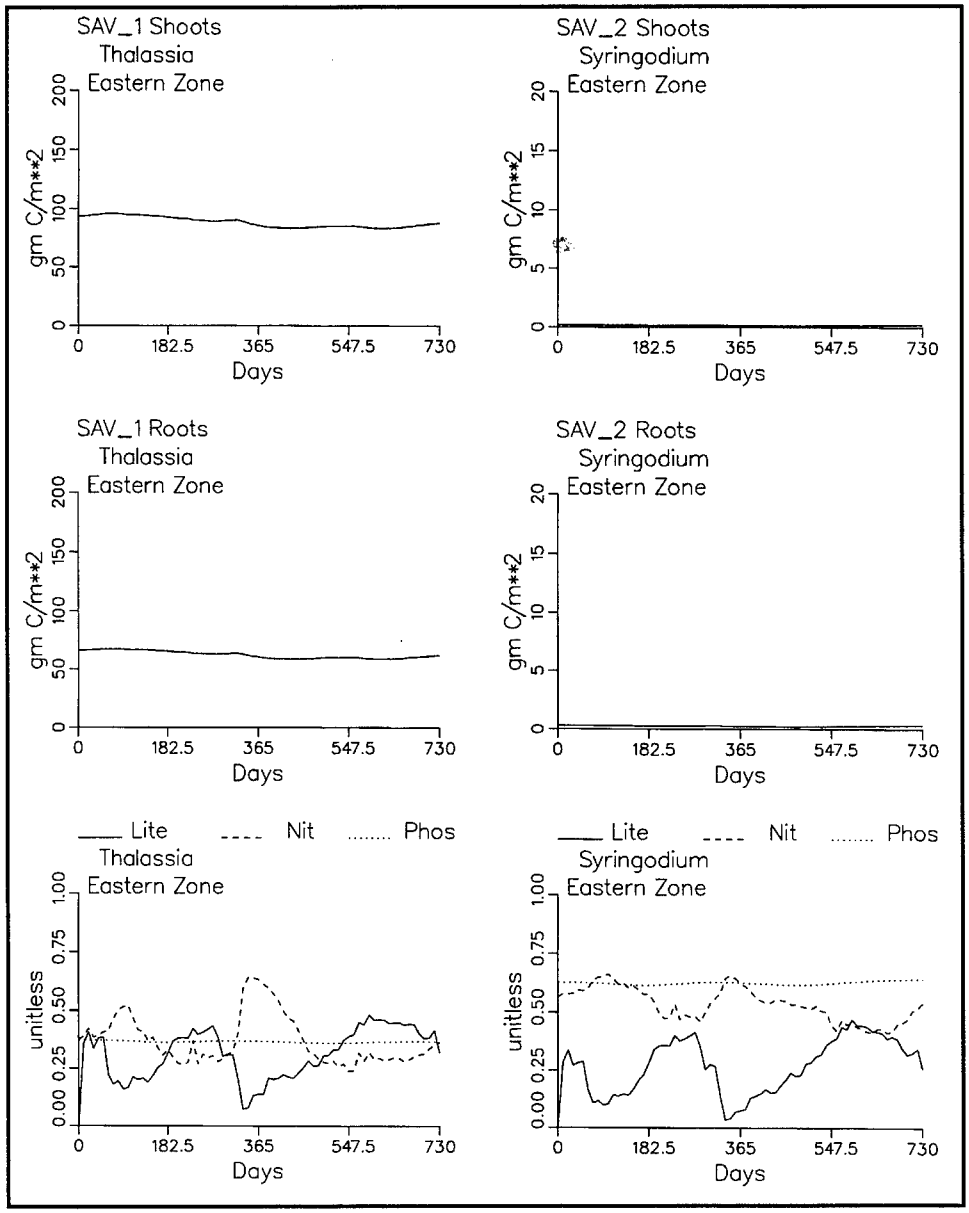

Figure 97. Computed densities and limiting factors, Eastern Zone (continued)

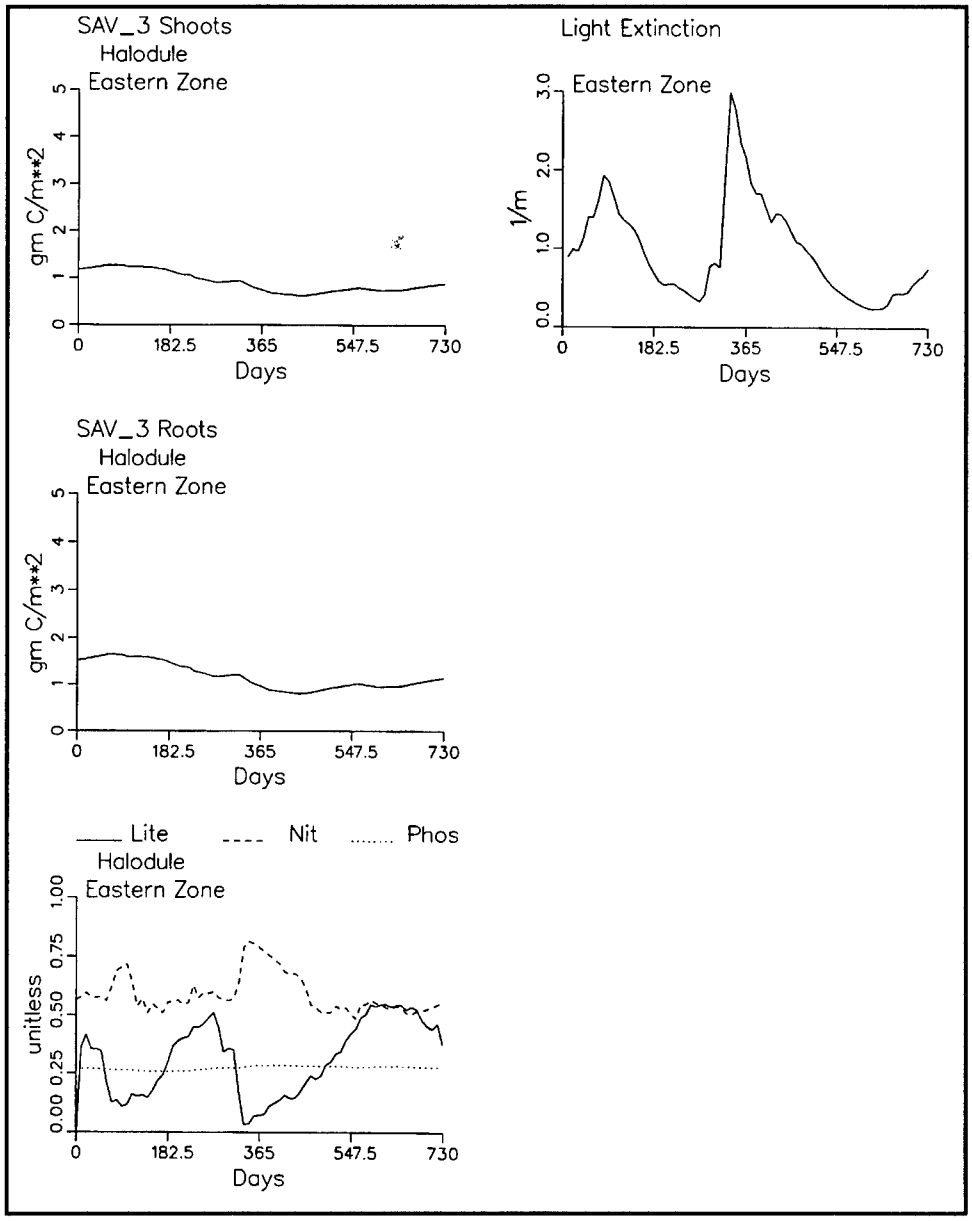

Figure 97. (concluded)

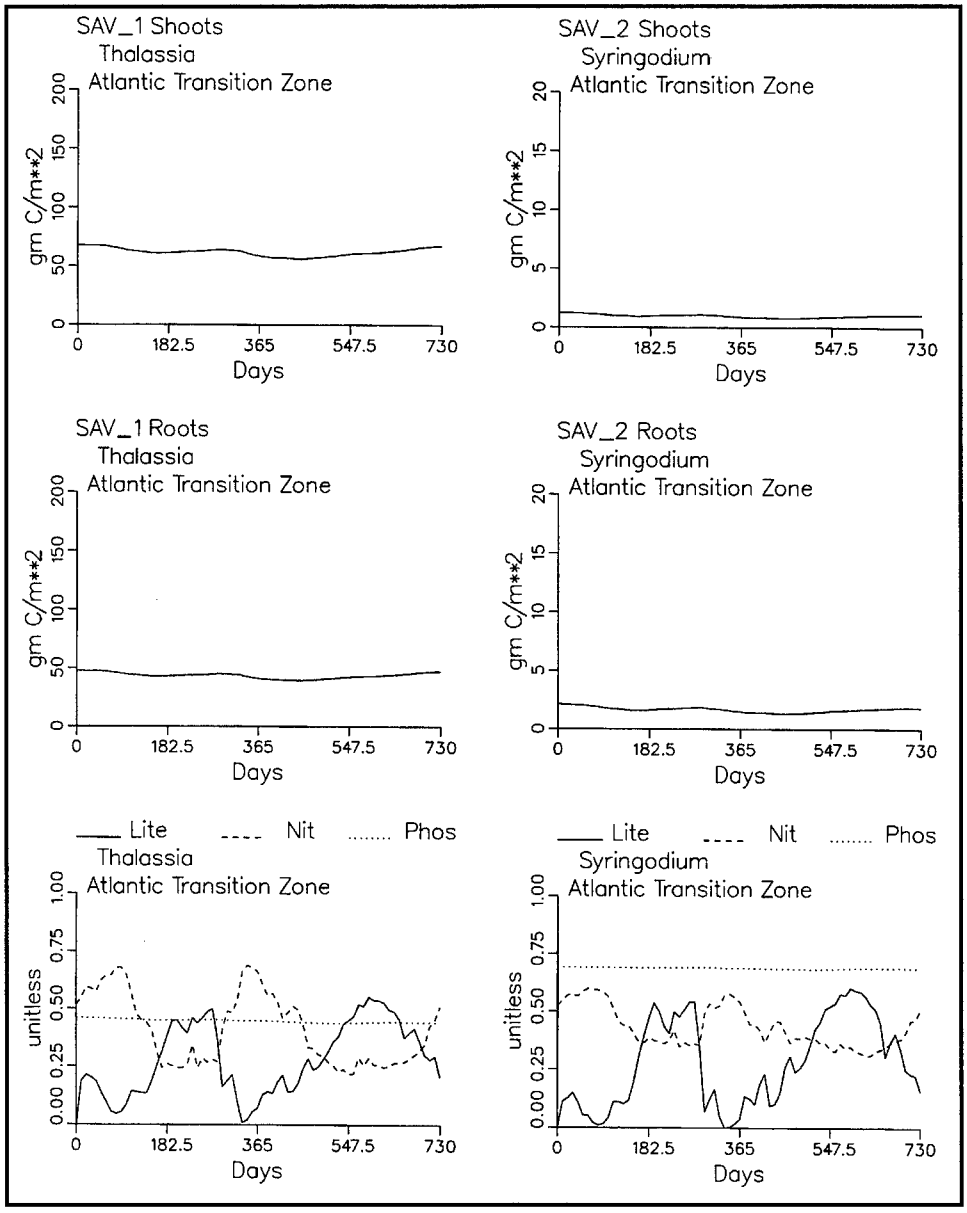

Figure 98. Computed densities and limiting factors, Atlantic Transition Zone (continued)

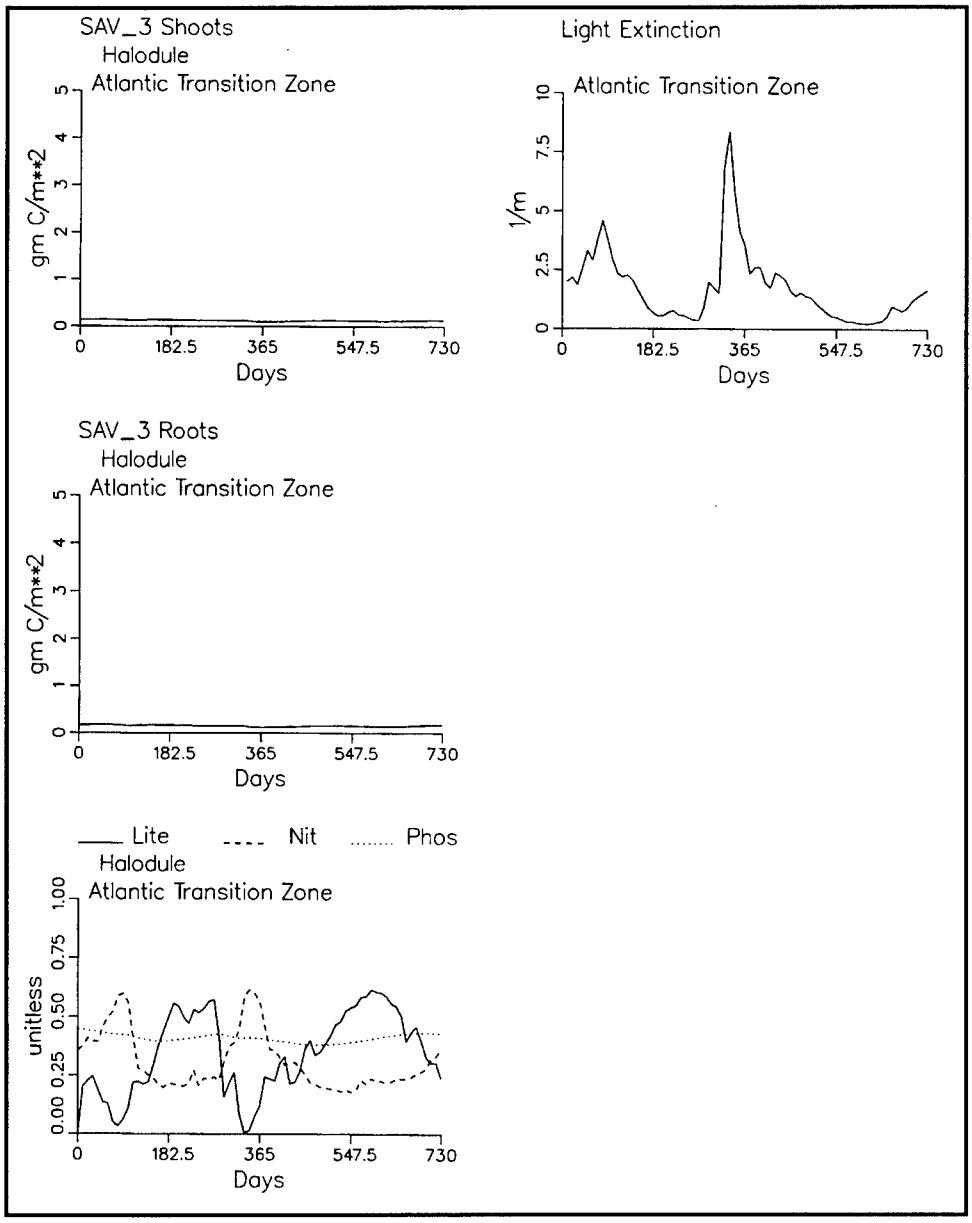

Figure 98. (concluded)

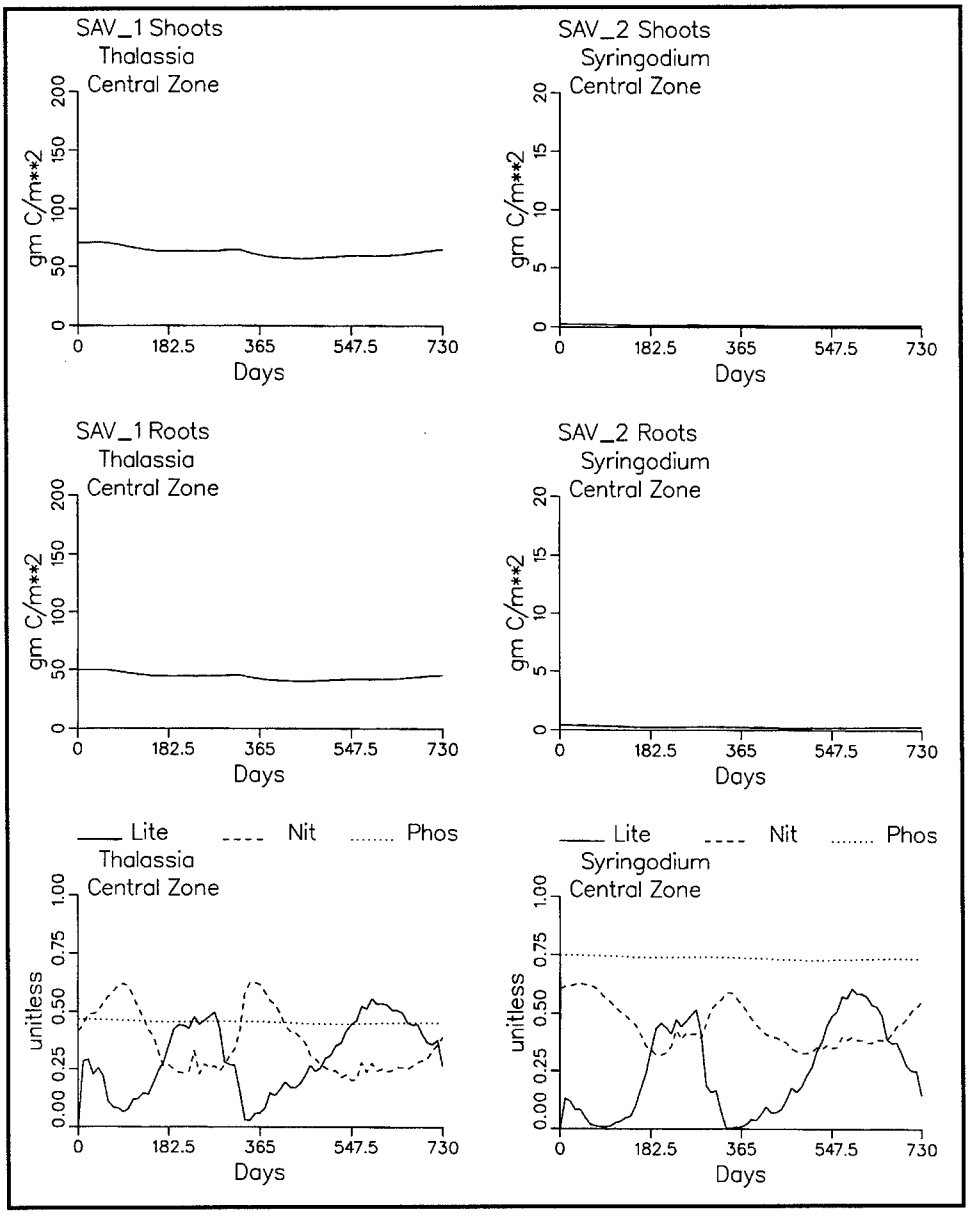

Figure 99. Computed densities and limiting factors, Central Zone (continued)

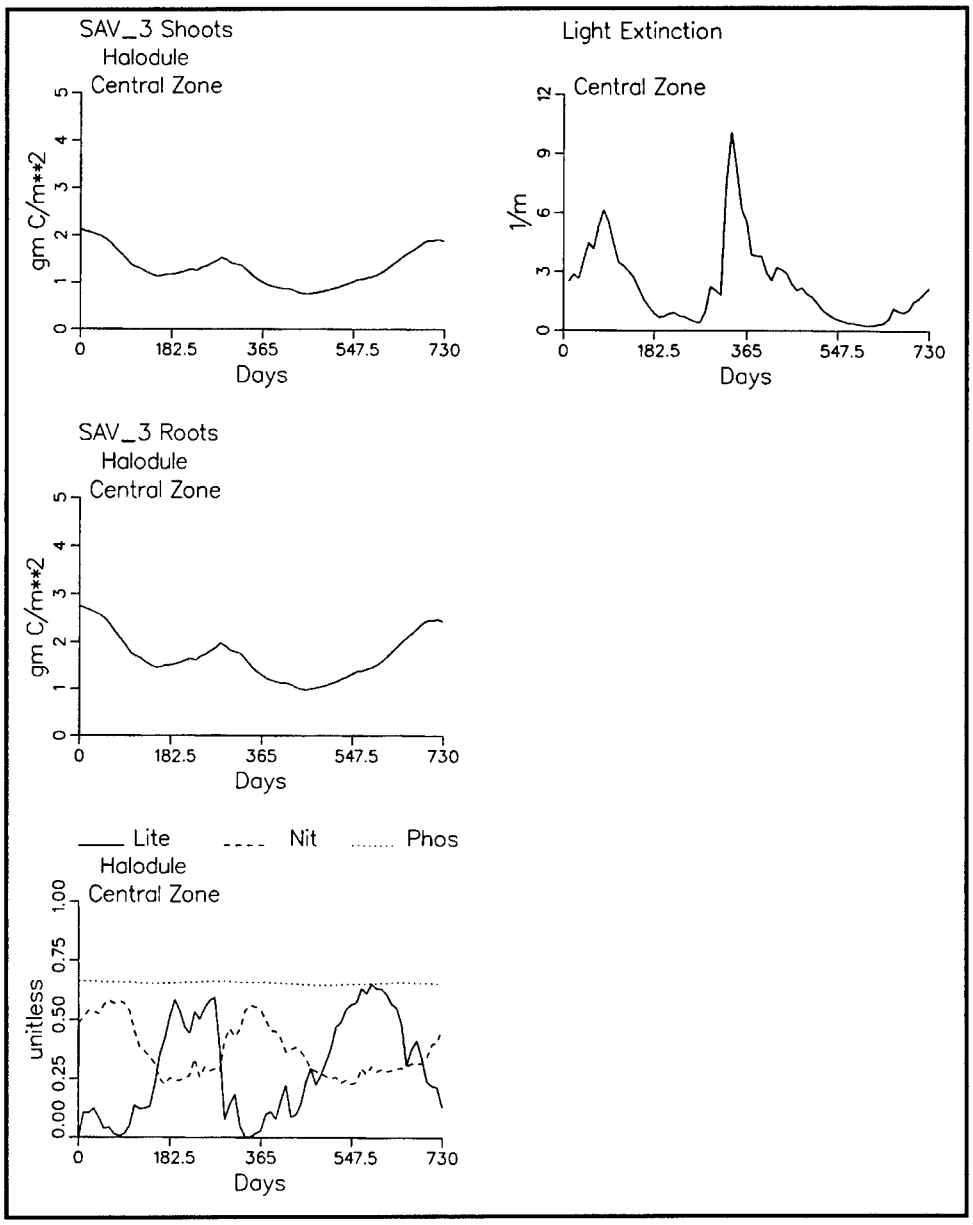

Figure 99. (concluded)

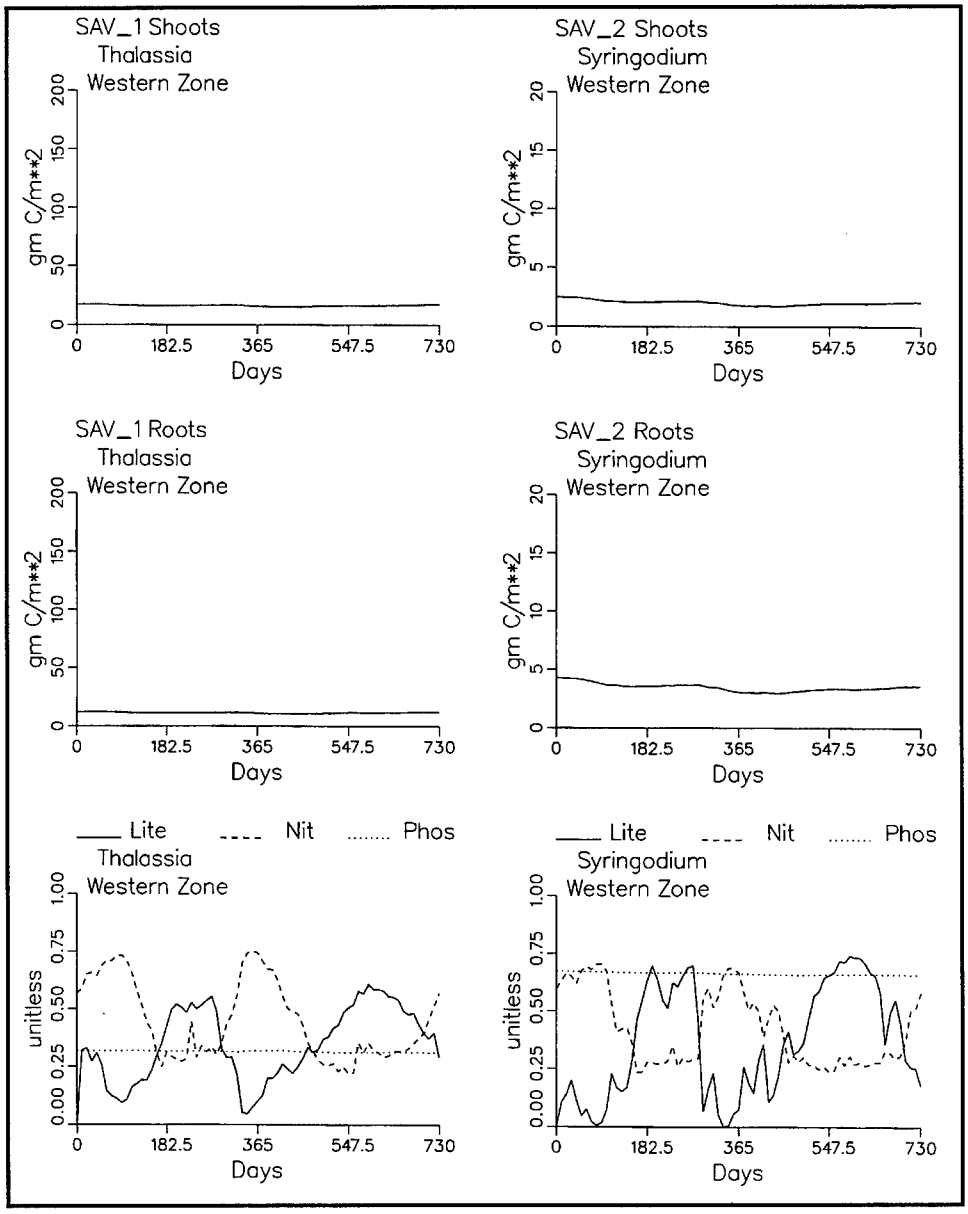

Figure 100. Computed densities and limiting factors, Western Zone (continued)

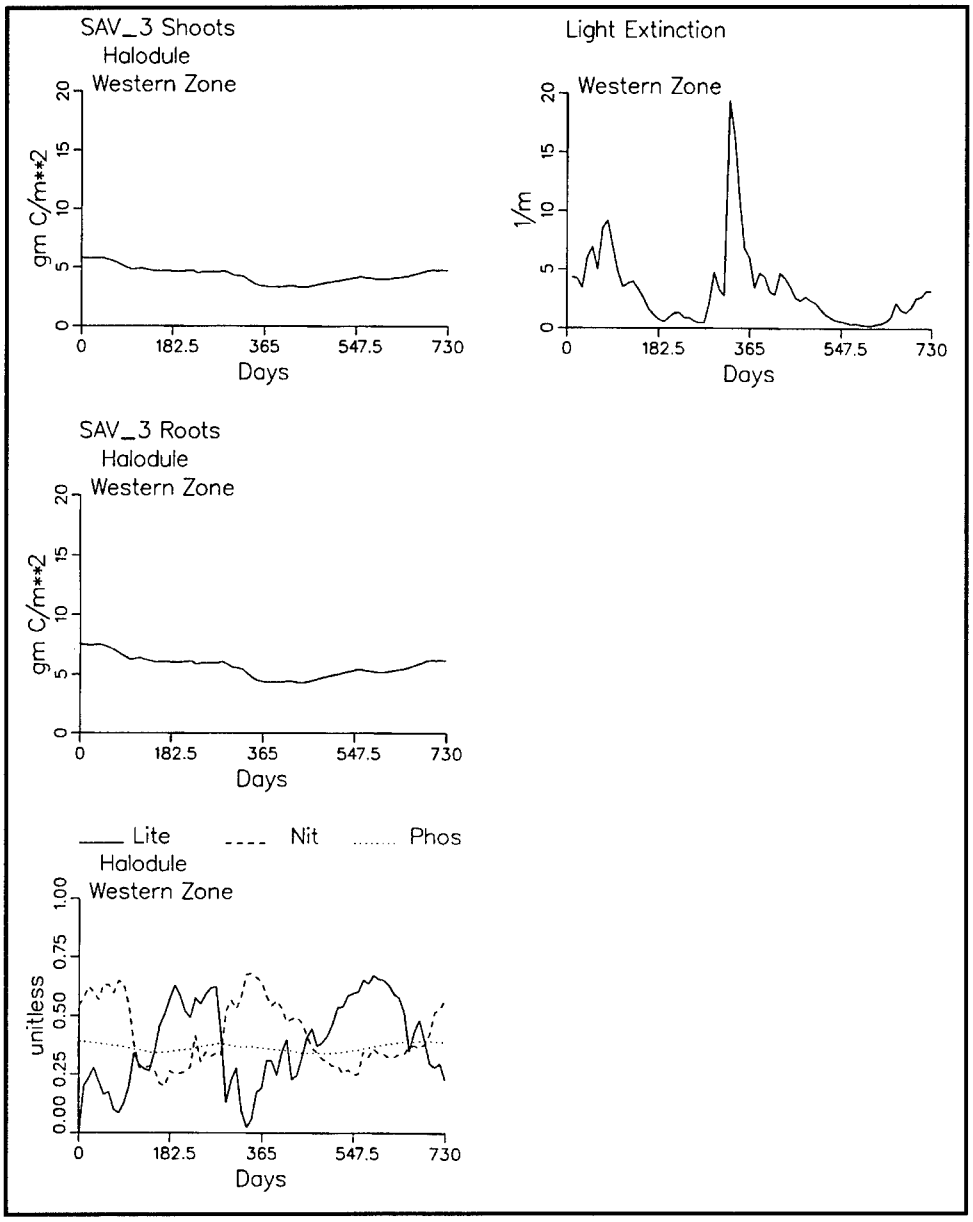

Figure 100. (concluded)

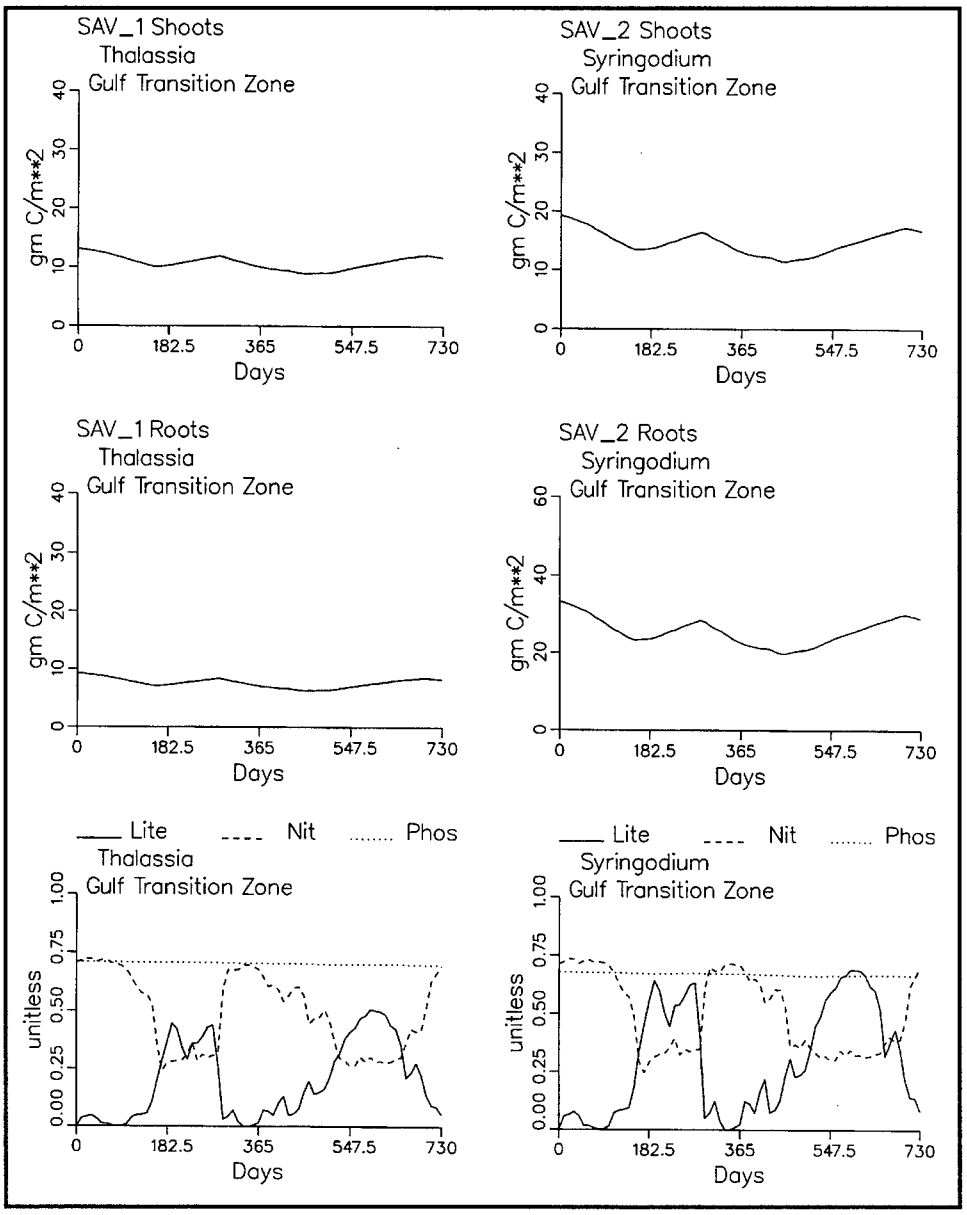

Figure 101. Computed densities and limiting factors, Gulf Transition Zone (continued)

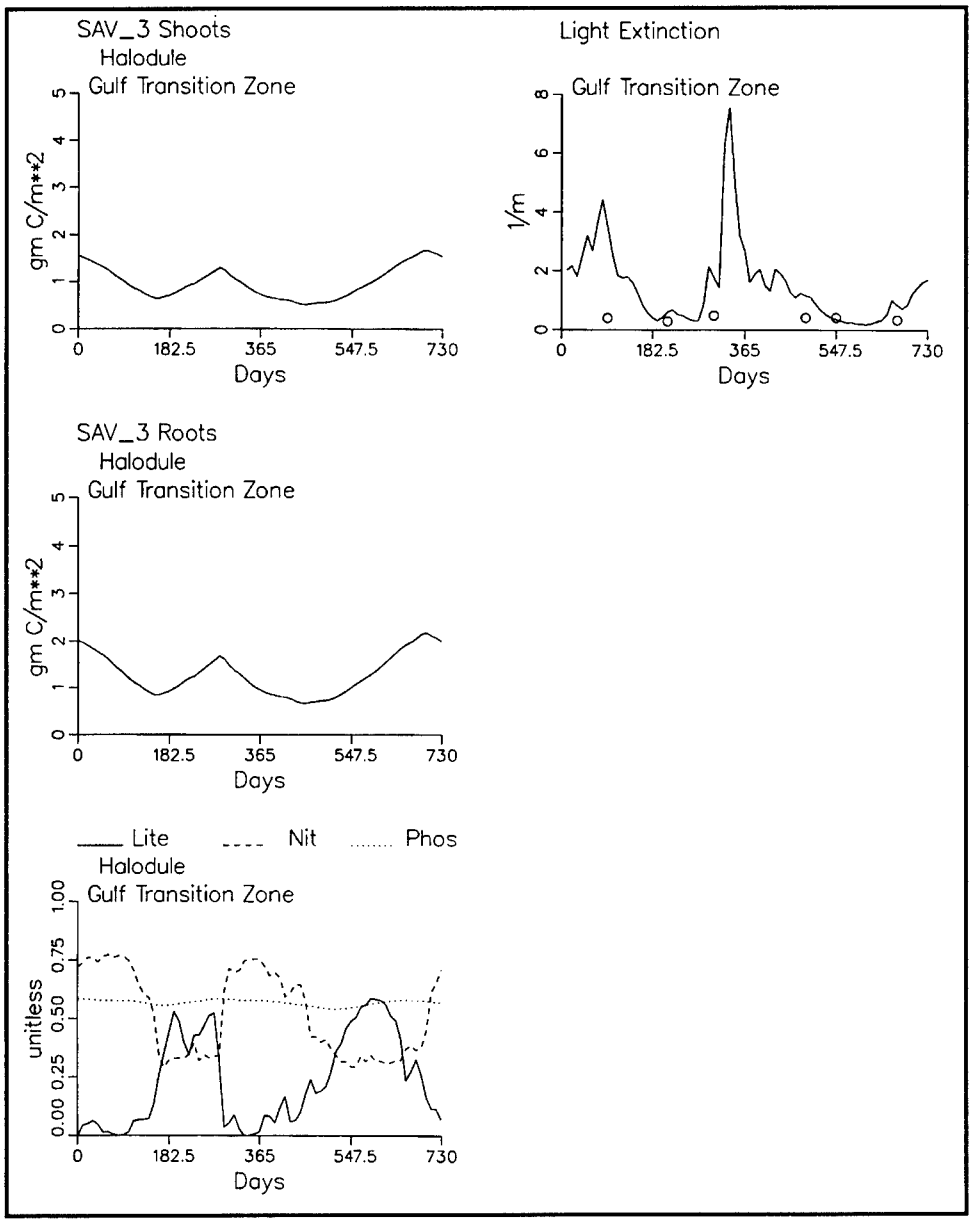

Figure 101. (concluded)

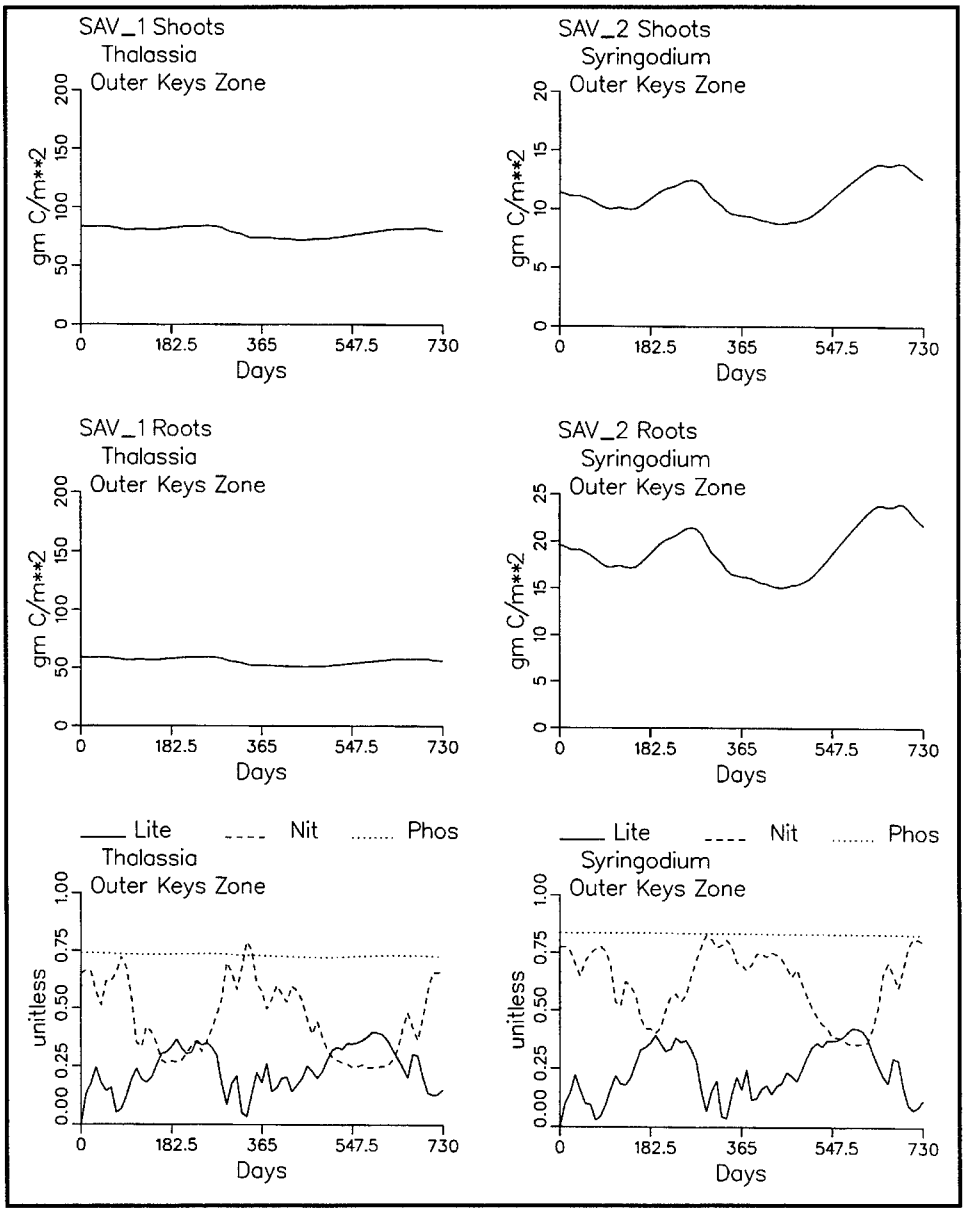

Figure 102. Computed densities and limiting factors, Outer Keys (continued)

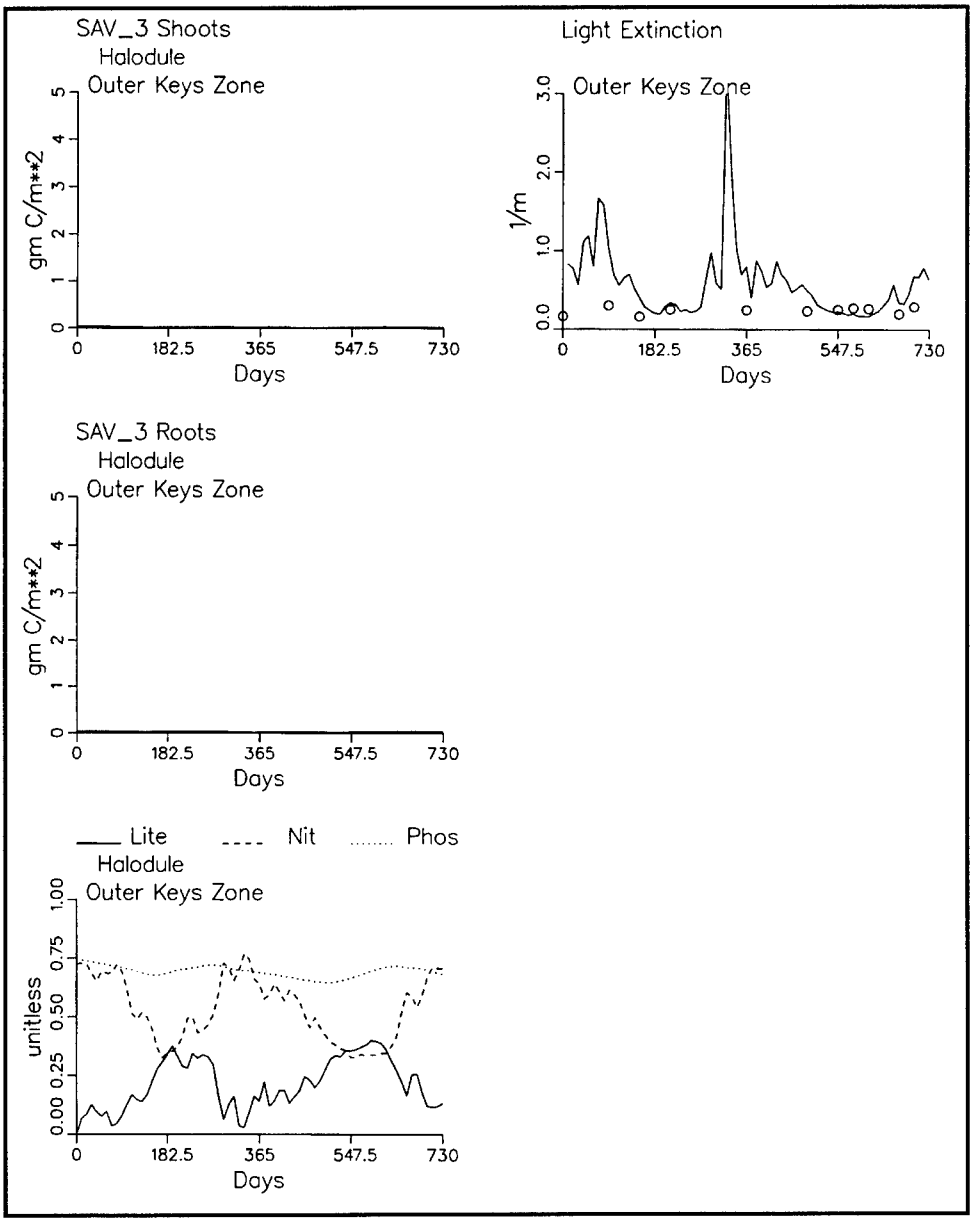

Figure 102. (concluded)

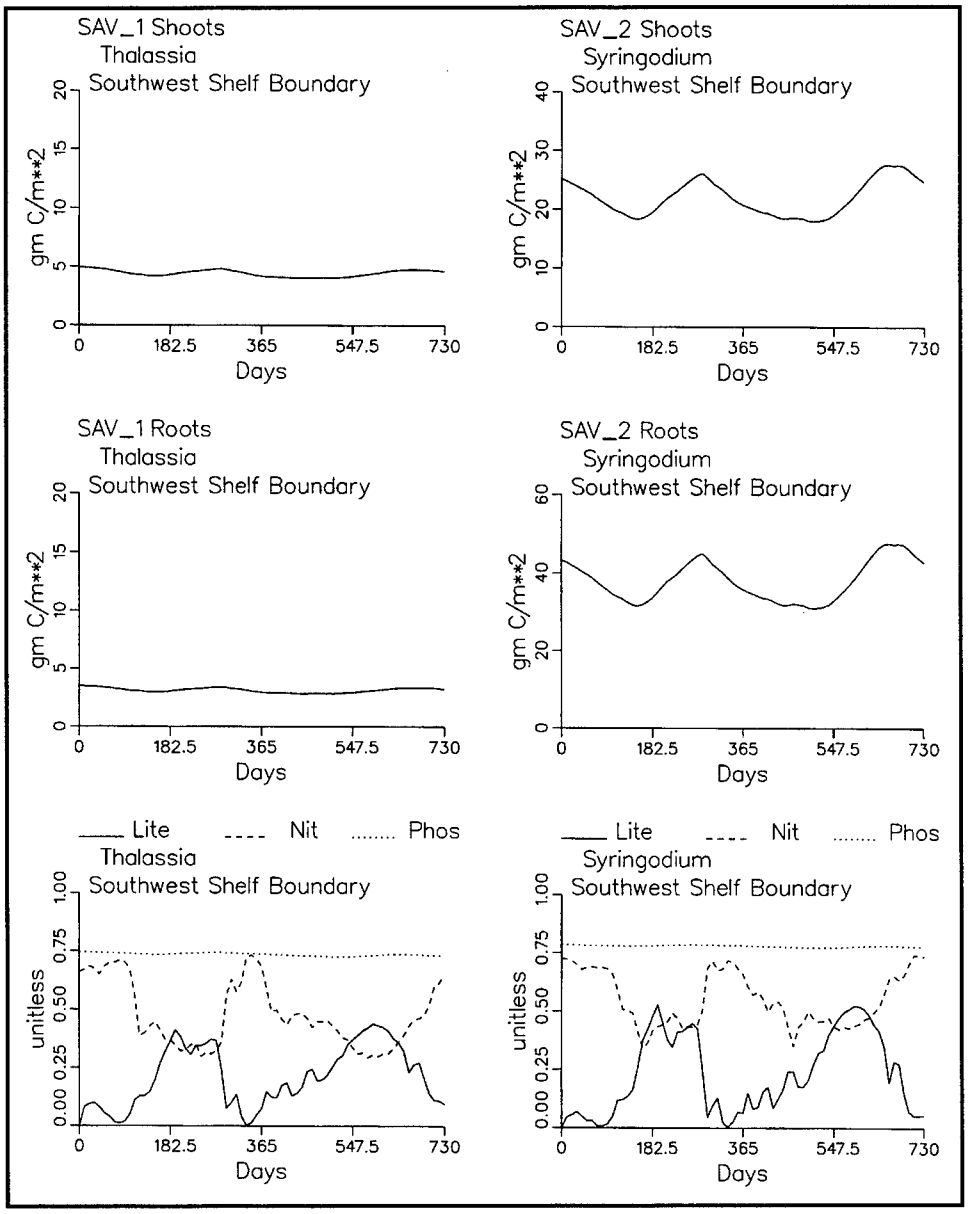

Figure 103. Computed densities and limiting factors, Southwest Shelf (continued)

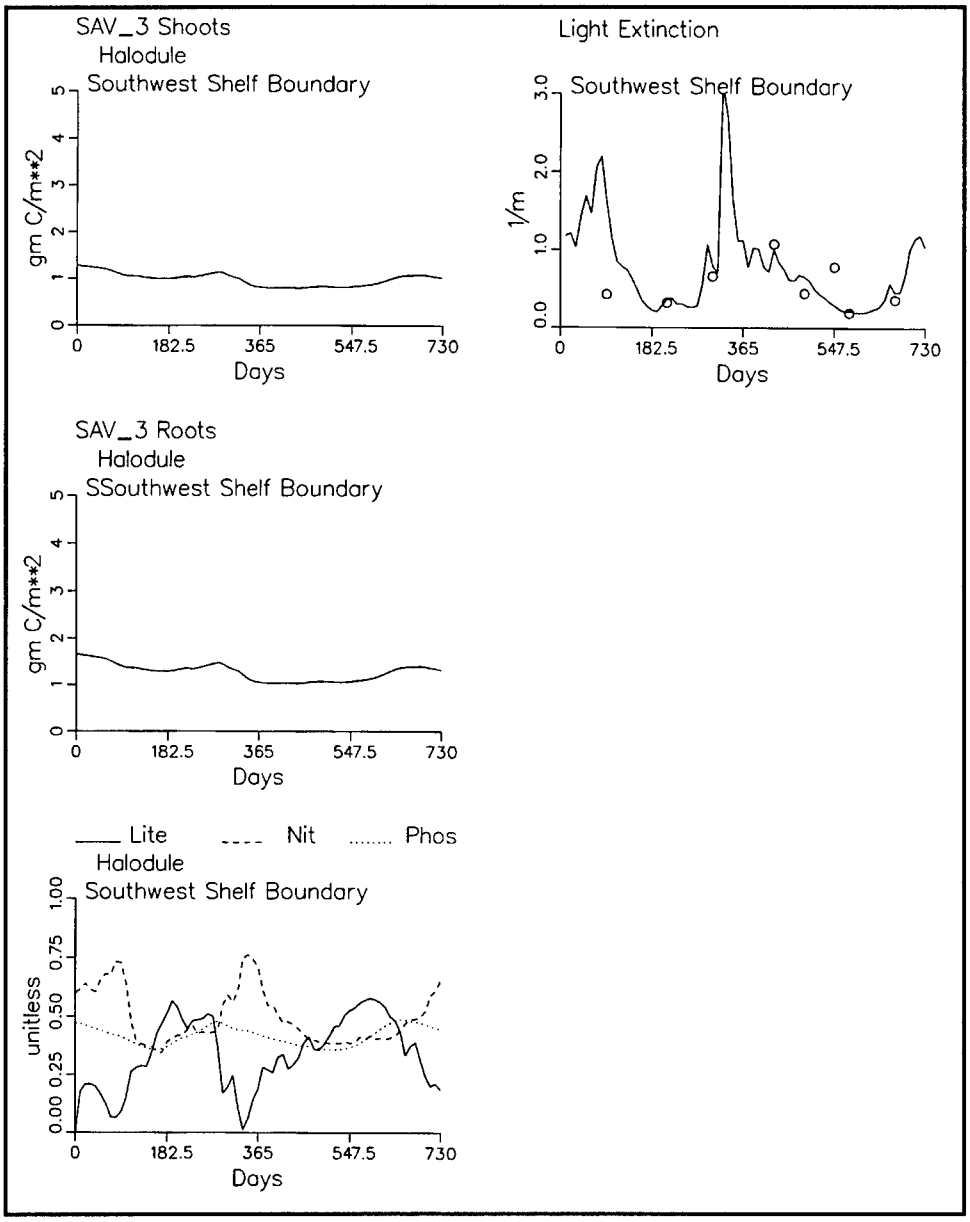

Figure 103. (concluded)

11 Benthic Sediment Calibration Results

Introduction

The present chapter compares three computed and observed properties of the benthic sediments. These are: benthic algal abundance, sediment nitrogen and phosphorus concentrations, and sediment-water fluxes of nutrients, carbon, and oxygen.

Benthic Algae

Benthic algae were reported for summer and winter of 1997 (see Chapter 6). Both seasons indicated concentrations from less than 20 to more than 100 mg Chl m^{-2}. Consistent spatial or seasonal patterns were not evident although the highest concentrations were observed in summer. For comparison purposes, observations digitized from summer 1997 are compared to model mean concentrations during the wet season of the same year (Figure 104). The preponderance of observations are in the range 20 to 100 mg Chl m^{-2} as are the computations in the same vicinity. A few observations in excess of 100 mg Chl m^{-2} were not matched by the model in the interior of Florida Bay but were computed elsewhere where phosphorus is more abundant.

Computed biomass, as carbon, attains peak values of 5 g C m^{-2} during the summer months (Figure 105). In the shallow interior portions of the Bay (e.g. the Northern Transition and Eastern Zones) phosphorus limits the benthic algal concentration. In deeper waters (e.g. Atlantic Transition Zone) light becomes more important as the limiting factor. Along the western and southern extremes of the domain, light and nitrogen are most limiting to benthic algal biomass.

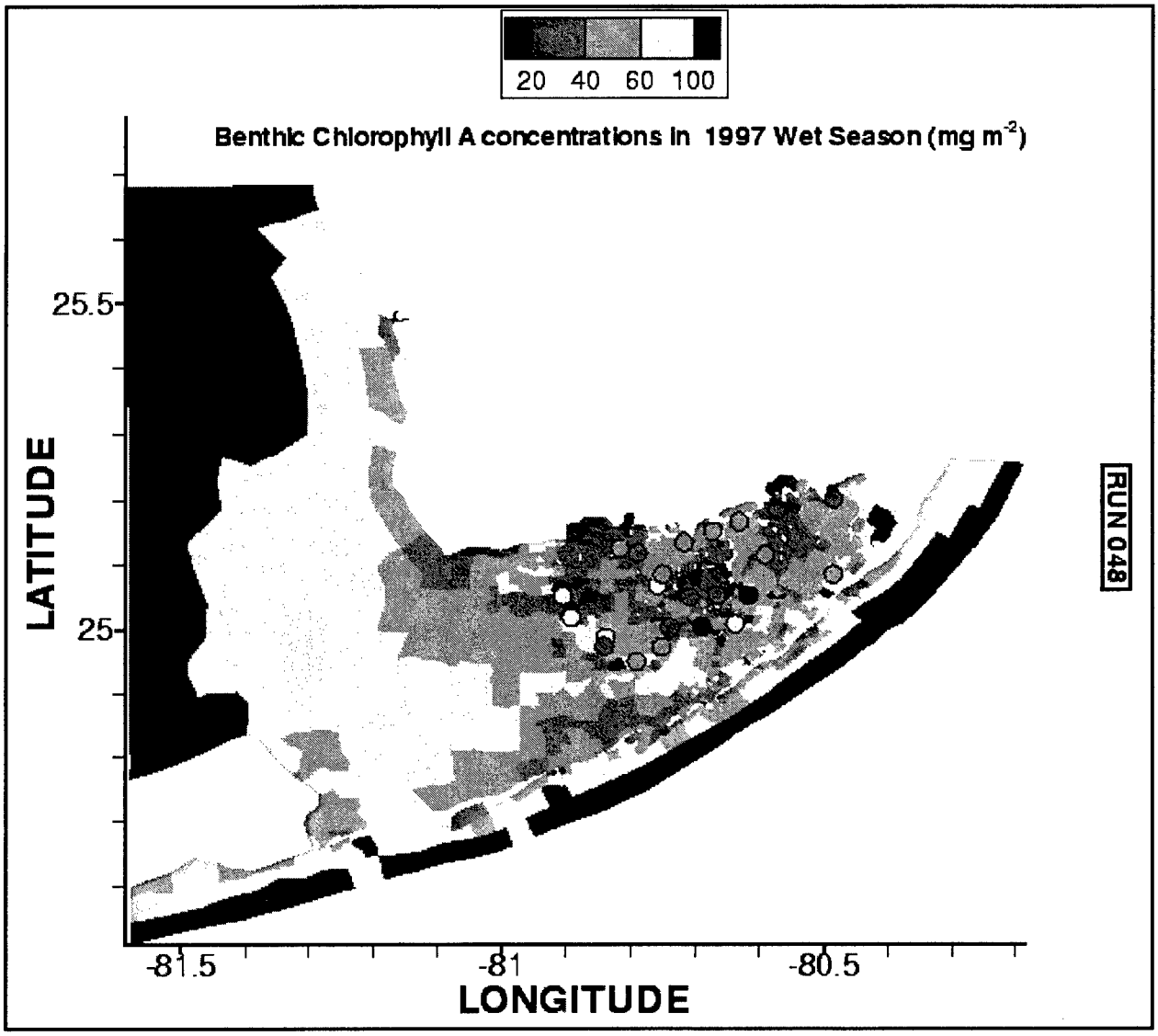

Figure 104. Observed and computed benthic algal chlorophyll, wet season 1997

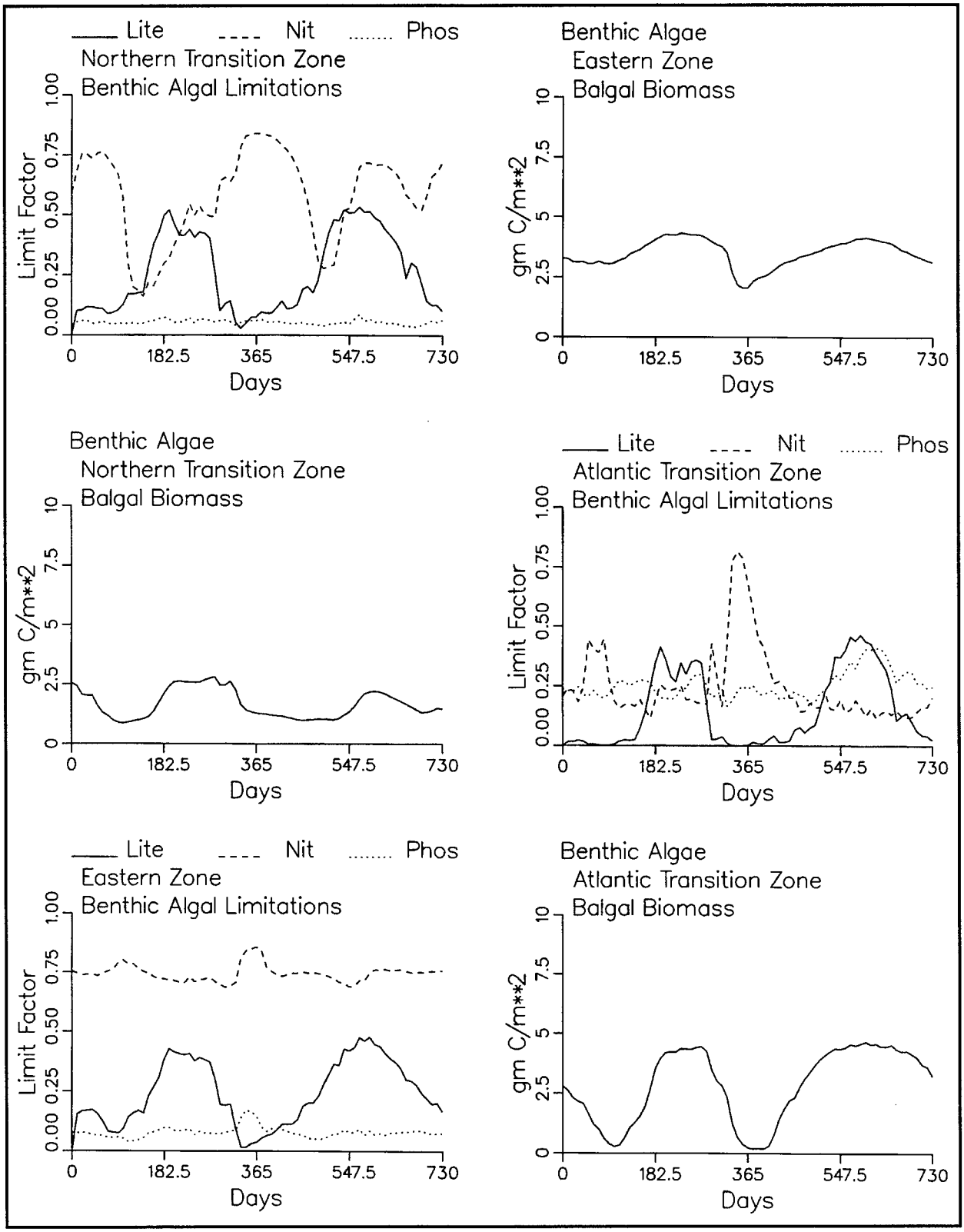

Figure 105. Computed algal biomass, as carbon, and computed limiting factors (sheet 1 of 3)

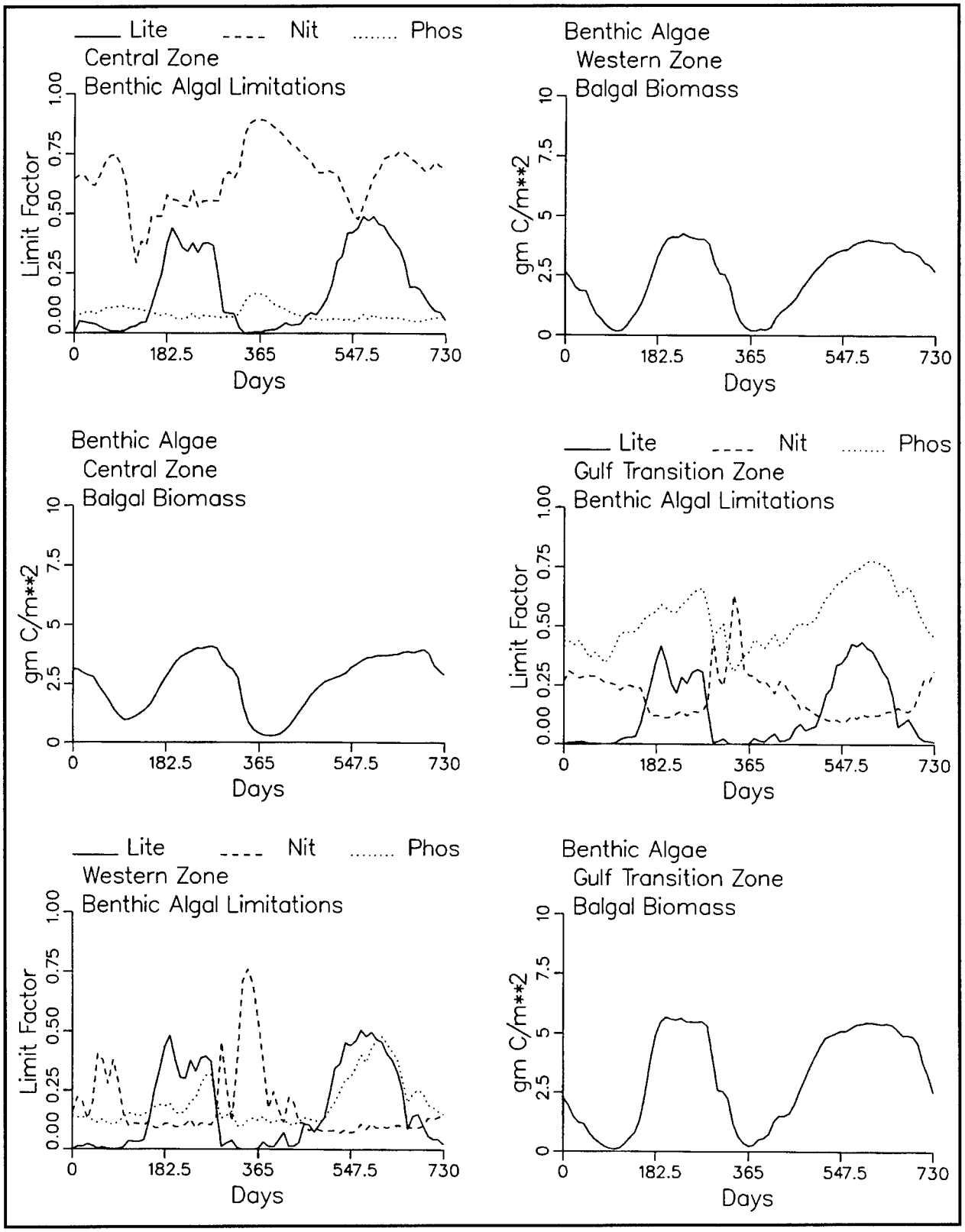

Figure 105. (sheet 2 of 3)

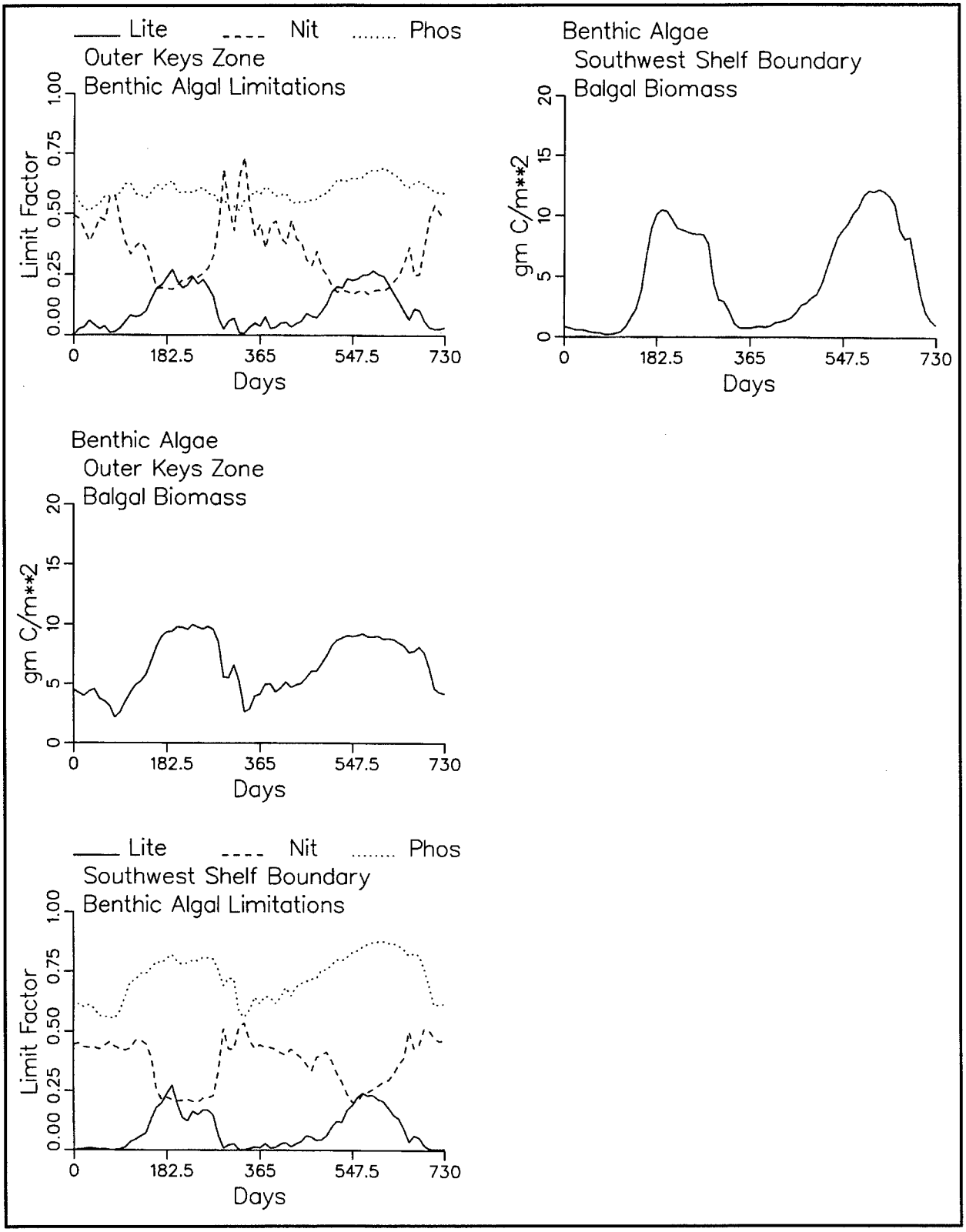

Figure 105. (sheet 3 of 3)

Sediment Nitrogen and Phosphorus

Bulk nitrogen

Observed sediment bulk nitrogen is in the range 20 to 500 μg at N g^{-1} sediment (Figure 106). Computed concentrations are frequently much less than observed. The most likely reason for the shortfall in nitrogen is a loading shortfall. This issue will be investigated in subsequent sensitivity analyses.

Bulk phosphorus

Observed sediment bulk phosphorus shows a pattern in which concentrations are in the range 1 to 6 μg at P g^{-1} sediment in the interior of the bay and between 6 and 19 μg at P g^{-1} sediment at the western extreme of the observations, south of Cape Sable (Figure 107). The lower concentrations in the interior are well matched by the model although the high concentrations in the Western Zone are not. The reason for the computed shortfall is not apparent. Examination of the computed total phosphorus in the Western Zone water column (Figure 86) indicates a small shortfall as well. Perhaps

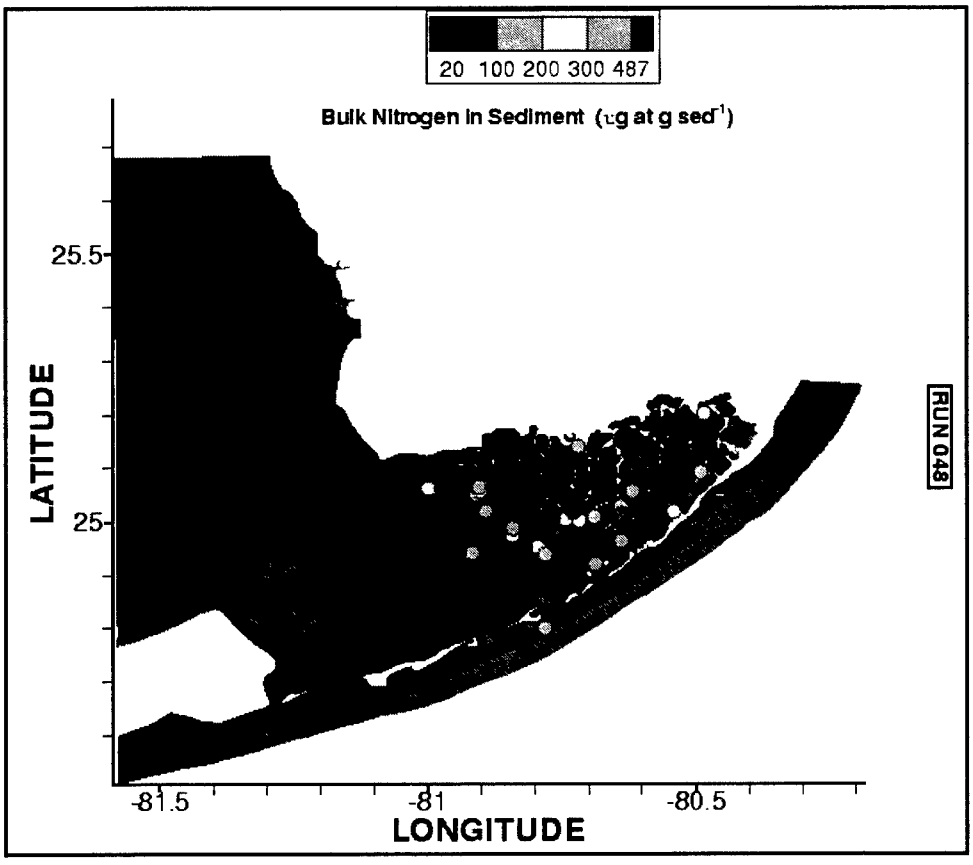

Figure 106. Observed and computed sediment bulk nitrogen

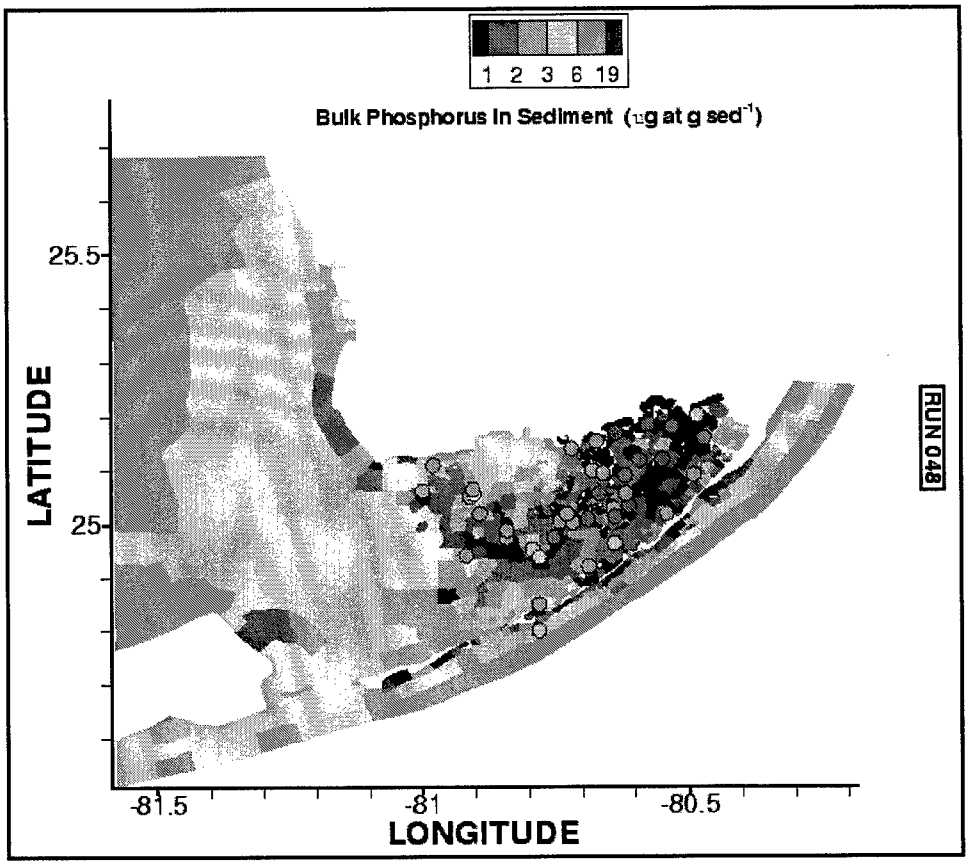

Figure 107. Observed and computed sediment bulk phosphorus

a loading shortfall or error in computed circulation is the root of the sediment shortfall.

Available phosphorus

Observations were reported for available phosphorus, defined as the sum of porewater and sorbed phosphate. The observations were in the range 0.02 to 1.0 µg at P g^{-1} sediment (Figure 108). Within the domain of the observations, computed concentrations were in the same range as the observations. Almost everywhere else, however, computed concentrations exceeded the maximum observed in the interior of the bay. The computed phosphate in the sediments largely reflects the abundance of phosphorus in the overlying water. Computed sediment concentrations are higher in the western portions of the domain and outside the Keys.

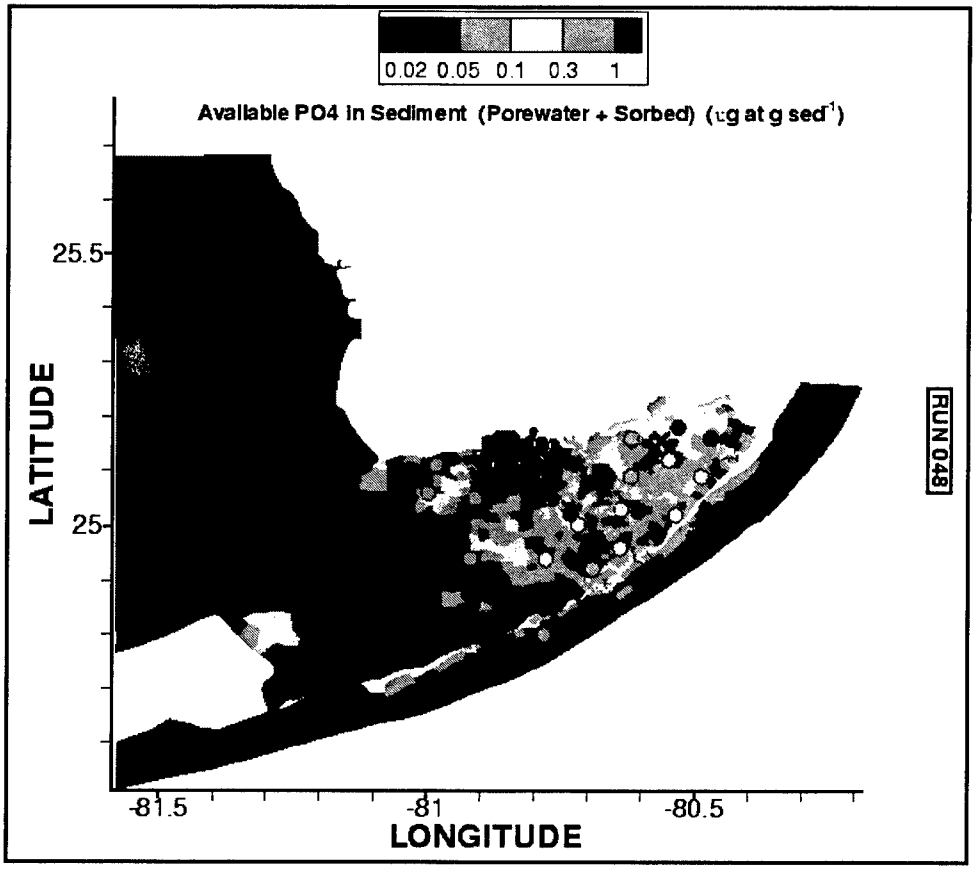

Figure 108. Observed and computed sediment phosphate

Nutrient, Carbon, and Oxygen Fluxes

Flux measurements were conducted over a period extending from 1996 to 1999 (see Chapter 2). The observations measured the net exchange between the water column and the community of benthic sediments, benthic algae, and SAV. For comparison with the observations, computed diagenetic processes, benthic algal processes, and SAV processes were summed. The model was sampled at thirty-day intervals, at noon and midnight, at the location of the sample stations. A model population of 72 computations was obtained for comparison with the Rudnick data set and 144 computations for comparison with the Carlson data set.

The variability in observed nutrient fluxes was large (Tables 23, 24). For many substances, both community release to the water column and uptake from the water column were observed. Computed fluxes also showed a large range but the direction of the fluxes was mostly uniform, either to or from the water column but seldom both. The summary below concentrates on median values from both observations and model.

Table 23
Summary of Observed (Rudnick) and Computed Fluxes

		Observed		Model	
		Dark	Light	Dark	Light
NH4 (mg m^{-2} d^{-1})	Mean	17.09558	3.406548	8.390278	-13.3694
	Median	9.751138	0.917895	8.1	-13.65
	Max	74.27676	38.20771	19.7	1.1
	Min	-8.05318	-26.3398	1	-31.9
	Std	21.70762	12.34671	3.877823	5.630391
NO3 (mg m^{-2} d^{-1})	Mean	-0.89645	-0.79173	-0.36944	-3.22917
	Median	-0.7453	-0.35044	-0.1	-2.2
	Max	1.196465	1.922013	0	-0.6
	Min	-3.13224	-5.56111	-4.6	-13.2
	Std	1.169327	1.678481	0.932759	2.990899
DON (mg m^{-2} d^{-1})	Mean	26.80068	4.156434	3.511111	3.958333
	Median	14.52839	-13.6407	3.6	4
	Max	225.8793	738.0739	6.9	7.3
	Min	-126.28	-255.731	1.1	1.2
	Std	89.89672	174.4383	1.261405	1.30608
PO4 (mg m^{-2} d^{-1})	Mean	0.023212	0.047132	0.858333	-1.42778
	Median	-0.02024	0.016217	0.9	-1.4
	Max	2.180919	1.020349	1.7	0
	Min	-1.13955	-0.53755	0.3	-3.8
	Std	0.493015	0.298626	0.29491	0.616949
DOP (mg m^{-2} d^{-1})	Mean	-0.23433	-0.19648	0.379167	0.406944
	Median	-0.04461	-0.10932	0.4	0.4
	Max	1.18524	0.867559	0.8	0.8
	Min	-3.30539	-1.80029	0.1	0.1
	Std	0.973349	0.614331	0.156491	0.160392
DOC (mg m^{-2} d^{-1})	Mean	75.34842	118.5581	56.82639	68.73472
	Median	12.01972	117.5088	57.25	67.45
	Max	1398.453	2158.631	118.8	128.4
	Min	-492.605	-1264.1	14.5	20.3
	Std	386.1082	556.5053	22.37407	23.2292
DO (mg m^{-2} d^{-1})	Mean	-1974.23	2898.41	-506.839	747.0722
	Median	-1805.18	2474.979	-504.25	756.85
	Max	-775.344	6816.54	-164.8	1181.2
	Min	-4588.14	-5.376	-964.5	78.6
	Std	791.3934	1568.497	176.1479	171.7529

Table 24
Summary of Observed (Carlson) and Computed Fluxes

		Observed		Model	
		Dark	Light	Dark	Light
NH4 (mg m^{-2} d^{-1})	Mean	10.60563		7.656522	-12.5877
	Median	7.777224		6.6	-7.8
	Max	52.45733		21	8.5
	Min	-2.78376		-0.1	-82.1
	Std	13.76213		5.077012	13.38578
DON (mg m^{-2} d^{-1})	Mean	-3.2236		2.829167	3.154861
	Median	0		2.4	2.7
	Max	41.08978		7.4	8.2
	Min	-160.29		0.1	0.1
	Std	34.30294		1.917307	2.132985
PO4 (mg m^{-2} d^{-1})	Mean	-0.02101		0.763194	-1.40208
	Median	0.021576		0.7	-1.1
	Max	1.47684		1.9	0.3
	Min	-3.02064		0	-9.4
	Std	0.91518		0.529381	1.359734
DOP (mg m^{-2} d^{-1})	Mean	0.699211		0.334028	0.347222
	Median	0.049476		0.3	0.3
	Max	5.931168		0.9	0.9
	Min	-1.36673		0	0
	Std	1.65576		0.254515	0.261503

Nitrogen

Observations and computations agreed that the dark ammonium flux is to the water column at a rate of 5 to 10 mg N m^{-2} d^{-1} (Figure 109). The majority of the computed release originates in excretion from SAV (Table 25). The model indicates daylight ammonium uptake, roughly equal in magnitude to the dark release. The uptake originates with benthic algae which strip ammonium from the water as well as intercept diagenetic ammonium release. Corresponding uptake is absent from the observations, however.

Both observations and model indicate nitrate removal, less than 5 mg N m^{-2} d^{-1}, from the water column in both dark and light (Figure 109). The largest computed component of this flux is daylight uptake by benthic algae (Table 25).

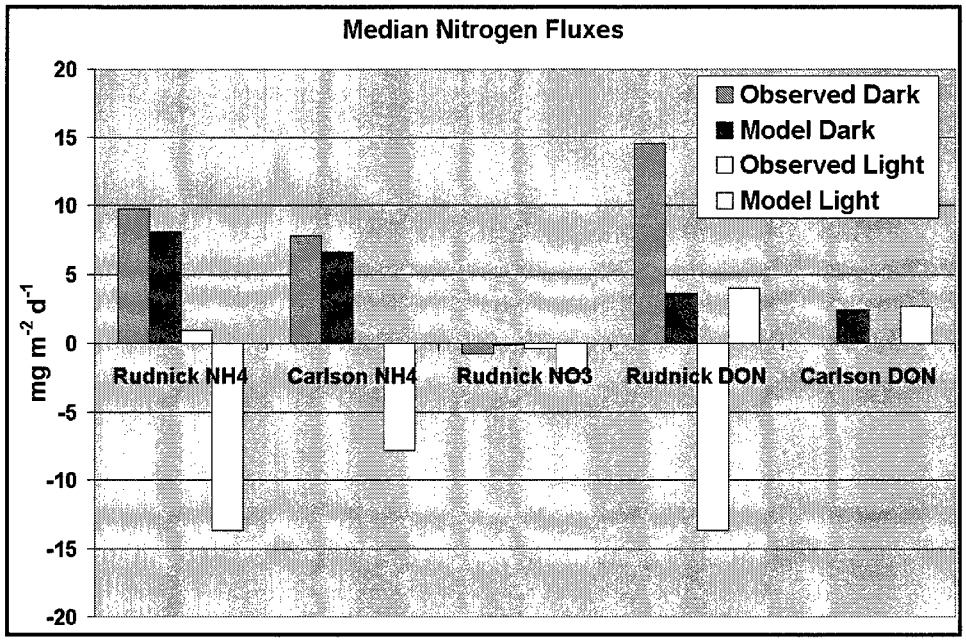

Figure 109. Median observed and computed nitrogen fluxes

Table 25
Components of Computed Fluxes

	Light SAV ($mg\ m^{-2}\ d^{-1}$)	Dark SAV ($mg\ m^{-2}\ d^{-1}$)	Light Algae and Diagenesis ($mg\ m^{-2}\ d^{-1}$)	Dark Algae and Diagenesis ($mg\ m^{-2}\ d^{-1}$)
Ammonium	5.233333	5.729167	-18.6028	2.661111
Nitrate	-0.14861	0	-3.08056	-0.36944
DON	1.941667	1.515278	2.016667	1.995833
Phosphate	0.240278	0.184722	-1.7375	0.663889
DOP	0.069444	0.040278	0.3375	0.338889
DO	646.4708	-225.808	100.6014	-281.031
DOC	54.86528	43.06944	13.86944	13.75694

The range of observed dissolved organic nitrogen fluxes is enormous relative to the other nitrogen components (Tables 23, 24). In the Rudnick data set, median dissolved organic nitrogen flux is to the water at night and out of the water during daylight (Figure 109). The magnitude of the median, relative to the range, casts doubt on interpretation of the statistic, however. In the Carlson data set, median flux is close to zero. Computed dissolved organic nitrogen fluxes are exclusively to the water and show no diurnal variation. Magnitude of the median release, less than 5 mg N m^{-2} d^{-1}, is close to the median of the Carlson database but much less than the median from the Rudnick database. Modeled fluxes originate in excretion from benthic algae and SAV in roughly equal proportions. No mechanism exists in the model to create uptake of dissolved organic nitrogen nor is the origin of the observed uptake apparent.

Phosphorus

Phosphate fluxes of 1 to 2 mg P m^{-2} d^{-1} were observed into and out of the water column (Tables 23, 24). Median observed fluxes were close to zero (Figure 110). Modeled fluxes showed a strong diurnal variation, with release to the water during dark and uptake during daylight. Median modeled fluxes were comparable to extremes in the observations. The diurnal variation originated in the computed benthic algae (Table 25). SAV contributed a lesser background release via excretion.

Extreme observed dissolved organic phosphorus fluxes, 3 to 6 mg P m^{-2} d^{-1}, exceeded extreme phosphate fluxes (Tables 23, 24). As with phosphate, fluxes were observed into and out of the water, such that medians of the observations were close to zero (Figure 110). Median modeled fluxes, less than 0.5 mg P m^{-2} d^{-1}, were greater than median observations but less than extreme observations. Modeled fluxes were exclusively into the water and originated primarily in excretion from benthic algae (Table 25). As with nitrogen, no mechanism exists in the model to create uptake of dissolved organic phosphorus nor is the origin of the observed uptake apparent.

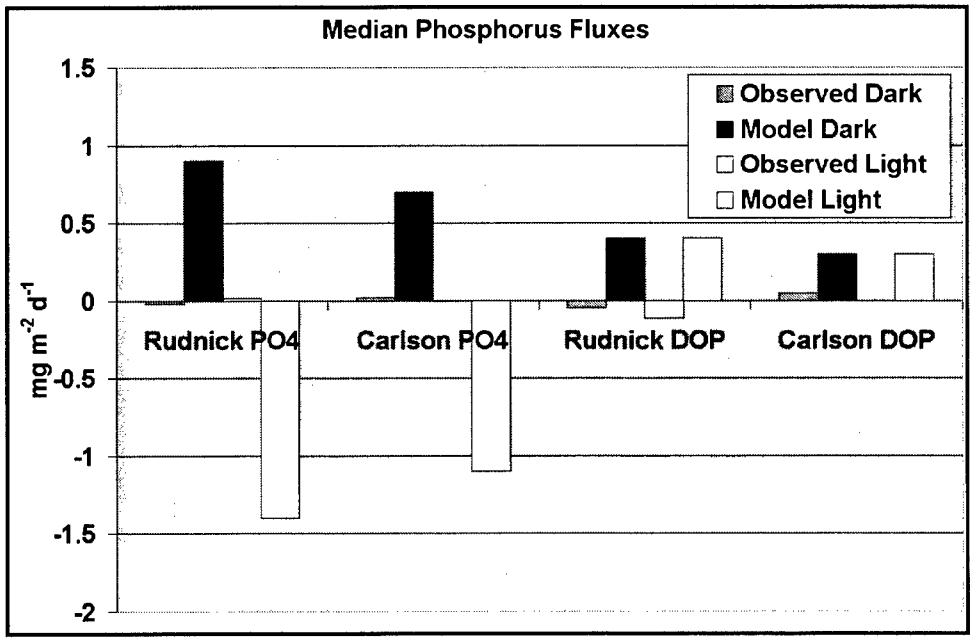

Figure 110. Median observed and computed phosphorus fluxes

Carbon and oxygen

Dissolved organic carbon fluxes in excess of 1 g C m^{-2} d^{-1} were observed both into and out of the water (Table 23). In darkness and light, median fluxes, roughly 10 and 100 mg C m^{-2} d^{-1} respectively, were into the water (Figure 111). Model fluxes were exclusively into the water and were of the same magnitude as median observations. The preponderance of the modeled DOC originated in SAV excretion (Table 25).

Observed dissolved oxygen fluxes showed a clear pattern of removal from the water at night and release to the water during day. Median release to the water, roughly 2.5 g DO m^{-2} d^{-1}, exceeded uptake, roughly 1.8 g DO m^{-2} d^{-1}, in magnitude (Figure 111). Modeled fluxes showed the same pattern as observed, but were less than half the observed values. Production by SAV accounted for the majority of the daylight flux (Table 25). Uptake via SAV respiration and via the combined effects of benthic algae and sediment diagenesis were roughly equal.

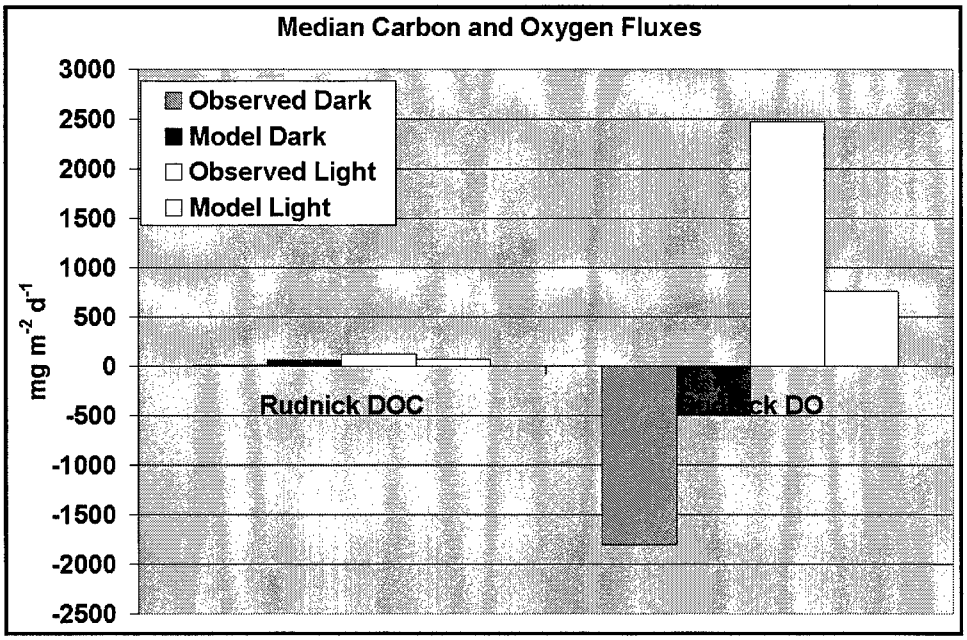

Figure 111. Median observed and computed carbon and oxygen fluxes

12 Sensitivity Analyses

Introduction

Sensitivity analyses are intended to provide insights into the behavior of the model and the modeled system. Six sensitivity runs were performed on the calibrated model. These were:

- Sensitivity to loads from mainland and Keys
- Sensitivity to atmospheric loads
- Sensitivity to boundary conditions
- Sensitivity to resuspension
- Sensitivity to benthic algae
- Sensitivity to nitrogen fixation

All sensitivity analyses were performed in identical fashion. One input or parameter was altered from the calibration value. A two-year "spin-up" was run that was otherwise identical to the calibration. Conditions at the end of the spin-up were used as initial conditions to the sensitivity run. This sensitivity run duplicated the calibration in all regards except the factor under investigation and the initial conditions.

For comparison with the sensitivity runs, a "base" run was conducted. The base was initiated with a two-year spin up that was a repeat of the calibration run. Conditions at the end of the spin-up were employed as initial conditions for a production run that also duplicated the calibration. The base run was identical to the calibration run except for the small difference in initial conditions that resulted from the spin-up.

Three regions of the bay (Figure 57) were selected for examination: the Eastern Zone, the Central Zone, and the Gulf Transition Zone.

Sensitivity to Loads from the Mainland and Keys

For this analysis, nitrogen and phosphorus loads from the mainland and Keys were doubled from loads employed in the calibration. As expected, the primary impact of the load increase appears in the Eastern Zone (Figure 112) which abuts both the mainland and the Keys. Within the Central Zone (Figure 113), an effect on nitrogen from the load increase is visible but the impact on computed phosphorus is negligible. Within the Gulf Transition Zone (Figure 114), effects on both nitrogen and phosphorus are barely detectable.

A major conclusion from this run is that the widespread shortfalls in computed nitrogen are likely not due to shortfalls in loading. Or else, the computed loads are low by much more than a factor of two. Similarly, shortfalls in computed phosphorus are likely not due to shortfalls in loading. The analysis also suggests that nitrogen and phosphorus from the mainland and Keys make up only a small fraction of the observed totals in the waters of Florida Bay.

Sensitivity to Loads from the Atmosphere

For this analysis, atmospheric nitrogen and phosphorus loads were doubled from loads employed in the calibration. Impact from the increased load is most evident in the Eastern and Central Zones (Figures 115, 116) but is negligible throughout the system. Within the Eastern and Central Zones, the impact of atmospheric nitrogen loading is less than loads from the mainland and Keys. Within the Eastern Zone, the impact of atmospheric phosphorus loading is less than loads from the mainland and Keys. In the Central Zone, impact of atmospheric phosphorus loading is larger than impact of loads from the mainland and Keys. In the Gulf Transition Zone (Figure 117), effects of atmospheric loads on both nitrogen and phosphorus are barely detectable.

As with the previous sensitivity run, a major conclusion is that computed shortfalls in nitrogen or phosphorus are likely not the result of errors in estimating atmospheric loads. Or else, the computed loads are low by much more than a factor of two. The analysis also suggests that nitrogen and phosphorus from the atmosphere make up only a small fraction of the observed totals in the waters of Florida Bay.

Sensitivity to Boundary Conditions

For this analysis, nitrogen and phosphorus concentrations at the open boundaries of the grid were doubled from concentrations employed in the calibration. Major impact of the change in boundary conditions is evident

in the Gulf Transition Zone (Figure 120). Negligible concentration increases are evident in the Central Zone (Figure 119) and no change is detected in the Eastern Zone (Figure 118).

This run indicates that concentration shortfalls and discrepancies between computed and observed concentrations in the Gulf Transition Zone may be partly attributed to uncertainties in the boundary conditions although consistent factor-of-two errors in specified boundary conditions are not likely. Within the interior of Florida Bay, specification of boundary conditions has little impact on model results. By inference, conditions in the Gulf of Mexico and outside the Keys have minimum impact on conditions in the interior of Florida Bay.

Sensitivity to Resuspension

For this analysis, resuspension of sediment nutrients was eliminated from the model. Resuspension of suspended solids remained in the computation, however. Resuspension affects total phosphorus more than total nitrogen with maximum impact in the Central Zone (Figure 122). Lesser impact is visible in the Gulf Transition Zone (Figure 123) and virtually no impact is evident in the Eastern Zone (Figure 121). The distribution of impacts is affected by local depth and by specified erodibility (Chapter 5). Zones with greater depth are expected to show less sensitivity to resuspension but this generalization is subject to alteration due to specified erosion potential of a region.

A secondary effect of resuspension is visible on chlorophyll and on nitrogen fractions, especially in the Central Zone. Absent resuspension, total and soluble reactive phosphorus diminish in the water column, causing a decline in abundance of phosphorus-limited phytoplankton. Diminished phytoplankton uptake of ammonium and nitrate leads to an increase in these fractions. Total nitrogen changes little, however. The additional ammonium and nitrate in the sensitivity run was present in the base run but was incorporated in phytoplankton biomass. Resuspension influences the distribution of total nitrogen into fractions but not the total itself.

Sensitivity to Benthic Algae

For this analysis, benthic algae were removed from the model. The impact on the water column in the interior of the bay is enormous (Figures 124, 125), far greater than any of the other sensitivity runs. Within the Gulf Transition Zone (Figure 126), the impact is noticeable, but less than that in the interior zones. The difference is puzzling, at first, since computed benthic algal concentration in the Gulf Transition Zone is, at times, as high or higher than in the interior zones (Figure 105). The difference in

effects is attributable to the difference in depths of the zones. The shallower zones demonstrate more impact than deeper zones from processes at the sediment-water interface.

Within the Eastern and Central Zones, computed total nitrogen in the water column doubles in the absence of benthic algae. Computed total phosphorus increases by an even greater amount. Fueled by the additional nutrients, computed chlorophyll jumps to values far in excess of any observations. Computed total nitrogen in the Central Zone is still less than observed, however. Computed total nitrogen and total phosphorus in the Gulf Transition Zone also remain on the low side.

This run suggests that the benthic algae play an important role in mediating sediment-water exchange processes in Florida Bay and in determining nutrient concentrations in the overlying water. The model calibration, potentially, could be improved by revision of the benthic algal component or by "tuning" of the existing representation. At present, however, little basis exists for improving the model. The only information available to the modelers is sporadic observations of sediment chlorophyll and the advice that "benthic algae cover half the bottom of Florida Bay."[1] The observed sediment chlorophyll concentrations are well matched by the model (Figure 104) and a patchiness factor of 0.5 was employed to convert computed algae, as g C m^{-2}, to total algae, as g C, in each model cell. Some additional tuning is possible, but clearly additional field and process investigation is necessary.

Sensitivity to Nitrogen Fixation

For this analysis, nitrogen fixation at the shoots and roots of submerged aquatic vegetation was doubled over the rate employed in the calibration. Within the Eastern Zone (Figure 127), additional nitrogen fixation results in an increase in water-column ammonium, nitrate, and total nitrogen. The increase in nitrate occurs because the additional ammonium substitutes for nitrate taken up by phytoplankton and SAV. Little impact of the additional nitrogen on phytoplankton is visible, however, since algal production in this region of the bay is largely limited by availability of phosphorus. While the rate of nitrogen fixation in SAV beds is poorly known, the rate would have to be many times larger than employed in the model to make up the computed shortfall in total nitrogen.

Within the Central Zone (Figure 128), the additional nitrogen fixation stimulates phytoplankton to a small degree. The stimulation indicates that, on occasion or in isolated locations, nitrogen availability is computed to be more limiting to algae than phosphorus availability. Zone-wide, however, phosphorus availability is still more limiting than nitrogen (Figure 88). As

[1] Ellen Prager, United States Geological Survey, St. Petersburg, FL, May 1998.

with the Eastern Zone, the computed shortfall in total nitrogen is unlikely to be made up by increasing the rate of nitrogen fixation in SAV beds.

The effect of added nitrogen fixation on the Gulf Transition Zone (Figure 129) is similar to the Central Zone. Phytoplankton concentrations increase slightly but the impact on total nitrogen is small relative to the computed shortfall.

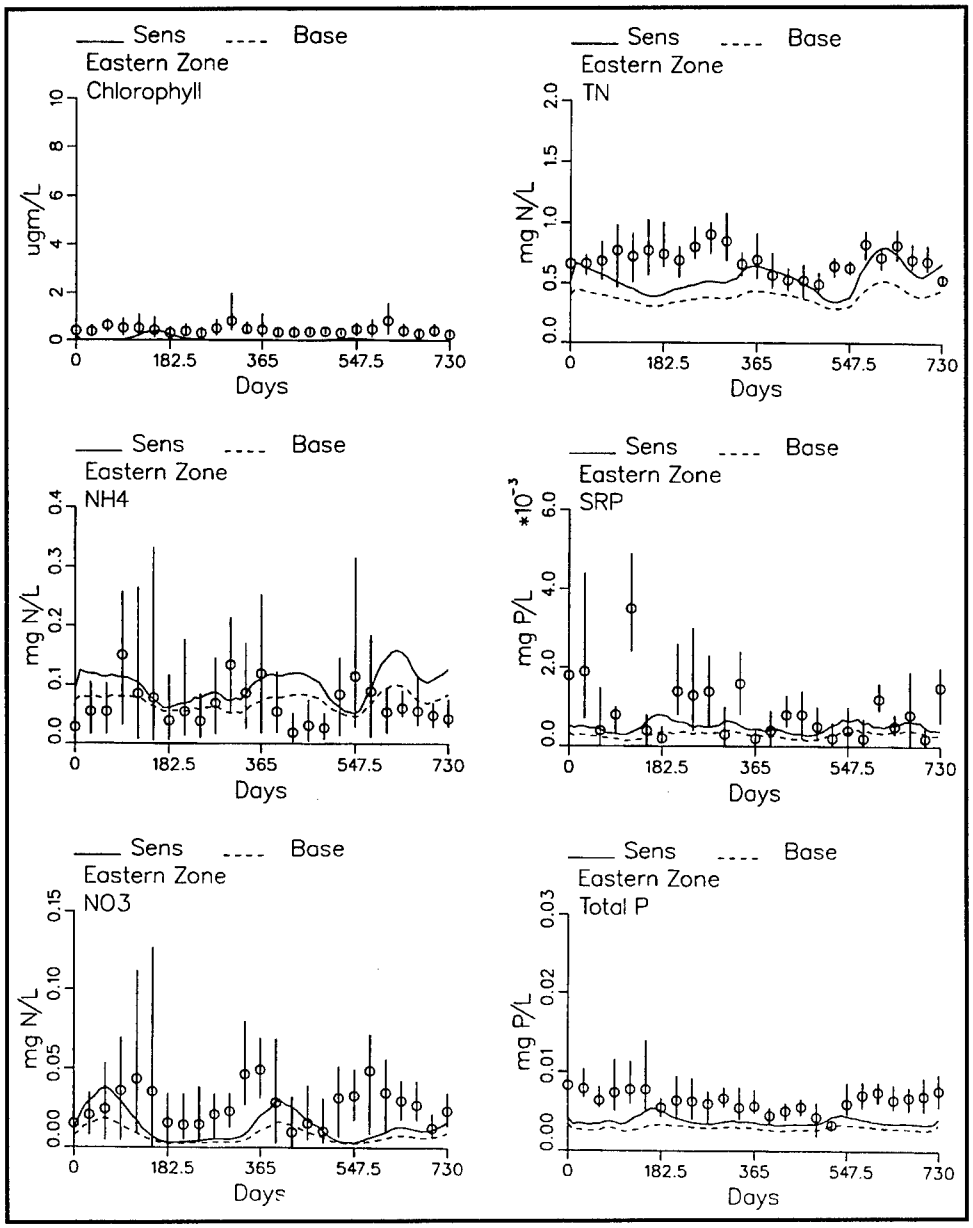

Figure 112. Effect of loads from mainland and Keys on waters in the Eastern Zone

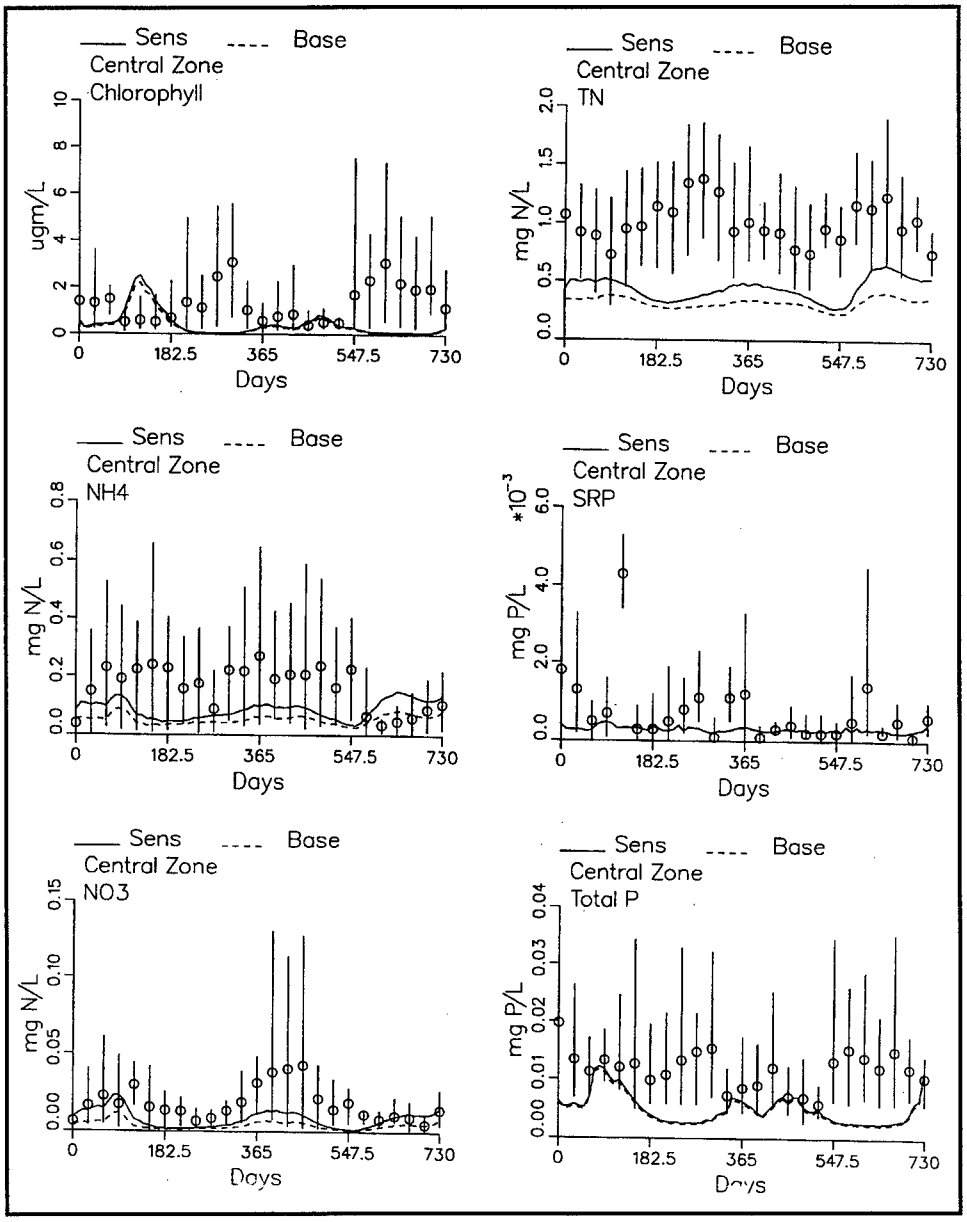

Figure 113. Effect of loads from mainland and Keys on waters in the Central Zone

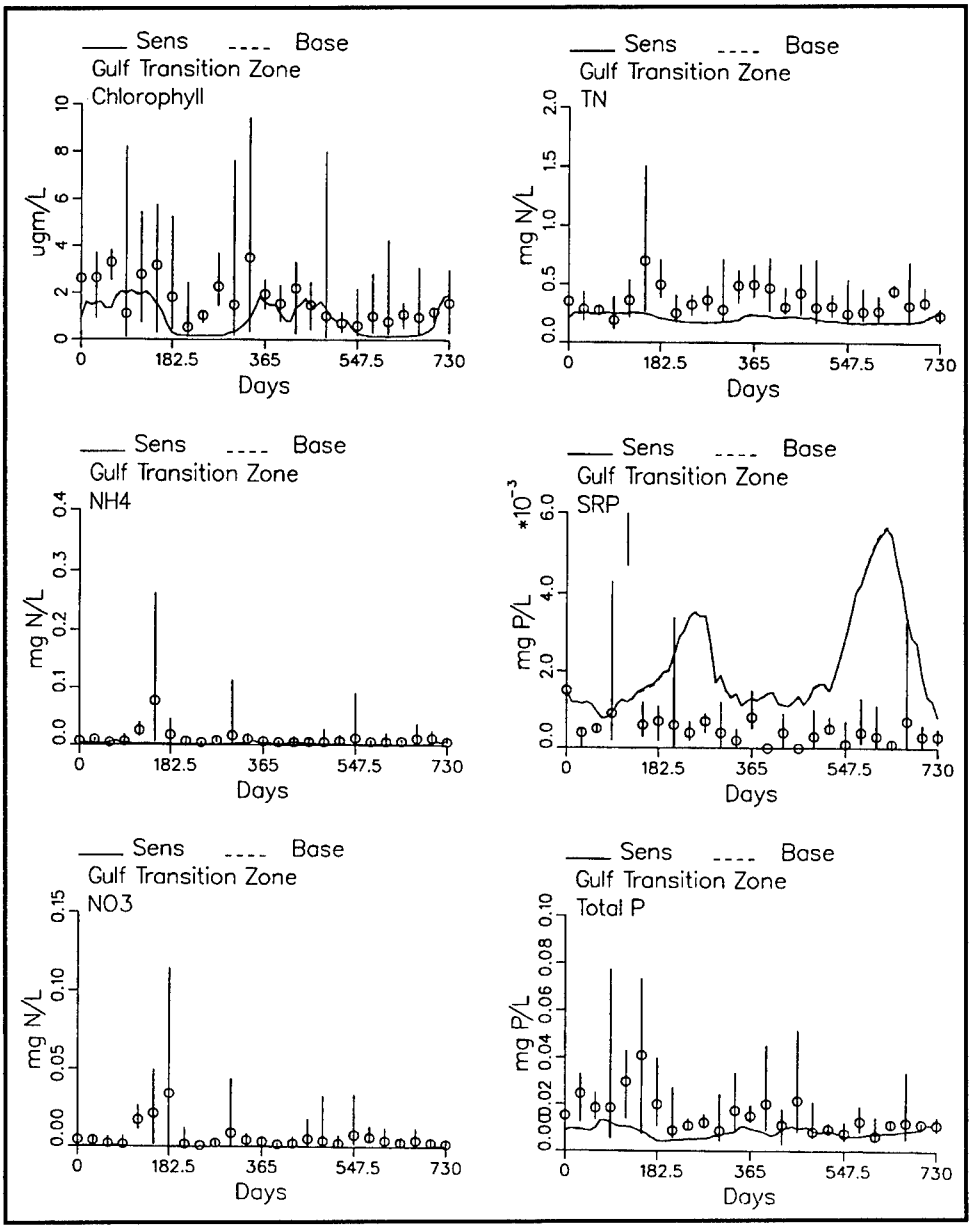

Figure 114. Effect of loads from mainland and Keys on waters in the Gulf Transition Zone

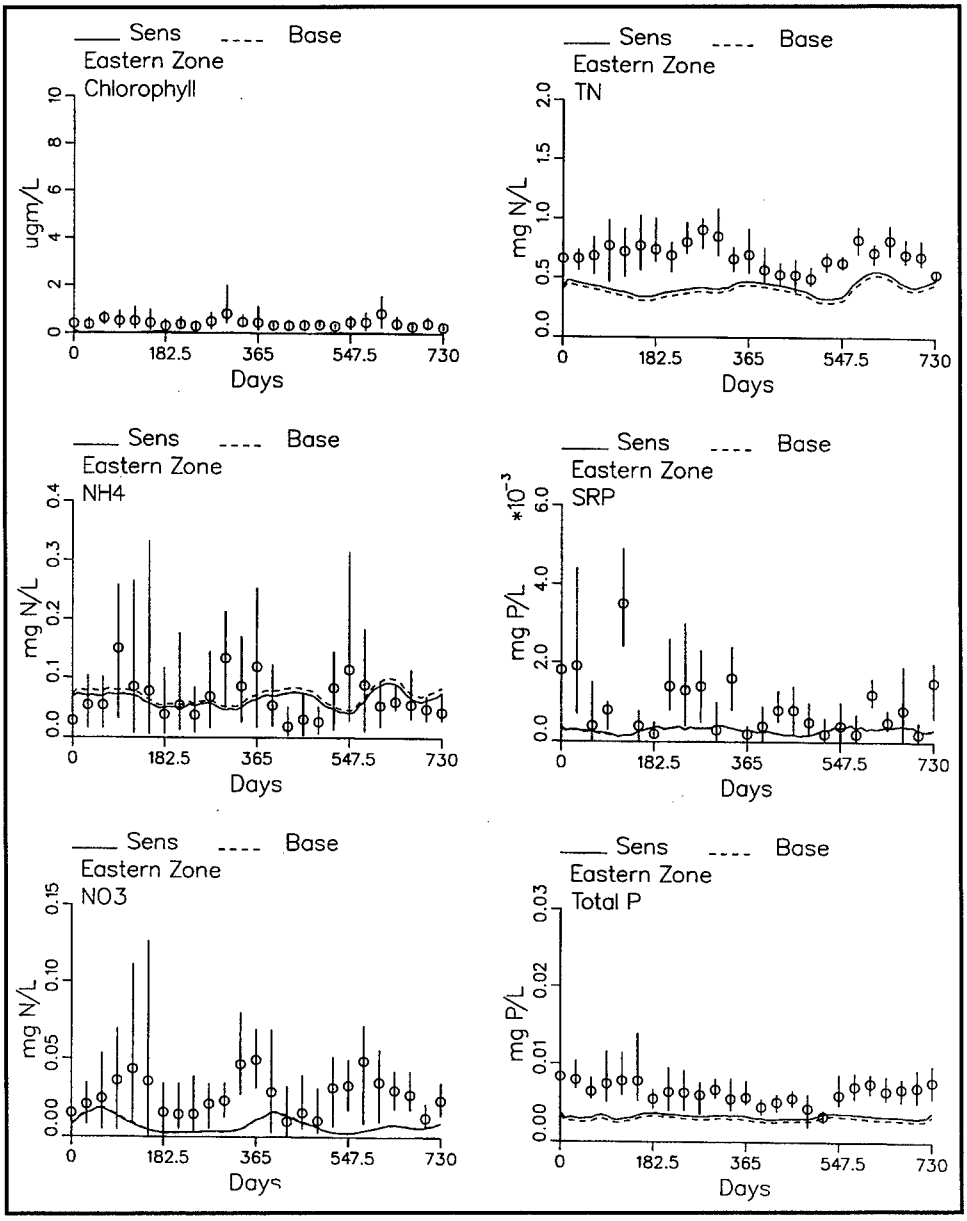

Figure 115. Effect of loads from the atmosphere on waters in the Eastern Zone

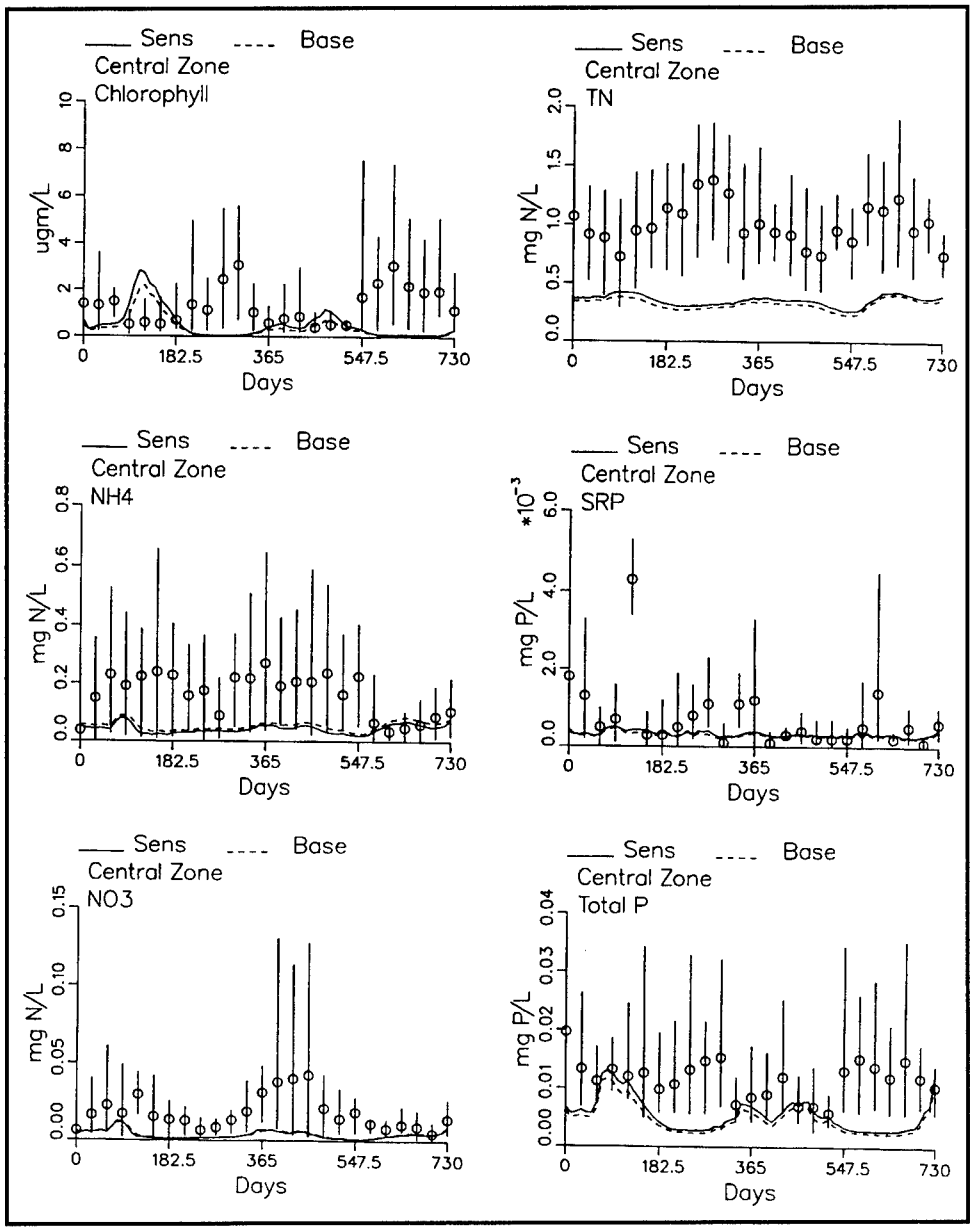

Figure 116. Effect of loads from the atmosphere on waters in the Central Zone

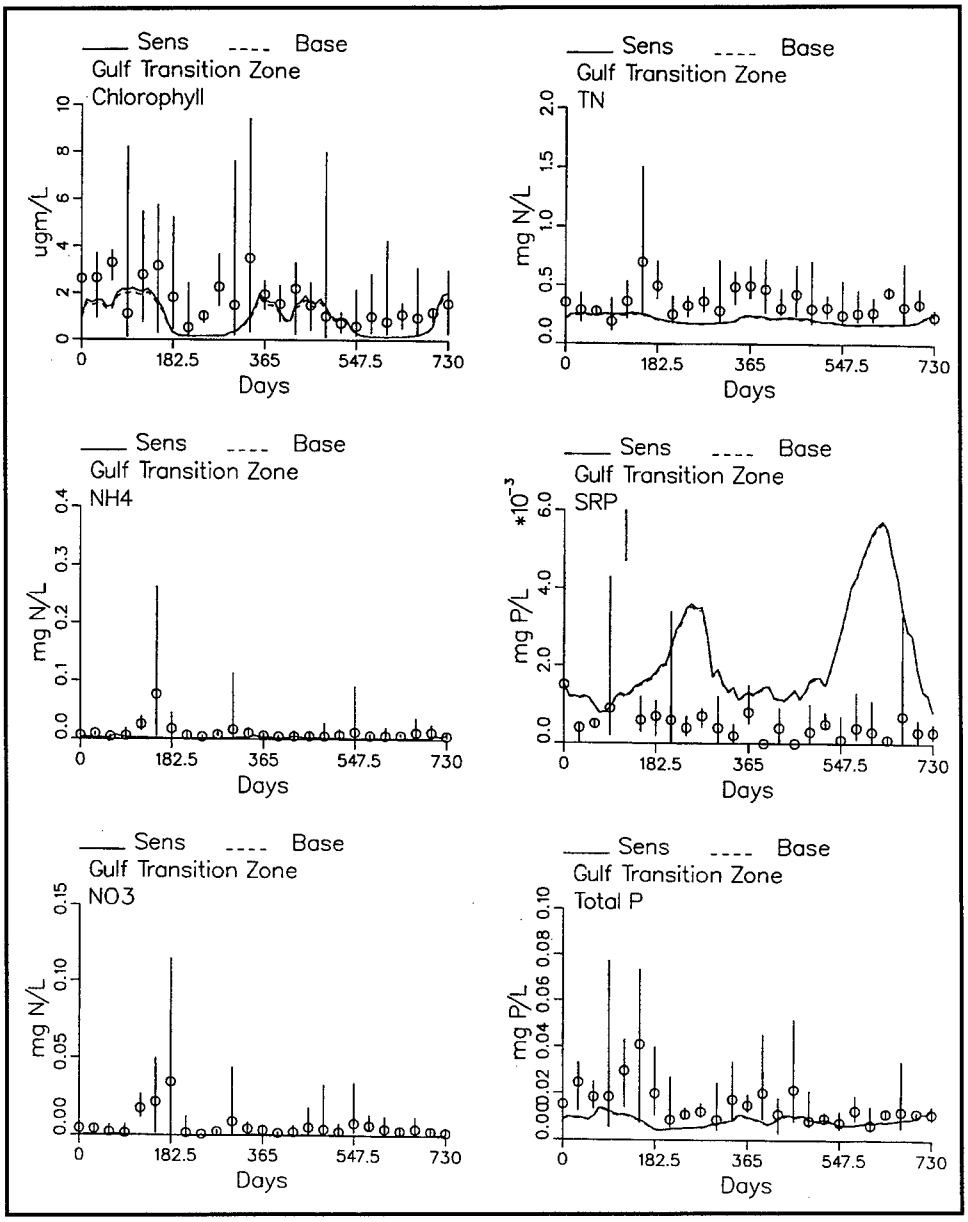

Figure 117. Effect of loads from the atmosphere on waters in the Gulf Transition Zone

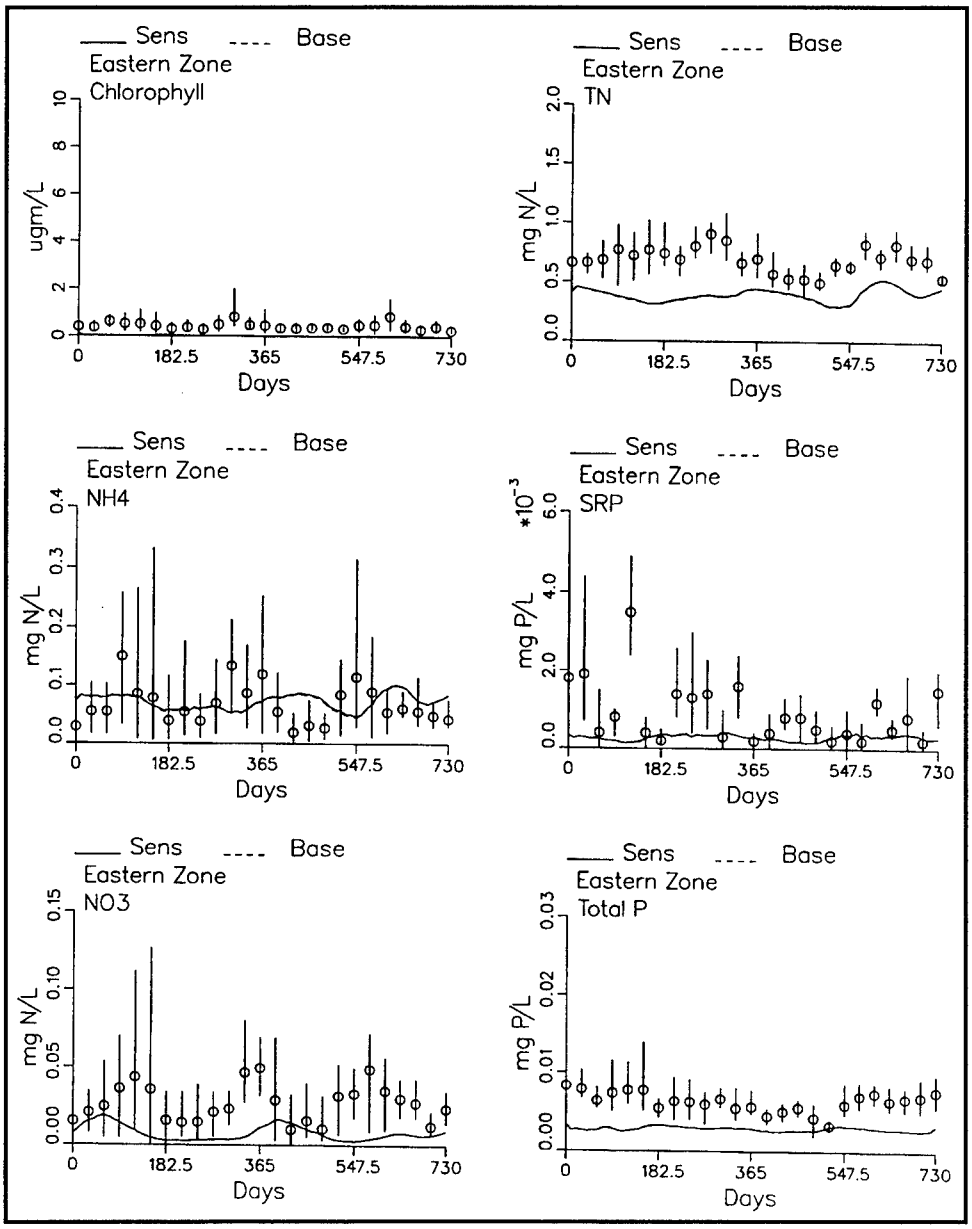

Figure 118. Effect of boundary conditions on waters in the Eastern Zone

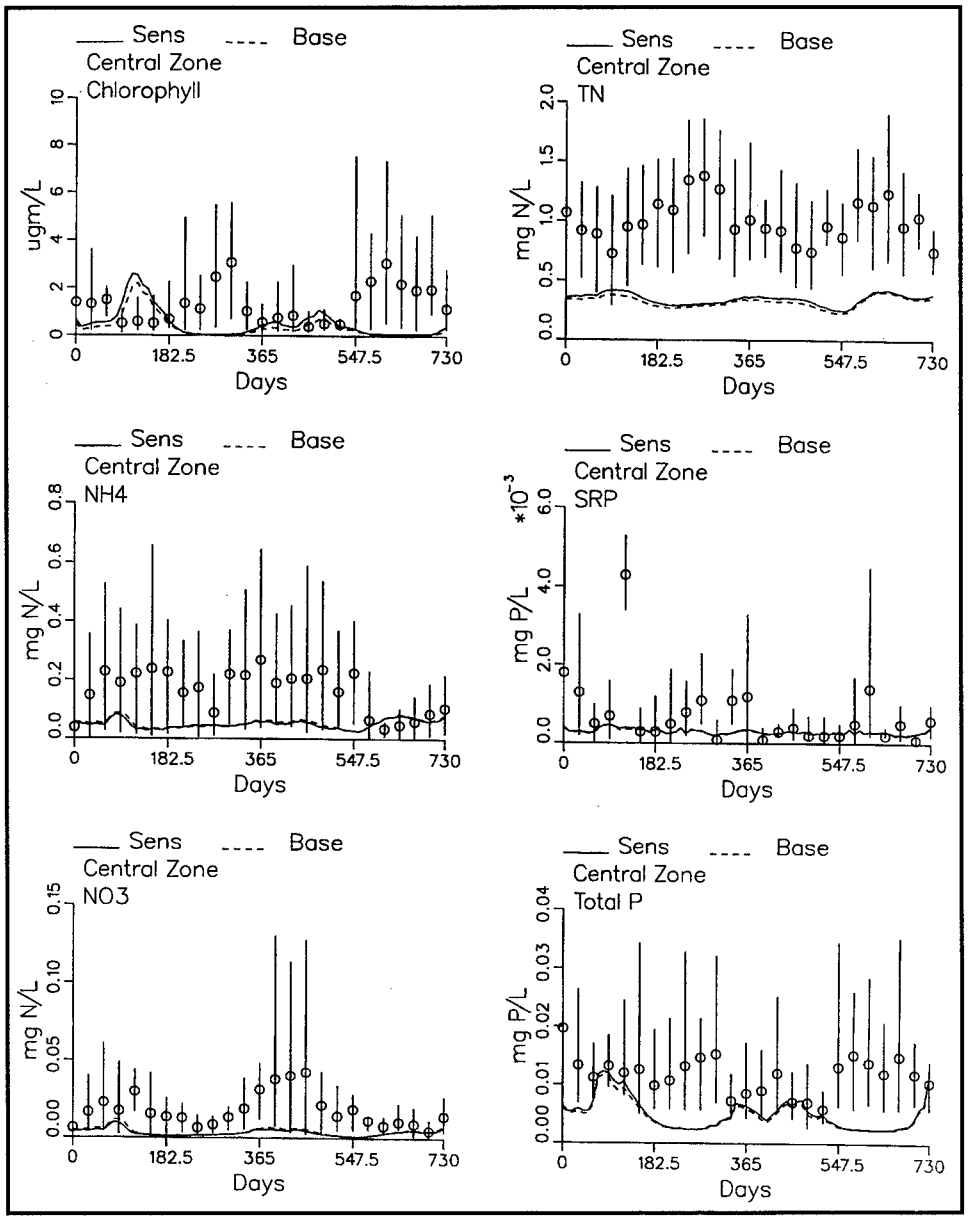

Figure 119. Effect of boundary conditions on waters in the Central Zone

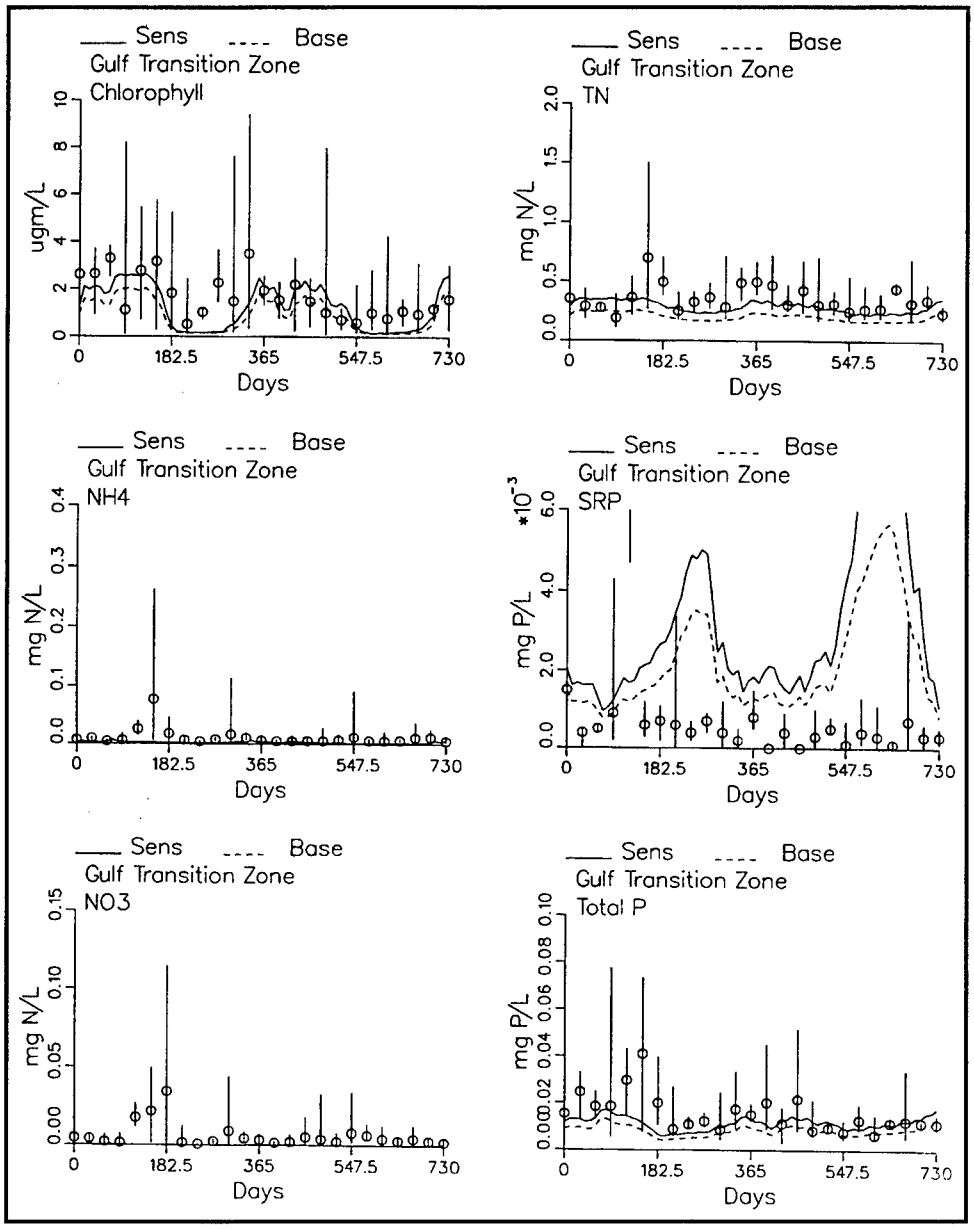

Figure 120. Effect of boundary conditions on waters in the Gulf Transition Zone

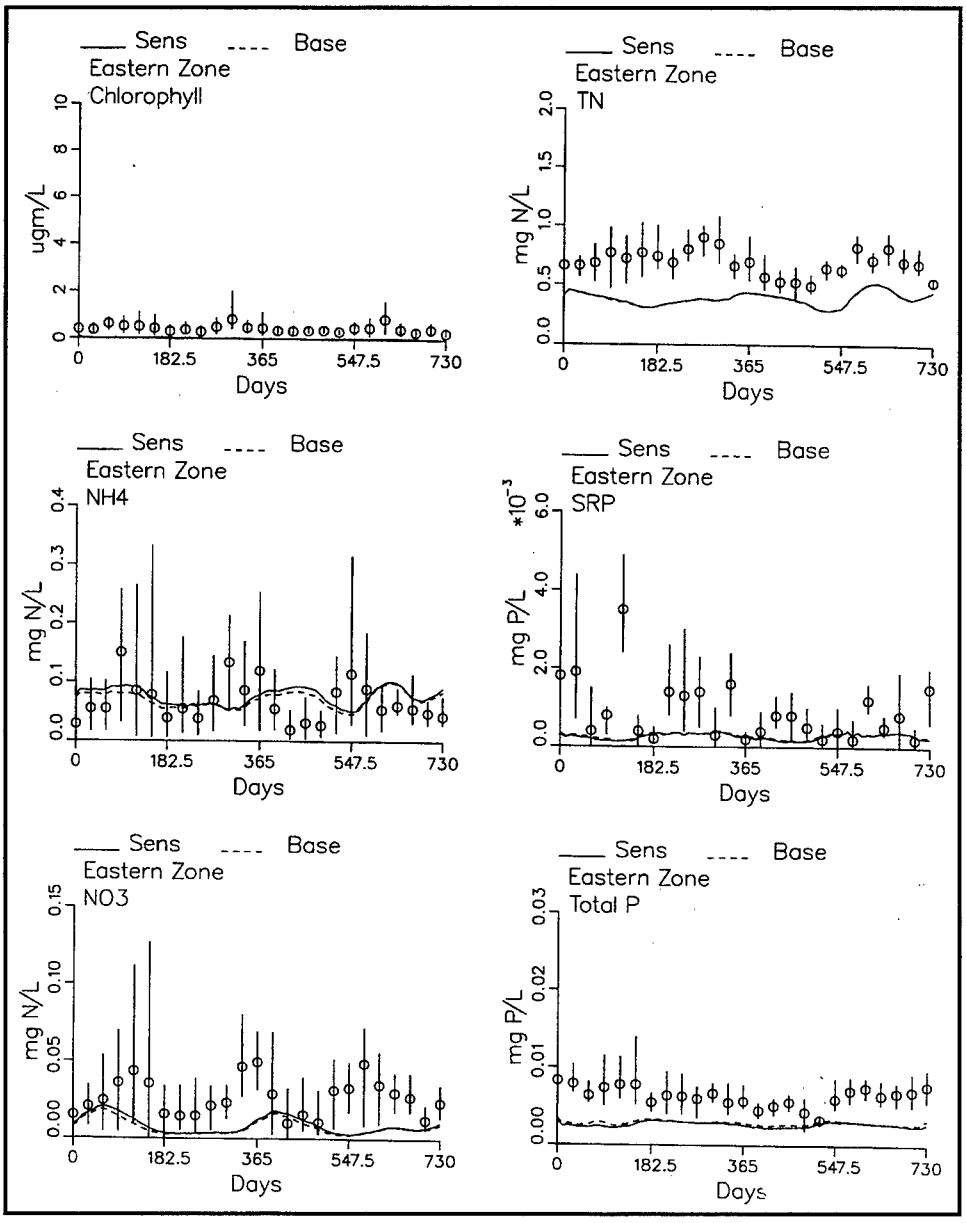

Figure 121. Effect of nutrient resuspension on waters in the Eastern Zone

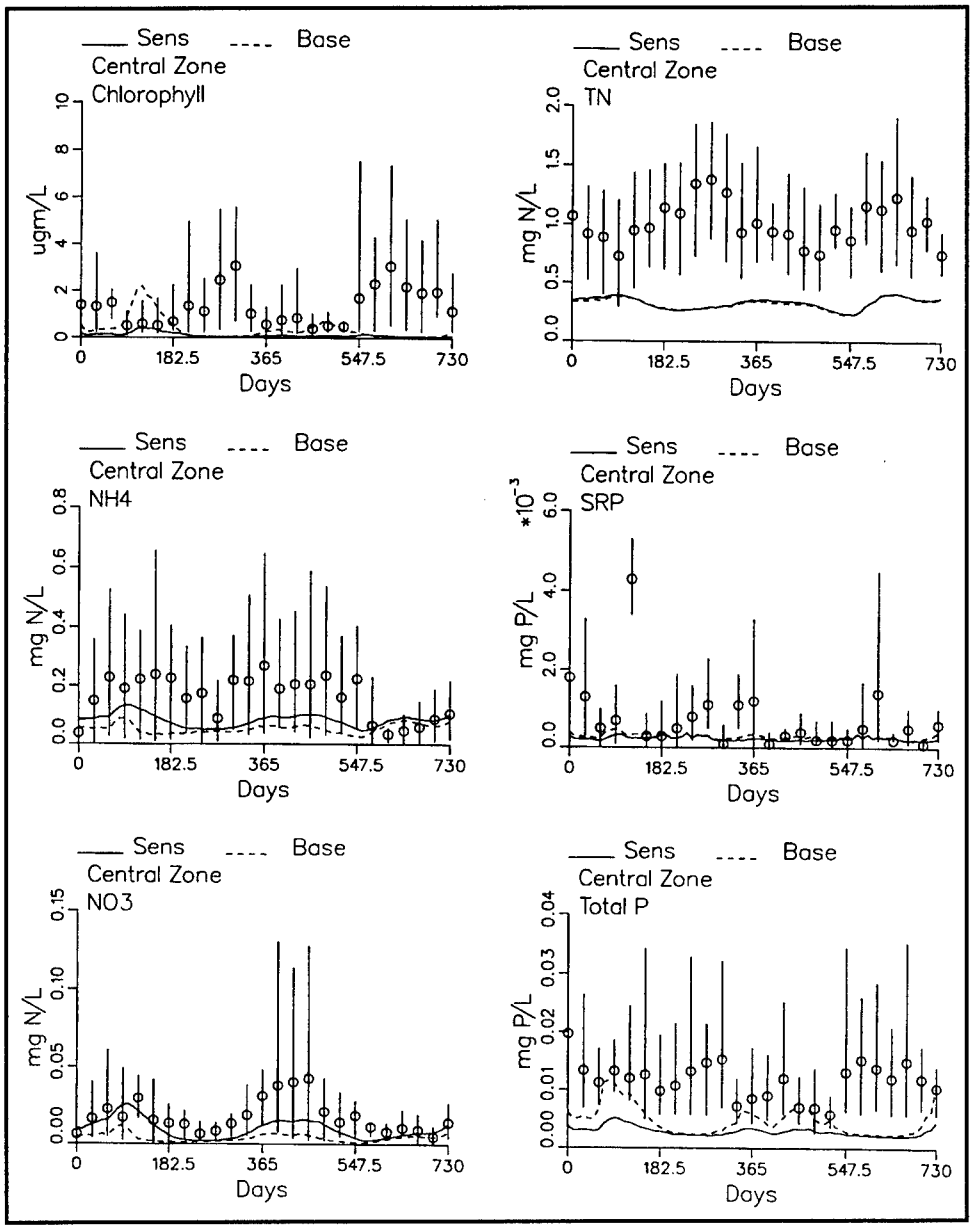

Figure 122. Effect of nutrient resuspension on waters in the Central Zone

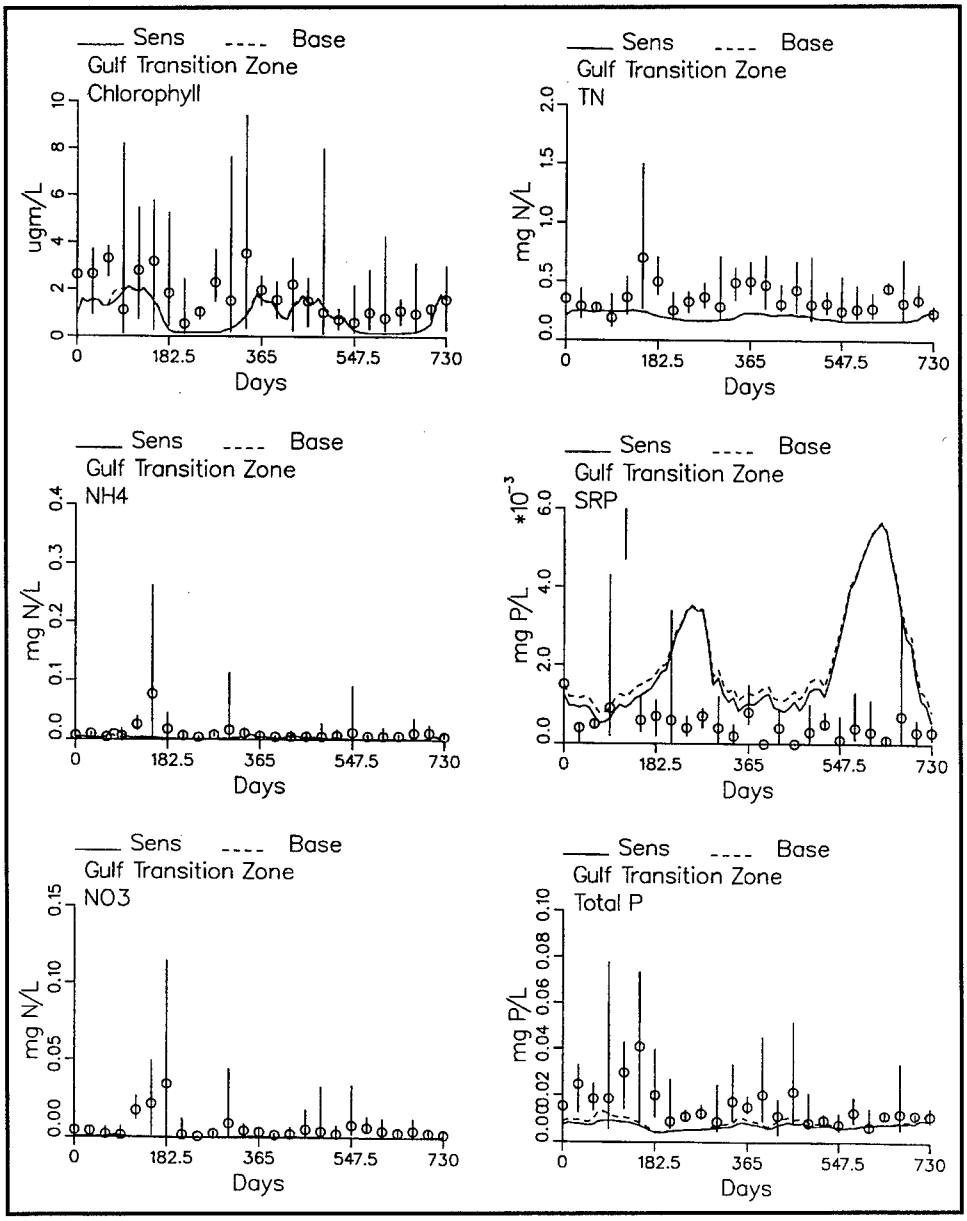

Figure 123. Effect of nutrient resuspension on waters in the Gulf Transition Zone

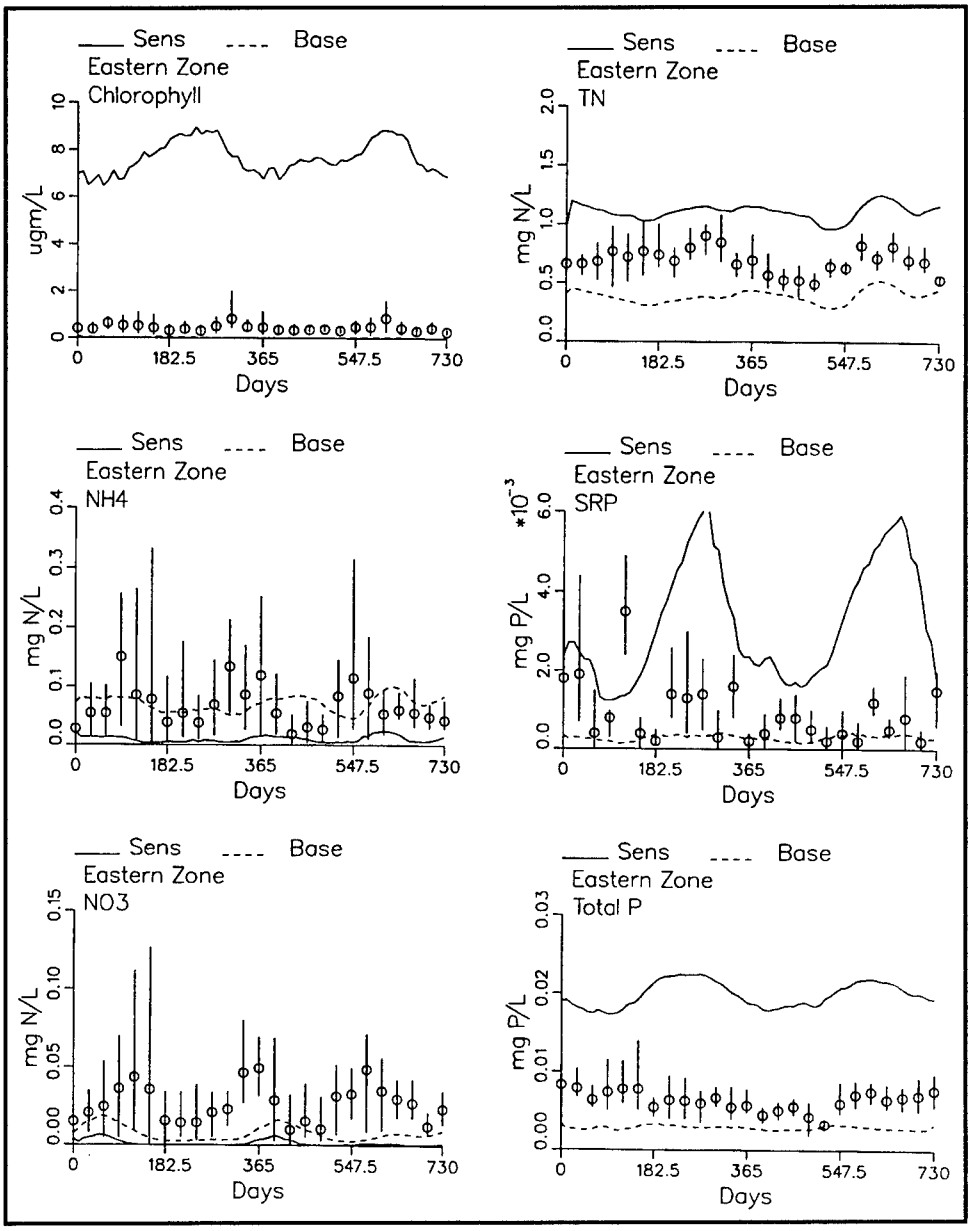

Figure 124. Effect of benthic algae on waters in the Eastern Zone

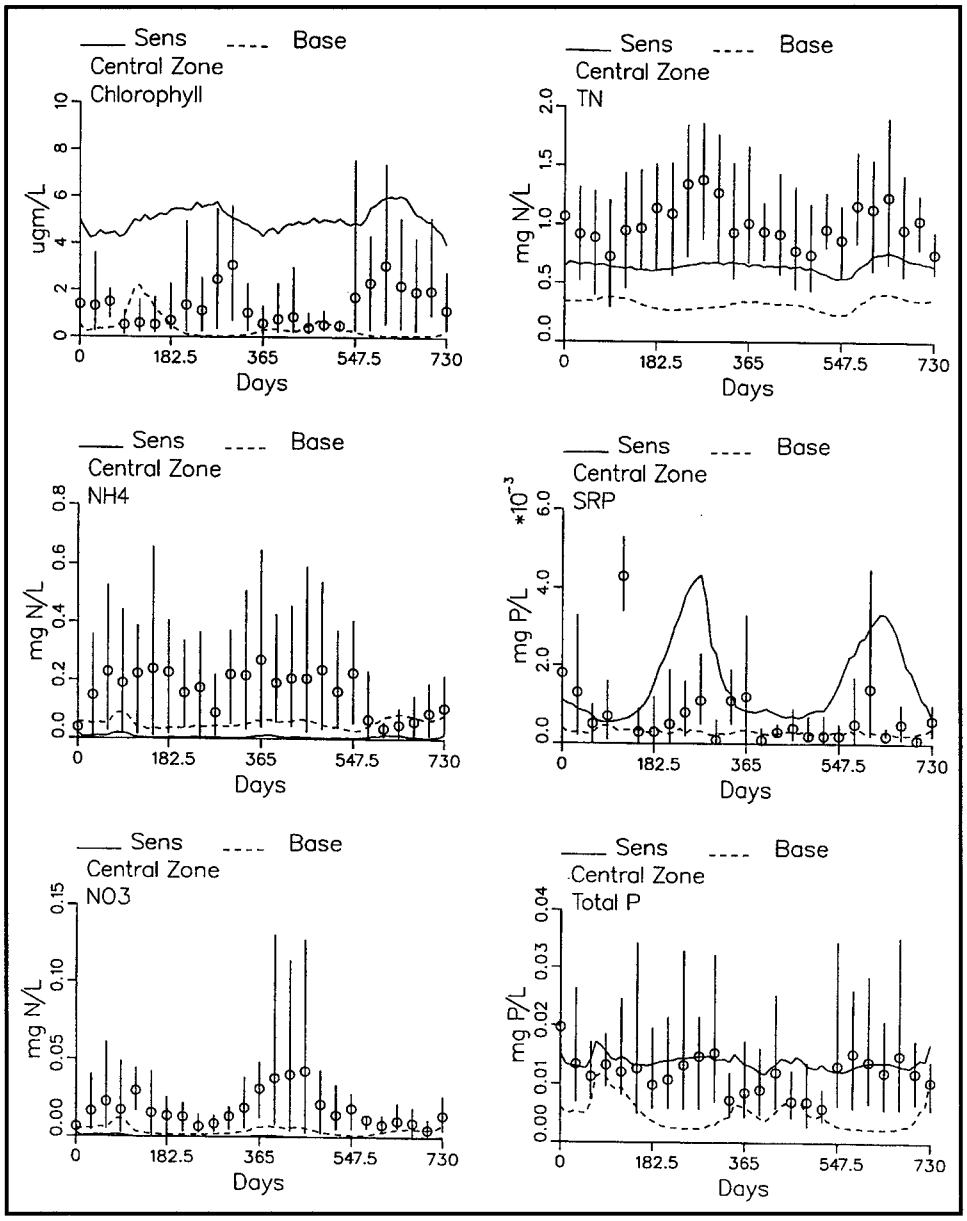

Figure 125. Effect of benthic algae on waters in the Central Zone

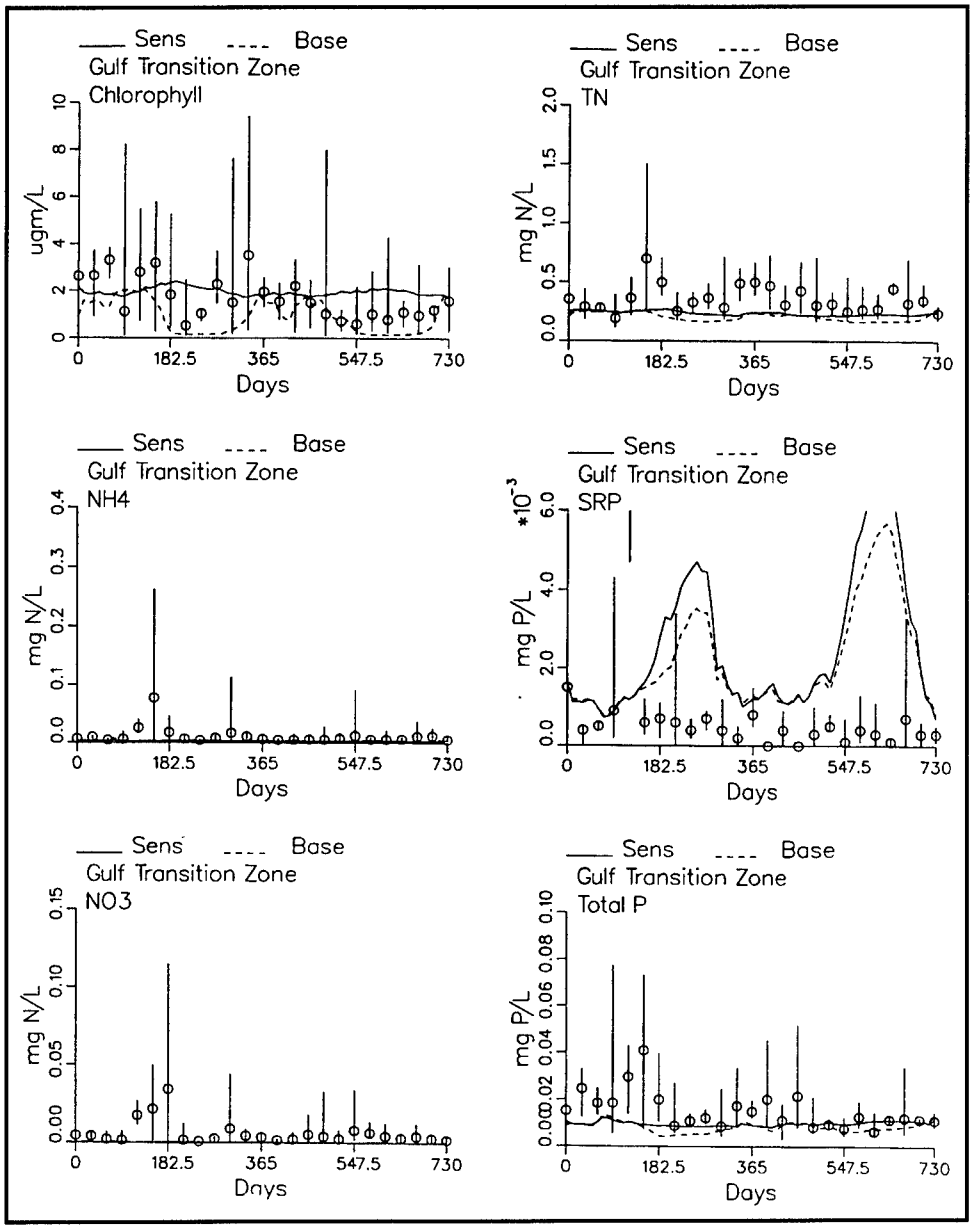

Figure 126. Effect of benthic algae on waters in the Gulf Transition Zone

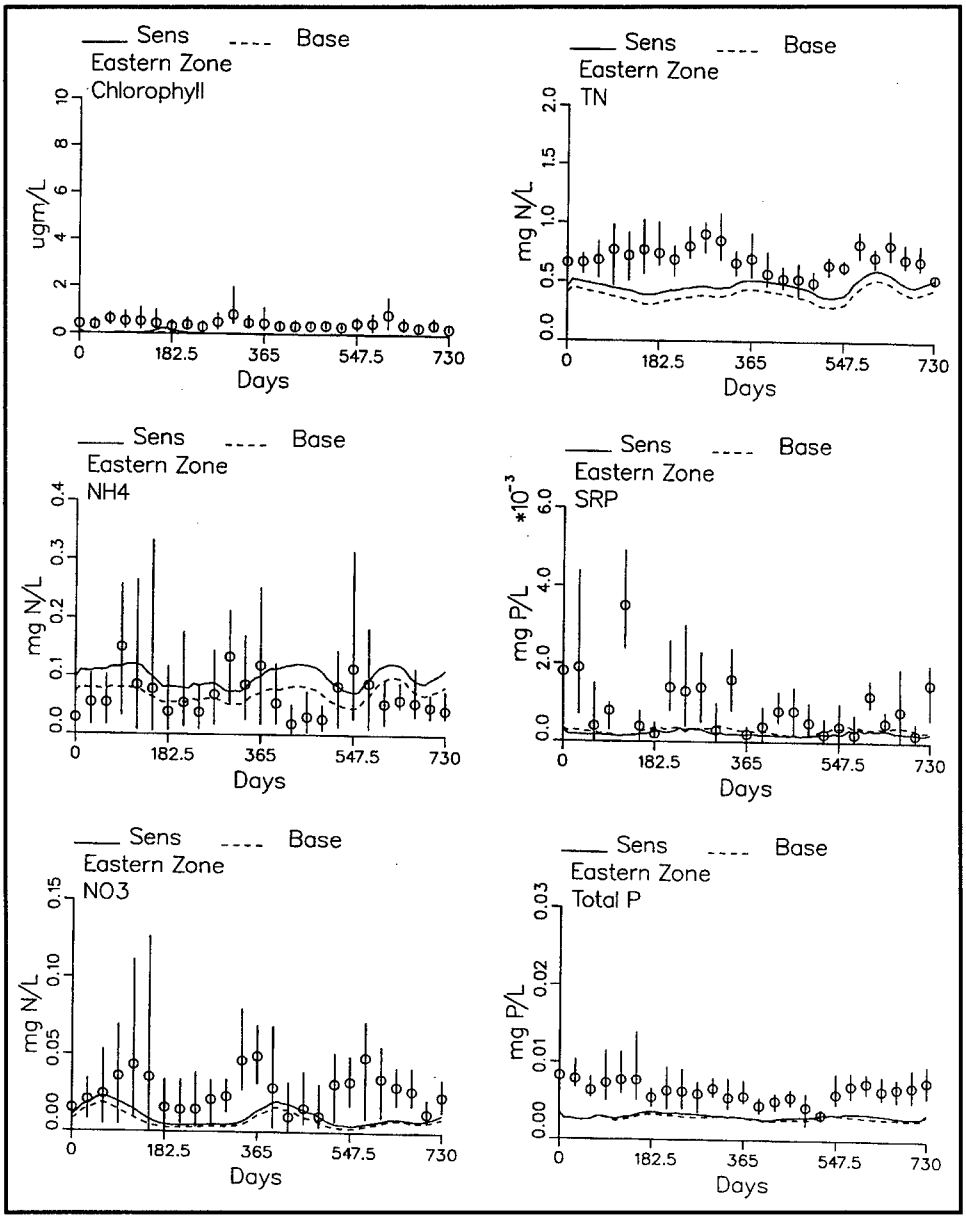

Figure 127. Effect of nitrogen fixation in SAV on waters in the Eastern Zone

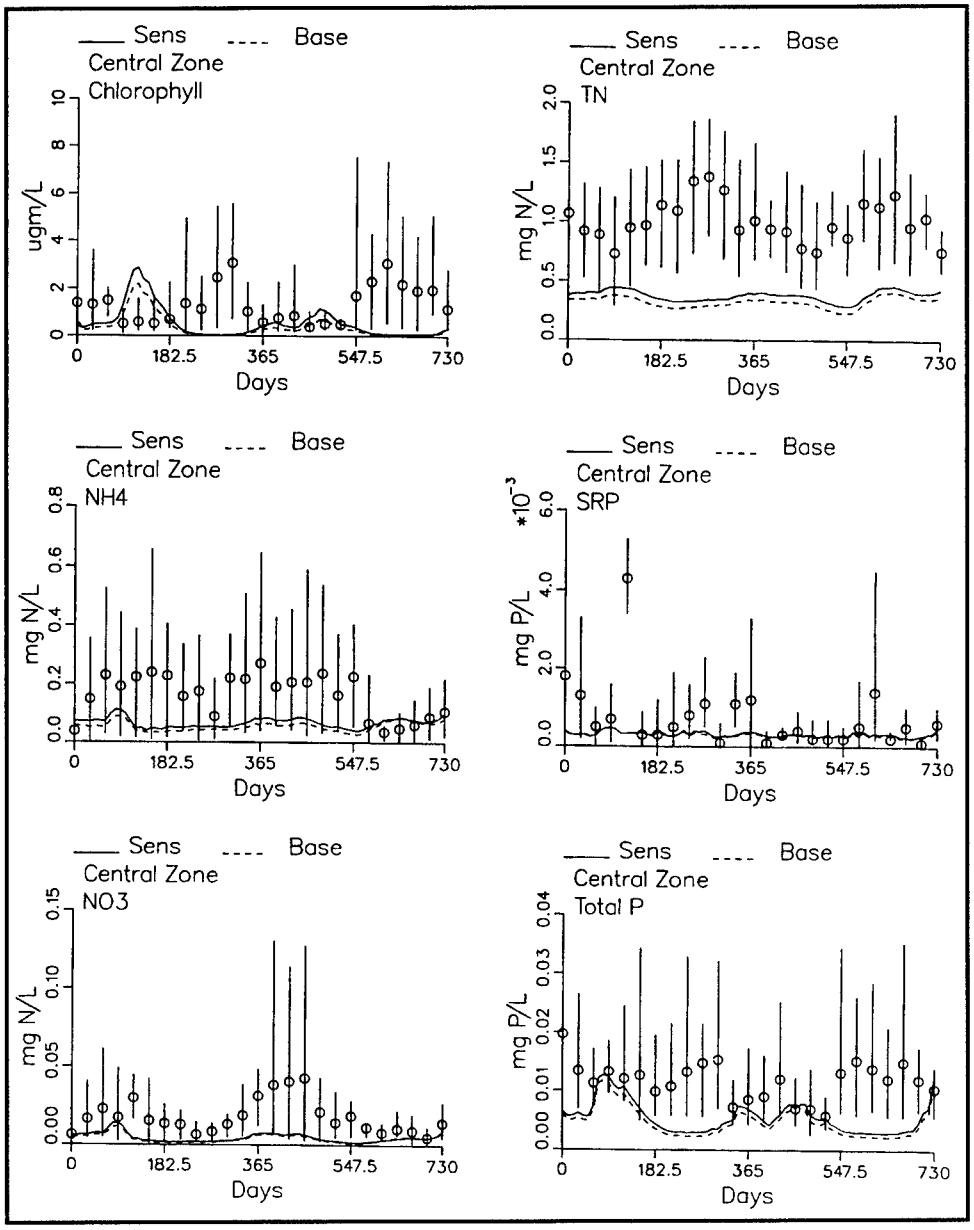

Figure 128. Effect of nitrogen fixation in SAV on waters in the Central Zone

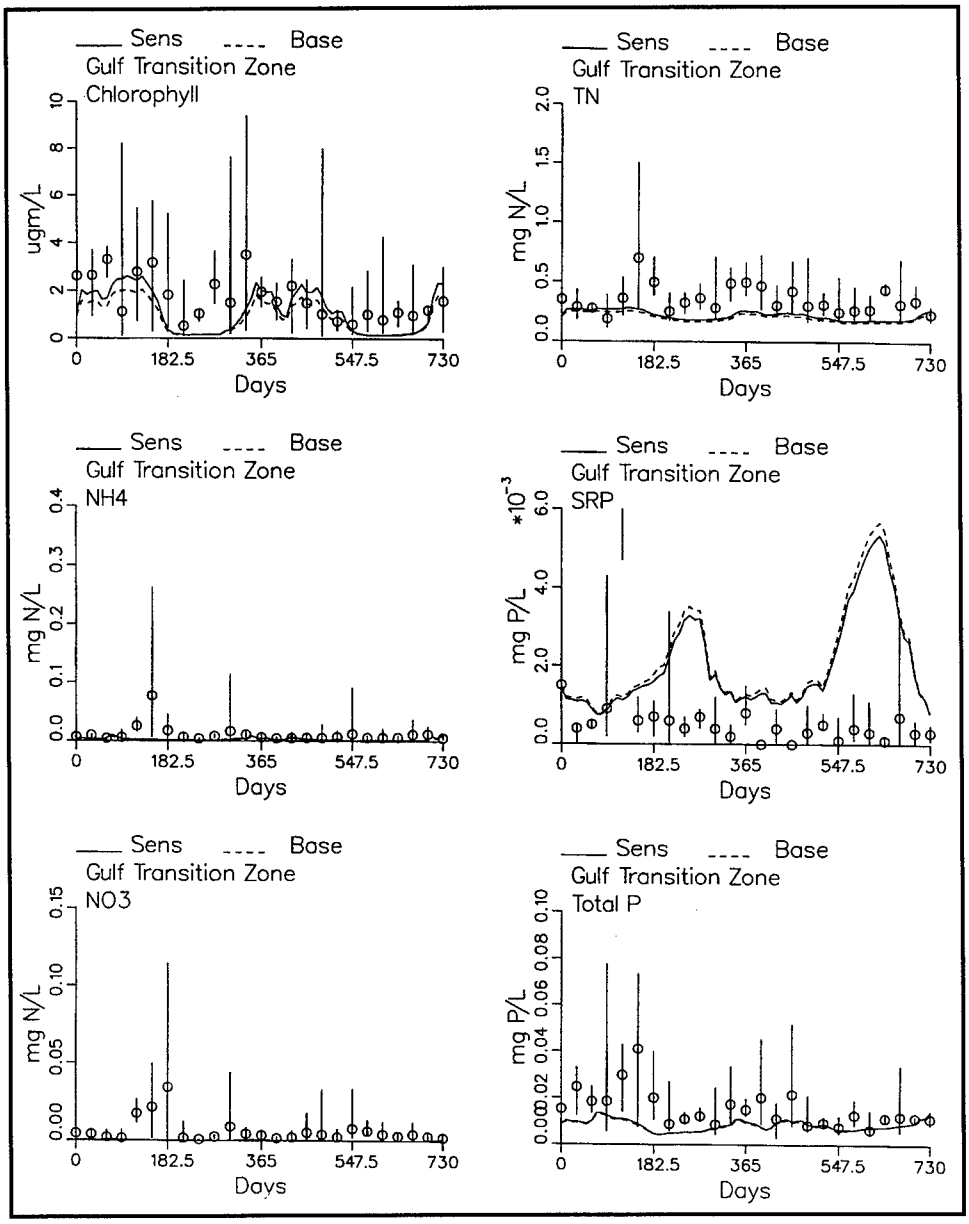

Figure 129. Effect of nitrogen fixation in SAV on waters in the Gulf Transition Zone

13 Ten-Year Water Quality Simulation

Introduction

In late 1987, portions of Florida Bay experienced a severe seagrass die-off (Roblee et al. 1991). Subsequent to the die-off, turbidity and phytoplankton abundance increased and other ecological indicators declined (Fourqurean and Roblee 1999). The succession of the die-off by alterations in multiple environmental factors suggests a cause and effect relationship but a direct linkage has not been established (Boyer, Fourqurean, and Jones 1999). Neither has the cause of the die-off been definitively determined.

One major objective of the model study was to simulate a ten-year period in Florida Bay, commencing with the seagrass die-off. The purposes of the simulation were to test the model's ability to simulate a wide range of environmental conditions and to provide insight into the processes that caused the environmental changes. The ten-year run encompassed the interval from January 1, 1988, to December 31, 1997.

Model Inputs

Initial conditions

Observations to initialize the model were not available. The initial conditions employed were the same as those used for the two-year calibration. These were obtained by running the model for an eight-year period, allowing the system to come into quasi-equilibrium with flows and loads.

Die-off zones (Figure 130) were indicated on the model grid.[1] For a period of ninety days, in these grid cells, seagrass production was eliminated, respiration was increased by an order of magnitude over normal values, and sloughing of above-ground biomass was instituted. These conditions caused seagrass to diminish to negligible abundance. At the end of the ninety-day period, production and respiration were returned to normal values and sloughing was eliminated.

Hydrodynamics

Plans called for the ten-year hydrodynamics to be pieced together from a sequence of seasonal hydrodynamic model runs. These runs were to include seasons of extremely low flow, to simulate the drought conditions in 1989-1990 (Figures 4, 5). Hydrodynamic simulations of the drought seasons were never satisfactorily completed. Consequently, the ten-year sequence was pieced together from available seasonal hydrodynamic simulations. These included the wet and dry seasons of 1996 and 1997, and the dry season of 1992. The simulated hydrodynamics were based on freshwater flows substantially higher than the estimated flows in 1989 and 1990, especially during the anomalous wet seasons of those years (Figure 131). Simulations during the seasons of greatest flow (e.g. the wet season of 1995) were based on runoff less than estimated, although the consequences of these discrepancies are likely not as great as the discrepancies during the low-flow periods.

In determining the hydrodynamic sequencing, attention was paid to matching wet seasons with wet seasons and dry seasons with dry seasons. In retrospect, a superior matching of runoff could have been achieved by matching flows, regardless of season (e.g. the dry season of 1997 is a good match for the wet season of 1989; Figure 131). Matching runoff, regardless of season, would have resulted in mismatching other influences such as prevailing winds, however. Ultimately, no substitute exists for the employment of appropriate hydrodynamics.

Loads

Nutrient load estimates were input monthly, based on the Walker estimates (Chapter 3). The actual ten-year sequence of loads was employed. No substitutions were made.

---

1 Personal Communication, February 2000, Dr. Michael Roblee, United States Geological Survey.

Boundary conditions

Observations sufficient to set concentration boundary conditions at the edges of the model domain were available for 1995-1997 from the FIU data set. For earlier years, boundary conditions were based on three-month averages of the 1995-1997 data.

Water Quality Model Results

The observed seagrass die-off was concentrated in three areas: Rankin Key, Johnson Key, and Rabbit Key (Figure 130). These areas are located within the Central Zone and at the junctures of the Central and Western Zones and the Central and Atlantic Transition Zones (Figure 57). Examination of model results in these three zones (Figures 132-134) indicates, first, that observed concentrations of numerous substances are higher in the early years of the simulation than in later years. The second dominating feature is that the wide range of observed conditions is not captured by the model.

Observed salinities in all three zones indicate the occurrence of hyper-saline conditions. Hyper-salinity results from a local excess of evaporation over precipitation and is especially severe in the Central Zone from 1989 through 1994 (Figure 132). The hyper-saline conditions are not captured by the model. The temptation to ascribe the low computed salinities to the excess runoff input in 1989 and 1990 is irresistible. Certainly the excess runoff is a contributing factor, but likely not the only influence. Our attention focuses, rather, on two issues. The first is the overall accuracy of the hydrodynamic model. The second is the influence of the overlay grid employed in the water quality model. To our knowledge, the ability of the hydrodynamic model to compute salinity, especially hyper-salinity, in Florida Bay has not been fully demonstrated. To compound the problem, the hydrodynamic grid was overlain with a coarser water quality grid. We suspect cells in the overlay grid span mud banks and other features that restrict flow. Overlay of flow-restricting features creates artificial transport across these features and prevents concentration buildup via an excess of evaporation over precipitation. In addition, the larger overlay cells increase numerical diffusion which also diminishes concentration gradients.

Observations in the Central and Atlantic Transition Zones exhibit elevated concentrations of inorganic nutrients (ammonium, nitrate, and soluble reactive phosphorus) in the early years of the simulation. These elevated concentrations are likely the result of the same process that produced hyper-salinity: excess of evaporation over precipitation in basins with restricted circulation. Remedying the computed shortfalls requires detailed modeling of actual hydrodynamics on a highly resolved grid.

Within the Central Zone and elsewhere, model computations of total nitrogen are less than observed. Three factors may contribute to the shortfall. The first is the inability of the model to concentrate material, as demonstrated for salt. The second is, potentially, an underestimation of nitrogen loading to the system. Sensitivity analyses demonstrated, however, that major revisions to the loads are required to make up the total nitrogen deficit. The third factor is the model treatment of dissolved organic nitrogen. Within the model, all dissolved organic nitrogen is reactive and subject to ammonification. The ammonium is subject to subsequent uptake and removal from the water column by seagrass, phytoplankton, and benthic algae. In reality, a substantial portion of the dissolved organic nitrogen input to the bay, from the Everglades and at the boundaries, is refractory in nature and not biologically available. Correct representation of total nitrogen requires addition of a refractory dissolved organic nitrogen state variable.

Correct representation of the wide range of conditions observed over a decade should be demonstrated before the model is employed to predict the range of conditions that will result from flow diversions and other anthropogenic alterations to the system. Correct representation is impossible with the current hydrodynamic model and overlay grid. A much more comprehensive long-term hydrodynamic simulation on a fine grid with detailed representations of wind, flow, and other forcing factors is required for further progress in modeling Florida Bay.

Seagrass Model Results

Two ten-year simulations were conducted to examine the seagrass model. In one simulation, a die-off was imposed, as described previously. In a second run, no die-off was imposed. This second run represented a continuation of the equilibrium conditions that prevailed at initiation of the model. Results of these two runs (Figures 135-137) were examined only in the model cells in which die-off was imposed.

At Rankin Key, the dominant computed equilibrium seagrass was *Thalassia* with minor stands of *Halodule* and *Syringodium* (Figure 135). Following the die-off, *Halodule* was computed to become the dominant and virtually exclusive seagrass species. At Johnson and Rabbit Keys, *Thalassia* was the dominant computed equilibrium seagrass with no *Halodule* present (Figures 136, 137). After the die-off, *Halodule* was computed to be the exclusive seagrass present.

The appearance of *Halodule* as the first seagrass following the die-off is consistent with a conceptual model of seagrass succession. *Halodule* is viewed as an early colonizer of disturbed areas (Zieman 1982). *Halodule* has an advantage in this regard due to its relatively high growth rate and low light requirement (Fourqurean 1992). *Halodule* is a poor competitor with *Thalassia* for sediment phosphorus, however. Consequently, over

time, Halodule is replaced by *Thalassia* in stable environments in which light availability is sufficient for *Thalassia* growth.

According to this conceptual model, computed *Thalassia* should have recovered its dominance in the die-off locations. This recovery did not occur within the ten-year simulation although computed *Halodule* did decline during the last five years of the simulation. Perhaps, if the model run were longer, *Thalassia* would have become dominant. Alternatively, some environmental factor required for re-establishment of *Thalassia* may be missing from the simulation.

Computed properties in the water column show little difference with and without the seagrass die-off (Figures 135-137). In particular, computed solids, light attenuation, and chlorophyll are virtually identical in the two simulations. One hypothesis for the observed diminished water quality following the die-off calls for resuspended sediment in the die-off zones to increase light attenuation, thereby shading out the recovery of seagrass. Nutrients no longer taken up by seagrass become available to phytoplankton, resulting in algal blooms. This succession of events does not occur in the model. The likely cause for lack of difference in the two simulations is the rapid recovery of *Halodule* following the die-off. We cannot state conclusively whether the model should be revised to reflect the hypothetical succession of events or if the model indicates the hypothesis is not a good one.

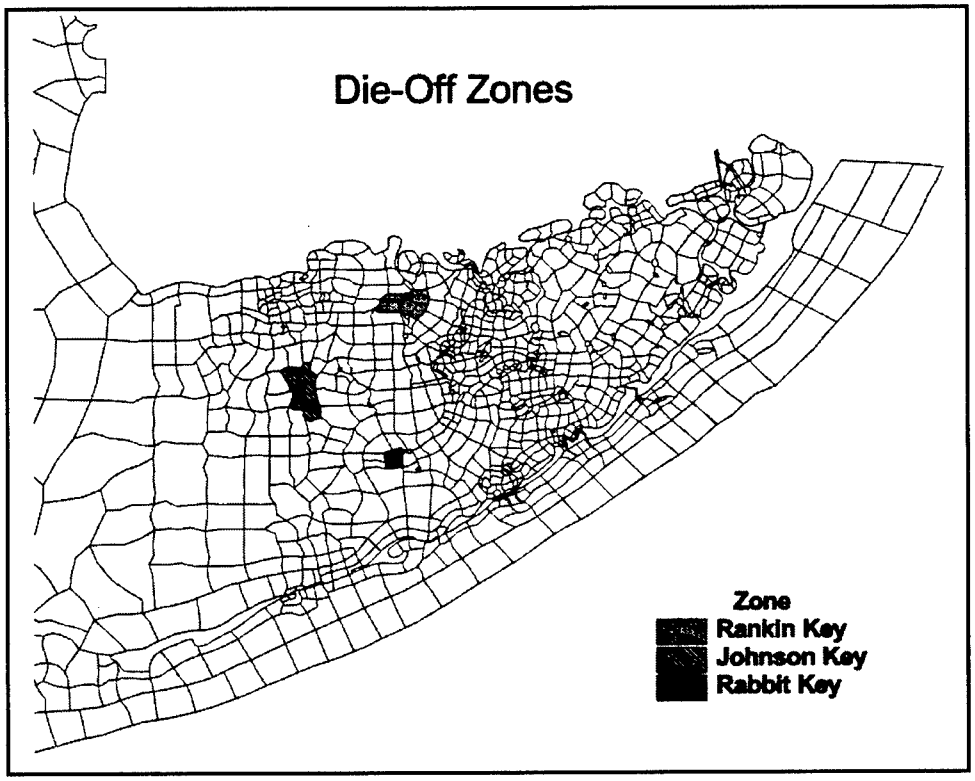

Figure 130. Seagrass die-off locations

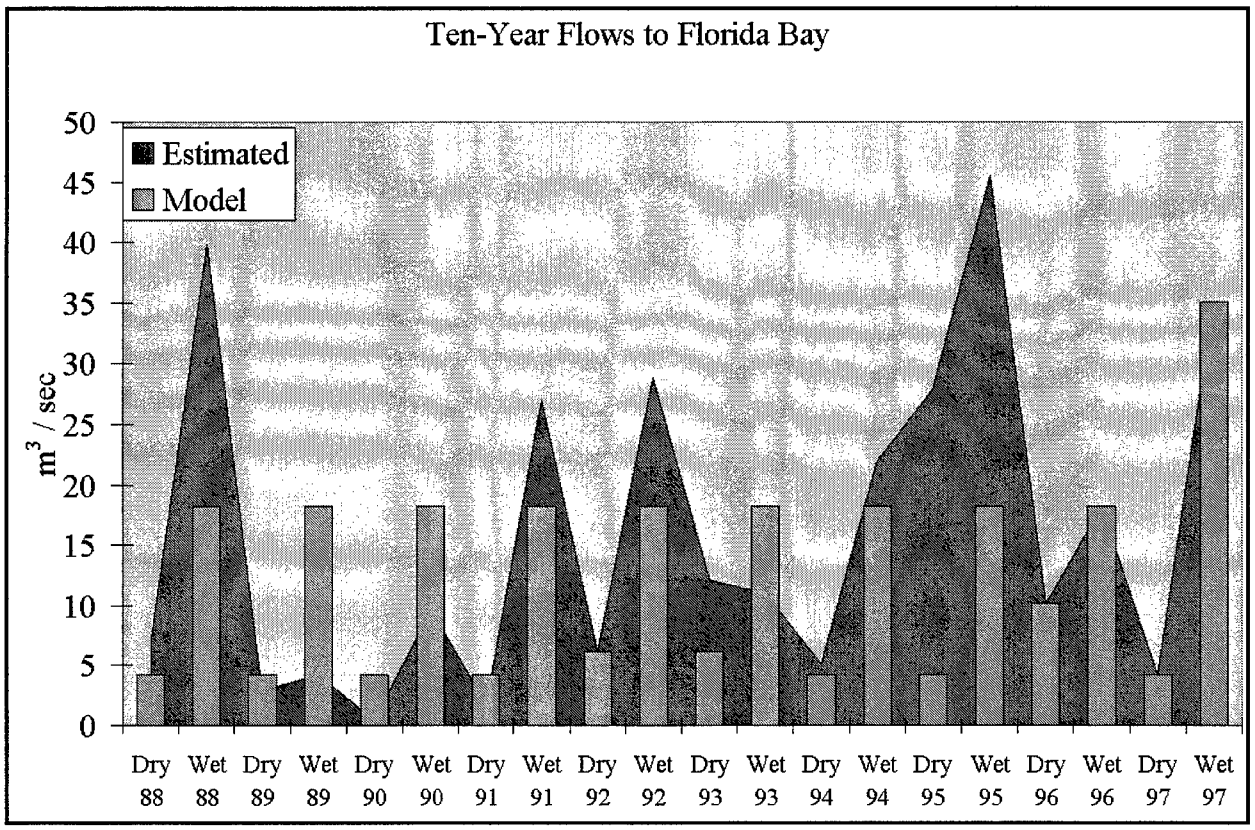

Figure 131. Estimated and modeled runoff to Florida Bay, 1988-1997

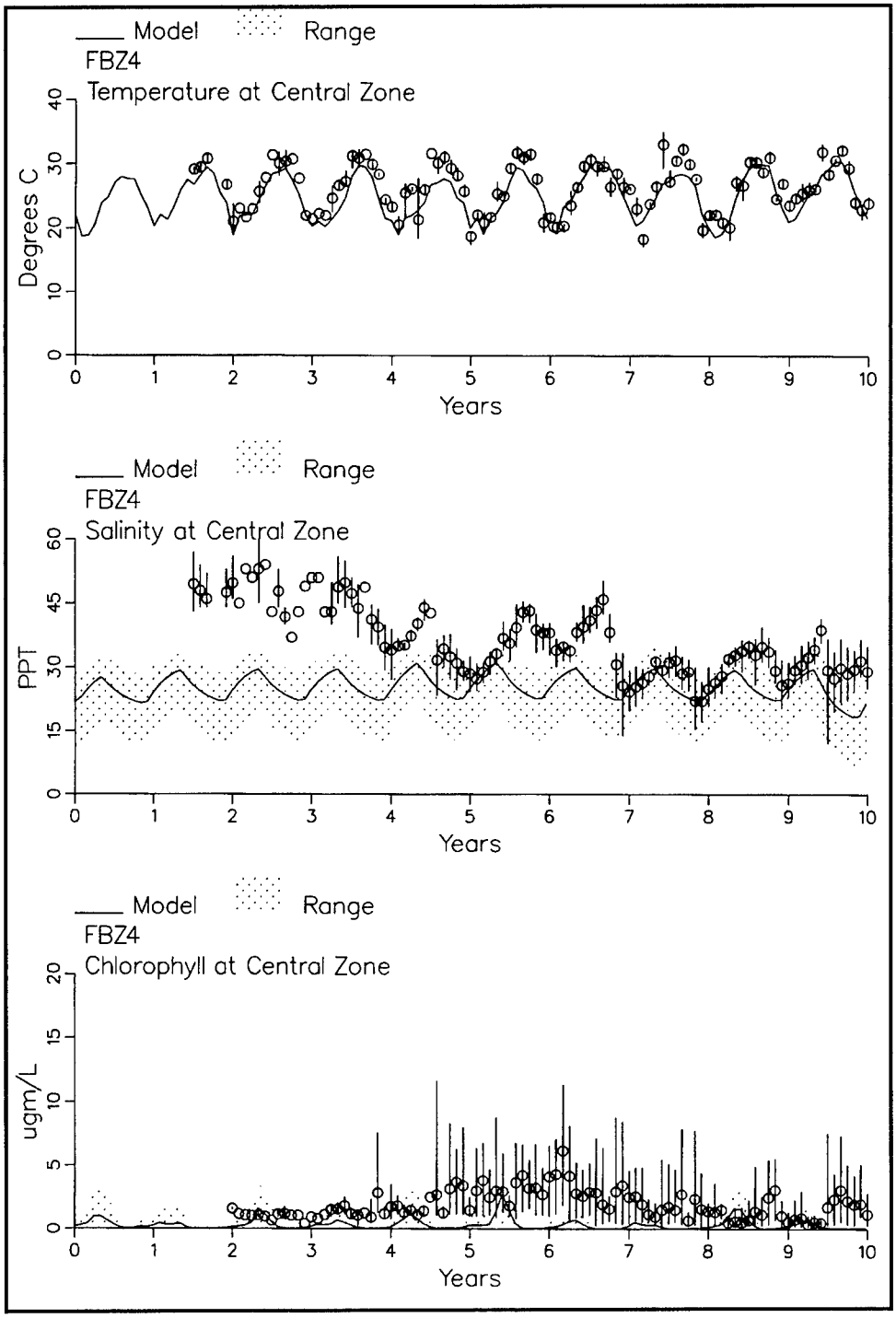

Figure 132. Observed and computed water quality in the Central Zone, 1988 (Year 0.0) to 1997 (Year 10.0) (sheet 1 of 4)

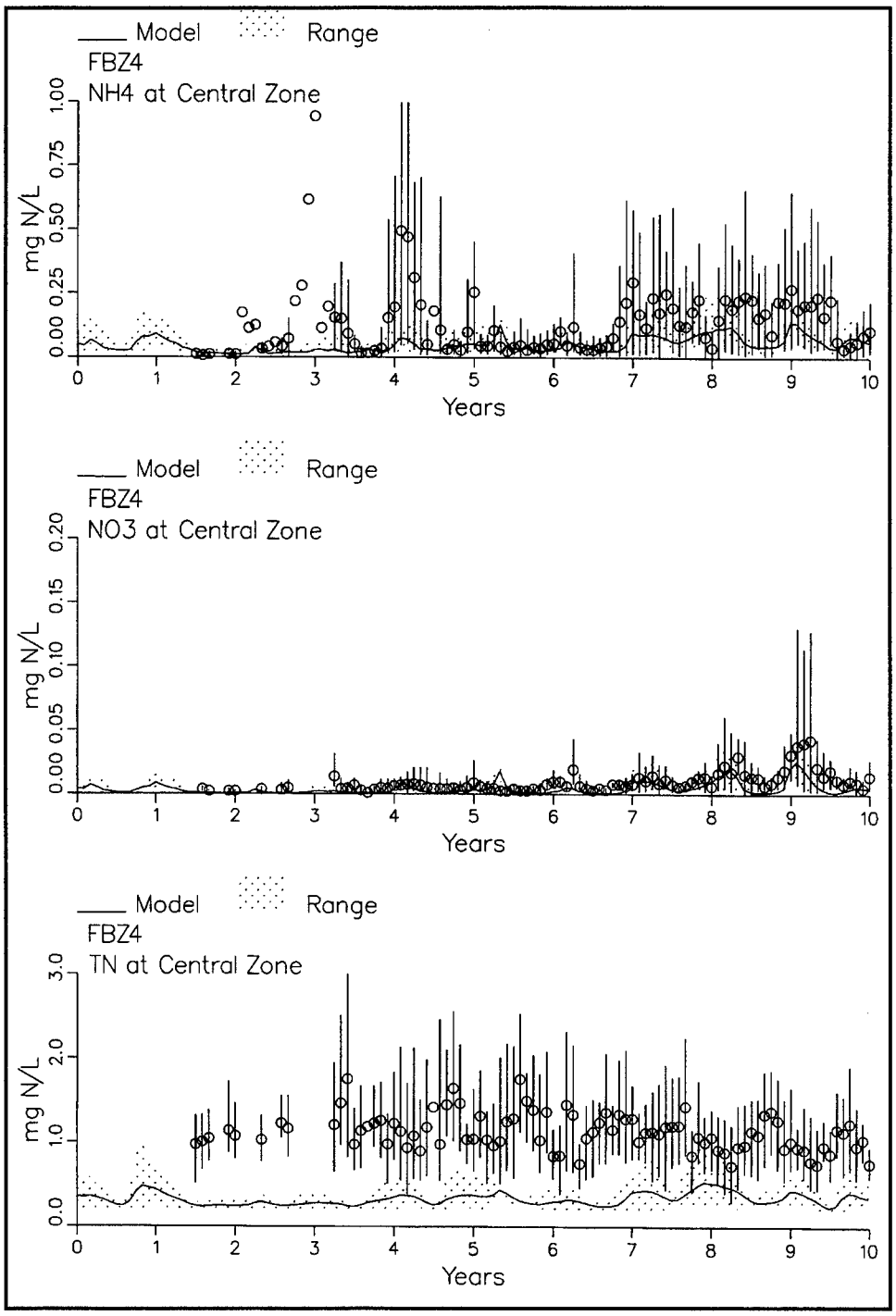

Figure 132. (sheet 2 of 4)

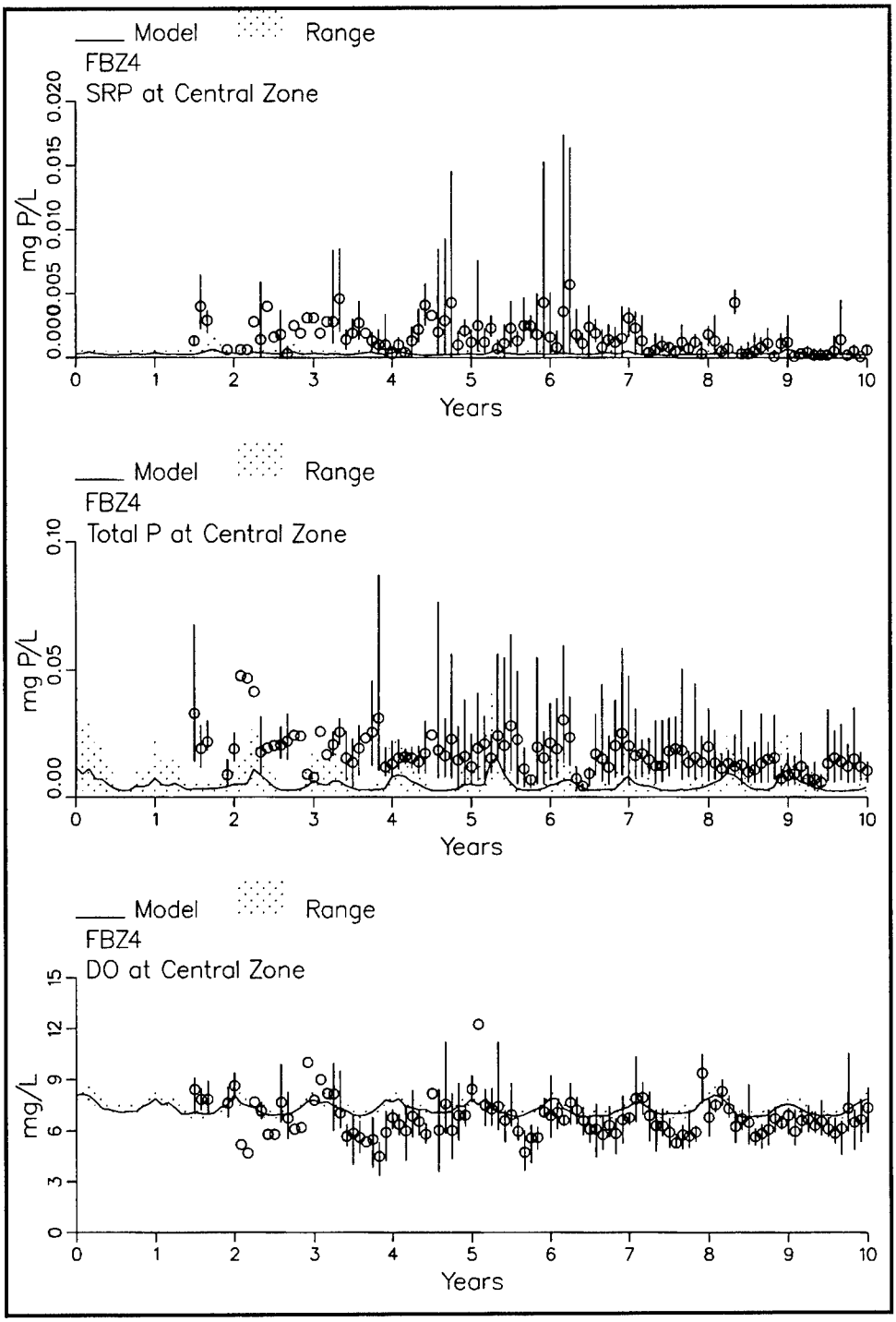

Figure 132. (sheet 3 of 4)

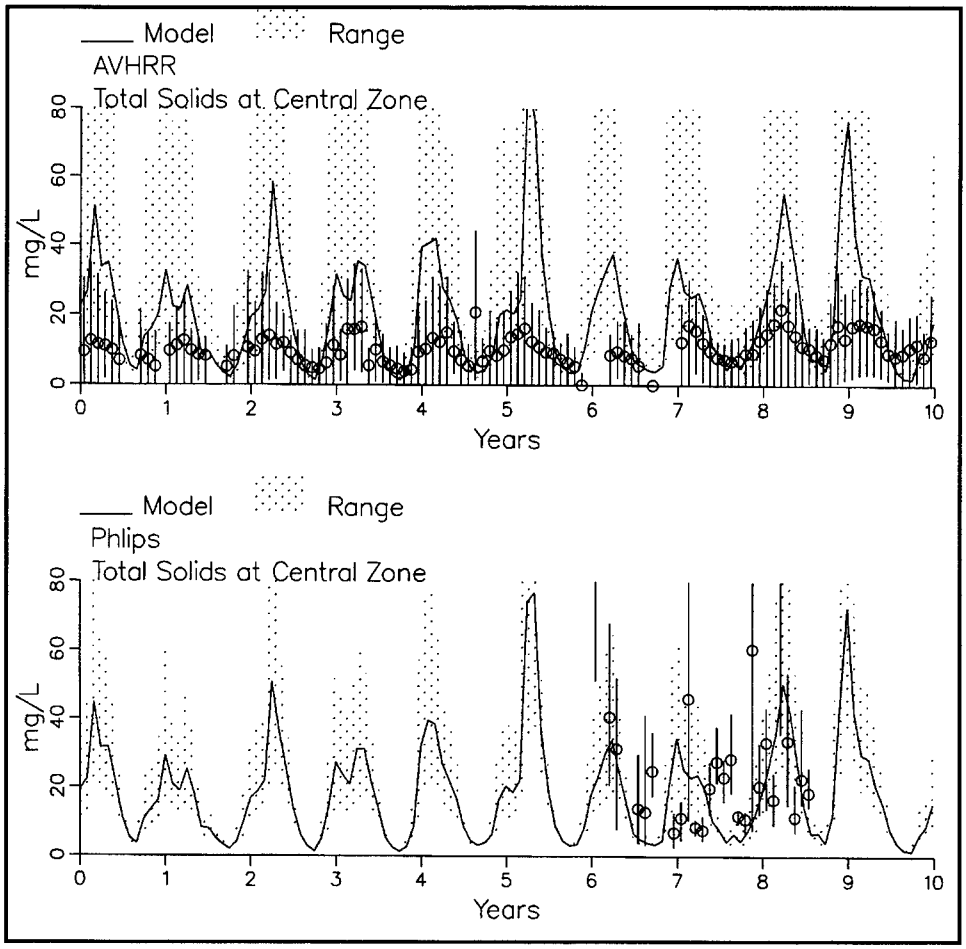

Figure 132. (sheet 4 of 4)

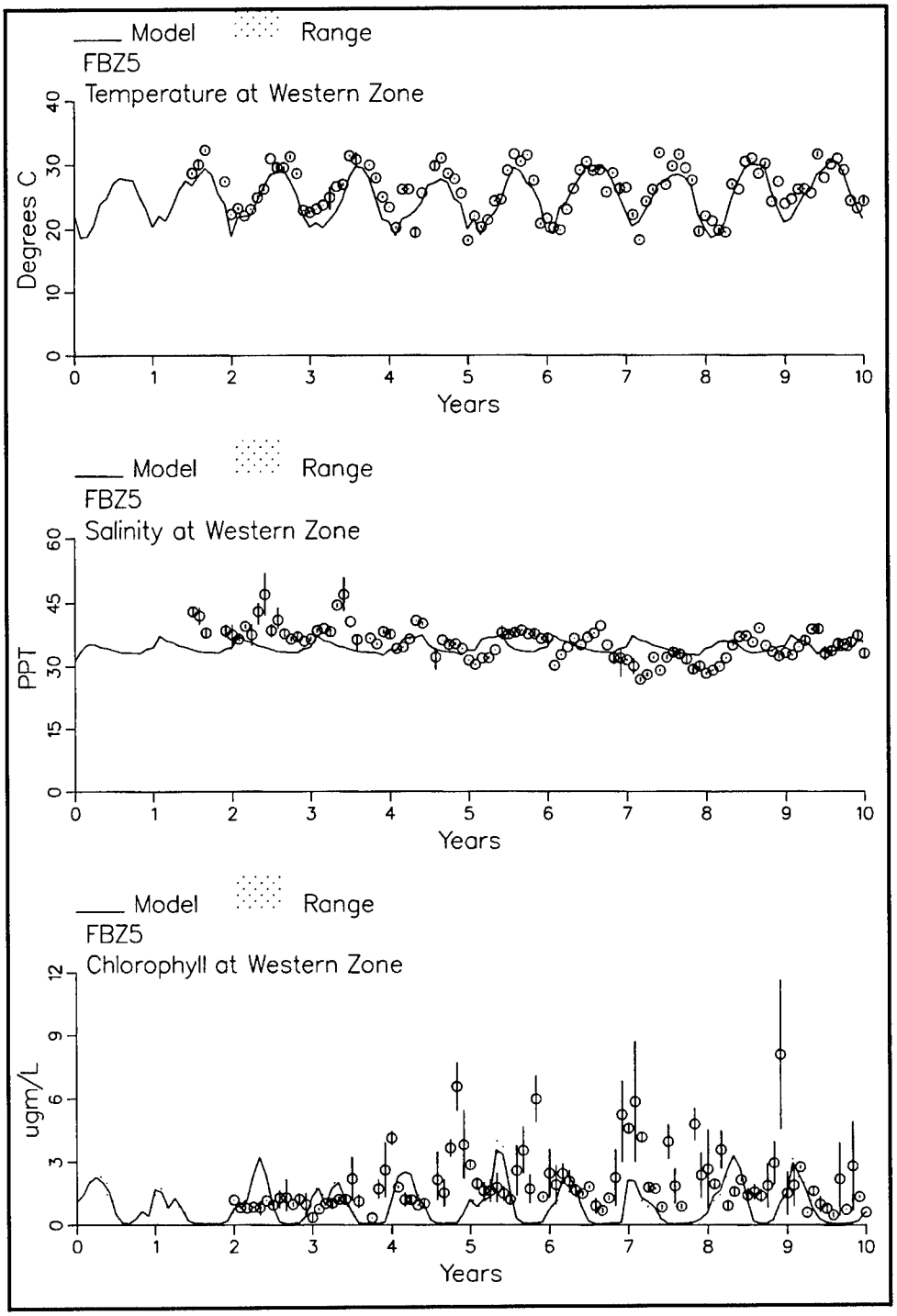

Figure 133. Observed and computed water quality in the Western Zone, 1988 (Year 0.0) to 1997 (Year 10.0) (sheet 1 of 4)

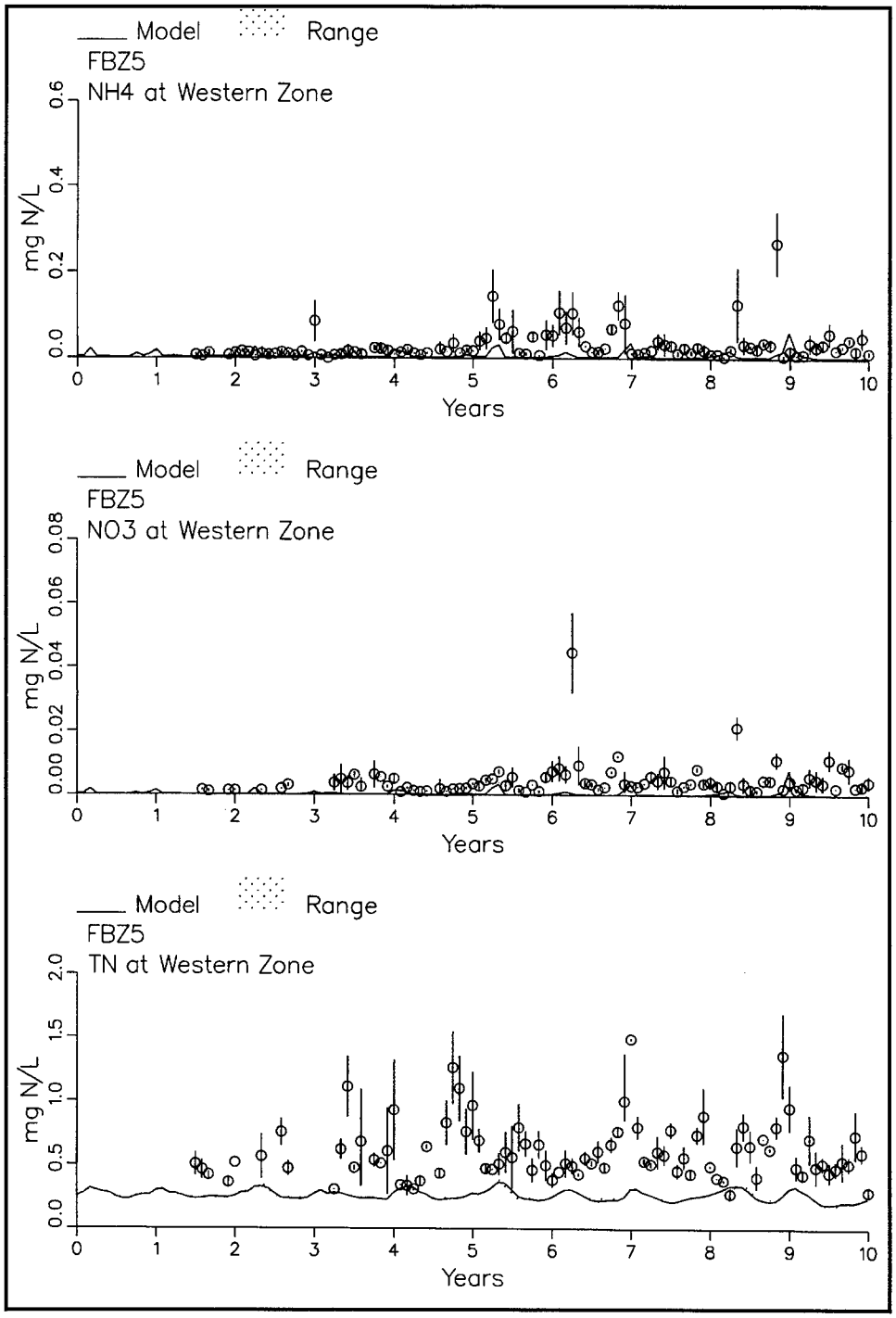

Figure 133. (sheet 2 of 4)

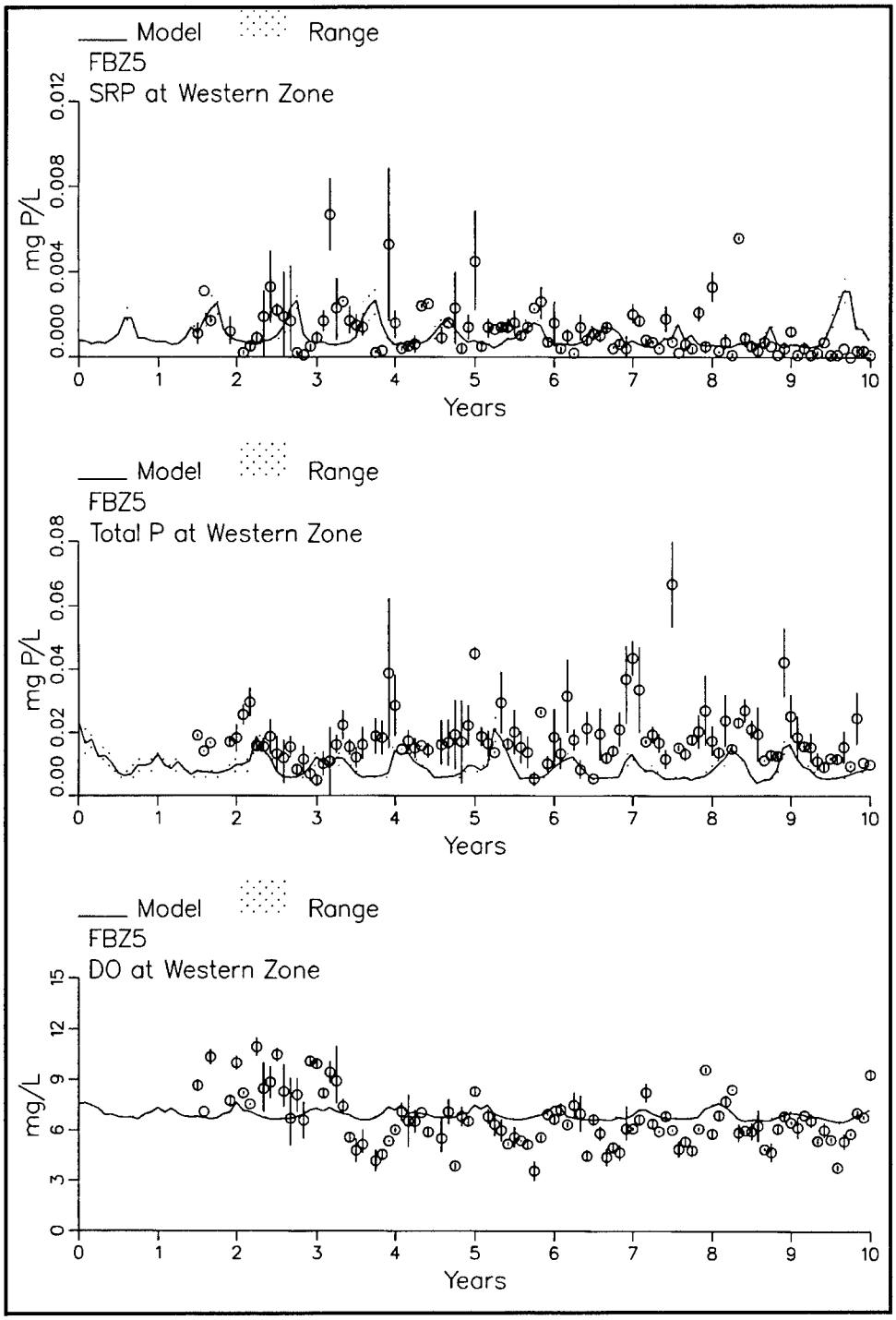

Figure 133. (sheet 3 of 4)

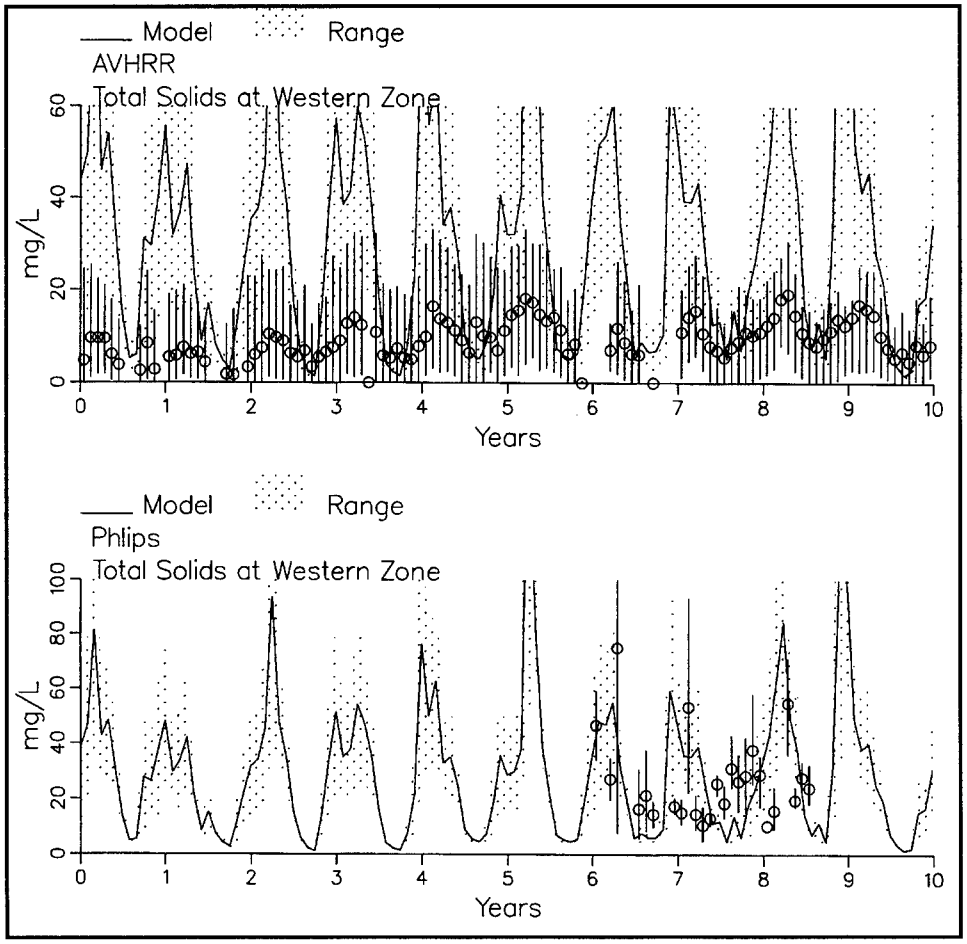

Figure 133. (sheet 4 of 4)

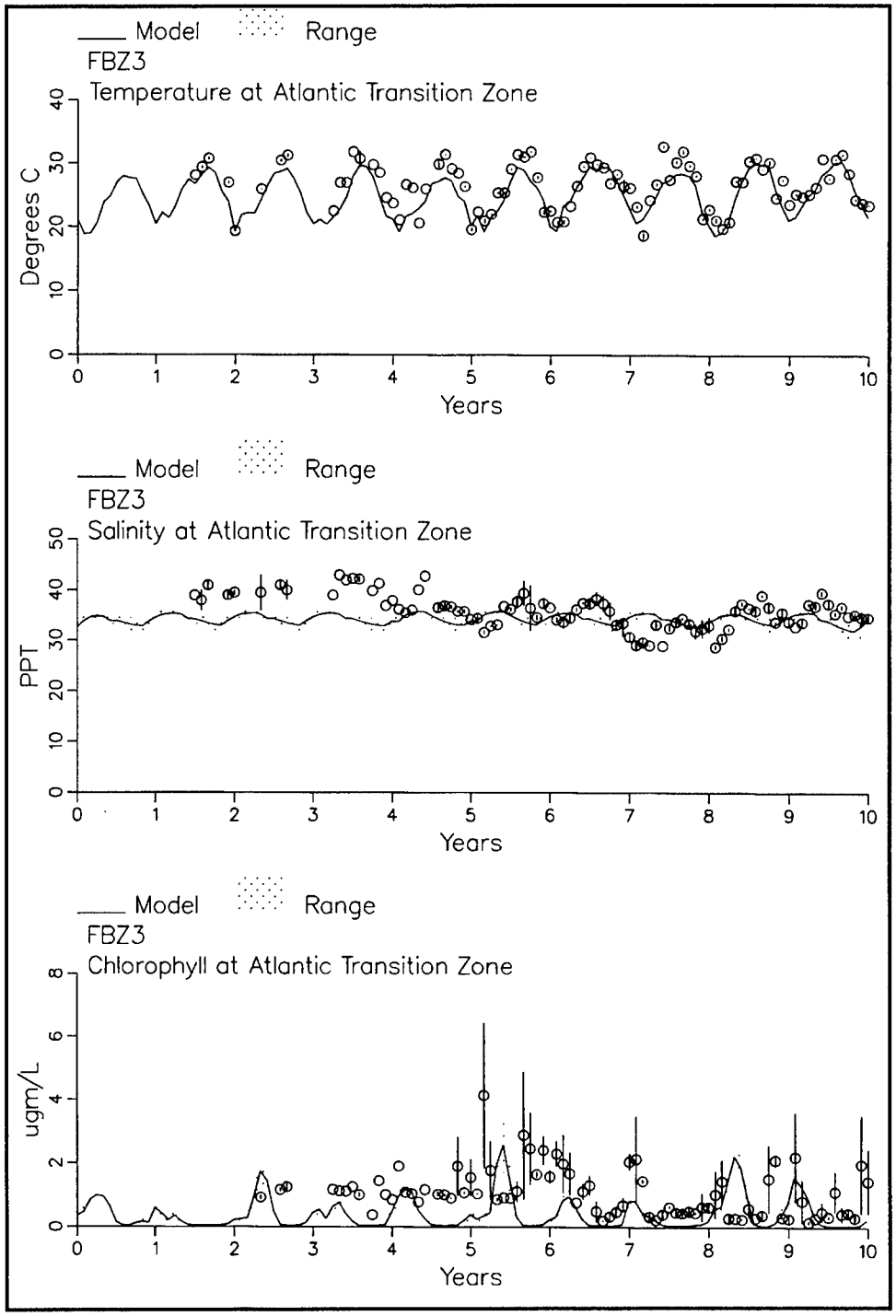

Figure 134. Observed and computed water quality in the Atlantic Transition Zone, 1988 (Year 0.0) to 1997 (Year 10.0) (sheet 1 of 4)

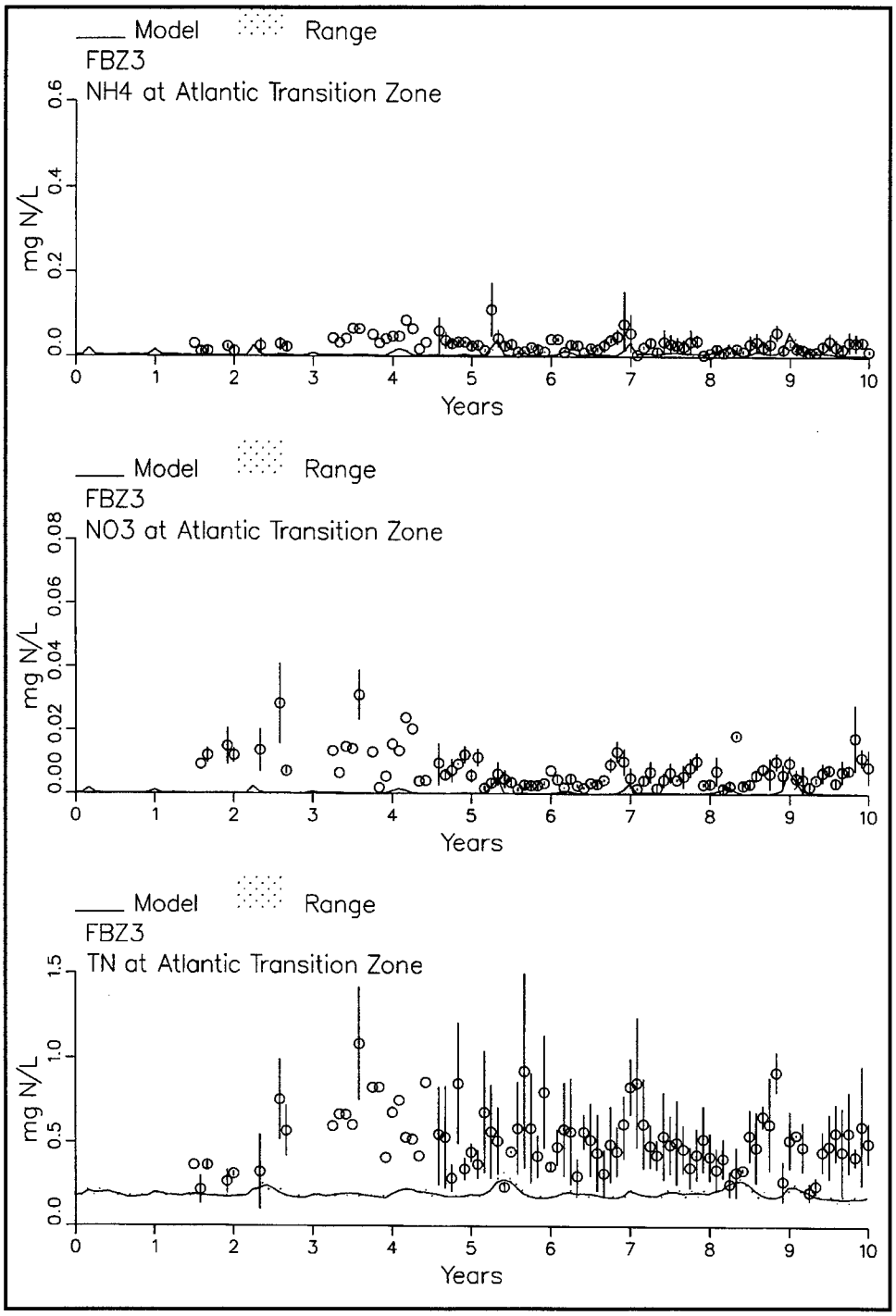

Figure 134. (sheet 2 of 4)

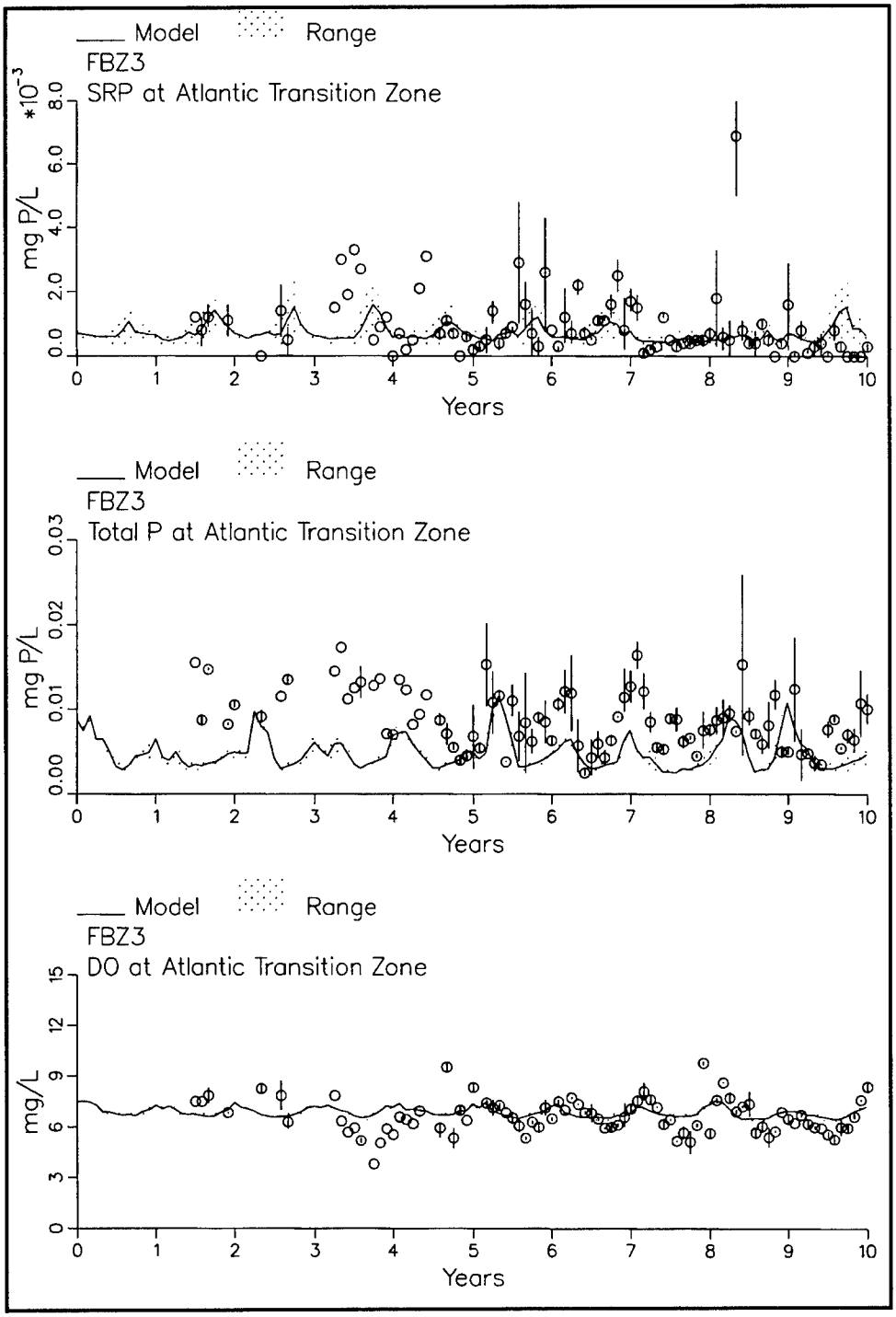

Figure 134. (sheet 3 of 4)

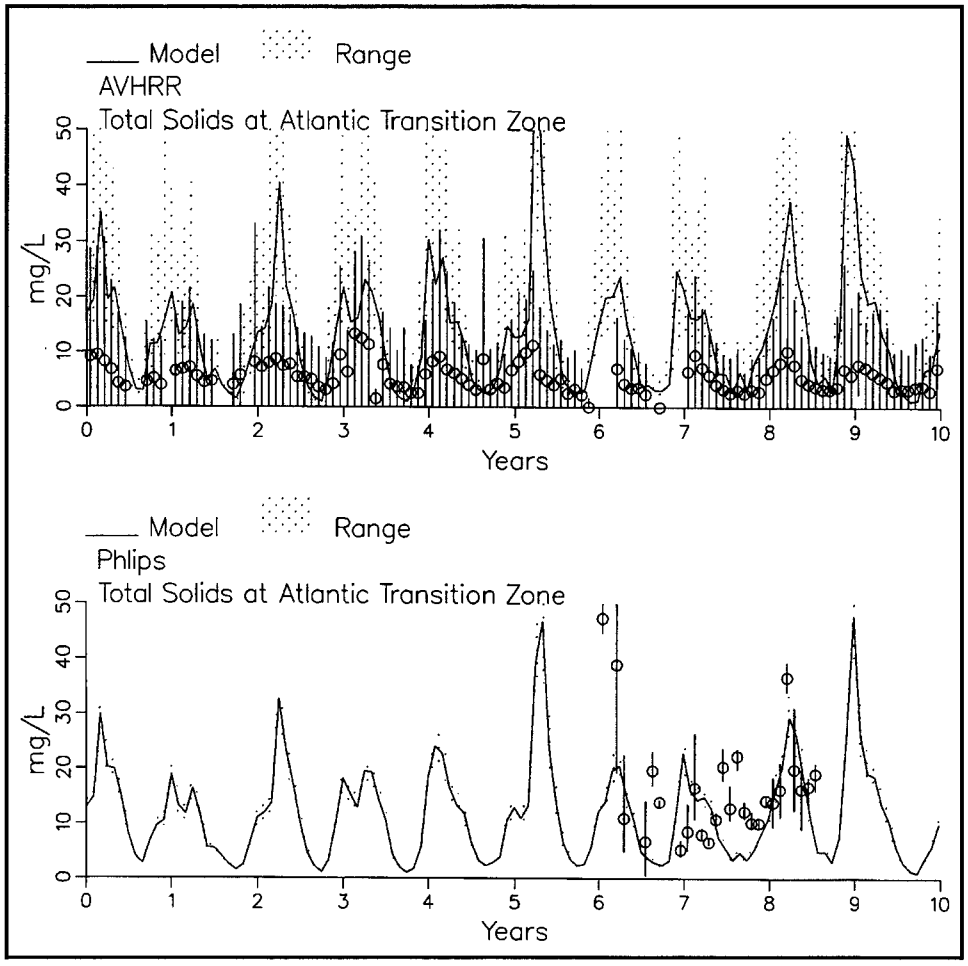

Figure 134. (sheet 4 of 4)

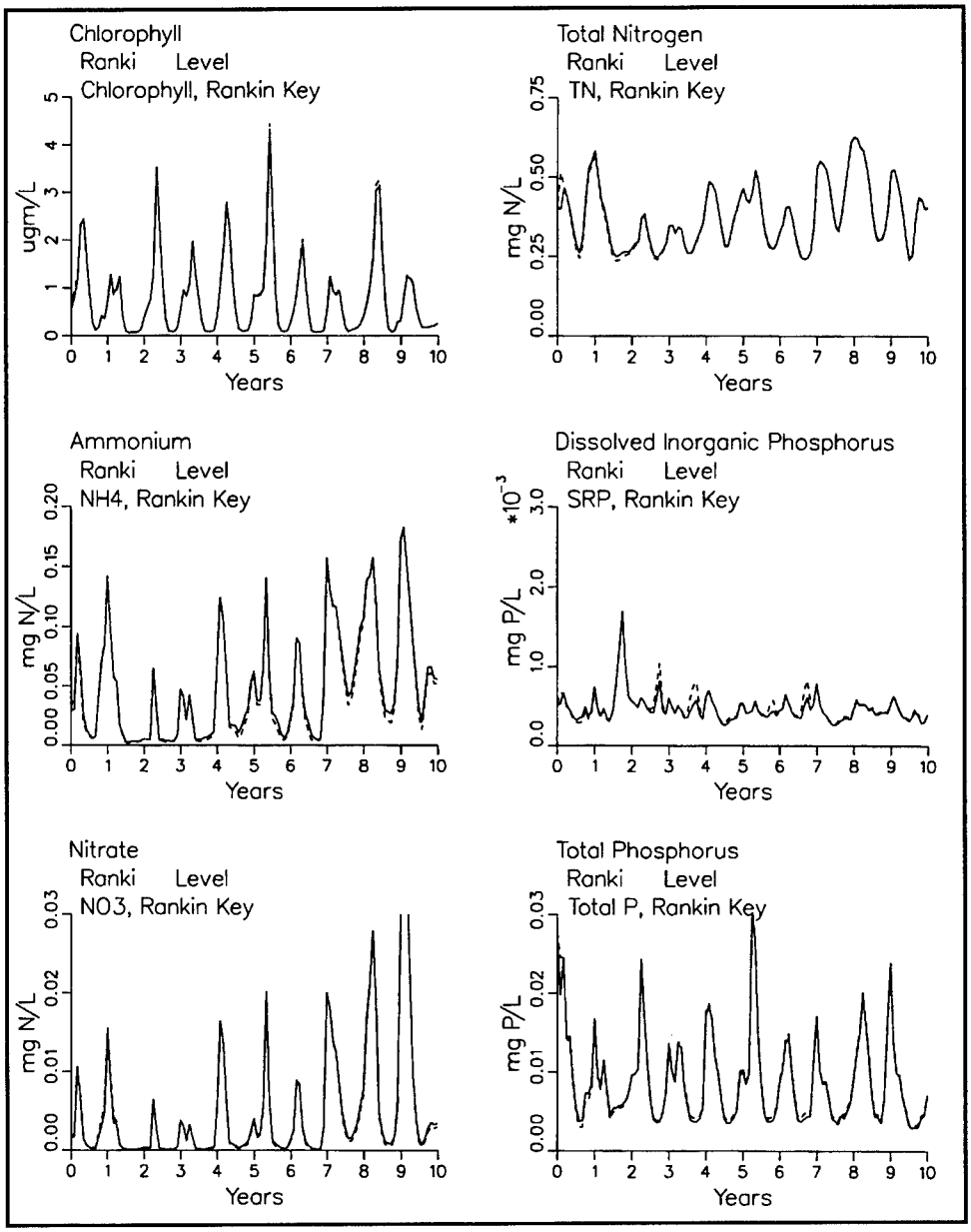

Figure 135. Ten-year model simulations at Rankin Key with seagrass die-off (dashed line) and without die-off (solid line) (continued)

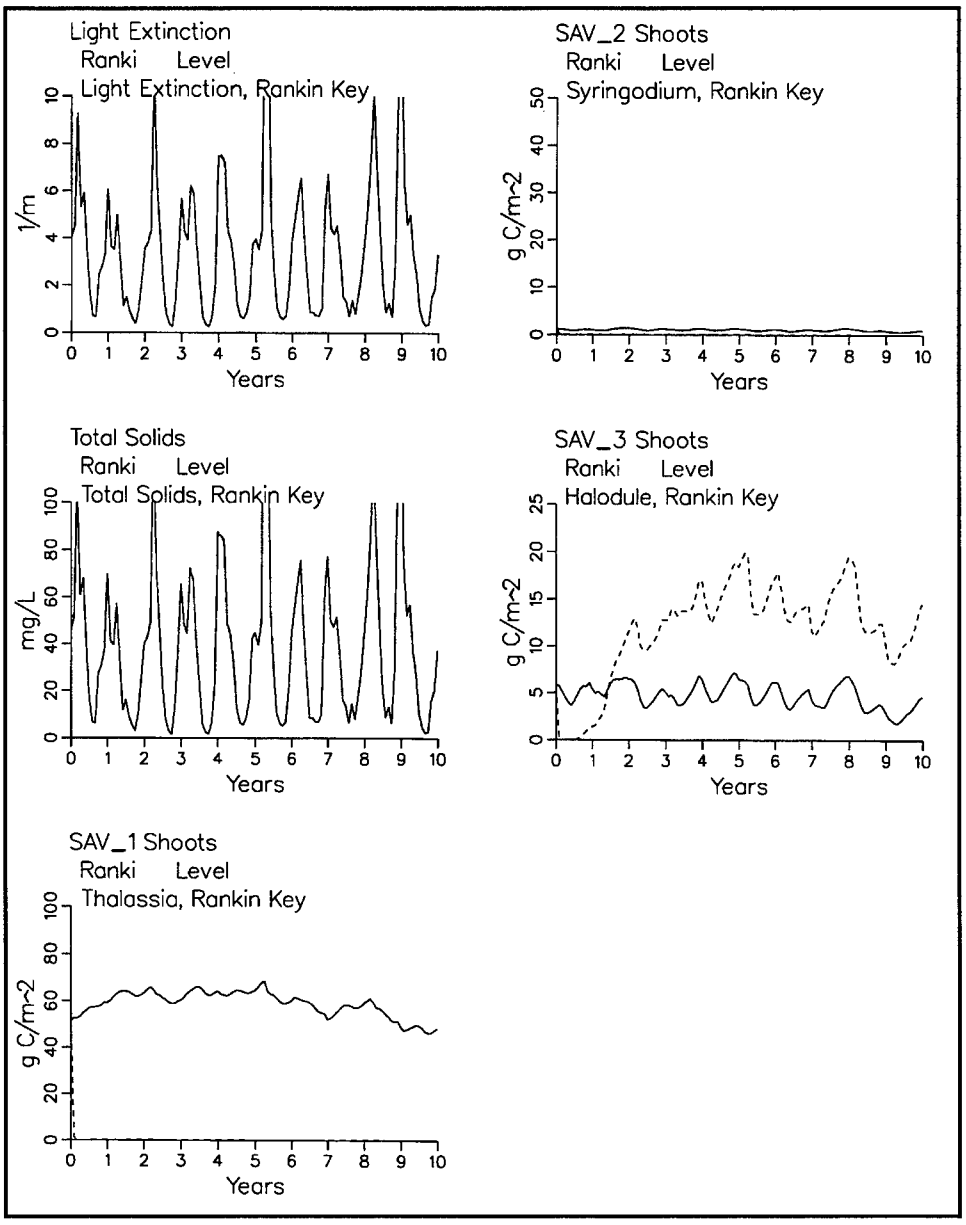

Figure 135. (concluded)

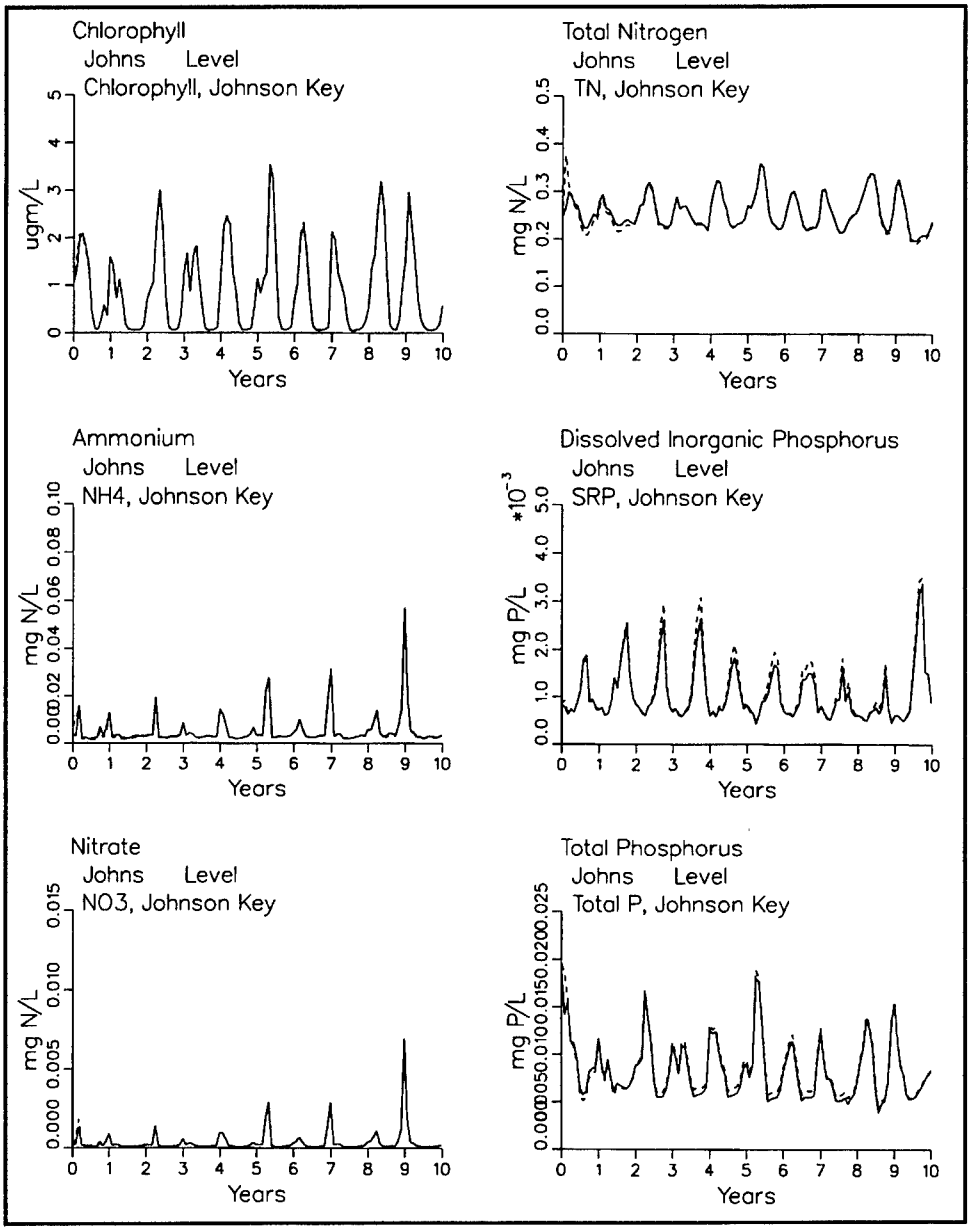

Figure 136. Ten-year model simulations at Johnson Key with seagrass die-off (dashed line) and without die-off (solid line) (continued)

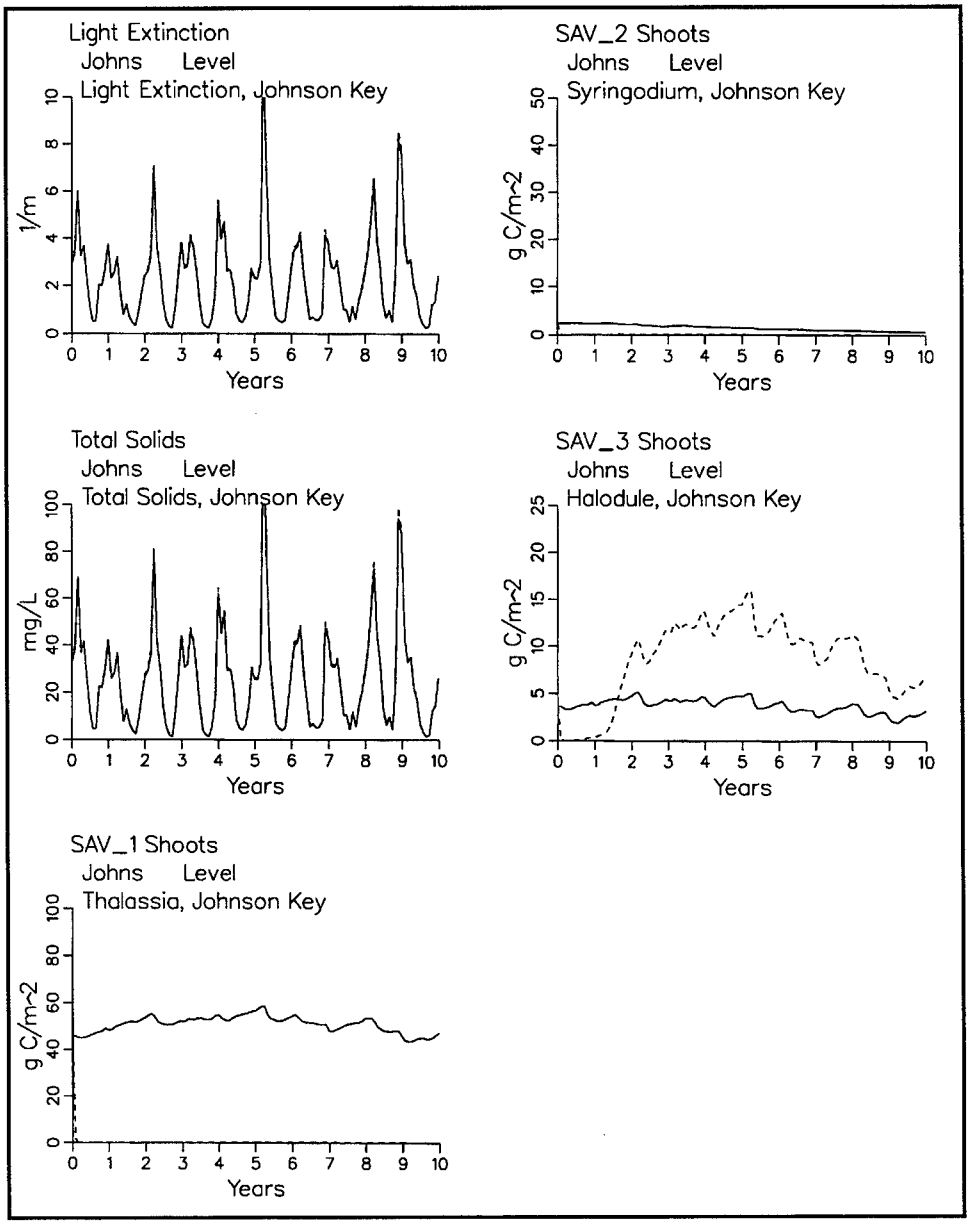

Figure 136. (concluded)

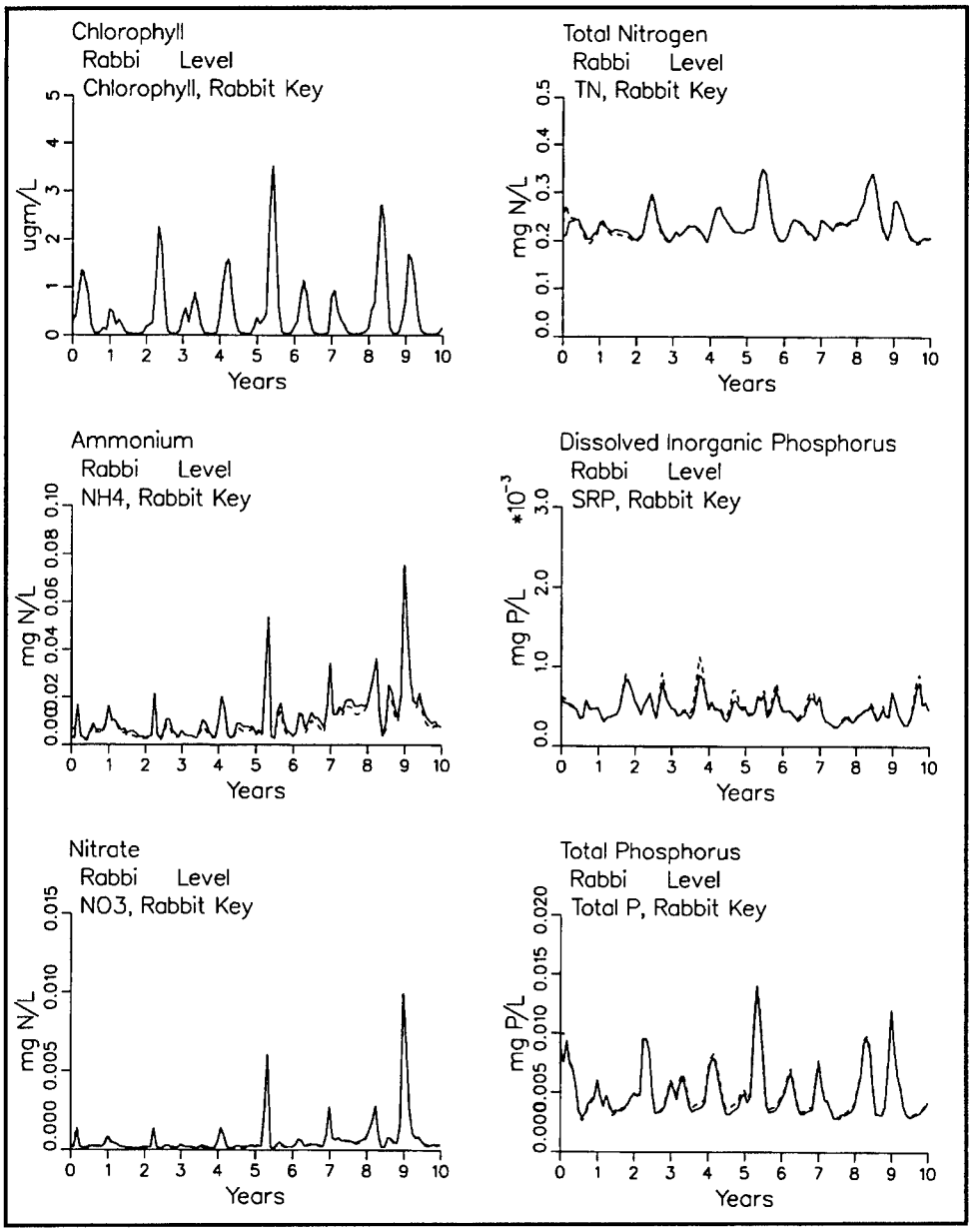

Figure 137. Ten-year model simulations at Rabbit Key with seagrass die-off (dashed line) and without die-off (solid line) (continued)

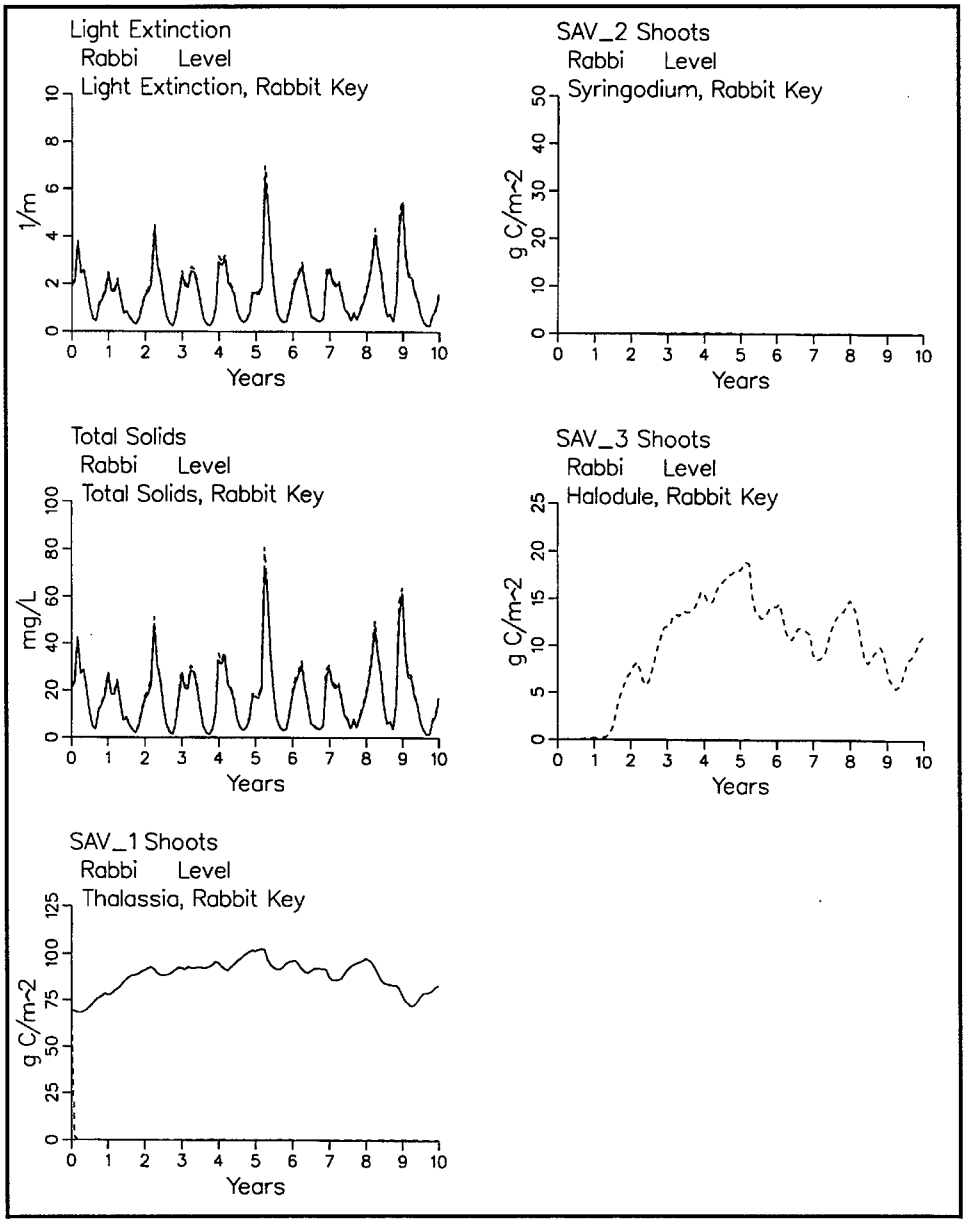

Figure 137. (concluded)

14 Flow and Nutrient Budgets

Florida Bay Net Flows

Net flows in Florida Bay were calculated for the wet and dry seasons of 1997. Rainfall (Figure 10) and runoff (Figure 12) for these seasons were reasonably close to ten-year mean values. Flows were calculated for the basins employed in time series analysis of the calibration (Figure 57). Only Florida Bay was considered, not the entire model domain.

Net flows were obtained from the 29-day hydrodynamics files that represented average conditions in each season. First, arithmetic (Eulerian) mean flows were computed at each interface between model cells. Next these flows were summed for all interfaces along boundaries between basins.

During the dry season (Figure 138), major flows were into the system through a passage in the upper Keys and out of the system in a westerly

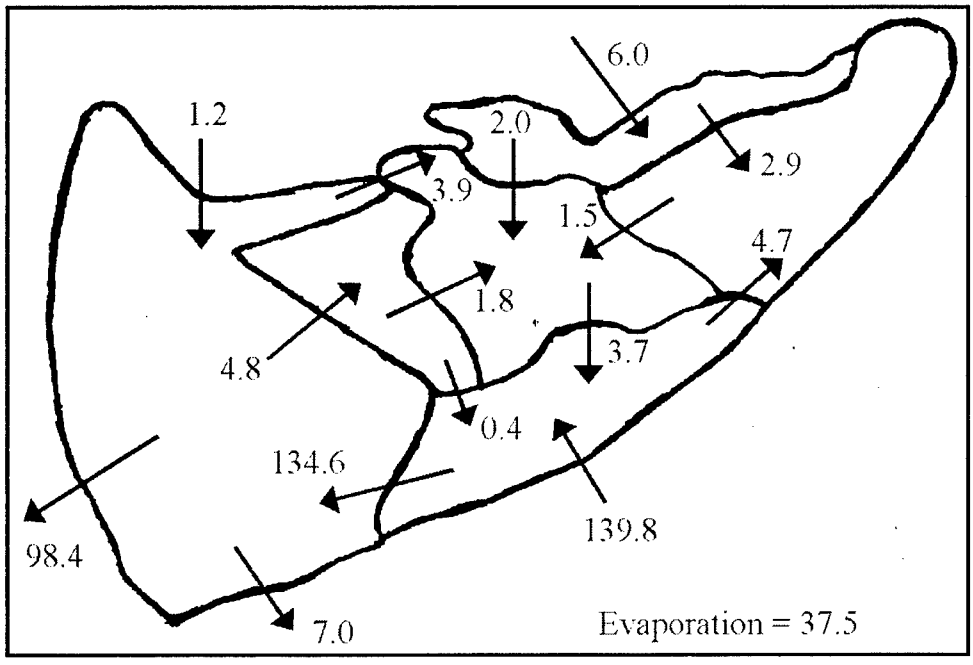

Figure 138. Net flows ($m^3 s^{-1}$) during 1997 dry season

direction onto the Western Shelf. In the interior of the bay, net flows between basins were two orders of magnitude smaller than this major circulation. Net flows suggest a small flow in an easterly direction along Cape Sable. This flow is reversed near the apex of the bay and joins the westerly circulation onto the Western Shelf.

During the wet season (Figure 139), major flows in the system are eastward, in from the Western Shelf, and out through a lower passage in the Keys. Flows between basins in the interior of the bay are an order of magnitude smaller than the major circulation from the west through the Keys passage. A small eastward flow persists along Cape Sable but the general flow in the interior is from Taylor Slough south and west, then out through the Keys.

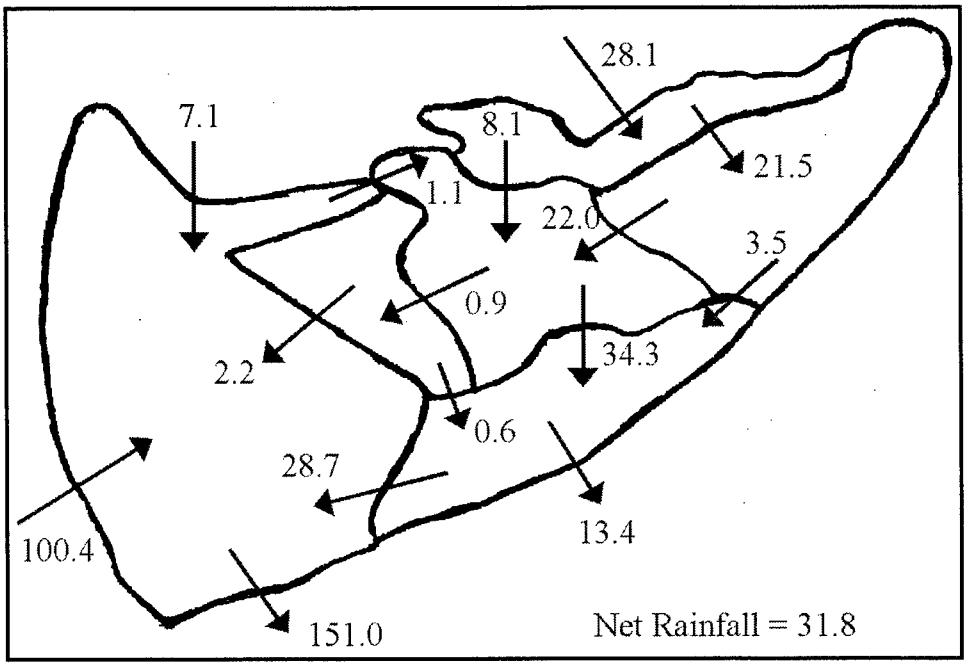

Figure 139. Net flows ($m^3 s^{-1}$) during 1997 wet season

Rudnick et al. (1999) analyzed current-meter measurements and concluded annual mean flow is into the bay in the northern and central portions of the boundary between the bay and the Western Shelf. They concluded annual mean flow is out of the bay at the southern end of the boundary. Net annual flow, derived from their estimates, is 722 $m^3 s^{-1}$ into the bay along the western boundary.

We did not analyze flows in sufficient detail to differentiate flows across the northern, central, and southern portions of the western boundary. Net flow across the entire boundary is into the bay during the wet season and out of the bay during the dry season. Seasonal flows are roughly equivalent in magnitude, 100 $m^3 s^{-1}$, but in opposite directions, so that annual net flow between the bay and the Western Shelf is negligible. We cannot account for the difference in the estimates from current meters and

model except to note that only three current meters were deployed and extrapolation from three points to the entire boundary must entail a lot of uncertainty.

Florida Bay Nutrient Budget

Loads

Loads to the system were presented in Chapter 3. A nutrient budget for Florida Bay was completed by computing nutrient transport across the western and southern boundaries. Total nitrogen and total phosphorus transport across the boundaries were computed for the wet and dry seasons of 1997. At each model time step, the product of concentration and flow was computed at cell interfaces along the boundary. This product was averaged into seasonal values at each interface and then summed for all interfaces along basin boundaries.

Rudnick et al. (1999) completed an annual nutrient budget for Florida Bay. Their analysis was adapted for comparison with the model. Adaptations included units conversion and summary of net transport across the western boundary.

Comparison of the published and present budgets (Table 26) indicates that estimated loadings from the Everglades and atmosphere are in reasonable agreement. A factor of two differentiates loadings from the Keys. Estimates of Keys loadings are affected by numerous assumptions regarding sources, destination, and attenuation. One major difference between the two estimates is that Walker assumed 50% load attenuation between source and receiving water while Rudnick et al. (1999) did not. Correction for the assumed attenuation provides reasonable agreement between the published loads and the loads used in this study.

Table 26
Florida Bay Nutrient Budgets (positive into system)

	Rudnick et al.		Model Dry Season		Model Wet Season	
	Total Phosphorus ($kg\ d^{-1}$)	Total Nitrogen ($kg\ d^{-1}$)	Total Phosphorus ($kg\ d^{-1}$)	Total Nitrogen ($kg\ d^{-1}$)	Total Phosphorus ($kg\ d^{-1}$)	Total Nitrogen ($kg\ d^{-1}$)
Everglades	7.1	685	3.0	679	9.1	1753
Atmosphere	104.1	1945	127.0	2393	127.0	2393
Keys loads	115.1	466	54.9	238	54.9	238
Western boundary	1112.3	21918	192.7	3105	-589.6	-6217
Keys passes	-493.2	-32877	101.8	2068	158.4	4154
Net	845.5	-7863	479.4	8483	-240.2	2321

Transport across boundaries

That independent load estimates agree is reassuring but not surprising since the estimates are based on the same databases. Major discrepancies occur in the estimates of transport across the boundaries. The fluxes of Rudnick et al. (1999) are an order of magnitude larger than the fluxes computed from the model. In view of the differences in estimated flows, large differences in nutrient transport are expected. The direction of transport and the net system budgets also differ. Rudnick et al. (1999) indicate the western boundary is a source of nitrogen and phosphorus and the Keys passes are sinks. In the model, the Keys passes are sources of nutrients to the bay. The western boundary is a source of phosphorus and of nitrogen in the dry season but a sink in the wet season. Overall, Rudnick et al. (1999) estimate the bay accumulates phosphorus and exports nitrogen. The model accumulates phosphorus and nitrogen.

The most significant difference in the two budgets is the relative size of the transport across the boundaries relative to system loads. The Rudnick et al. (1999) budget indicates transport across boundaries is an order of magnitude larger than the largest loading sources. The model budget indicates transport across the boundaries is comparable in magnitude to the loads. The size of the boundary transports relative to loads has substantial implications on management of the system through load controls.

The major source of discrepancies in the two budgets is the discrepancies in flows. Differences also occur, to some extent, due to computed model concentrations. If the model computed additional total nitrogen, the model bay might change from a net importer to a net exporter of nitrogen.

Nitrogen fixation and denitrification

Rudnick at al. (1999) acknowledged nitrogen fixation and denitrification as potential nitrogen sources and sinks but were unable to evaluate these processes. Nitrogen fixation was specified as part of the seagrass model (Chapter 7). Values used in the model were 2300 kg N d^{-1} to the water column of Florida Bay and 8450 kg N d^{-1} to the sediments. The amount delivered to the water column is equivalent to the estimated atmospheric nitrogen load. The amount delivered to the water and sediments makes nitrogen fixation the largest net source to the system.

Denitrification within bottom sediments is calculated as part of the sediment diagenesis model (Chapter 8). Calculated denitrification within Florida Bay sediments amounts to 10,700 kg N d^{-1}. Calculated denitrification exceeds nitrogen fixation within the sediments and almost exactly equals total nitrogen fixation in water and sediments. Consequently, within the model, the system net nitrogen flux due to combined nitrogen fixation and denitrification is essentially zero. We caution that this result is based on extrapolation of rates from other systems and is subject to modification as flux measures from Florida Bay become available.

Carbon and Nutrient Pools

Organic carbon and nutrients in organic and mineral form exist in numerous pools in Florida Bay. Among these are the water column, seagrass, and benthic sediments. The size of these pools was estimated from the model for the wet and dry seasons of 1997.

The benthic sediments are, by far, the largest pool of organic carbon (Figure 140). The size of this pool can be misleading, however, since much of the carbon is refractory G3 organic matter. Seagrasses comprise the second largest carbon pool, followed by dissolved organic carbon in the water column. Benthic algae are computed to contain more carbon than phytoplankton, especially during the wet season.

The size sequence of the nitrogen (Figure 141) and phosphorus (Figure 142) pools largely follows the sequence of organic carbon although the relative sizes of the pools may differ, especially for phosphorus. For carbon and nitrogen, the sediments contain three to five times more material than seagrass, the next largest pool. For phosphorus, the sediments contain nearly 100 times as much phosphorus than seagrass. Benthic algae rival the water column for phosphorus content while they contain less nitrogen and substantially less carbon than the water column.

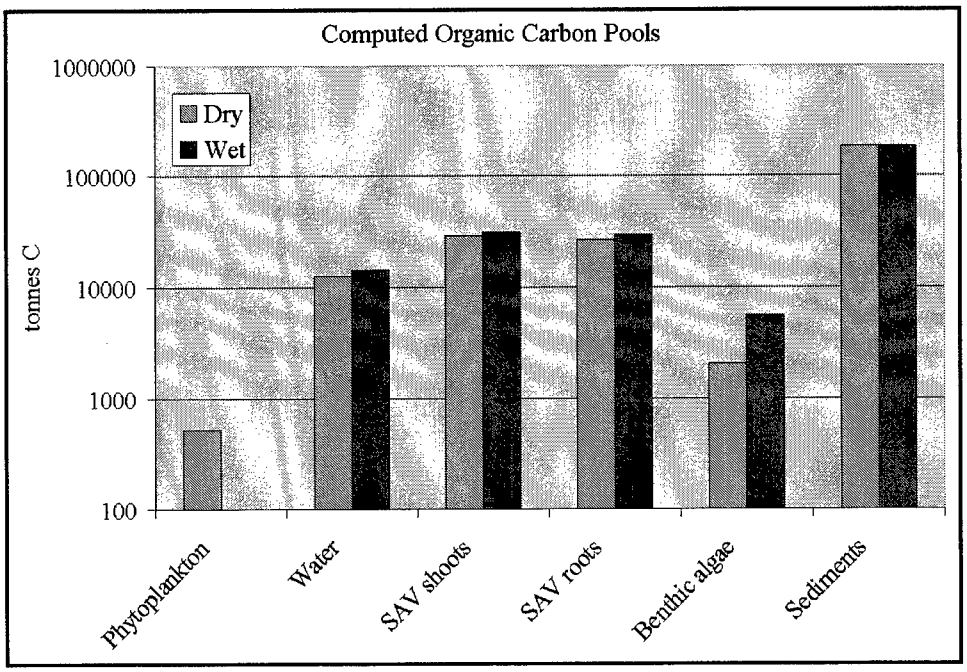

Figure 140. Computed organic carbon pools

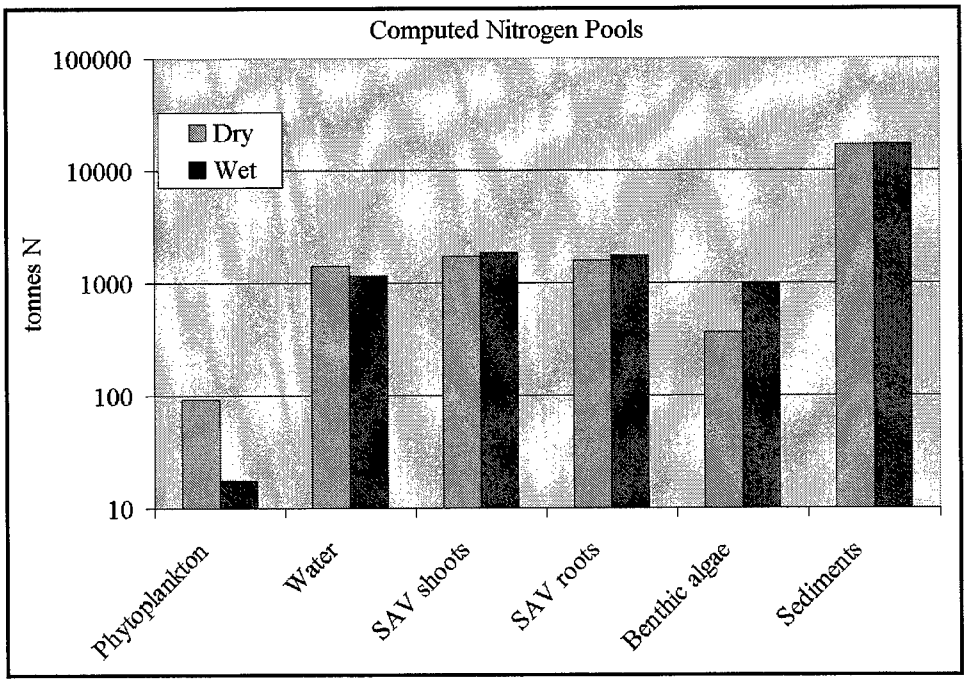

Figure 141. Computed total nitrogen pools

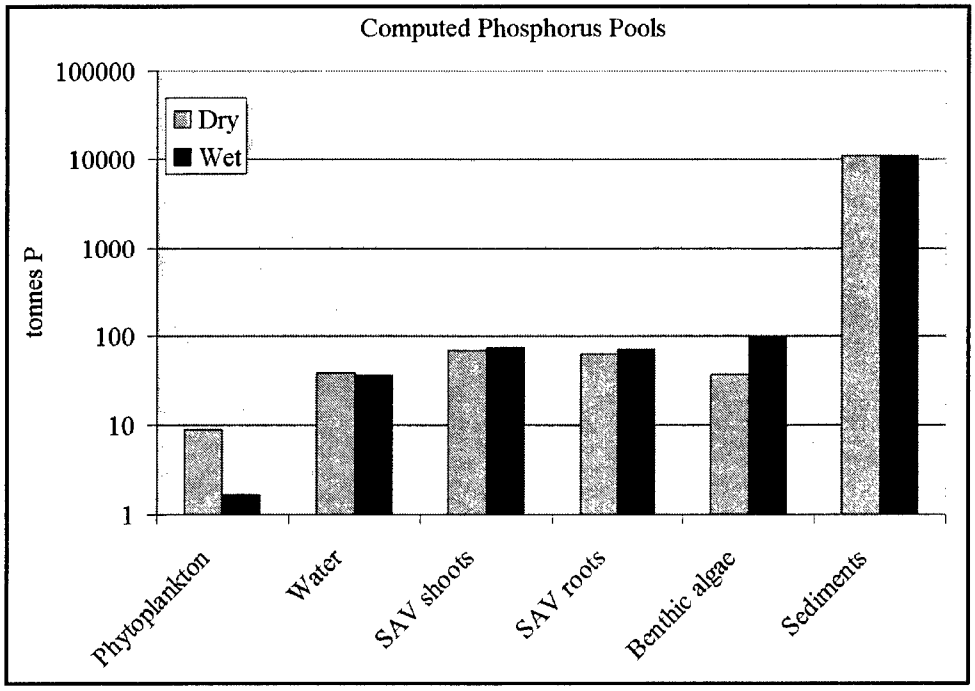

Figure 142. Computed total phosphorus pools

15 Summary, Conclusions, and Recommendations

Introduction

Florida Bay is a shallow, triangular water body bordered on the north by the Florida mainland and on the southeast by the Florida Keys. The waters of Florida Bay are characterized by low nutrient and chlorophyll concentrations and high water clarity. The system is distinguished by a dense, highly developed seagrass community that covers 95% of the bottom. Recent occurrences of algal blooms, periods of elevated turbidity, and seagrass die-offs have led to enhanced concern for the viability of the bay.

A Florida Bay nutrient workshop was held in Key Largo, July 1-2, 1996, to exchange information and derive inferences about nutrient enrichment and how it might change in association with hydrologic restoration of South Florida. A primary recommendation of the Science Oversight Panel convened for this workshop was that a numerical circulation/water quality model of Florida Bay should be developed.

In response to the need for a Florida Bay water quality model, the U.S. Army Engineer District, Jacksonville, requested the U.S. Army Engineer Waterways Experiment Station to assist with model planning. The original work plan called for a four-year effort. The need for rapid initial insights as well as resource constraints resulted in the present, two-year study. The revised work plan included the following tasks: 1) Data Acquisition; 2) Hydrodynamic Model Application for Water Quality Model Calibration; 3) Linkage Setup and Testing; 4) Resuspension Module Development; 5) Physical Modifications to Water Quality Model; 6) Seagrass Model Modifications; 7) Loading and Boundary Concentration Estimates; 8) Initial Water Quality Model Application and Nutrient Budget Analysis; 9) Hydrodynamic Model Application for Water Quality Model Confirmation; 10) Water Quality Model Confirmation/Evaluation; and 11) Documentation Report. The present report comprises the documentation called for in item 11.

Databases

The primary database for calibration of the water quality model consisted of observations collected monthly in the period 1991 to 1997. These were supplemented with observations collected at roughly monthly intervals from June 1989 through March 1991.

Additional data assembled for comparison with the model included seagrass abundance, measurements of sediment-water nutrient, carbon, and oxygen fluxes, observations of sediment chlorophyll and nutrients, observations of in situ suspended solids, and remotely sensed suspended solids.

Runoff and Loading

Monthly runoff for the period 1987-1997 was computed for eight South Florida drainage basins, six of which discharge into the model domain. Shark Slough, located on the west coast, was the largest discharger to the model domain. Taylor Slough was the largest discharger into Florida Bay itself. Runoff and other flows from the Keys were negligibly small.

Nitrogen and phosphorus loads from the mainland, Keys, and atmosphere were computed for the 1987-1997 period. A summary of long-term mean nutrient loads to the Western Shelf and to Florida Bay indicates atmospheric loads are the dominant source. Atmospheric loads comprise roughly 80% of the phosphorus loads to the Western Shelf and two-thirds the total loading to Florida Bay. Phosphorus loads from the Keys comprise most of the remaining load to Florida Bay. Phosphorus in runoff to Florida Bay is insignificant by comparison. Atmospheric nitrogen loads are more than a third of the total loading to the shelf and two-thirds of the loading to Florida Bay. The Keys are the least source of nitrogen directly to the bay.

Linkage to Hydrodynamic Model

The RMA-10-WES finite-element hydrodynamic model was used to generate a flow field for the CE-QUAL-ICM water quality model. Computed hydrodynamics were projected onto a water-quality model grid that was an overlay of the hydrodynamic grid. The projection algorithm generated a locally and globally conservative flow field for the water-quality model. Transport comparisons between RMA-10-WES and CE-QUAL-ICM using a conservative tracer indicated that the projection algorithm approach is working. Use of an overlay did not impact water-quality results in the area of focus, Florida Bay. The use of a coarse overlay along the western boundary resulted in numerical diffusion which influenced computations in that region. Overall, the results indicate that CE-QUAL-ICM and

RMA-10-WES were linked together properly and that RMA-10-WES could be used to generate hydrodynamic flow fields for water-quality modeling.

Suspended Sediment Modeling

A sediment resuspension module was developed and implemented in the Water Quality Model for this study. The module accounts for resuspension of a single sediment class by wind-driven waves. Damping effects of seagrass on resuspension are included. The module successfully reproduced in situ observed suspended sediment concentrations. The best agreement between model and observations was in a statistical sense, however, rather than one-to-one comparisons of computations and observations. Further refinement of the algorithm is possible but requires synoptic information on wind, wave, and suspended sediment concentrations over bare and seagrass-covered bottoms. More information is also needed on the short-term variability of suspended sediment fields.

Water Quality Model Formulation

The CE-QUAL-ICM water quality model was applied to the system. CE-QUAL-ICM is a flexible, widely applicable eutrophication model. As applied to Florida Bay, the model provided computations of variables listed in Table 27.

Table 27
Water Quality Model State Variables

Temperature	Salinity
Fixed Solids	Algal Biomass
Dissolved Organic Carbon	Labile Particulate Organic Carbon
Refractory Particulate Organic Carbon	Ammonium
Nitrate	Dissolved Organic Nitrogen
Labile Particulate Organic Nitrogen	Refractory Particulate Organic Nitrogen
Total Phosphate	Dissolved Organic Phosphorus
Labile Particulate Organic Phosphorus	Refractory Particulate Organic Phosphorus
Chemical Oxygen Demand	Dissolved Oxygen

The Seagrass Model

The seagrass model incorporates two state variables: shoots (above-ground biomass) and roots (below-ground biomass). Shoots exchange nutrients with the water-column component of the eutrophication model while roots exchange nutrients with the diagenetic sediment component. Light available to the shoots is computed via a series of sequential attenuations by color, fixed and organic solids in the water column, epiphytes, and self-shading.

The basic model formulation was applied to three seagrass species: *Thalassia testudinum*, *Syringodium filiforme*, and *Halodule wrightii*. Species were differentiated by species-specific parameter sets derived from observations collected in Florida Bay.

Sediment-Water Interactions

Representations of sediment-water interactions in Florida Bay employ three interactive submodels: a sediment diagenesis model, a benthic algae model, and a resuspension model. The diagenesis model computes the diagenesis (decay) of organic matter in the sediments, the resulting production of oxygen demand and nutrients, and the movement of diagenesis products between sediments and water column. Benthic algae occupy the sediment-water interface. They intercept nutrients released from sediments and may remove nutrients from the water column as well. The resuspension model transfers particulate carbon and nutrients from the sediments to the water column as a result of wind-driven wave action.

Water Column Calibration Results

Initial application of the model was to a two-year period, 1996–1997. Hydrodynamics for the calibration were obtained by sequencing dry-season and wet-season hydrodynamic files of 29 days in length. The hydrodynamics were generated using seasonal-average flows and winds and an intertidal sequence of surface elevations at the open boundaries. Loads were updated on a monthly basis.

The model captured the seasonal-average salinity distribution except at the interface with the mainland. There, the solid model boundary did not represent the permeable nature of the true interface. In the interior of the bay, on a monthly time scale, the model did not reproduce the observed salinity, especially the highest observed values.

The model captured the spatial distribution of chlorophyll and computed the occurrence of algal blooms. Little correlation was noted between observed and computed blooms, however. Random algal blooms are among the most difficult phenomena to model. Both increased understanding and more intense modeling effort are required to improve model capabilities in this area.

The model calculates strong phosphorus limitation on algal growth within the interior of the bay. The most limiting nutrient transitions from phosphorus to nitrogen in the southern and western extremes of the bay and becomes almost exclusively nitrogen along the open boundaries of the model domain. Occasionally, during resuspension events, light is computed to limit growth more than either nutrient but nutrient limitations generally prevail over light as limiting factors.

The dominant feature of total nitrogen observations and computations is the great excess of organic nitrogen over other forms. Observed total nitrogen demonstrates a pronounced "hot spot" in the Central Zone that persists through wet and dry seasons. The model reproduces the spatial pattern but tends to underestimate total nitrogen over a broad portion of the bay. The origin of the deficit cannot be clearly identified from the calibration. Possible causes include loading shortfalls and failure to isolate water in enclosed basins.

Observed total phosphorus exhibits highest concentrations in an arc that extends from the Western Shelf around Cape Sable into the Central Zone. The model duplicates the broad pattern of higher concentrations to the west and lower concentrations in the interior of the bay. The model reproduces the low soluble reactive phosphorus concentrations well in the interior of the bay but tends to overestimate soluble reactive phosphorus elsewhere. Observations indicate 30% of total phosphorus is in particulate form and 65% is in dissolved organic form. In the model, these distributions are reversed. The largest phosphorus fraction is particulate and about half of that fraction is inorganic. The distribution of total phosphorus into fractions can be addressed through additional calibration of the model.

Computed total organic carbon in the interior of the bay is uniformly less than observed. To match the observations, the model should include a large fraction of refractory dissolved organic carbon and a small fraction of labile dissolved organic carbon. This improvement can be readily installed in the model but is not of primary importance in Florida Bay.

Comparison of observed and computed total suspended solids for the calibration period is problematic. The solids resuspension algorithm was developed based on in situ solids observations collected in 1993-1994. For the calibration period, only remotely sensed solids data were available. During the calibration period, the model roughly reproduced the magnitudes and spatial distribution of suspended solids observed in situ during the earlier years. Compared to the remotely sensed observations, however, modeled solids are most often higher than observed. The model can be

recalibrated to reproduce the widespread remotely sensed database but cannot simultaneously reproduce the in situ and remotely sensed observations.

A data set was assembled to provide an indication of the model's ability to compute light attenuation. The observations show a spatial trend in which attenuation is highest near the mainland and declines with distance away from the mainland to reach minimum values outside the Keys. The model reproduces both the magnitude and the trend in the observations.

Seagrass Model Calibration Results

The computed distribution of *Thalassia* agrees well with observations. *Thalassia* is computed almost exclusively in Florida Bay and in the shallow waters adjacent to the Keys. Computed *Syringodium* is nearly absent from Florida Bay and is concentrated instead on the Western Shelf and outside the Keys. The model also computes extensive Syringodium along the west coast of Florida where none is found. Apparently, computed *Syringodium* is occupying regions that should be dominated by *Halophila* which is not represented in the model. As with the observations, computed *Halodule* is sporadically distributed within Florida Bay.

Overall, computed seagrass density (standing crop) is lower than reported mean values. More careful comparison of computed values at the exact locations of the samples may alter this conclusion. Comparisons of observed and computed densities may also be affected by the numerical algorithms used to derive regional mean values from model computations in individual cells.

Nitrogen limits computed seagrass growth to a greater extent than reported. Additional nitrogen loading to the system, routed to the sediments, may alleviate this limit and contribute to overall higher seagrass density.

Benthic Sediment Calibration Results

Computed benthic algae, as mg Chl m^{-2}, largely agrees with observations. Overall, computed bulk nitrogen in the sediments is much less than observed values. Computed bulk sediment phosphorus agrees with observations in the interior of Florida Bay but is less than observations in the western portion of the bay. Regions in which sediment nitrogen and phosphorus are less than observed tend to underlie water in which computed total nutrients are also less than observed. Within the domain of the observations, computed sediment available phosphorus is within the range of the observations.

Observations and computations agreed that the dark ammonium flux is to the water column. The majority of the computed release originates in excretion from seagrass. The model indicates daylight ammonium uptake, roughly equal in magnitude to the dark release. The uptake originates with benthic algae which strip ammonium from the water as well as intercept diagenetic ammonium release. Corresponding uptake is absent from the observations.

Both observations and model indicate nitrate removal from the water column in both dark and light. The largest computed component of this flux is daylight uptake by benthic algae.

The range of observed dissolved organic nitrogen fluxes is enormous relative to the other nitrogen components. The observed range, relative to the mean or median, confounds interpretation of the observations, especially in an average sense. Computed dissolved organic nitrogen fluxes are exclusively to the water and show no diurnal variation. Modeled fluxes originate in excretion from benthic algae and seagrass in roughly equal proportions.

Phosphate fluxes were observed into and out of the water column. Median observed fluxes were close to zero. Modeled fluxes showed a strong diurnal variation, with release to the water during dark and uptake during daylight. The diurnal variation originated in the computed benthic algae. Seagrass contributed a lesser background release via excretion.

As with phosphate, dissolved organic phosphorus fluxes were observed into and out of the water, such that medians of the observations were close to zero. Modeled fluxes were exclusively into the water and originated primarily in excretion from benthic algae.

Median observed dissolved organic carbon fluxes were into the water. Model fluxes were exclusively into the water and were of the same magnitude as median observations. The preponderance of the modeled DOC originated in seagrass excretion. Observed dissolved oxygen fluxes showed a clear pattern of removal from the water at night and release to the water during day. Modeled fluxes showed the same pattern as observed, but were less than half the observed values. Production by seagrass accounted for the majority of the daylight flux. Respiration by seagrass and benthic algae and sediment diagenesis all contributed to oxygen consumption.

Sensitivity Analyses

Six sensitivity runs were performed on the calibrated model. These were: 1) Sensitivity to loads from mainland and Keys; 2) Sensitivity to atmospheric loads; 3) Sensitivity to boundary conditions; 4) Sensitivity to resuspension; 5) Sensitivity to benthic algae; and 6) Sensitivity to nitrogen fixation.

One major conclusion from these runs is that shortfalls in computed nitrogen are not likely due to shortfalls in loading. Or else the computed loads must be low by more than a factor of two. Neither can the shortfalls in nutrients in the interior of the bay be attributed to boundary conditions which exert limited influence in the interior.

The impact of removing benthic algae from the model was enormous, far greater than any other sensitivity runs. This run suggests that benthic algae play an important role in mediating sediment-water exchange processes in Florida Bay and in determining nutrient concentrations in the overlying water. The model calibration, potentially, could be improved by revision of the benthic algal component or by "tuning" of the existing representation. At present, however, little basis exists for improving the model. Clearly, additional field and process investigation is necessary.

While the rate of nitrogen fixation in seagrass beds is poorly known, the rate would have to be many times larger than employed in the model to make up the computed shortfall in total nitrogen.

Ten-Year Water Quality Simulation

One major objective of the model study was to simulate a ten-year period in Florida Bay, commencing with the seagrass die-off. The ten-year run encompassed the interval from January 1, 1988, to December 31, 1997. Plans called for the ten-year hydrodynamics to be pieced together from a sequence of seasonal hydrodynamic model runs. These runs were to include seasons of extremely low flow, to simulate the drought conditions. Hydrodynamic simulations of the drought seasons were never satisfactorily completed. Consequently, the ten-year sequence was pieced together from available hydrodynamic simulations including one season from 1992, and two seasons each from 1996 and 1997.

Examination of model results concentrated on the zones in which seagrass die-offs occurred. Results in these three zones indicate, first, that observed concentrations of numerous substances are higher in the early years of the simulation than in later years. The second dominating feature is that the wide range of observed conditions are not captured by the model.

In interpreting the behavior of the model, our attention focuses on two issues. The first is the overall accuracy of the hydrodynamic model. The second is the influence of the overlay grid employed in the water quality model. To our knowledge, the ability of the hydrodynamic model to compute salinity, especially hyper-salinity, in Florida Bay has not been fully demonstrated. To compound the problem, the hydrodynamic grid was overlain with a coarser water quality grid. We suspect cells in the overlay grid span mud banks and other features that restrict flow. Overlay of flow-restricting features creates artificial transport across these features and may prevent concentration buildup that should result from an excess of

evaporation over precipitation. The larger overlay cells also increase numerical diffusion which diminishes concentration gradients.

Two ten-year simulations were conducted to examine the seagrass model. In one simulation, a die-off was imposed. In a second run, no die-off was imposed. The major impact of the die-off was rapid succession of the dominant *Thalassia* with *Halodule*. *Halodule* persisted through the remainder of the ten-year simulation.

Computed properties in the water column show little difference with and without the seagrass die-off. Computed solids, light attenuation, and chlorophyll are virtually identical in the two simulations. One hypothesis for the observed diminished water quality following the die-off calls for resuspended sediment in the die-off zones to increase light attenuation, thereby shading out the recovery of seagrass. Nutrients no longer taken up by seagrass become available to phytoplankton, resulting in algal blooms. This succession of events does not occur in the model. The likely cause for lack of difference in the two simulations is the rapid recovery of *Halodule* following the die-off. We cannot state conclusively whether the model should be revised to reflect the hypothetical succession of events or if the model indicates the hypothesis is not a good one.

Flow and Nutrient Budgets

Florida Bay flow and nutrient budgets were computed for the wet and dry seasons of 1997. During the dry season, major flows were into the system through a passage in the upper Keys and out of the system in a westerly direction onto the Western Shelf. During the wet season, major flows in the system were eastward, in from the Western Shelf, and out through a lower passage in the Keys. In the interior of the bay, net flows between basins were one or two orders of magnitude smaller than the major circulation via the western boundary and Keys passes.

Comparison of a published nutrient budget and the model budget indicates that estimated loadings from the Everglades, the atmosphere, and the Keys are in reasonable agreement. Major discrepancies occur in the estimates of transport across the boundaries. The published budget indicates nutrient transport across boundaries is an order of magnitude larger than the largest loading sources. The model budget indicates transport across the boundaries is comparable in magnitude to the loads. The size of the boundary transports relative to loads has substantial implications on management of the system through load controls. The direction of transport and the net system budgets also differ. The previous estimate indicates the bay accumulates phosphorus and exports nitrogen. The model bay accumulates phosphorus and nitrogen.

Conclusions and Recommendations

The accomplishments of this study should not be underestimated. First, the study successfully linked a finite-element hydrodynamic model with a conventional eutrophication model based on local conservation of volume. To our knowledge, this study represents the first time such a linkage has been accomplished. Although the linkage methodology is not perfected, the major hurdles have been cleared. With a little more effort, the method can be perfected. One obstacle to perfection in the linkage was the requirement to accomplish the linkage in the context of a practical study with deliverables and deadlines. Additional development of the linkage should be conducted as a research project solely devoted to the linkage effort.

The water quality model linked modules including water-column eutrophication, seagrass dynamics, sediment diagenesis, solids and nutrient resuspension, and benthic algal production. To our knowledge, this is a first for Florida Bay. In fact, we know of few systems that presently have a model application to rival the current effort in Florida Bay. The model does require substantial upgrading, however, to fully represent processes in the bay.

Nutrient loads to the bay and surrounding waters from various sources were calculated for this study. Estimates indicate the atmosphere is the largest of the loading sources to the bay. Runoff from the mainland is the least source of phosphorus and second least source of nitrogen. Paradoxically, runoff appears to be the most intensely studied loading source while large degrees of uncertainty exist in the greatest loads. Attention should be devoted to accurately quantifying atmospheric loads and phosphorus loads from the Keys.

No in situ measures of nitrogen fixation were available to us. Rates associated with seagrass beds, measured in other systems, were adapted for the model. Estimated nitrogen fixation associated with seagrass leaves equals the estimated atmospheric nitrogen load. The sum of nitrogen fixed in the leaves and roots makes nitrogen fixation the largest single source to the system. To our knowledge, measures of nitrogen fixation are currently being conducted. These measures should be swiftly incorporated into the model and into system nutrient budgets.

Neither were measures of denitrification within benthic sediments available. Rates of denitrification were calculated by the sediment diagenesis model with parameters adapted from Chesapeake Bay. Calculated denitrification roughly equals total nitrogen fixation. Denitrification rates should be measured and used to verify the computations provided by the model.

The model underestimates the amount of nitrogen in both the sediments and water column. Sensitivity analysis indicates the shortfall is unlikely to originate in loading estimates. Either a source of nitrogen has been omitted

or the estimated loads are greatly in error. Potential sources of omission or error include groundwater, nitrogen fixation, and denitrification.

The model does not concentrate material in the central basins, e.g. hypersalinity. This behavior may be attributed to several factors. First, the underlying hydrodynamic calculations may not concentrate material. Second, the linkage method may introduce errors in the computed hydrodynamic field. Third, the water-quality grid and numerics may introduce artificial dispersion. Dye tracer tests indicate the water quality model qualitatively tracks transport in the hydrodynamic model in Florida Bay. (Transport is not equivalent on the Western Shelf, due to artificial dispersion and boundary condition specification.) The tracer tests lead us to the conclusion that the underlying hydrodynamics prevent computation of hypersalinity and concurrent concentration of nitrogen and other materials.

Interpretation of results from the water quality model was severely compromised by lack of a verified hydrodynamic model operable on the same time scale as the water quality model. Successful simulation of a ten-year sequence of water quality was virtually impossible without corresponding hydrodynamics. The highest priority should be given to application of a detailed, volume-conservative hydrodynamic model to the bay and adjoining waters. The model should simulate a ten-year period, at least, and provide good agreement to salinities observed within that period.

The major uncertainty in the system nutrient budget is transport across the western boundary and through the Keys passes. This transport cannot be observed on a long-term basis. Computation via a model is the only alternative for long-term budget estimates. High priority should be given to estimating flow across system boundaries once a verified hydrodynamic model is available.

Sensitivity analysis indicates model computations are very sensitive to the biological activity at the sediment-water interface. In the present model, this activity is represented by the benthic algal component. The model, as formulated, cannot represent all observed fluxes, especially of dissolved organic matter. Attention should be devoted to quantifying sediment-water fluxes, to investigating the nature of the benthic community, and to process-based modeling of this community.

A great deal of observations have been collected in the bay since this study commenced and a good deal more is known about the bay than was known a few years ago. Once suitable hydrodynamics are available, the water quality model should be re-applied, on a ten-year time scale, and validated with the latest observations of conditions and processes in the bay. Concurrent with the re-application, first-order improvements (e.g. division of dissolved organic matter into labile and refractory components) can be incorporated into the water quality model.

References

Ambrose, R., Wool, T., Martin, J., Connolly, J., and Schanz, R. (1991). "WASP4, a hydrodynamic and water quality model - model theory, user's manual, and programmer's guide," Environmental Research Laboratory, Office of Research and Development, U.S. Environmental Protection Agency, Athens, GA.

Ammermaan, J., and Azam, F. (1985). "Bacterial 5'-nucleodase in aquatic ecosystems: a novel mechanism of phosphorus regeneration," Science 227, 1338-40.

Arfi, R., Guiral, D., and Bouvyi, M. (1993). "Wind induced resuspension in a shallow tropical lagoon," *Estuarine, Coastal, and Shelf Science*, 36, 587-604.

Boni, L., Carpene, E., Wynne, D., and Reti, M. (1989). "Alkaline phosphatase activity in Protogonyaulax Tamarensis," Journal of Plankton Research 11, 879-85.

Borum, J. (1985). "Development of epiphytic communities on eelgrass (*Zostera marina*) along a nutrient gradient in a Danish estuary," *Marine Biology* 87, 211-18.

Bosence, D. (1989). "Surface sublittoral sediments of Florida Bay," *Bulletin of Marine Science*, 44(1), 434-53.

Boyer, J., Fourqurean, J., and Jones, R. (1999). "Seasonal and long-term trends in the water quality of Florida Bay (1989-1997)," *Estuaries* 22(2B), 345-57.

Bunch, B., Cerco, C., Dortch, M., Johnson, B., and Kim, K. (2000). "Hydrodynamic and water quality model study of San Juan Bay and Estuary," ERDC TR-00-1, U.S. Army Engineer Research and Development Center, Vicksburg MS.

Capone, D., and Taylor, B. (1980). "Microbial nitrogen cycling in a seagrass community." *Estuarine perspectives.* V. Kennedy, ed., Academic Press, New York, 153-62.

Cerco, C., and Bunch, B. (1997). "Passaic River tunnel diversion model study, Report 5, water quality modeling," Technical Report HL-96-2, U.S. Army Engineer Waterways Experiment Station, Vicksburg, MS.

Cerco, C., Bunch, B., Cialone, M., and Wang, H. (1994). "Hydrodynamic and eutrophication model study of Indian River and Rehoboth Bay, Delaware," Technical Report EL-94-5, U.S. Army Engineer Waterways Experiment Station, Vicksburg, MS.

Cerco, C., and Cole, T. (1994). "Three-dimensional eutrophication model of Chesapeake Bay," Technical Report EL-94-4, U.S. Army Engineer Waterways Experiment Station, Vicksburg, MS.

_____. (1995). "User's guide to the CE-QUAL-ICM three-dimensional eutrophication model," Technical Report EL-95-15, U.S. Army Engineer Waterways Experiment Station, Vicksburg, MS.

Cerco, C., and Moore, K. (2000). "System-wide submerged aquatic vegetation model for Chesapeake Bay," *Estuaries*, in review.

Chrost, R., and Overbeck, J. (1987). "Kinetics of alkaline phosphatase activity and phosphorus availability for phytoplankton and bacterioplankton in Lake Plubsee (north German eutrophic lake)," Microbial Ecology 13, 229-48.

Cloern, J., Grenz, C., and Vidergar-Lucas, L. (1995). "An empirical model of the phytoplankton chlorophyll:carbon ratio - the conversion factor between productivity and growth rate," *Limnology and Oceanography* 40(7), 1313-21.

Cole, T., and Buchak, E. (1995). "CE-QUAL-W2: a two-dimensional, laterally averaged, hydrodynamic and water quality model, version 2.0," Instruction Report EL-95-1, U.S. Army Engineer Waterways Experiment Station, Vicksburg, MS.

Dawson, F.H., and Charlton, F. G. (1988). "Bibliography on the hydraulic resistance or roughness of vegetated watercourses," Freshwater Biological Association Occasional Publication. No. 25, Dorset, England.

DiToro, D., O'Connor, S., and Thomann, R. (1971). "A dynamic model of the phytoplankton population in the Sacramento-San Joaquin Delta," *Nonequilibrium systems in water chemistry*, American Chemical Society, Washington, DC, 131-80.

DiToro, D., and Fitzpatrick, J. (1993). "Chesapeake Bay sediment flux model," Contract Report EL-93-2, U.S. Army Engineer Waterways Experiment Station, Vicksburg, MS.

Dortch, M., Cerco, C., Teeter, A., and McAdory, R. (1997). "Work plan for a water quality model of Florida Bay," Miscellaneous Paper EL-97-6, U.S. Army Engineer Waterways Experiment Station, Vicksburg, MS.

Edinger, J., Brady, D., and Geyer, J. (1974). "Heat exchange and transport in the environment," Report 14, Department of Geography and Environmental Engineering, Johns Hopkins University, Baltimore, MD.

Enos, P. (1989). "Islands in the Bay - a key habitat of Florida Bay," *Bulletin of Marine Science* 44(1), 365-86.

Fonseca, M. S., and Cahalan, J. A. (1992). "A preliminary evaluation of wave attenuation by four species of seagrass," *Estuarine, Coastal, and Shelf Science* 35, 565-76.

Fonseca, M. S., and Fisher, J. S. (1986). "A comparison of canopy friction and seagrass movement between four species of seagrass with reference to their ecological restoration," *Marine Ecology*, 29, 15-22.

Fourqurean, J. (1992). "The roles of resource availability and resource competition in structuring seagrass communities of Florida Bay," Ph.D. diss., University of Virginia, Charlottesville.

Fourqurean, J., Durako, M., Hall, M., and Hefty, L. (in press). "Seagrass distribution in south Florida: a multi-agency coordinated monitoring program." *Linkages between ecosystems in the south Florida hydroscape: the river of grass continues*. J. Porter and K. Porter eds.

Fourqurean, J., Jones, R., and Zieman, J. (1993). "Processes influencing water column nutrient characteristics and phosphorus limitation of phytoplankton biomass in Florida Bay, FL, USA: inferences from spatial distributions," *Estuarine, Coastal and Shelf Science*, 36, 295-314.

Fourqurean, J., and Roblee, M. (1999). "Florida Bay: A history of recent ecological changes," *Estuaries* 22(2B), 345-57.

Fourqurean, J., Zieman, J., and Powell, G. (1992a). "Relationships between porewater nutrients and seagrasses in a subtropical carbonate environment," *Marine Biology* 114, 57-65.

Fourqurean, J., Zieman, J., and Powell, G. (1992b). "Phosphorus limitation of primary production in Florida Bay: Evidence from C:N:P ratios of the dominant seagrass," *Limnology and Oceanography* 37(1), 162-71.

Frankovich, T., and Fourqurean, J. (1997). "Seagrass epiphyte loads along a nutrient availability gradient, Florida Bay, USA," *Marine Ecology Progress Series* 159, 37-50.

Genet, L., Smith, D., and Sonnen, M. (1974). "Computer program documentation for the Dynamic Estuary Model," U.S. Environmental Protection Agency, Systems Development Branch, Washington, DC.

Hamilton, D. P., and Mitchell, S. F. (1996). "An empirical model for sediment resuspension in shallow lakes," *Hydrobiologica* 317, 209-220.

Hartman, B., and Hammond, D. (1985). "Gas exchange in San Francisco Bay," *Hydrobiologia* 129, 59-68.

Hawley, N., and Lesht, B. M. (1992). "Sediment resuspension in Lake St. Clair," *Limnology and Oceanography*, 37(8), 1720-37.

Hsu, S.A. (1974). "A dynamic roughness equation and its application to wind stress determination at the air-sea interface," *Journal of Physical Oceanography* 4, 16-20.

James, W. F., and Barko, J. W. (1994). "Macrophyte influences on sediment resuspension and export in a shallow impoundment," *Lake and Reservoir Management* 10(2), 95-102.

Jassby, A., and Platt, T. (1976). "Mathematical formulation of the relationship between photosynthesis and light for phytoplankton," *Limnology and Oceanography* 21, 540-47.

Johnson, B., Kim, K., Heath, R., Hsieh, B., and Butler, L. (1993). "Validation of a three-dimensional hydrodynamic model of Chesapeake Bay," *Journal of Hydraulic Engineering*, 199(1), 2-20.

Kemp, W., Twilley, R., Stevenson, J., Boynton, W., and Means, J. (1983). "The decline of submerged vascular plants in the upper Chesapeake Bay: Summary of results concerning possible causes," *Marine Technology Science Journal* 17(2), 78-89.

Kruczynski, B. (1998). "White paper on water quality concerns in Florida Keys," DRAFT, National Oceanic and Atmospheric Administration, National Marine Sanctuary Program Florida Keys, Marathon FL.

Laws, E., and Chalup, M. (1990). "A microalgal growth model," *Limnology and Oceanography* 35(3), 597-608.

Lick, W., Lick, J., and .Ziegler, C. K. (1994). "The resuspension and transport of fine-grained sediments in Lake Erie," *Journal of Great Lakes Research* 20(4), 599-612.

Luettich, R., Harleman, D., and Somlyody, L. (1990). "Dynamic behavior of suspended sediment concentrations in a shallow lake perturbed by episodic wind events," *Limnology and Oceanography* 35(5), 1050-67.

Madden C., and Kemp, W. (1996). "Ecosystem model of an estuarine submersed plant community: Calibration and simulation of eutrophication responses," *Estuaries* 19(2B), 457-74.

Matavulj, M., and Flint, K. (1987). "A model for acid and alkaline phosphatase activity in a small pond," Microbial Ecology 13, 141-58.

Mitchum, G.T., and Sturges, W. (1982). "Wind-driven currents on the West Florida shelf," *Journal of Physical Oceanography* 12, 1310-17.

Monod, J. (1949). "The growth of bacterial cultures," *Annual Review of Microbiology* 3, 371-94.

O'Connor, D. (1983). "Wind effects on gas-liquid transfer coefficients," Journal of the Environmental Engineering Division 190, 731-52.

O'Connor, D., and Dobbins, W. (1958). "Mechanisms of reaeration in natural streams," Transactions of the American Society of Civil Engineers 123, 641-66.

Odum, E. (1971). *Fundamentals of ecology*, 3rd ed., W. B. Saunders, Philadelphia, PA, 106-7.

Parsons, T., Takahashi, M., and Hargrave, B. (1984). *Biological oceanographic processes.* 3rd ed., Pergamon Press, Oxford.

Pejrup, M. (1986). "Parameters affecting fine-grained suspended sediment concentrations in a shallow micro-tidal estuary, Ho Bugt, Denmark," *Estuarine, Coastal, and Shelf Science* 22, 241-54.

Phlips, E., Lynch, T., and Badylak, S. (1995). "Chlorophyll a, tripton, color, and light availability in a shallow tropical inner-shelf lagoon, Florida Bay, USA," *Marine Ecology Progress Series* 127, 223-34.

Phlips, E., Zeman, C., and Hansen, P. (1989). "Growth, photosynthesis, nitrogen fixation and carbohydrate production by a unicellular cyanobacterium, *Synechococcus* sp. (Cyanophyta)," *Journal of Applied Phycology* 1, 137-45.

Prager, E. J., Halley, R. B., and Hansen, M. (1996). "Sediment transport processes and sea-floor mapping in Florida Bay," Program and abstracts, 1996 Florida Bay Science Conference, Key Largo, FL.

Roblee, M., Barber, T., Carlson, P., Durako, M., Fourqurean, J., Muehlstein, L., Porter, D., Yarbro, L., Zieman, R., and Zieman, J. (1991). "Mass mortality of the tropical seagrass *Thalassia testudinum* in Florida Bay (USA)," *Marine Ecology Progress Series* 71, 297-99.

Rudnick, D., Chen, A., Childers, D., Boyer, J., and Fontaine, T. (1999). "Phosphorus and nitrogen inputs to Florida Bay: The importance of the Everglades watershed," *Estuaries* 22(2B), 398-416.

Sanford, L. P., and Halka, J. P. (1993). "Assessing the paradigm of mutually exclusive erosion and deposition of mud, with examples from upper Chesapeake Bay," *Marine Geology* 114, 37-57.

Schomer, N. S., and Drew, R. D. (1982). "An Ecological Characterization of the Lower Everglades, Florida Bay, and the Florida Keys," FWS/OBS-82/58.1, U.S. Fish and Wildlife Service, Office of Biological Services, Washington, D.C.

Sheng, Y. P., Eliason, D. E., and Chen, X.-J. (1992). "Modeling three-dimensional circulation and sediment transport in lakes and estuaries," Proceedings, 2nd International Conf. Est. Coastal Modeling, ASCE, New York.

Southard, J., Young, R., and Hollister, C. (1971). "Experimental erosion of calcareous ooze," *Journal of Geophysical Research* 76(24), 5903-09.

Stumpf, R., Frayer, M., Durako, M., and Brock, J. (1999). "Variations in water clarity and bottom albedo in Florida Bay from 1985 to 1997," *Estuaries* 22(2B), 431-44.

Sutula, M. (1999). "Processes controlling nutrient transport in the southeastern Everglades wetlands, Florida, USA," Ph.D. diss., Louisiana State University, Baton Rouge.

Tchobanoglous, G., and Schroeder, E. (1987). *Water quality*, Addison Wesley, Reading, MA.

Teeter. A.M. (2000). "Cohesive clay-silt sediment modeling using multiple grain classes; Part II: Application to shallow-water resuspension and deposition," (in review) Elsevier Publishing, New York.

Thomann, R., and Fitzpatrick, J. (1982). "Calibration and verification of a mathematical model of the eutrophication of the Potomac Estuary," HydroQual Inc., Mahwah, NJ.

Titus, J., and Adams, M. (1979). "Coexistence and comparative light relations of the submersed macrophytes *Myriophyllum spicatum L.* and *Vallisneria americana Michx.*," *Oecologia (Berl.)* 40, 273-86.

Tuffey, T., Hunter, J., and Matulewich, V. (1974). "Zones of nitrification," *Water Resources Bulletin* 10, 555-64.

Twilley, R., Kemp, W., Staver, K., Stevenson, J., and Boynton, W. (1985). "Nutrient enrichment of estuarine submersed vascular plant communities. 1. Algal growth and effects on production of plants and associated communities," *Marine Ecology Progress Series* 23, 179-91.

Ward, L. G., Kemp, W. M., and Boynton, W. R. (1984). "The influence of waves and seagrass communities on suspended particulates in an estuarine embayment," *Marine Geology* 59, 85-103.

Westerlink, J. J., Leuttich, R. A., Baptista, A. M., Scheffner, N. W., and Farrar, P. (1992). "Tide and storm surge predictions using a finite element model," *Journal of Hydraulic Engineering* 118, 1373-90.

Westrich, J., and Berner, R. (1984). "The role of sedimentary organic matter in bacterial sulfate reduction: the G model tested," *Limnology and Oceanography* 29, 236-49.

Wetzel, R., and Neckles, H. (1986). "A model of *Zostera marina L.* photosynthesis and growth: Simulated effects of selected physical-chemical variables and biological interactions," *Aquatic Botany* 26, 307-23.

Wezernak, C., and Gannon, J. (1968). "Evaluation of nitrification in streams," Journal of the Sanitary Engineering Division 94(SA5), 883-95.

Zieman, J. (1982). "The ecology of the seagrasses of south Florida: a community profile," FWS/OBS-82/25, U.S. Fish and Wildlife Service, Office of Biological Services, Washington, DC.

REPORT DOCUMENTATION PAGE

Form Approved
OMB No. 0704-0188

1. AGENCY USE ONLY *(Leave blank)*	2. REPORT DATE	3. REPORT TYPE AND DATES COVERED
	September 2000	Final report

4. TITLE AND SUBTITLE
Water Quality Model of Florida Bay

5. FUNDING NUMBERS

6. AUTHOR(S)
Carl F. Cerco, Barry W. Bunch, Allen M. Teeter, Mark S. Dortch

7. PERFORMING ORGANIZATION NAME(S) AND ADDRESS(ES)
U.S. Army Engineer Research and Development Center
Environmental Laboratory
3909 Halls Ferry Road, Vicksburg, MS 39180-6199

8. PERFORMING ORGANIZATION REPORT NUMBER
ERDC/EL TR-00-10

9. SPONSORING/MONITORING AGENCY NAME(S) AND ADDRESS(ES)
U.S. Army Engineer District, Jacksonville
Jacksonville, FL

10. SPONSORING/MONITORING AGENCY REPORT NUMBER

11. SUPPLEMENTARY NOTES

12a. DISTRIBUTION/AVAILABILITY STATEMENT
Approved for public release; distribution is unlimited.

12b. DISTRIBUTION CODE

13. ABSTRACT *(Maximum 200 words)*

This report describes the development and application of a two-dimensional, depth-integrated water quality model to Florida Bay. The model includes dynamically linked components for water column transport and eutrophication processes, sediment resuspension and effects on light attenuation, benthic sediment processes and interaction with the water column, and seagrass biomass and interactions with water column and sediments. The report describes linkage to a finite-element hydrodynamic model, estimation of freshwater inflows and nutrient loadings to the system, model formulations, and application. Application consists of calibrating the model to the two-year period 1996-1997, testing model sensitivity for the two-year period, and simulating the ten-year period 1988-1997 to evaluate model long-term performance. This is the first application of a detailed water quality simulation model to Florida Bay. The application provides improved understanding of nutrient transport, fate, and effects. Although significant progress was achieved through this initial effort, there were also many improvements identified that must be undertaken before the model can be advanced further.

14. SUBJECT TERMS

Florida Bay	Nutrients	Water quality
Loadings	Seagrass	
Model	Sediments	

15. NUMBER OF PAGES
275

16. PRICE CODE

17. SECURITY CLASSIFICATION OF REPORT	18. SECURITY CLASSIFICATION OF THIS PAGE	19. SECURITY CLASSIFICATION OF ABSTRACT	20. LIMITATION OF ABSTRACT
UNCLASSIFIED	UNCLASSIFIED		